



Universitat Autònoma de Barcelona

**ADVERTIMENT.** L'accés als continguts d'aquesta tesi queda condicionat a l'acceptació de les condicions d'ús establertes per la següent llicència Creative Commons:  [http://cat.creativecommons.org/?page\\_id=184](http://cat.creativecommons.org/?page_id=184)

**ADVERTENCIA.** El acceso a los contenidos de esta tesis queda condicionado a la aceptación de las condiciones de uso establecidas por la siguiente licencia Creative Commons:  <http://es.creativecommons.org/blog/licencias/>

**WARNING.** The access to the contents of this doctoral thesis it is limited to the acceptance of the use conditions set by the following Creative Commons license:  <https://creativecommons.org/licenses/?lang=en>



Universitat Autònoma  
de Barcelona

# **Supramolecular studies on the behaviour of different chiral cycloalkane-based compounds as receptors, gelators and surfactants**

**Bernat Pi i Boleda**

**Tesi Doctoral**

**Estudi de Doctorat en Química**

**Supervised by:**

**Prof. Vicenç Branchadell Gallo  
Prof. Rosa M<sup>a</sup> Ortuño Mingarro**

**Departament de Química  
Facultat de Ciències**

**2016**



Memòria presentada per aspirar al grau de Doctor per **Bernat Pi i Boleda**.

This thesis is presented for graduation as Doctor by **Bernat Pi i Boleda**.

Vist i plau,

Read and approved,

Prof. Vicenç Branchadell Gallo

Prof. Rosa M<sup>a</sup> Ortuño Mingarro

Bellaterra, 15 de setembre de 2016

Bellaterra, 15<sup>th</sup> of September, 2016



## Abstract

In this thesis, four different supramolecular systems were studied as receptors, gelators or surfactants. The influence of different structural factors of the single molecule on the final supramolecular properties was analysed. Different strategies were used to prepare the studied compounds. The combination of different techniques leads us to better understand these systems obtaining synergistic results. Results of this thesis are divided in four chapters:

- 1) Different tripodal anion receptors were synthesised and their complexation with different anions were studied. Using NMR, complexation Gibbs energies were calculated and the binding affinity were studied. Using theoretical calculations, the structure of the complexes were predicted. Also, thermodynamics of the host-guest system were calculated and theoretical calculations lead us to rationalise the experimental results.
- 2) Three different families of cycloalkane diamide-based gelators were studied to determine the influence of the ring size, the substitutions of the ring and the stereochemistry on the final gelation abilities. Using the tube inversion test and rationalising it with different solubility parameters, the gelation ability was determined. This study was accompanied by high resolution NMR. Self-assembly was studied using theoretical calculations and circular dichroism. Results show that all of the studied gels are chiral despite some of the monomers are *meso* compounds. Then, using SEM, the morphology of the aggregates was determined.
- 3) Four different bolaform amphiphiles were synthesised and their behaviour as surfactants were studied to determine the influence of the stereochemistry and the regiochemistry on the final surfactant behaviour. Using the pendant drop method, the variation of the surface tension with the concentration was analysed. We developed a new method to predict the structure of the self-assembled surfactants at the surface. CryoTEM and SAXS were used to determine the morphology and size of the aggregates.
- 4) In the last chapter, four pH-dependent  $\beta$ -amino acid-based surfactants were synthesised. Supramolecular properties of these systems were studied using pendant drop method, cryoTEM, theoretical calculations, different physicochemical titrations, circular dichroism, UV-vis absorption and DLS. These surfactants show interesting acid-base behaviour suitable for biological applications. They have been studied as potential new non-viral vectors for gene therapy using different biophysical and biological techniques. Results show that these surfactants are not toxic and they have interesting features to be used as vectors.



## Acknowledgements

This thesis has been carried out in the *Departament de Química* from the *Universitat Autònoma de Barcelona* (UAB) under the direction of Prof. Rosa M<sup>a</sup> Ortuño and Prof. Vicenç Branchadell. I really thank them for giving me the chance to work in their group, for their scientific and financial support and the confidence placed in me.

I would like to thank to *Universitat Autònoma de Barcelona* the financial support I received during this thesis through a *Personal Investigador en Formació (PIF)* grant, without which the realisation of the thesis would have not been possible.

Thank to Dr. Rita de Sousa Dias for giving me the opportunity to carry out a three months collaboration in the *Norwegian University of Science and Technology (Norges teknisk-naturvitenskapelige universitet NTNU, Trondheim, Norway)*. Also thank to Sravani K. Ramiseti for teaching me all different techniques we used during the collaboration. I would like to thank specially Dr. Dan Lundberg from Colloidal Resource Research Center (Lund, Sweden), without whom I would not been able to carry out the stay in Trondheim. I would like to thank again to *Universitat Autònoma de Barcelona* the financial support I received to carry out this stay.

I want to special thank Dr. Ramon Pons for giving me the possibility to work with him in the *Institut de Química Avançada de Catalunya (IQAC-CSIC)* in order to carry out the study of different surfactants and also for all the knowledge I have learnt with him.

In addition, I would like to thank Dr. Ona Illa for her scientific advices and to the labmates I have been working with: Sergi (Chapter 4), Alessandro (Chapter 6), Marta (Chapter 5 and 6), Jimena, Carme and Oriol, for teaching me how to work, for their advices and scientific discussions and for the after-work times and all other thesismates such as Ana María, Albert and others. Also thanks to the visiting members such as Yaroslav, Thomas and Christian. Moreover, thanks to Oriol, Kírian, Bohores and Alfons for sharing their knowledge in our interesting scientific discussions.

I would to acknowledge the work of all those who remove barriers in the way of science and especially to all the PhD students from around the world.



I would like to thank the technicians from the different services that we used in this thesis:

- HR-NMR: Dr. Pau Nolis, Servei de Ressonància Magnètica de la UAB.
- X-Ray diffraction: Dr. Àngel Álvarez, Servei de Difracció de Rajos X de la UAB.
- CryoTEM: Dr. Pablo Castro, Servei de Microscopia de la UAB.
- SAXS: Dr. Ramon Pons, Dr. Jordi Morros, Jordi Caelles and Imma Carreras, (IQAC-CSIC). Measurements were carried out in ALBA Synchrotron.
- SEM: Dr. Anna Esther Carrillo and Dr. Judith Oró, Servei de Microscopia Electrònica de l'Institut de Ciència dels Materials de Barcelona (ICMAB-CSIC).
- AFM: Dr. Gjertrud Maurstad, NTNU.
- DLS: Ann-Sissel Teialeret Ulset, NTNU.
- Biological assays: Dr. Nerea Gaztelumendi and Dr. Carme Nogués (Department of Cellular Biology, UAB)

I would like to thank Dr. Ramanathan Nagarajan and Dr. Gennaro Pescitelli for their kind answers and advices.

Finally, I want to thank specially my parents for all the scientific and vital discussions during the thesis as well as their support and Julieta for all the support she gave me during these years by listening all the discussions, assays of the seminars, talks, results and presentations. They gave me some external points of view of the research that have helped me to find out the way.

Chemistry can be likened to “language”. The atoms are the “letters”. The molecules are the “words”. Assemblies of molecules make up the “sentences”. The sets of assembled molecules or supermolecules are the “paragraphs”. The ways in which the molecular assemblies and supramolecular arrays contain and express information are the “chapters”. The manner in which this information is conveyed is the “book”. Ultimately, chemistry has to tell a “story”. The life sciences are composed of really wonderful chemical “stories”. They were written by nature using “ancient languages”.

Chemists are just starting to write their own “stories”. They know how to produce the “words”. Now, they are learning how to write the “sentences”. The “grammar” they will use will be dictated by the nature of the non-covalent bond. The “modern languages” are about to evolve. Materials science and the life sciences will be beneficiaries. As discipline, chemistry will be enriched. <sup>1</sup>

Part of the results reported in this thesis have been published in the following scientific articles:

- **Synthesis, Selectivity and Structural Study of New  $C_3$ -Symmetric Tripodal Amides as Anion Receptors. An Experimental and Theoretical Approach.**

Sergi Celis, Bernat Pi-Boleda, Pau Nolis, Ona Illa, Vicenç Branchadell and Rosa M. Ortuño  
*Chemistry Select*, **2016**, *1*,1887-1892.

- **Studies on cycloalkane-based bisamide organogelators: A singular case of chiral aggregates from *meso* molecules.**

Bernat Pi-Boleda, Marta Sans, María Campos, Pau Nolis, Ona Illa, Juan Carlons Estévez, Vicenç Branchadell and Rosa M. Ortuño  
*Submitted*

Other articles with the rest of the results will be published as soon as possible.

## Table of abbreviations

AFM	Atomic Force Microscopy
ATP	Adenosine Triphosphate
ATR	Attenuated Total Reflectance
bp	base pair
BSA	Bovine Serum Albumin
BSSE	Basis Set Superposition Error
CAC	Critical Aggregation Concentration
CD	Circular Dichroism
CMC	Critical Micellar Concentration
C-PCM	Conductor-like Polarizable Continuum Model
CryoTEM	Cryogenic Transmission Electron Microscopy
CTAB	Cetyltrimethylammonium Bromide
DAC	Dodecylammonium Chloride
DEA	Dye Exclusion Assay
DFPA	DNase Foot-Printing Assay
DFT	Density Functional Theory
DIPEA	<i>N,N</i> -Diisopropylethylamine
DLS	Dynamic Light Scattering
DLVO	Derjaguin-Landau-Verwey-Oberbeek
DMAP	4-dimethylaminopyridine
DMF	Dimethylformamide
DMSO	Dimethylsulfoxide
DNA	Deoxyribonucleic acid
dNTP	Deoxynucleoside triphosphate
dsDNA	double-stranded DNA
DTAB	Dodecyltrimethylammonium Bromide
EDX	Energy Dispersive X-ray
EMSA	Electrophoretic Mobility Shift Assay
ESI	Electrospray Ionization
FDPP	Pentafluorophenyl Diphenylphosphinate
GABA	$\gamma$ -Aminobutyric acid
GFP	Green Fluorescent Protein
HRMS	High Resolution Mass Spectroscopy
HR-NMR	High Resolution Nuclear Magnetic Resonance
HSPs	Hansen Solubility Parameters
IR	Infrared
kbp	kilobase pair
L-CPL	Left-handed Circularly Polarised Light
LMWG	Low Molecular Weight Gelator
LMWOG	Low Molecular Weight Organogelator
<i>mgc</i>	minimum gelation concentration
MRI	Magnetic Resonance Imaging
NBO	Natural Bond Orbital
NMR	Nuclear Magnetic Resonance
NTA	Nitrilotriacetic acid

PCR	Polymerase Chain Reaction
PDI	Polydisperse factor
PLE	Pig Liver Esterase
PyBOP	(Benzotriazol-1-yloxy)tripyrrolidinophosphonium hexafluorophosphate
R-CPL	Right-handed Circularly Polarised Light
RNA	Ribonucleic Acid
SAXS	Small Angle X-Ray Scattering
SDS	Sodium Dodecylsulphate
SEM	Scanning Electron Microscopy
SMD	Solvation Model based on solute electron Density
ssDNA	Single-stranded DNA
TBA	Tetrabutylammonium
TBDMS	<i>tert</i> -Butyldimethylsilyl
THF	Tetrahydrofuran
TLC	Thin Layer Chromatography
<i>tren</i>	2,2',2''-Tris-(2-aminoethyl)amine
UV	Ultraviolet light
Vis	Visible light

## 1. Table of contents

2. General Introduction .....	19
3. Formative Objectives.....	25
4. Synthesis, selectivity and structural study of new $C_3$ -symmetric tripodal amides as anion receptors. An experimental and theoretical approach.....	29
4.1 Introduction.....	31
4.2 Objectives .....	36
4.3 Results and Discussion .....	37
4.3.1 Dissociation of the TBA <sup>+</sup> salts .....	37
4.3.2 Complexation of the $\alpha$ -glycine-based tripodal receptor <b>18</b> with different anions .....	38
4.3.3 Complexation of the $\beta$ -alanine and $\gamma$ -aminobutyric acid-based tripodal anion receptors <b>19</b> and <b>20</b> , respectively, with H <sub>2</sub> PO <sub>4</sub> <sup>-</sup> .....	42
4.3.4 The tripodal anion receptor derived from (-)-verbenone as a selective fluoride receptor .....	44
4.3.5 Study of the formation of bifluoride in F <sup>-</sup> complexes.....	47
4.3.6 Possibility that tripodal receptors form complexes of other stoichiometries with H <sub>2</sub> PO <sub>4</sub> <sup>-</sup> .....	50
4.3.7 Preparation of single crystals of the studied complexes .....	52
4.4 Summary and Conclusions .....	54
5. Cycloalkane diamide-based low molecular weight organogelators: influence of ring size, substitution and stereochemistry .....	55
5.1 Introduction.....	57
5.2 Objectives .....	63
5.3 Results and Discussion .....	64
5.3.1 Gelation study of Family 1.....	66
5.3.1.1 High-resolution NMR spectroscopy .....	68

## 1. Table of contents

5.3.1.2 Scanning Electron Microscopy (SEM) .....	72
5.3.1.3 Theoretical Calculations .....	74
5.3.1.4 Circular Dichroism .....	79
5.3.2 Gelation study of Family 2.....	84
5.3.2.1 Hansen Solubility Parameters .....	86
5.3.2.2 Scanning Electron Microscopy (SEM).....	90
5.3.2.3 Theoretical Calculations .....	91
5.3.2.4 Circular Dichroism .....	99
5.3.3 Gelation study of Family 3.....	104
5.3.3.1 Theoretical Calculations .....	105
5.3.3.2 Circular Dichroism .....	107
5.4 Summary and Conclusions .....	108
6. Cationic bolaamphiphiles with a cyclobutane scaffold: behaviour as surfactants .....	111
6.1 Introduction.....	113
6.2 Objectives .....	120
6.3 Results and Discussion .....	121
6.3.1 Synthesis.....	121
6.3.2 Measurements of the surface tension .....	125
6.3.3 Cryogenic Transmission Electron Microscopy (cryoTEM) .....	129
6.3.4 Small Angle X-Ray Diffraction (SAXS) .....	131
6.3.5 Theoretical calculations.....	134
6.4 Summary and Conclusions .....	143
7. Chiral pH-dependent $\beta$ -amino acid-based surfactants: synthesis, study of their properties and study as potential new vectors for gene therapy.....	145
7.1 Introduction.....	147
7.2 Objectives .....	153

7.3 Results and Discussion .....	154
7.3.1 Synthesis.....	154
7.3.2 Supramolecular analysis.....	155
7.3.2.1 Determination of the pK <sub>a</sub> .....	155
7.3.2.1.1 Dependence of the pH on the concentration of surfactant .....	157
7.3.2.1.2 Acid-Base titration of the surfactant aggregates.....	162
7.3.2.2 Measurements of the surface tension .....	164
7.3.2.3 Cryogenic Transmission Electron Microscopy (CryoTEM).....	169
7.3.2.4 Theoretical Calculations .....	171
7.3.2.5 Dynamic Light Scattering (DLS) .....	175
7.3.2.6 Circular Dichroism .....	178
7.3.3 Biophysical study.....	184
7.3.3.1 Dye Exclusion Assay (DEA).....	185
7.3.3.2 Electrophoretic Mobility Shift Assay (EMSA) .....	192
7.3.3.3 Atomic Force Microscopy (AFM).....	195
7.3.3.4 Compaction using CD .....	197
7.3.3.5 DNase Foot Printing Assays (DFPA).....	200
7.3.3.6 Decompaction and release of the complexed DNA .....	204
7.3.4 Biological application.....	210
7.3.4.1 Cytotoxicity – MTT assay .....	210
7.3.4.2 Cell Transfection.....	212
7.4 Summary and Conclusions .....	214
8. General Conclusions .....	215
9. Computational Details.....	219
9.1 General methodology.....	221



## 1. Table of contents

9.2 Tripodal anion receptors .....	221
9.3 Organogelators .....	223
9.4 Bolaamphiphiles .....	223
9.5 pH-Dependent surfactants .....	224
10. Experimental Details.....	225
10.1 Spectroscopy and spectrometry .....	227
10.2 Infrared spectroscopy (IR) .....	227
10.3 High Resolution Mass Spectra (HRMS).....	227
10.4 Measurements of the surface tension .....	227
10.5 Measurements of the proton activity of the surfactants.....	229
10.5.1 pKa measurements.....	229
10.5.2 pH-Surfactant Concentration Measurements.....	229
10.6 Microscopy .....	230
10.6.1 Cryogenic Transmission Electron Microscopy (CryoTEM).....	230
10.6.2 Scanning Electron Microscopy (SEM).....	231
10.6.3 Atomic Force Microscopy (AFM) .....	231
10.7 Circular dichroism (CD).....	231
10.7.1 CD in solution .....	231
10.7.2 Solid state CD of the xerogels.....	232
10.7.3 CD of DNA-containing samples .....	233
10.8 Gelation studies.....	234
10.9 Flash chromatography.....	235
10.10 Dynamic Light Scattering (DLS) .....	235
10.11 Polymerase Chain Reaction (PCR protocol) .....	236
10.12 Gel electrophoresis.....	239

10.13 NanoDrop Measurements.....	240
10.14 Dye Exclusion Assay.....	241
10.15 DNase Foot Printing Assay .....	242
10.16 Biological assays .....	242
10.17 General tools .....	243
10.18 Synthetic procedures.....	244
11. Bibliography.....	283
12. Annex.....	297
12.1 CryoTEM images of pH-dependent surfactants .....	299
12.2 Correlation curves of DLS .....	303
12.3 Emission Spectra of DNA-GelStar® complexes at different surfactant concentrations.....	304
12.4 Comparison between the results obtained from DEA and EMSA.....	305
12.5 DNase Foot Printing Assay.....	307
12.6 Transfection studies .....	309
12.7 Program “Calculs” .....	311
12.8 Posters .....	315



## **2. General Introduction**

---



## 2. General Introduction

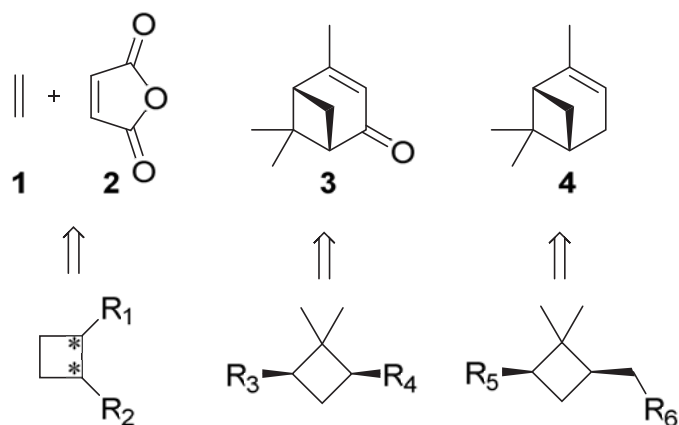
During the last few decades, the field of supramolecular chemistry has grown exponentially as indicated in the large number of articles, reviews and books.<sup>2-7</sup> Molecular chemistry consists in forming covalent bonds between atoms to obtain molecules and then to study their properties and applications. On the other hand, supramolecular chemistry consists in forming intermolecular bonds between molecules to obtain the so-called supermolecules and to study their properties and applications, which in most cases are completely different from those of the single molecules. As Lehn said in his Nobel Prize lecture, supramolecular chemistry is “the chemistry beyond molecules”.<sup>8</sup>

Supramolecular studies involve multidisciplinary fields such as organic synthesis, physicochemical studies or computational calculations. The combination of different techniques is crucial to be able to understand the complexity of supramolecular systems. Thus, supramolecular chemistry lead us to take advantage of different techniques achieving a synergistic result.

During the last years, our research group *Synthesis, Structure and Chemical Reactivity (SERQ)* has been interested in the use of cyclobutane as a conformational restriction element in a wide variety of applications. Different enantioselective syntheses were developed in order to obtain enantiopure compounds. The cyclobutane ring provides a rigid platform to the substituents of the ring, enhancing their properties in different fields.

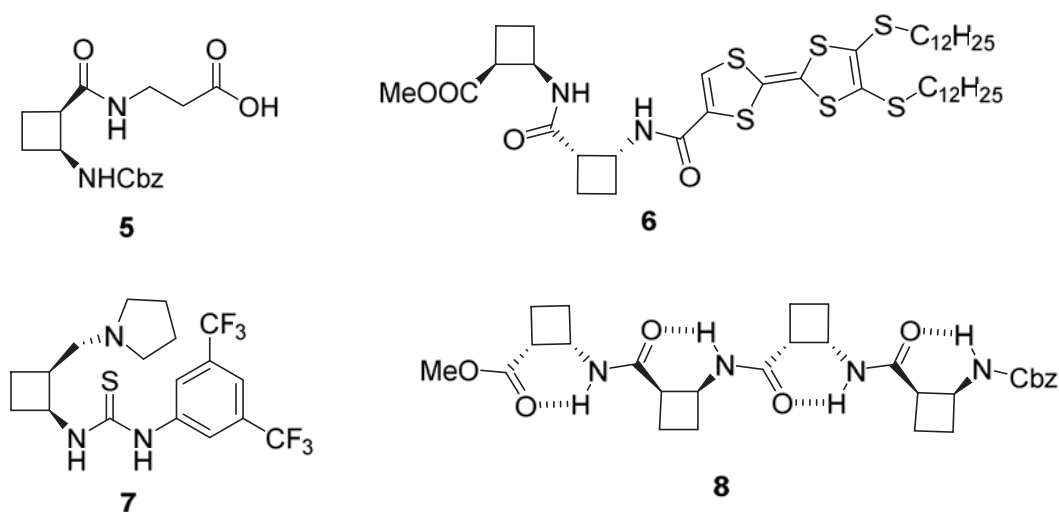
Two main different types of substituted chiral cyclobutane-based compounds were studied: substitution in 1,2- and in 1,3- (Figure 1). The 1,2- substituted cyclobutane-based compounds are obtained from a photochemical reaction between ethylene and maleic anhydride and the resulting product can be easily desymmetrised using an enzyme. The 1,3-substituted cyclobutane-based compounds can be obtained from (–)- $\alpha$ -verbenone (**3**) and from (–)- $\alpha$ -pinene (**4**), which are commercially available, depending on the desired substituents. Depending on the substituents of the ring, these molecules could have application in a wide range of different fields. The synthesis and use of chiral  $\beta$ -,  $\gamma$ - and  $\epsilon$ -amino acid-based compounds as building blocks has been one of main research lines.

## 2. General Introduction



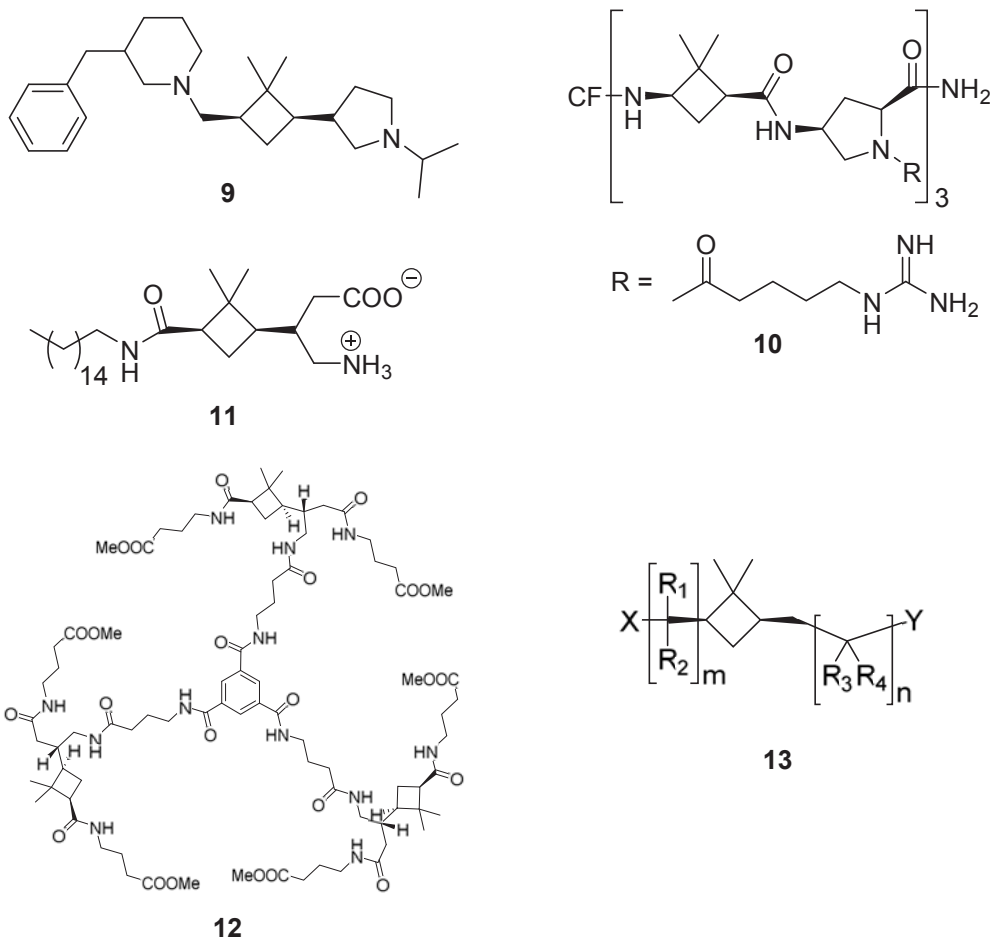
**Figure 1.** Schematic representation of the 1,2- and 1,3-substituted cyclobutanes studied in our research group.

Figure 2 shows some examples of 1,2-substituted cyclobutane-based compounds as metallocoxypeptidase inhibitors (**5**),<sup>9</sup> conductive materials (**6**),<sup>10</sup> bifunctional organocatalysts (**7**),<sup>11</sup> organobridged silsesquioxanes<sup>12</sup> or homochiral  $\beta$ -peptide foldamers (**8**).<sup>13,14</sup>



**Figure 2.** Examples of 1,2-substituted chiral cyclobutane-based compounds synthesised in our research group.

Figure 3 shows some examples of 1,3-substituted chiral cyclobutane-based compounds as nanocatalyst stabilizers (**9**),<sup>15</sup> cell-penetrating peptides (**10**),<sup>16</sup> zwitterionic surfactant (**11**),<sup>17</sup> tripodal dendrimers (**12**)<sup>18</sup> or ligands for MRI (**13**).<sup>19,20</sup>



**Figure 3.** Examples of 1,3-substituted chiral cyclobutane-based compounds synthesised in our research group.

In this thesis, different supramolecular systems based on chiral cyclobutane scaffolds were studied. Additionally, some other systems were also considered in order to find out the effect of the cyclobutane ring. The main aim of this work is to combine different techniques in order to understand the supramolecular systems and especially to carry out basic research to determine the influence of different structural factors of the single molecule such as stereochemistry, regiochemistry, ring size, length of an alkyl chain or an spacer on the final properties of the supermolecule.

The study of supramolecular systems carried out in this thesis can be divided in host-guest chemistry (Chapter 4), molecular self-assembly (Chapter 5, 6 and 7) and biophysical chemistry (Chapter 7). All of them lead us to better understand the supramolecular behaviour of different chiral cyclobutane-based compounds in different environments and applications.



## 2. General Introduction

Results are presented as four different chapters; each of them contains an Introduction, Objectives, Results, Discussion and Conclusions section. Then, General Conclusions of all the results are shown in a separate chapter. Finally, Computational and Experimental Details are disclosed in the last chapters.

### **3. Formative Objectives**

---



### 3. Formative Objectives

During the elaboration of this thesis, different specific scientific objectives were proposed in order to determine the path of the research. Scientific objectives are crucial for the elaboration of a scientific research. In this way, for the elaboration of a PhD thesis, which is a formative period, also some formative objectives were proposed.

- To **learn**. To learn a lot.

The most important objective of a PhD thesis is to learn. To learn different techniques, methodologies, ways to work, ways to think... Knowledge has no limit and thus, depends only on each researcher to decide how much he wants to learn during the PhD thesis. The objective is to deepen in different topics in order to get as wide knowledge as possible.

- To work as part of a **team**.

A researcher has to know to work not only as a part of a group but also as a part of a team. Each member of a team has to have some responsibilities to carry out in order to assure that the team can work without problems. Sharing ideas and points of view can enrich the way we see the daily work. The objective is to learn to work with different teammates during the thesis sharing responsibilities, thoughts and ideas.

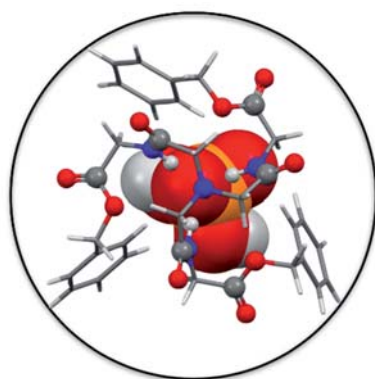
- To be **critical** with oneself.

Only being critical with one-self, a researcher can be a better researcher and a better person. During the PhD thesis, to be critical with one-self as well as with the obtained results will lead the researcher to be self-confident with himself. The objective is to be critical with one-self as a researcher and as a person in order to improve in both senses.

- To be able to find **solutions** of some daily/scientific problems.

The last but not least is to be able to find solutions to the daily problems during the thesis as well as the scientific decisions that one has to take alone.





**4. Synthesis, selectivity and structural study of new C<sub>3</sub>-symmetric tripodal amides as anion receptors. An experimental and theoretical approach**

---



## 4. Synthesis, selectivity and structural study of new $C_3$ -symmetric tripodal amides as anion receptors. An experimental and theoretical approach

### 4.1 Introduction

Host-guest chemistry deals with an important type of supramolecular systems providing useful tools to recognize and entrap specific chemical species by using appropriate receptors.<sup>2</sup> Specially, the formation of complexes between anions and suitable ligands has received particular attention since anions play fundamental roles in a wide range of chemical, biological and environmental processes.<sup>6</sup> Therefore, a great interest is devoted to the development of synthetic receptors able to recognize anions with high selectivity and affinity.

Among the diversity of the receptors described, podands have emerged as simple and effective ligands because of their easier synthesis and low cost compared with big macrocycles, which were earlier developed.<sup>2</sup> The name podand comes from the Greek word  $\pi\acute{o}\delta\iota$  (podi), which means foot but it is commonly referred as arm. These three branches provide to the receptor a three-legged piano-stool-like structure (Figure 4).

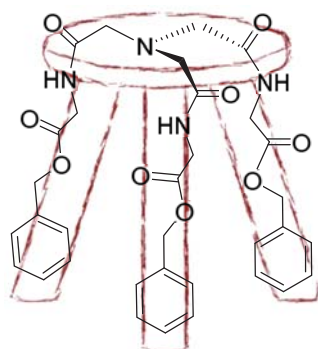


**Figure 4.** Three-legged piano-stool-like structure.

Often, podands are defined as multidentate organic ligands, host molecules with pendant binding sites<sup>21</sup> or multidonor-site host molecules, whose characteristic structural feature is the alignment of donor atoms in the open-chain backbone.<sup>22</sup> Podands can display a wide scope of binding groups in their structure and they can modulate the flexibility degree with different levels of preorganization, allowing diversity in host design



to fit almost any analytical and sensing application. Probably, anion recognition is the major focus of work in the podand field at present. On the other hand, amides as binding sites in receptors have conferred to hosts with high selectivity and good affinity. Thus,  $C_3$ -symmetric analogues of tripodal 2,2',2''-nitrilotris(*N*-amides) were tested for anion recognition and present entrapping properties for several kinds of monovalent anions. Tris(2-aminoethyl)amine (*tren*) derivatives were prepared for these purposes and

Figure 5 shows compound **14**, which was synthesised and used by Reinhoudt becoming one of the most used tripodal scaffolds for the receptors with three branches.<sup>23</sup> Thus, tripodal *tren*-based receptors differing in the aromatic end-group presented selective affinity for fluoride<sup>24</sup> or nitrate<sup>25</sup> (compounds **15** and **16**, respectively, Figure 5). Moreover, tripodal (*tren*)-*N*-amide-based receptors, which show high affinity towards dihydrogenphosphate,  $H_2PO_4^-$ , were used for the development of some redox sensors.<sup>26</sup>

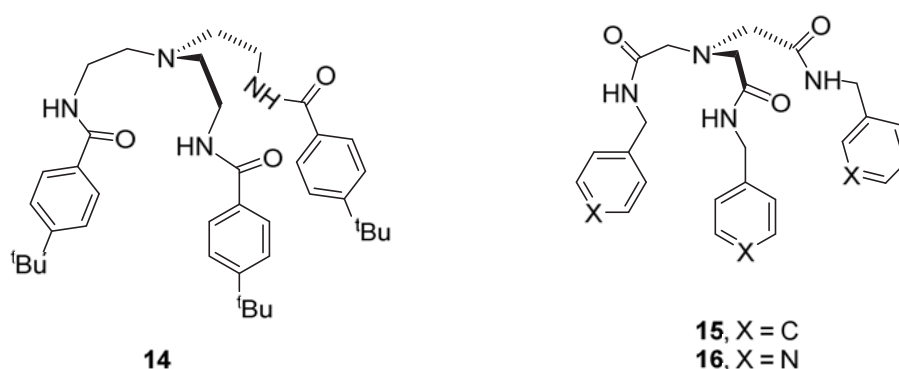


**Figure 5.** Examples of tripodal *tren*-based receptors (compound **14**)<sup>24,25</sup> and NTA-based amide receptors (compounds **15** and **16**)<sup>27</sup>.

Amides derived from nitrilotriacetic acid (NTA) were also prepared and used as monoanion receptors.

Figure 5 shows examples of the NTA-based amides (compound **15** and **16**) with ability for the recognition of several anions as in their tetrabutylammonium salt form.<sup>27</sup>

Concerning the most relevant anions described in the literature for host-guest chemistry with similar tripodal receptors,<sup>6</sup>  $H_2PO_4^-$  was widely employed for the study of host-anion systems and its interest is usually related to mimic active sites of phosphate-binding proteins, which are necessary for the ATP formation. It is a versatile anion due to

its acidic properties together with the intrinsic basicity derived from its anionic nature. Among carboxylate anions, acetate,  $\text{CH}_3\text{CO}_2^-$ , and benzoate,  $\text{PhCO}_2^-$ , are a common source of trigonal planar anions. Benzoate anion usually presents similar host-guest behaviour to that of acetate although their differences normally rise from their distinct bulkiness in the binding sites of receptors. Chloride anion,  $\text{Cl}^-$ , is interesting since membrane transport agents therefore can be found in many biological systems. A key structural feature to bind chloride in an effective manner is a cavity with the proper size to entrap it. The main reason is related to the fact that spherical anions cannot be bound by directionality of the negative charge density.  $\text{F}^-$  is a useful chemical for many industrial applications, and was used in human diet. Nevertheless, recently, it has found to be responsible for several human pathologies and, therefore, it is motivating to find systems for its sensing and separation. Some interesting complexation studies have emphasised the different behaviour of fluoride as a guest due to its small size and basic nature in some organic solvents.

In our laboratory, taking into account the relevance of chemical recognition in several interesting applications and according to our research program on the use of small peptides in supramolecular chemistry, we have studied their hierarchical aggregation to afford low molecular weight gelators (LMWGs), as well as the properties of the resulting organogels.<sup>28-30</sup>

More recently, searching for new anion receptors, we envisaged the synthesis of new neutral  $C_3$ -symmetric tripodal amides based on the NTA core, using alkyl chains or synthetic amino acids as branches. Dr. Sergi Celis, in his PhD thesis,<sup>31</sup> synthesised and studied several tripodal anion receptors (Figure 6). These can be linear and achiral (compounds **17-21**) or cyclic and chiral (compounds **22-24**). The C-terminus carboxylic ester protecting end-groups varied for some derivatives (Me or Bn).

During a part of my Master thesis<sup>32</sup> and in this PhD thesis, the synthesis of receptors **18** and **23** (Figure 6) was carried out in order to try to obtain single crystal of the complexes with different anions suitable for X-Ray diffraction studies. Furthermore, a complete theoretical study of the geometries of some selected complexes and the thermodynamics of the complexation processes of some receptors was carried out to find out differences between receptors and between anions. In addition, theoretical calculations could help us to understand the experimental behaviour of these receptors.

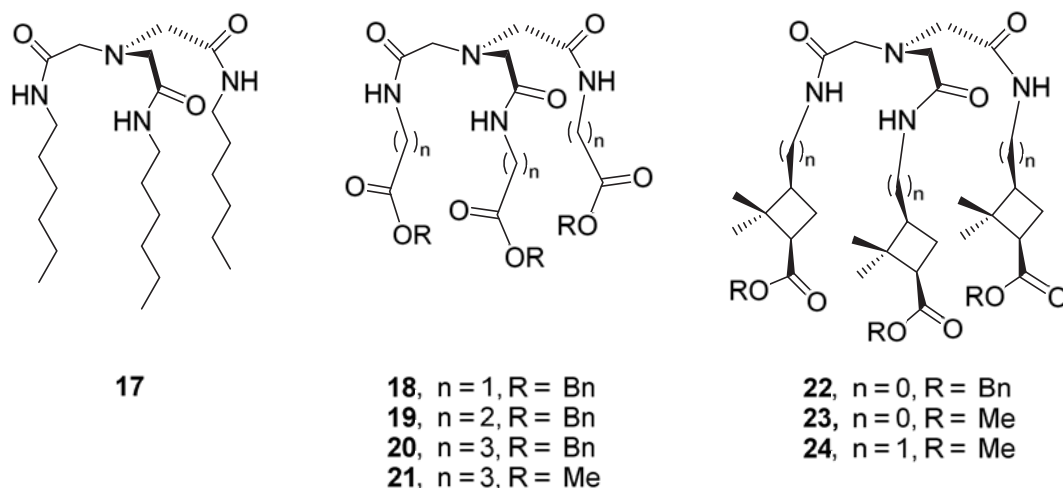


**Figure 6.** Tripodal receptors synthesised and studied by Dr. Sergi Celis.

All studied monovalent anionic guests ( $\text{H}_2\text{PO}_4^-$ ,  $\text{CH}_3\text{COO}^-$ ,  $\text{Cl}^-$  and  $\text{F}^-$ ) were obtained as different salts with tetrabutylammonium ( $\text{TBA}^+$ ) cation, because it cannot interact with the receptor neither by hydrogen bond nor by  $\pi$ - $\pi$  stacking and because  $\text{TBA}^+$  salts are known to be a good source of anions.<sup>33</sup> Furthermore,  $\text{TBA}^+$  is a big cation and it cannot fit the available cavity of a receptor.

The experimental values of the formation Gibbs energy of the complexes in DMSO were obtained graphically. The binding affinities were further assessed by fitting the changes observed by NMR in the resonance of the  $\text{NH}$  proton signals to 1:1 and 1:2 binding stoichiometries using the WinEQNMR2 program<sup>34</sup>. This program fits NMR data to several possible stoichiometries providing statistical data for each case. It allows to determine which complexation event is taking place and the determination of binding parameters through a non-linear fitting. Most of the studied systems show a 1:1 stoichiometry determined with the graphical Job's plot method and/or the WinEQNMR2 program. Nevertheless, in three cases there are some deviations from the rest. For receptor **20** with  $\text{H}_2\text{PO}_4^-$ , the NMR data could not be fitted clearly into a 1:1 or a 1:2 binding model, but the statistical results using WinEQNMR2 program suggested a much better fitting for a 1:1 stoichiometry. For receptors **18** and **23** with  $\text{F}^-$ , the NMR data could not be fitted into any clear stoichiometry, and the data obtained using the statistical method showed that both stoichiometries 1:1 and 1:2 are plausible. In some other supramolecular studies, Job's plot seems not to work properly.<sup>7</sup> Theoretical calculations could help us to understand the geometries and the stoichiometry of the complexes.

Table 1 shows some of the experimental results obtained by Dr. Sergi Celis of the complexation Gibbs energies of the studied processes and the error associated to each value. Firstly, receptor **18** was studied with four anions. Secondly, three receptors (**18**, **19** and **20**) were studied with  $\text{H}_2\text{PO}_4^-$ . Results show that the longer is the chain the lower is the value of  $\Delta G$  in absolute value. Moreover, receptor **23** was studied with  $\text{F}^-$  and  $\text{H}_2\text{PO}_4^-$  and it was found that it is selective to bind  $\text{F}^-$  ( $\Delta\delta$  was 4.16 for  $\text{F}^-$  while it was only 0.03 for  $\text{H}_2\text{PO}_4^-$  during the titration followed by NMR). Finally, the presence of bifluoride anion was found in  $\text{F}^-$  complexes but the mechanism for its formation is not clear.

**Table 1.** Experimental complexation Gibbs energies and binding constants of complexes between different anions and receptors **18**, **19**, **20** and **23**. All the values are shown in kcal mol<sup>-1</sup>.

Receptor	Anion	Graphical method		WinEQNMR2 method	
		log $K_{1:1}$	$\Delta G$ (kcal mol <sup>-1</sup> )	Log $K_{1:1}$	$\Delta G$ (kcal mol <sup>-1</sup> )
<b>18</b>	$\text{H}_2\text{PO}_4^-$	2.80 ± 0.03	-3.66 ± 0.06	3.31 ± 0.02	-4.32 ± 0.05
	$\text{CH}_3\text{CO}_2^-$	2.32 ± 0.02	-3.03 ± 0.05	2.37 ± 0.03	-3.08 ± 0.08
	$\text{Cl}^-$	1.83 ± 0.07	-2.40 ± 0.16	1.65 ± 0.09	-2.15 ± 0.20
	$\text{F}^-$	-- <sup>a</sup>	-- <sup>a</sup>	1.77 ± 0.30 <sup>b</sup>	-2.3 ± 0.4 <sup>b</sup>
<b>19</b>	$\text{H}_2\text{PO}_4^-$	2.02 ± 0.06	-2.60 ± 0.14	2.38 ± 0.03	-3.10 ± 0.07
<b>20</b>	$\text{H}_2\text{PO}_4^-$	-- <sup>a</sup>	-- <sup>a</sup>	2.03 ± 0.22 <sup>c</sup>	-2.64 ± 0.51 <sup>c</sup>
<b>23</b>	$\text{F}^-$	-- <sup>a</sup>	-- <sup>a</sup>	2.94 ± 0.33 <sup>d</sup>	-3.8 ± 0.4 <sup>d</sup>

<sup>a</sup> Isotherm could not be fitted to a 1:1 or 1:2 binding model. <sup>b</sup> Note that a 1:2 stoichiometry could also be plausible (log  $K_1$  = 2.26 ± 0.76; log  $K_2$  = 5.86 ± 0.24;  $\Delta G$  = -7.6 ± 0.3 Kcal/mol) <sup>c</sup> Results fit better to a 1:1 binding model because errors for a 1:2 stoichiometry are too big ((log  $K_1$  = 2.27 ± 1.06; log  $K_2$  = 3.52 ± 3.70;  $\Delta G$  = -4.6 ± 4.8 Kcal/mol) <sup>d</sup> Note that a 1:2 stoichiometry could also be plausible (log  $K_1$  = 3.88 ± 0.36; log  $K_2$  = 8.22 ± 0.18;  $\Delta G$  = -10.7 ± 0.2 Kcal/mol).

## 4.2 Objectives

The main objectives of this part of the thesis are:

- 1) Prediction of the geometries of the complexes formed by receptor **18** with different anions, **19** and **20** with  $\text{H}_2\text{PO}_4^-$  and **23** with  $\text{F}^-$  and with  $\text{H}_2\text{PO}_4^-$ .
- 2) Calculation of the Gibbs energies of the formation of the selected complexes.
- 3) Rationalization of the obtained results with the experimental data, especially with those experimental results which are not clear.
- 4) Synthesis of tripodal anion receptors **18** and **23** and their complexes with  $\text{F}^-$  and  $\text{H}_2\text{PO}_4^-$  in order to obtain single crystals suitable for X-Ray diffraction.

## 4.3 Results and Discussion

The aim of this part of the work is the study of the complexation of some anion receptors. Firstly, we have studied the dissociation processes of the TBA<sup>+</sup> salts (section 4.3.1). Secondly, the affinity of receptor **18**, which is based on  $\alpha$ -glycine, was studied towards four different anions (section 4.3.2). Then, we have studied anion receptors based on  $\beta$ -alanine (**19**) and  $\gamma$ -aminobutyric acid (**20**) and their affinity to act as dihydrogenphosphate receptors (section 4.3.3) In addition, we have studied a receptor derived from (-)-verbenone (**23**) and its affinity to bind selectively fluoride instead of dihydrogenphosphate, and it was compared with receptor **18** (section 4.3.4). Then, the formation of bifluoride was studied (section 4.3.5). Finally, different stoichiometries of complexation of six receptors with H<sub>2</sub>PO<sub>4</sub><sup>-</sup> were studied (section 4.3.6). Additionally, the synthesis of these receptors is described (section 4.3.7).

### 4.3.1 Dissociation of the TBA<sup>+</sup> salts

All the anions were obtained as TBA<sup>+</sup> salts. First of all, it is important to determine if our calculations can predict correctly whether these salts are dissociated or not in the medium where the experiments are carried out.



The four studied anions are dihydrogenphosphate, acetate, chloride and fluoride. All the salts were studied in dimethylsulfoxide (DMSO) solution. Table 2 shows the dissociation energy ( $\Delta E$ ) and the dissociation Gibbs energy ( $\Delta G$ ) of these salts in solution using diffuse function in the optimization step and without them.

**Table 2.** Computed dissociation energies and dissociation Gibbs energies of the TBA<sup>+</sup> salts in DMSO. All the values are in kcal mol<sup>-1</sup>.

X <sup>-</sup>	$\Delta E^a$	$\Delta E'^b$	$\Delta G^a$	$\Delta G'^b$
H <sub>2</sub> PO <sub>4</sub> <sup>-</sup>	7.5	5.5	-2.9	-2.1
CH <sub>3</sub> COO <sup>-</sup>	4.3	3.9	-5.4	-4.8
Cl <sup>-</sup>	0.6	1.4	-2.4	-1.7
F <sup>-</sup>	-6.4	-1.4	-10.5	-4.8

<sup>a</sup> M06-2X / 6-311++G(2df,2pd) // M06-2X / 6-31G(d) level of theory

<sup>b</sup> M06-2X / 6-311++G(2df,2pd) // M06-2X / 6-31+G(d) level of theory

Results show that our calculations predict correctly that all dissociation processes are spontaneous, because dissociation Gibbs energies are negative.

The calculation of the energy of an anion requires the use of diffuse functions in the basis set. In order to determine if diffuse functions are also important in the optimization of the molecular geometries of the TBAX salts, we can compare the values of dissociation energy obtained from geometries optimised without ( $\Delta E$ ) and with ( $\Delta E'$ ) diffuse functions. As it is observed, diffuse functions have the main importance in the optimised geometry of TBAF (5 kcal mol<sup>-1</sup>), while in the other salts their effect is much smaller (0.4-2 kcal mol<sup>-1</sup>). In addition, comparing the results of dissociation Gibbs energy obtained from geometries without ( $\Delta G$ ) and with ( $\Delta G'$ ) diffuse functions, it is observed that diffuse functions only have importance in TBAF calculated geometries. F<sup>-</sup> is the smallest anion (ionic radius = 1.33 Å) and has the same negative charge as the others, so it has the larger value of charge density and diffuse functions play an important role to describe it correctly. According to these results, diffuse functions in the optimization of the molecular geometries will be considered only when F<sup>-</sup> is present.

### 4.3.2 Complexation of the $\alpha$ -glycine-based tripodal receptor **18** with different anions

We have studied the complexation of  $\alpha$ -glycine-based tripodal anion receptor (**18**) with four anions (H<sub>2</sub>PO<sub>4</sub><sup>-</sup>, CH<sub>3</sub>COO<sup>-</sup>, Cl<sup>-</sup> and F<sup>-</sup>).

The structures of the complexes are shown in Figure 7. Complexation energies ( $\Delta E$ ) and Gibbs energies ( $\Delta G$ ) of the complexation of receptor **18** with the four anions and the net charge transfer (Q) from the anion to the receptor are shown in Table 3.

In both **18**-H<sub>2</sub>PO<sub>4</sub><sup>-</sup> and **18**-CH<sub>3</sub>COO<sup>-</sup> complexes, one of the oxygen atoms of H<sub>2</sub>PO<sub>4</sub><sup>-</sup> and CH<sub>3</sub>COO<sup>-</sup> forms hydrogen bonds with the three NH groups of the receptor. The three arms of the receptor involve the anion H<sub>2</sub>PO<sub>4</sub><sup>-</sup> forming a nearly symmetrical internal cavity with a C<sub>3</sub> axis. In the case of CH<sub>3</sub>COO<sup>-</sup>, there is another hydrogen bond formed by one NH and the oxygen of the carbonyl group of the acetate. The three arms of the receptor involve the anion acetate forming an internal cavity similar to the cavity with H<sub>2</sub>PO<sub>4</sub><sup>-</sup>, but quite deformed.

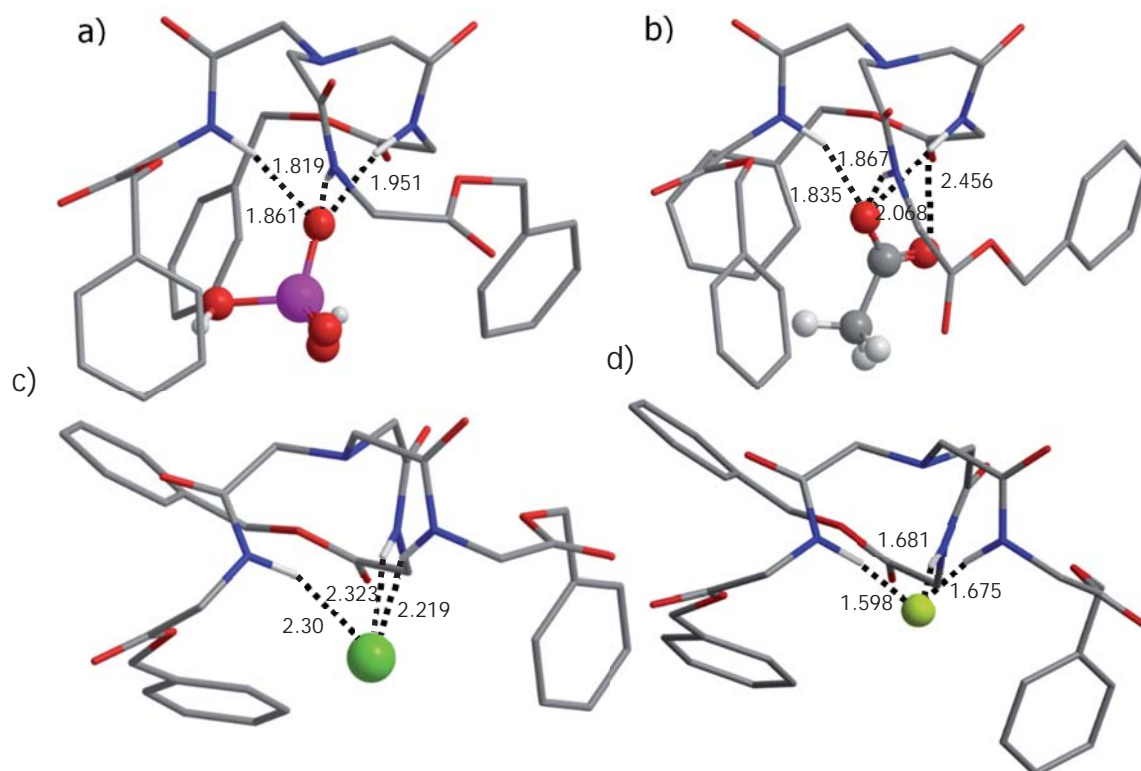


**Figure 7.** Structures of **18** complexed with anions: a)  $\text{H}_2\text{PO}_4^-$ , b)  $\text{CH}_3\text{COO}^-$ , c)  $\text{Cl}^-$  and d)  $\text{F}^-$ . All the distances of the hydrogen bonds are in Å. Non polar hydrogen atoms were omitted for clarity.

Both **18**- $\text{Cl}^-$  and **18**- $\text{F}^-$  complexes have more or less the same structure. The anion is at the same distance from the three NH groups, forming hydrogen bonds. In this case, the cavity differs from the other two previous cases. Here, only two branches of the tripodal anion receptor are involving the anion. One explanation can be that the ions are small and if the three branches were close to each other, there would be more repulsion between them.

Table 3 shows that the affinities of receptor **18** to bind anions in DMSO are sorted as  $\text{H}_2\text{PO}_4^- > \text{CH}_3\text{COO}^- > \text{Cl}^-$  in good qualitative agreement with the experimental results (Table 1). Experimentally, despite it cannot be calculated, receptor **18** has more affinity for  $\text{F}^-$  than for  $\text{Cl}^-$  in DMSO. The discrepancy between theoretical and experimental results for  $\text{F}^-$  was already reported,<sup>35,36</sup> and it was attributed to the difficulty of finding “free”  $\text{F}^-$  ions under common experimental conditions.



**Table 3.** Complexation energies and Gibbs energies corresponding to the formation of **18**-X<sup>-</sup> complexes in DMSO and net charge transfer (Q) from the anion to receptor **18**. All the energies are in kcal mol<sup>-1</sup>.

X <sup>-</sup>	ΔE	ΔG	Q
H <sub>2</sub> PO <sub>4</sub> <sup>-</sup>	-20.8 (-49.7) <sup>a</sup>	-11.3	-0.147
CH <sub>3</sub> COO <sup>-</sup>	-21.5 (-54.0)	-10.8	-0.153
Cl <sup>-</sup>	-13.3 (-50.5)	-10.3	-0.149
F <sup>-</sup>	-17.9 (-76.7)	-8.8	-0.249

<sup>a</sup> Results in parentheses were computed in the gas phase.

Looking at the results of the Cl<sup>-</sup> and F<sup>-</sup> complexes, it is shown that the **18**-Cl<sup>-</sup> complex has a ΔG value larger than **18**-F<sup>-</sup> complex in absolute value, while ΔE for the formation of the former is lower than for the formation of the latter in absolute value. This fact can be explained calculating the increment of entropy (ΔS) of the complexation processes. While for Cl<sup>-</sup>, ΔS = -19.54 cal K<sup>-1</sup> mol<sup>-1</sup>, for F<sup>-</sup> ΔS = -31.87 cal K<sup>-1</sup> mol<sup>-1</sup>. This means that the F<sup>-</sup> complex is more ordered than the Cl<sup>-</sup> one and entropic factors favour the **18**-Cl<sup>-</sup> complex with respect to the **18**-F<sup>-</sup> complex. To compare the geometries of both Cl<sup>-</sup> and F<sup>-</sup> complexes, we must take into account that the sum of the X<sup>-</sup> ionic radius and the van der Waals radius of H are 2.39 Å for F<sup>-</sup> and 2.87 Å for Cl<sup>-</sup>, and that the mean NH-X<sup>-</sup> distance in the complex is 1.65 Å for F<sup>-</sup> and 2.28 Å for Cl<sup>-</sup>. In the F<sup>-</sup> complex, the distance is a 31 % shorter than the sum of radii, while for Cl<sup>-</sup> the reduction is only a 21 %.

The values of the binding energies in gas phase can be compared with other studies with anion receptors,<sup>37</sup> in which they obtain Gibbs energy values of the same order of magnitude and the values with these anions can be compared (-72 kcal mol<sup>-1</sup> for a F<sup>-</sup> complex and -43 for a Cl<sup>-</sup> complex). In addition, NH-X<sup>-</sup> distances can be compared (NH-F<sup>-</sup> ≈ 1.65 Å and NH-Cl<sup>-</sup> ≈ 2.35 Å). Thus, our results are in good agreement with those from other studies.

If we compare **18**-F<sup>-</sup> with **18**-Cl<sup>-</sup> complexes, and **18**-H<sub>2</sub>PO<sub>4</sub><sup>-</sup> with **18**-CH<sub>3</sub>COO<sup>-</sup> complexes, we can observe that there is a correlation between the magnitude of charge

transfer (Q) and the complexation energy. Therefore, it is important to transfer as much charge as possible to the receptor to have a more favourable process.

Computed complexation Gibbs energies are more negative than the experimental ones. While experimental results are in the range between  $-2.4$  and  $-5.3$  kcal mol<sup>-1</sup>, computational results are comprised between  $-8.8$  and  $-11.3$  kcal mol<sup>-1</sup>. There are several possible explanations for this discrepancy.

First, our calculations are based on a static system while complexation is a dynamic process. In addition, other computational approximations and experimental errors can vary the value of the energies. Another approximation is that we are assuming the solvent as a cavity around the host and the guest but we are not considering explicit molecules of solvent, which have a carbonyl group and they could interact with the NH groups of the receptor giving a competitive reaction. The complexation process taking into account an explicit molecule of solvent was studied and results show that the process is not favourable, so no competitive reaction takes place.

Moreover, in our calculations we did not consider the presence of TBA<sup>+</sup> cations in the medium because the dissociation of the salts is very favourable. To reduce this problem, we have also carried out the calculations of the complexes in the presence of the cation.

Assuming that the BSSE is not affected by the presence of the cation, complexation Gibbs energies in DMSO are  $-10.1$  kcal mol<sup>-1</sup> for F<sup>-</sup>,  $-7.6$  kcal mol<sup>-1</sup> for H<sub>2</sub>PO<sub>4</sub><sup>-</sup>,  $-3.9$  kcal mol<sup>-1</sup> for CH<sub>3</sub>COO<sup>-</sup> and  $-3.7$  kcal mol<sup>-1</sup> for Cl<sup>-</sup>. Results show that the order is the same as before (Table 3), but now the values are closer to the experimental results (Table 1) and now receptor **18** has the larger affinity for F<sup>-</sup>. However, these calculations are very time-consuming<sup>†</sup> and so the presence of the cation will not be further considered.

---

<sup>†</sup> For instance, for the smallest system, **18**-F<sup>-</sup>, the optimization of the geometry requires 38 h without TBA<sup>+</sup>, and 10.5 days with TBA<sup>+</sup>. (Parallel calculations with 12 processors)

### 4.3.3 Complexation of the $\beta$ -alanine and $\gamma$ -aminobutyric acid-based tripodal anion receptors **19** and **20**, respectively, with $\text{H}_2\text{PO}_4^-$

In this section, we have studied two more different tripodal anion receptors with a C-NTA core. These receptors are based on  $\beta$ -alanine ( $n=2$ ) (**19**) and  $\gamma$ -aminobutyric acid ( $n=3$ ) (**20**). We have studied the affinity of these compounds to bind  $\text{H}_2\text{PO}_4^-$  in DMSO solution. The structures of the complexes of receptors **19** and **20** with  $\text{H}_2\text{PO}_4^-$  are shown in Figure 8. The computed complexation energies ( $\Delta E$ ), complexation Gibbs energies ( $\Delta G$ ), and the net charge transfer from the anion to the receptor ( $Q$ ) are shown in Table 4. Results for complex **18**- $\text{H}_2\text{PO}_4^-$  were also included for comparison.

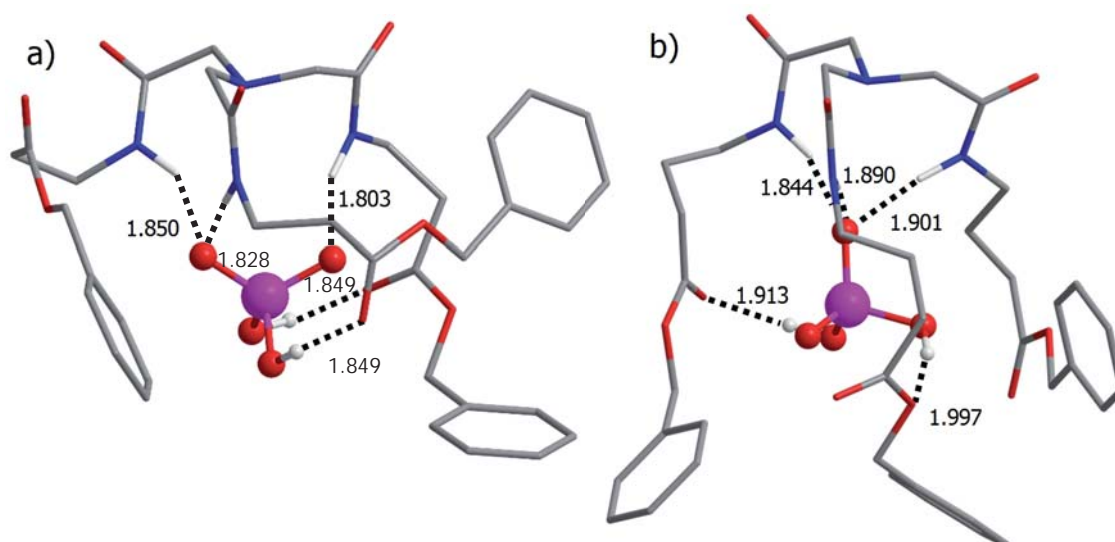


**Figure 8.** Structure of the complexes a) **19**- $\text{H}_2\text{PO}_4^-$  and b) **20**- $\text{H}_2\text{PO}_4^-$ . All the distances of the hydrogen bonds are in Å. Non polar hydrogen atoms were omitted for clarity.

In both complexes **19**- $\text{H}_2\text{PO}_4^-$  (a) and **20**- $\text{H}_2\text{PO}_4^-$  (b), one of the oxygen atoms of  $\text{H}_2\text{PO}_4^-$  forms hydrogen bonds with the NH groups from the receptor forming two and three hydrogen bonds, respectively. In complex **19**- $\text{H}_2\text{PO}_4^-$ , the other oxygen atom forms another hydrogen bond with the remaining NH group. In the two complexes, the two OH groups of  $\text{H}_2\text{PO}_4^-$  form hydrogen bonds with the carbonyl groups of two of the terminal esters of the receptor. The three branches of the receptor involve the anion forming an irregular cavity. In the case of complex **18** there are only three hydrogen bonds because of the length of the branches (Figure 8a).

**Table 4.** Complexation energies, Gibbs energies for the complexes of **18**, **19** and **20** with  $\text{H}_2\text{PO}_4^-$  in DMSO, and net charge transfer (Q) from the anion to the receptor. All the energy results are in  $\text{kcal mol}^{-1}$ .

Receptor	$\Delta G_{\text{exp}}$	$\Delta E$	$\Delta G$	Q
<b>18</b>	-4.3	-20.8 (-49.7) <sup>a</sup>	-11.3	-0.147
<b>19</b>	-3.1	-21.7 (-48.9)	-10.0	-0.100
<b>20</b>	-2.7	-25.6 (-54.8)	-11.8	-0.092

<sup>a</sup> Results in parentheses were computed in gas phase.

As it is observed, **19** has the lowest complexation Gibbs energy in absolute value, followed by **18**, and finally **20**. These three receptors have more or less the same affinity to bind  $\text{H}_2\text{PO}_4^-$ ; all of them are in a range of  $1.8 \text{ kcal mol}^{-1}$ . Experimental results show that the affinity order is **18** ( $-4.32 \pm 0.03$ ) > **19** ( $-3.1 \pm 1.1$ ) > **20** ( $-2.7 \pm 0.3$ ). As it is observed, experimental values of  $\Delta G$  are within a range of  $1.6 \text{ kcal mol}^{-1}$ . In addition, experimental values of  $\Delta G$  of receptor **20** are inside the range of values of  $\Delta G$  of **19**, taking into account the errors. Thus, we are not able to distinguish within them. In this case, the shorter is the chain the larger is the value of net charge transfer, but this result does not correlate with the order of complexation energies.

As in the previous section, the presence of the cation was considered in order to try to minimize the error of the calculations. The complexation Gibbs energy for the receptors is  $-7.6 \text{ kcal mol}^{-1}$  for **18**,  $-4.1 \text{ kcal mol}^{-1}$  for **19** and  $-9.5 \text{ kcal mol}^{-1}$  for **20**.

Experimental errors and experimental conditions can modify the magnitude of the values, and hence, the order of affinity. It is known that measured binding constants for the same system can vary by up to a factor of 10 (a difference in  $\Delta G$  about  $1\text{-}2 \text{ kcal mol}^{-1}$ ), depending on the assay conditions.<sup>38,39</sup> In order to be able to discriminate within receptors, Gibbs energy values should have a difference bigger than  $2\text{-}3 \text{ kcal mol}^{-1}$  (a factor of 100 in the binding constant). In this way, the error due to the experimental factors is reduced. Also, absolute binding free energies can be computed with an accuracy of only about  $2\text{-}3 \text{ kcal mol}^{-1}$ ,<sup>40</sup> which is bigger than  $1.8 \text{ kcal mol}^{-1}$  (range of values of the experimental results). Thus, is not possible to find quantitative differences within them.

However, looking at the predicted structures it is shown that the structures of complexes with **19** and **20** form three hydrogen bonds between the anion and the NH groups of the amides, but also two more hydrogen bonds between the anion and the carbonyl groups of the branches. Due to the length of the branches, only in these two cases these additional hydrogen bonds can be formed. Taking into account that a hydrogen bond promotes a reduction of energy of the final product, these two additional hydrogen bonds will further stabilize the complex. Nevertheless, the experimental Gibbs energies were calculated taking into account the signal of the NH in the  $^1\text{H}$  NMR spectrum and, thus, only the contribution of the three hydrogen bonds with the amides were taken into account. The contribution of the two additional hydrogen bonds cannot be monitored by  $^1\text{H}$  NMR, but even in the case it could be monitored, the contribution of the five hydrogen bonds is not the same and thus, the experimental Gibbs energy cannot be calculated using  $^1\text{H}$ -NMR. This fact explains why theoretical calculations are not in agreement with the experimental values.

Thus, to find out the influence of the chain length in the complexation process, the obtained calculated values in the presence of the cation are the most relevant ones. Therefore, the order of affinity should be **20** > **18** > **19**. Taking this order of affinity and comparing it with the predicted structures of the complexes, we could conclude that **18** can form a symmetrical cavity involving the anion where the chain does not play any role. As the length of the chain increases, it starts to interact with the anion. **19** has a length that leads it to interact with the anion but is not long enough to stabilize the final complex. It would be the transition distance. Finally, **20** has a chain long enough to involve the anion forming five hydrogen bonds between the receptor and the anion, which stabilize the complex.

#### **4.3.4 The tripodal anion receptor derived from (–)-verbenone as a selective fluoride receptor**

We have studied the interaction of the tripodal anion receptor derived from (–)-verbenone (**23**) with  $\text{F}^-$  and  $\text{H}_2\text{PO}_4^-$ . This receptor is an esterified  $\gamma$ -amino acid with a cyclobutane containing the three carbons between the amine group and the carboxylic

group. Experiments have shown that this compound has more affinity to bind  $F^-$  than  $H_2PO_4^-$ .

The values of complexation energy ( $\Delta E$ ) of the receptor with anion, complexation Gibbs energy ( $\Delta G$ ) and the recalculated Gibbs energy ( $\Delta G'$ ) taking into account the complexation energy in solution and also taking into account the cation and the BSSE error, and the net charge transfer ( $Q$ ) from the anion to the receptor are shown in Table 5. The structures of complexes **23**- $H_2PO_4^-$  and **23**- $F^-$  are shown in Figure 9.

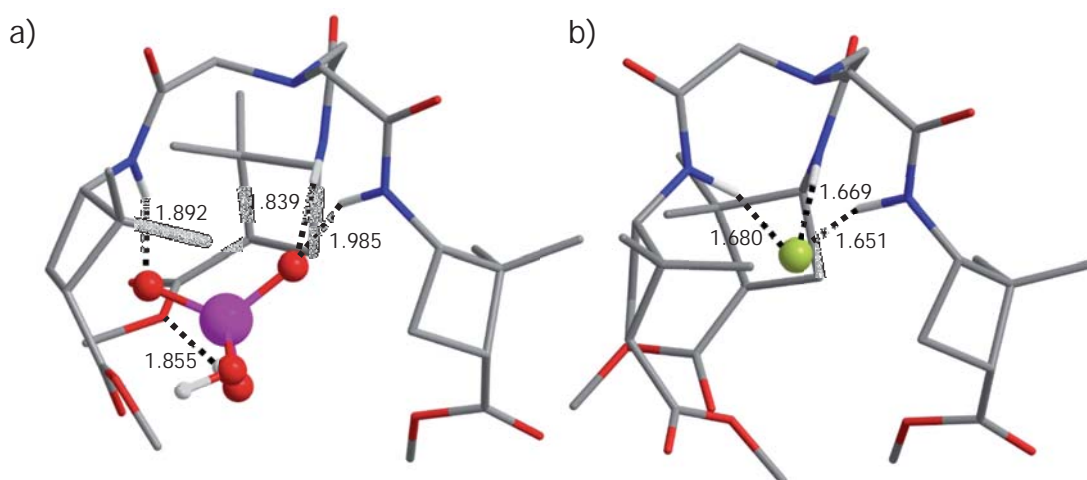


**Figure 9.** Structures of a) **23**- $H_2PO_4^-$  and b) **23**- $F^-$ . All the distances of the hydrogen bonds are in Å. Non polar hydrogen atoms were omitted for clarity.

**Table 5.** Values of the complexation energies ( $\Delta E$ ), Gibbs energies without the cation ( $\Delta G'$ ), with the cation ( $\Delta G$ ) and the net charge transfer ( $Q$ ) of the complexation of **23** and **18** with  $H_2PO_4^-$  and  $F^-$  in DMSO. All energies are in  $\text{kcal mol}^{-1}$ .

Complex	$\Delta E$	$\Delta G$	$\Delta G'$	$Q$
<b>23</b> - $H_2PO_4^-$	-21.7	-9.7	-5.3	-0.092
<b>23</b> - $F^-$	-22.8	-17.3	-17.4	-0.154
<b>18</b> - $H_2PO_4^-$	-20.8	-11.3	-7.6	-0.147
<b>18</b> - $F^-$	-15.5	-8.8	-10.1	-0.249

As it is observed, receptor **23** has more affinity to bind  $F^-$  than  $H_2PO_4^-$  because it has a value of  $\Delta G$  in solution about  $7 \text{ kcal mol}^{-1}$  more negative with  $F^-$  than with  $H_2PO_4^-$ , so it can bind selectively  $F^-$  instead of  $H_2PO_4^-$ . Looking at complexation energy values ( $\Delta E$ ), it is observed that there is no difference between ions. Calculating the  $\Delta S$  of complexes of **23**, it is shown that for **23**- $H_2PO_4^-$   $\Delta S$  is  $-42.0 \text{ cal K}^{-1} \text{ mol}^{-1}$  and for **23**- $F^-$   $\Delta S$  is  $-25.3 \text{ cal K}^{-1} \text{ mol}^{-1}$ .

Regarding the geometries, in **2**- $H_2PO_4^-$ , there are four hydrogen bonds:

- two of them between an oxygen from the anion with two of the three NH groups from the receptor,
- another one between the other oxygen of  $H_2PO_4^-$  with the other NH group of the receptor, and
- the last one between an OH group from the anion and an oxygen from a terminal ester.

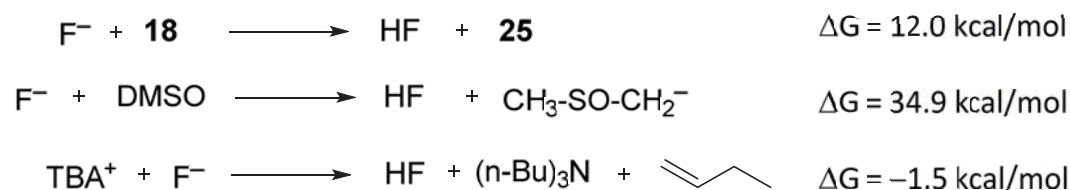
The three branches of the receptor involve the ion but form an irregular cavity. On the other hand, in complex **23**- $F^-$ , the three branches of the receptor involve the anion forming a  $C_3$  symmetrical cavity and forming three hydrogen bonds with the three NH groups from the receptor.

Within receptors **18** and **23**, there are no quantitative differences to bind  $H_2PO_4^-$ , but looking at the values of complexation energies, it is shown that there is a difference between complexes **23**- $F^-$  and **18**- $F^-$  (Table 5). This difference can be explained calculating the energy of deformation of the structure of the receptor. The energy necessary to distort receptor **23** from its isolated geometry until the final geometry in the complex is  $14.9 \text{ kcal mol}^{-1}$  in the case of  $F^-$  and  $22.6 \text{ kcal mol}^{-1}$  in the case of  $H_2PO_4^-$ , while for receptor **18** the distortion energies are around  $20\text{-}22 \text{ kcal mol}^{-1}$  for the four studied anions in section 4.3.2. These values show that receptor **23** is more preorganised than receptor **18** to bind  $F^-$  than to bind  $H_2PO_4^-$ .

### 4.3.5 Study of the formation of bifluoride in F<sup>-</sup> complexes

Experimentally, it was found a triplet at 16-17 ppm in the <sup>1</sup>H NMR spectra of fluoride complexes due to the presence of a coordinated bifluoride anion (FHF<sup>-</sup>).<sup>41</sup> Thus, fluoride is able to act as a base<sup>41,42</sup> removing a proton and forming a new anion. Bifluoride anion can be understood as a fluoride solvated by hydrogen fluoride by an extremely strong hydrogen bond,<sup>43</sup> which is the strongest hydrogen bond ever found (39 kcal mol<sup>-1</sup>).<sup>44</sup> Its crystalline structure in a complex was already determined.<sup>41</sup>

In order to study the basicity of the fluoride ion and to determine which proton is removed, we have carried out some calculations. Taking into account the species that are in the solution, the proton can come from three different sources: receptor **18** forming the deprotonated receptor (**25**), the solvent or TBA<sup>+</sup>. First of all, we have studied some possible acid-base reactions in order to determine which proton can be abstracted by the fluoride anion (Scheme 1).

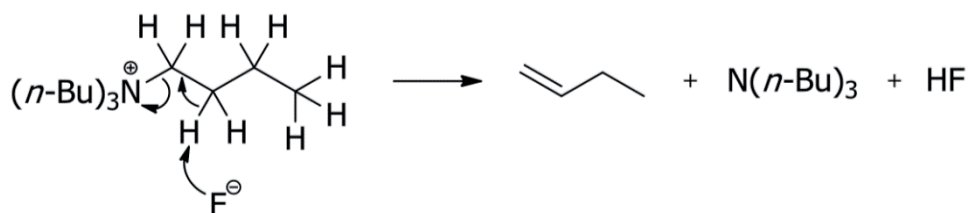


**Scheme 1.** Acid-base reactions of the possible formation of HF.

As it can be observed, the only favourable process that could explain the formation of HF from the interaction between TBAF and receptor **18** in DMSO solution corresponds to the proton abstraction from TBA<sup>+</sup>. The increase of the number of molecules involves an entropic contribution that favours the process. Decomposition of TBAF is a well-known procedure that undergoes via an E2 elimination (Scheme 2).<sup>33</sup> This process is favoured in hydrated DMSO solutions, despite being a slow process. TBAF is very hygroscopic and thus, it provides the necessary amount of water to overcome the kinetic barriers of the reaction. Our TBAF not only has traces of water, but also the salt is hydrated because of the difficulty of working with anhydrous TBAF. TBAF is very sensitive to hydroxylic impurities in polar aprotic solvents and thus bifluoride can be formed by abstracting a proton from water



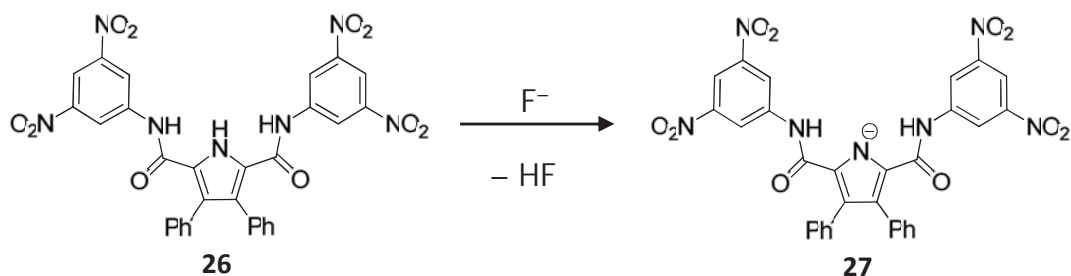
instead of undergoing via E2 elimination.<sup>45,46</sup> The concentration of bifluoride is usually less than 2 % of the concentration of TBAF.<sup>47</sup>



**Scheme 2.** Mechanism of the acid-base reaction between TBA and  $F^-$ .

However, experimentally, neither the formation a gas nor tributylamine were observed. Thus, other options have to be taken into account.

In addition, we have calculated the deprotonation by  $F^-$  of a previously described receptor **26** (Scheme 3),<sup>48</sup> in order to determine if our calculations predict correctly this process.



**Scheme 3.** Example of the deprotonation of a receptor by a  $F^-$ .

The calculated value of the  $\Delta G$  of this process is  $-4.3 \text{ kcal mol}^{-1}$ . Thus, this result shows that our calculations predict satisfactorily the deprotonation process and  $F^-$  can remove the proton of this pyrrole but cannot remove an NH proton of receptor **18**.

The formation of bifluoride from HF and  $F^-$  is thermodynamically very favourable ( $\Delta G = -17.2 \text{ kcal/mol}$ ). Therefore, the formation of bifluoride from the deprotonation of **18**, could also be possible if the two steps process were considered ( $\Delta G = -5.2 \text{ kcal/mol}$ ). We have carried out conformational searches of the deprotonated receptor **25** complexed with  $F^-$ , HF and  $FHF^-$ , but none of them led to any stable conformation.

TBAF salt was analysed in DMSO- $d_6$ . In the  $^1\text{H}$  NMR, any signal of bifluoride is not observed, but in the  $^{19}\text{F}$ , the signal corresponding to  $\text{FHF}^-$  is clear (Figure 10). As said before, only the 2 % of the TBAF is in  $\text{FHF}^-$  form, which is able to exchange the proton with a deuterium. Furthermore, other authors have demonstrate that the concentration of the  $\text{FHF}^-$  ion is inversely proportional to the concentration of TBAF. Experimentally, the signal of the  $\text{FHF}^-$  in the  $^1\text{H}$  spectrum appeared when the concentration of the receptor increased. This can be explained because when the concentration of the receptor is increased,  $\text{F}^-$  is complexed, and then, the concentration of  $\text{FHF}^-$  increased. According to these results, the interaction of  $\text{F}^-$  with the tripodal receptors is more complex than the interaction with other anions and there are side reactions to be taken into account.

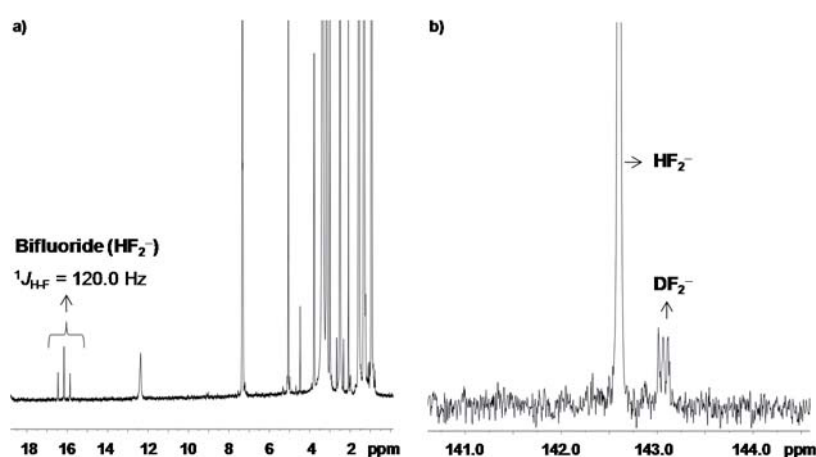


**Figure 10.** a)  $^1\text{H}$  NMR and b)  $^{19}\text{F}$  NMR  $^1\text{H}$ -decoupled spectrum of **18** titration (2.0 mM) with TBAF (12 mM) (DMSO- $d_6$ , 400 MHz, 25 °C).

We have calculated the formation of complexes of receptors **18** and **23** with  $\text{FHF}^-$ . The resulting structures are shown in Figure 11 and the values of complexation Gibbs energies are shown in Table 6.

**Table 6.** Values of the complexation energies ( $\Delta E$ ) and the calculated Gibbs energies ( $\Delta G$ ) of the complexation of **23** and **18** with  $\text{FHF}^-$  in DMSO. All the results are in kcal mol $^{-1}$ .

Receptor	$\Delta E$	$\Delta G$
<b>18</b>	-10.3	-6.3
<b>23</b>	-14.3	-5.9

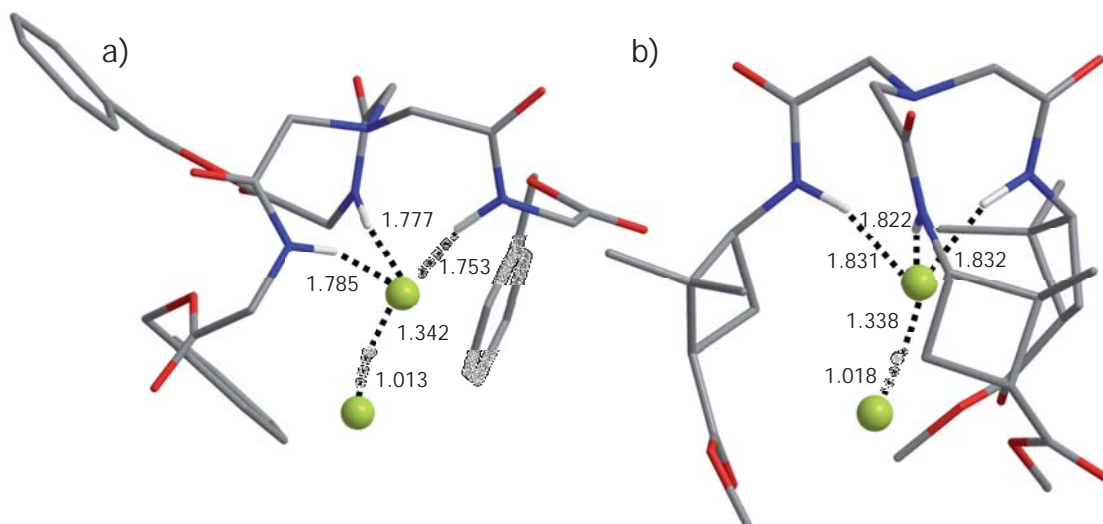


**Figure 11.** Structures of complexes a) **18**-(FHF<sup>-</sup>) and b) **23**-(FHF<sup>-</sup>). All the distances are in Å. Non polar hydrogens were omitted for clarity.

The structure of these complexes show that the coordination is similar to the coordination of the F<sup>-</sup>. Results show that receptors **18** and **23** can coordinate bifluoride forming new complexes that were not taken into account. This fact would explain the different behaviour of F<sup>-</sup> complexes.

#### 4.3.6 Possibility that tripodal receptors form complexes of other stoichiometries with H<sub>2</sub>PO<sub>4</sub><sup>-</sup>

Complexes of **18**, **19** and **20** with H<sub>2</sub>PO<sub>4</sub><sup>-</sup> have a structure in which two OH groups and one of the oxygen atoms of H<sub>2</sub>PO<sub>4</sub><sup>-</sup> point away from the receptor cavity, so that they could interact with another H<sub>2</sub>PO<sub>4</sub><sup>-</sup> anion as schematically shown in Figure 12. We have thought about the possibility that some receptors are able to form complexes with stoichiometries different from 1:1. In particular, these receptors could form complexes with 1:2 and 2:2 stoichiometries.

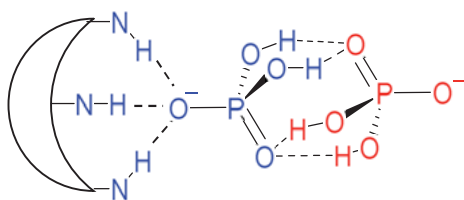


**Figure 12.** Proposed structure for the H<sub>2</sub>PO<sub>4</sub><sup>-</sup> dimer.

Thus, we have studied the formation of such complexes for receptors **18**, **19** and **20**. Figure 13 shows the resulting structures of the complexes with 1:2 and 2:2 stoichiometries for receptor **18**. Structures of complexes with the other receptors are not shown because they are similar to the structures shown in Figure 13.

The values of complexation Gibbs energies for the formation of the complexes with 1:1, 1:2 and 2:2 stoichiometries are presented in Table 7.

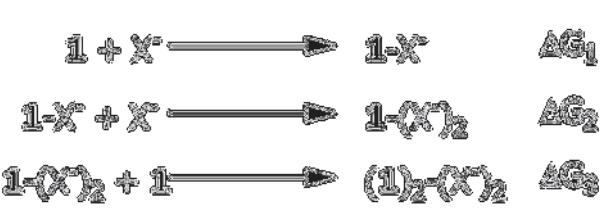
**Table 7.** Complexation Gibbs energies for the complexation of different tripodal anion receptors with  $\text{H}_2\text{PO}_4^-$ , with a 1:1, 1:2 and 2:2 stoichiometries. All the results are in  $\text{kcal mol}^{-1}$ .

Receptor	$\Delta G_1$	$\Delta G_2$	$\Delta G_3$
<b>18</b>	-11.3	-7.5	0.9
<b>19</b>	-10.0	-4.5	6.0
<b>20</b>	-11.8	-6.4	-0.9

$$\mathbf{1} + \text{X}^- \longrightarrow \mathbf{1-X}^- \quad \Delta G_1$$

$$\mathbf{1-X}^- + \text{X}^- \longrightarrow \mathbf{1-(X^-)}_2 \quad \Delta G_2$$

$$\mathbf{1-(X^-)}_2 + \mathbf{1} \longrightarrow (\mathbf{1})_2\text{(X}^-\text{)}_2 \quad \Delta G_3$$



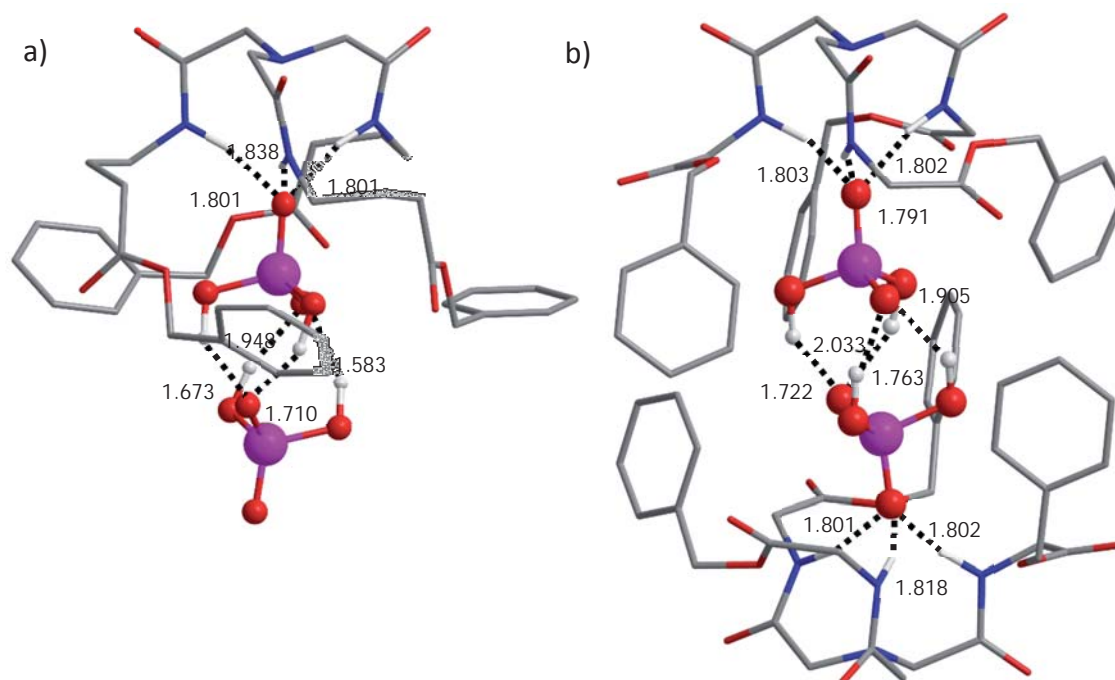
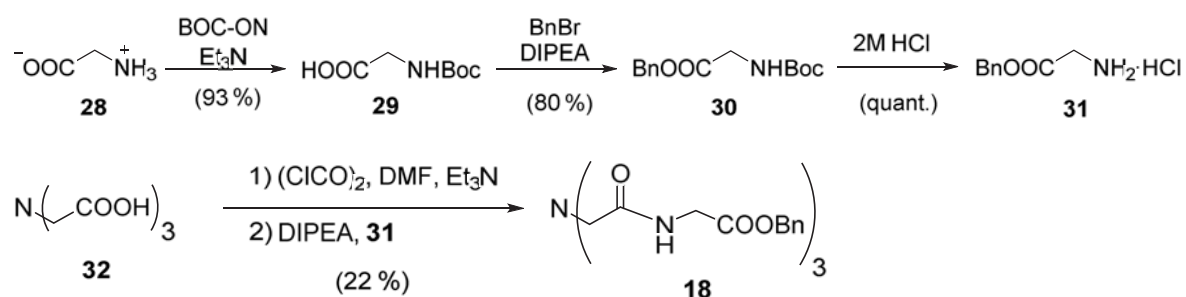


**Figure 13.** Structures of the complexes of receptor **18** with  $\text{H}_2\text{PO}_4^-$ . a) 1:2 stoichiometry and b) 2:2 stoichiometry. All the distances of the hydrogen bonds are represented in Å. Non polar hydrogens were omitted for clarity.

As it observed, all studied receptors can form complexes with 1:1 and 1:2 stoichiometries, while some of these can form also 2:2 complexes. **18** and **19** receptors can form up to 1:2 complexes, while **20** can form up to 2:2 complexes. However, and as we have discussed in section 4.3.2, the calculated complexation Gibbs energies are undervalued, so that, the results corresponding to the formation of 1:2 complexes and, specially, 2:2 complexes should be treated with caution. Results show that different complexes of receptors **18**, **19** and **20** with  $\text{H}_2\text{PO}_4^-$  could be obtained. Despite Job's plot shows that the stoichiometry of the complex is 1:1, the same results would fit a 2:2 complex. In order to verify the structure of all complexes, single crystal X-Ray diffraction should be carried out. Therefore, the synthesis of receptors **18** and **23** was carried out and their complexation with  $\text{F}^-$  and  $\text{H}_2\text{PO}_4^-$  was performed.

#### 4.3.7 Preparation of single crystals of the studied complexes

Receptors **18** and **23** were synthesised following the synthetic route shown in Scheme 4 and Scheme 5, respectively.

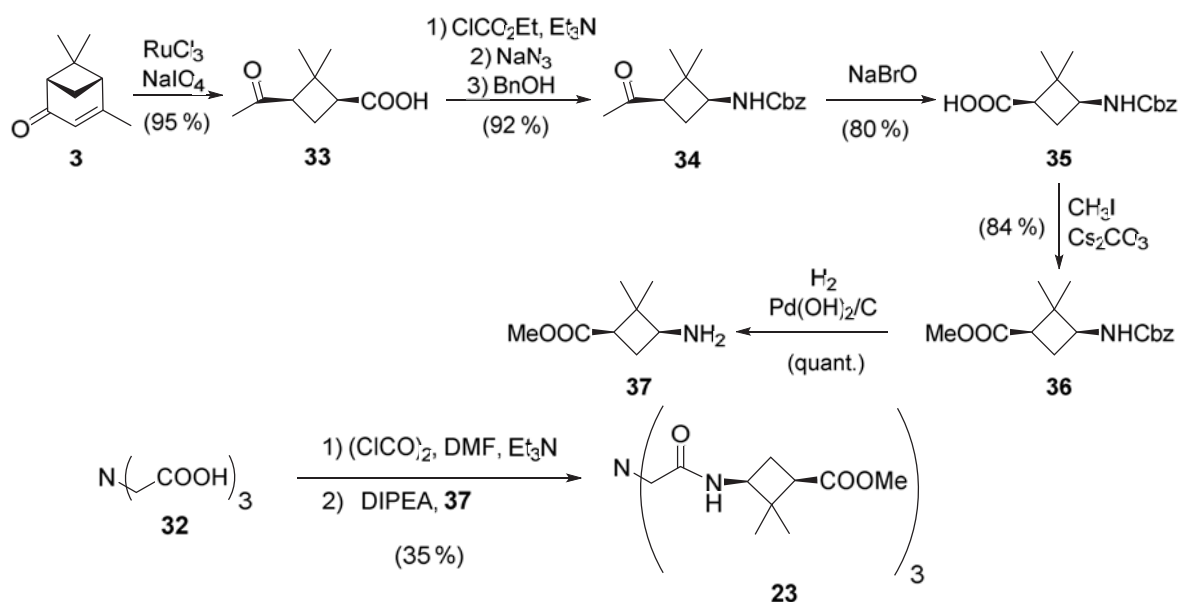


**Scheme 4.** Synthetic pathway of receptor **18**.

Once the products were obtained, some complexes were prepared and different techniques and solvents were used to obtain a crystal of a complex. In spite of the large number of attempts, solvents and conditions, none of them precipitates in form of a single crystal. The obtained precipitates were observed using an optical microscope with a camera attached. The pictures of the obtained solids are shown in Figure 14.

These images show that these complexes tend to form gummy solids and to obtain a single crystal turned to be a tough task. Some of the samples was lead trying to crystallise

for more than one year. Any crystal was not obtained and thus, the X-Ray diffraction analysis could not be carried out, which would lead us to compare the crystal structure with the predicted one.



**Scheme 5.** Synthetic pathway of receptor **23**.



**Figure 14.** Images from the obtained precipitates of different complexes of **18** and **23** with  $\text{H}_2\text{PO}_4^-$  and  $\text{F}^-$ . These images were taken using an 8 Megapixel cam incorporated in an optical microscope.

## 4.4 Summary and Conclusions

The structures of complexes between four tripodal receptors and several anions were determined through theoretical calculations.

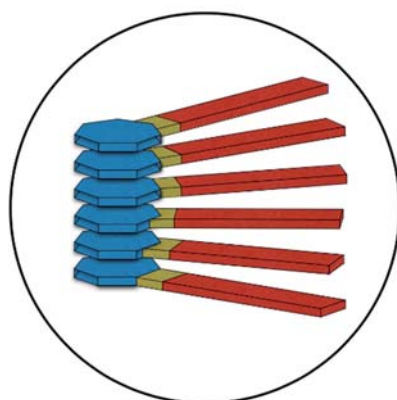
First of all, receptor **18** was studied with four anions and results show that the order of affinity is  $\text{H}_2\text{PO}_4^- > \text{CH}_3\text{COO}^- > \text{Cl}^-$ , which is in good qualitative agreement with the experimental results.  $\text{F}^-$  is a special case because of its nature and its side reactions. Calculated values of  $\Delta G$  are underestimated in relationship to the experimental values because of computational approximations and experimental conditions. We could say that we have a systematic error of around 7-8 kcal mol<sup>-1</sup>. The error decreases to 1-4 kcal mol<sup>-1</sup> when the calculations are done in the presence of  $\text{TBA}^+$ .

Complexes with  $\text{H}_2\text{PO}_4^-$  with different receptors lead to similar  $\Delta G$  values, but the chain length has an influence on the additional hydrogen bonds formed between the receptor and the anion, which can modify the affinity. Due to these additional hydrogen bonds, experimental Gibbs energies cannot be calculated with precision. Thus, each receptor needs to be studied separately.

Computational studies confirm that receptor **23** has more affinity to bind selectively  $\text{F}^-$  instead of  $\text{H}_2\text{PO}_4^-$  because of its preorganization. Thus, these results fit well with the experimental data. Moreover, we have found that  $\text{F}^-$  is able to abstract a proton from  $\text{TBA}^+$  forming  $\text{FHF}^-$ , which can bind receptors **18** and **23**, doing the system more complex.

Finally, the possibility that some receptors can form complexes having 1:2 or 2:2 stoichiometry with  $\text{H}_2\text{PO}_4^-$  was confirmed.

Receptors **18** and **23** were synthesised but, unfortunately, any crystal was not obtained and so, X-Ray diffraction could not be carried out.



**5. Cycloalkane diamide-based low molecular weight organogelators: influence of ring size, substitution and stereochemistry**

---





## 5. Cycloalkane diamide-based low molecular weight organogelators: influence of ring size, substitution and stereochemistry

### 5.1 Introduction

Gel state has been recognised for over 155 years when in 1861 Thomas Graham gave the following description: *“while the rigidity of the crystalline structure shuts out external expressions, the softness of the gelatinous colloid partakes of fluidity and enables the colloid to become a medium for liquid diffusion, like water itself”*.<sup>49</sup> During the following years and until today, scientists attempted to define the “gel” state in a more explicit manner. In 1926, Jordon Lloyd said that “if it looks like a gel it must be a gel” and that a gel is easier to identify than to define.<sup>50</sup> In 1997, Klaas te Nijenhuis said that “a gel is a gel, as long as one cannot prove that it is not a gel”.<sup>51</sup> Figure 15 shows a vial turned upside down to check if a gel is formed. The formed material remains on the bottom of the vial and it does not fall down, meaning that a gel is formed.



**Figure 15.** Picture of a vial turned upside down to check if a gel is formed.

Gels have been and are compounds that we use in our daily lives and in some cases without realising it. They can be found in shampoos, toothpastes, jellies, lubricants, food or in technology. Most of them can be classified as hydrogels because they are formed by polymeric compounds in aqueous solutions. Gels formed in organic solvents are known as organogels and they can be used for example as sensors,<sup>52</sup> catalysts,<sup>53,54</sup> liquid crystals<sup>55</sup> or electrophoretic and electrically conductive matrices,<sup>56</sup> for example. More recent biological applications have been found such as drug delivery, in vaccines, microbiological media, bioadhesives, suppositories and gelatin gels.<sup>57</sup>

Gels can be classified in two main categories: chemical gels, formed by covalent bonds; and physical gels, formed by intermolecular non-covalent interactions. Two different types of physical gels can be identified: those in which the gelator is an inorganic compound or those in which the gelator is a small organic molecule, also called as low molecular weight gelator (LMWG). Physical gels present reversibility, which means that the liquid phase can be recovered by applying a stimulus to the sample.

LMWGs are especially interesting because they consist of small molecules that can self-assemble due to the presence of different non-covalent interactions, such as van der Waals,  $\pi$ - $\pi$ , dipolar and Coulomb interactions and hydrogen bonding, forming fibrous nanostructures, which can further associate into higher hierarchically ordered architectures. Apart from those interactions, solvophobic effects play an important role. These solvophobic effects originate from moieties or functional groups in the gelator molecule that are poorly soluble in the solvent to be gelled. These contribute to the gelling ability by reducing the overall solubility of the gelator in that solvent. LMWG become even more interesting when chirality is introduced in the organogelator, because the soft material that is formed can present supramolecular chirality features and thus, “smart” chiral materials such as chiroptical devices, catalysts and chiral sensors can be developed.<sup>54,58–60</sup> Moreover, even achiral molecules could self-assemble forming chiral aggregates.<sup>61</sup> Nowadays, it is generally accepted that an organogel must consist of a low concentration (usually less than 2 wt. %) of a LMWG with a molecular mass lower than 3000 Da.<sup>62</sup>

Gelation process of LMWGs is considered to be a hierarchical assembly process including the following steps:<sup>63,64</sup>

1. Dimerization of two individual molecules.
2. Oligomer formation by interaction of dimers with further molecules, normally in only one dimension.
3. Formation of polymer fibrils of approximately the same width as the molecular building blocks by extension of the oligomers.
4. Fiber formation by bundling of fibrils.
5. Interactions of fibers to give an effectively infinite, interconnected network spanning the entire sample (the least well-understood aspect of the gelation process).

6. Immobilization of the solvent by the fiber network, generally by surface tension effects.

Rational design of small molecular gelators with specific and desired gelation properties has remained elusive, despite the rapid growing of the field based on the number of publications (more than 12000 articles during 2014).<sup>65</sup> Determining gelation of small molecules is still an empirical science, and the vast majority of new gelators are discovered serendipitously. Without exception, every study has shown only selected solvents are capable of being gelled by a given gelator. Therefore, the “Holy Grail” of this field of science may not be to develop a universal gelator but to create reliable *a priori* methodologies to understand why molecular gels form in specific solvents and not in others in order to be able someday to design a gelator with specific abilities. Therefore, the aim of this chapter is to provide information to the field in order to help in the research of the “Holy Grail”.

There are many different families of LMWGs depending on their structure, as shown in Figure 16, such as hydrocarbons (**38**),<sup>66,67</sup> fatty acids (**39**),<sup>68,69</sup> esters (**40**),<sup>70</sup> saccharides (**41**),<sup>71</sup> amides (**42**),<sup>72</sup> ureas,<sup>73</sup> amino acids (**43** and **44**),<sup>54,74</sup> steroids (**45**)<sup>75</sup> or combining different moieties with other functionalities (**46**).<sup>76</sup>

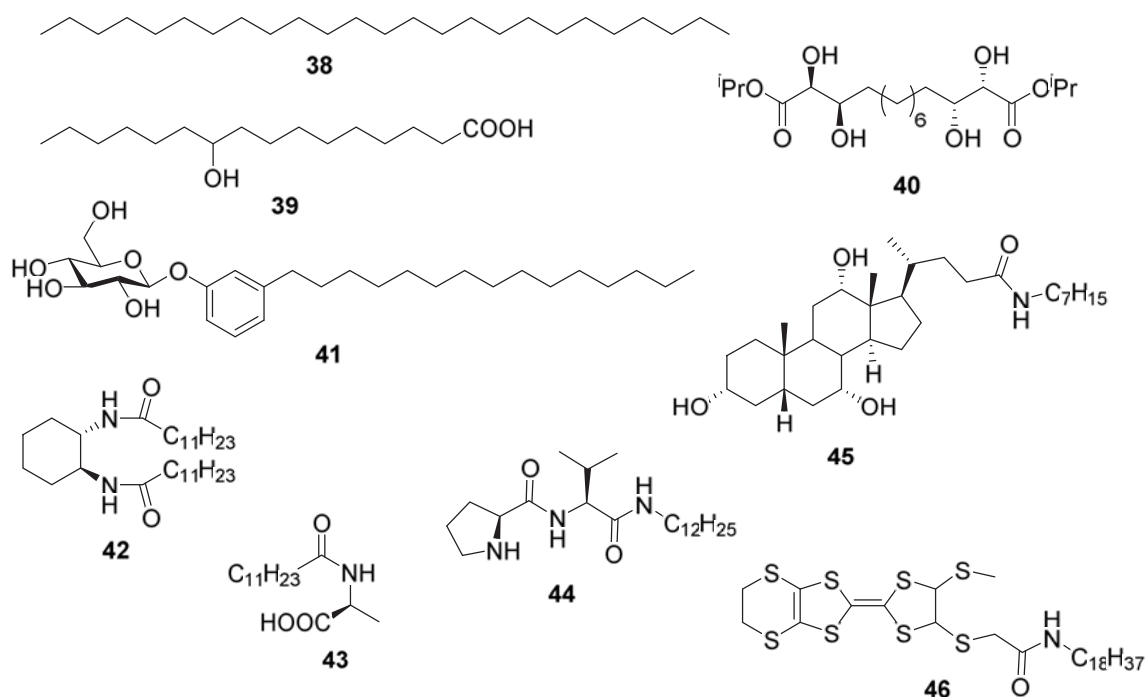


**Figure 16.** Examples of LMWGs.



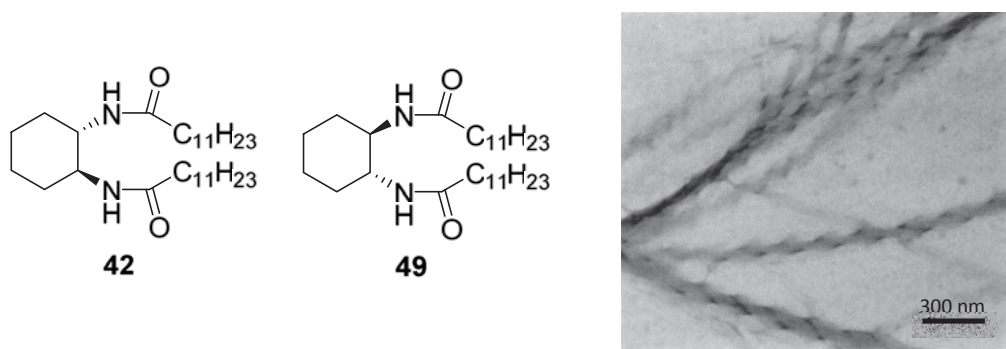


**Figure 18.** Cyclohexane diamide-based gelators studied by Hanabusa *et al.* and SEM image of **49** in acetonitrile (1 mM).<sup>72</sup>

To follow the procedures in this thesis it is important to distinguish within the terms organogel and xerogel. While an organogel is a gel made of a LMWG and any kind of organic solvent, a xerogel is a solid formed after evaporation of the solvent in a hydrogel or by drying an organogel. Xerogels usually retain high porosity (15–50%) and enormous surface area (150–900 m<sup>2</sup> g<sup>-1</sup>), along with very small pore size (1–10 nm).

Taking into account previous works, in this chapter, three different families of carbocyclic diamide-based LMWGs were studied using different techniques in order to try to find a relationship between the structure of a single molecule and the gelation properties. Techniques such as tube inversion test,<sup>79</sup> High Resolution NMR (HR-NMR), Circular Dichroism (CD), Scanning Electron Microscopy (SEM) and theoretical calculations gave us information about the supramolecular system.

Using HR-NMR, the gelation process can be monitored by cooling down the system stepwise. CD is a useful technique to analyse chiral gelators by studying a solution of the gelator and the xerogel of chiral aggregates. In this way, information about self-assembly could be obtained by looking at the chirality of the molecule through the “eyes” of the chromophore group.<sup>80</sup> Theoretical calculations is a useful technique to predict the structure of the aggregate from the molecular point of view while SEM gives information about the morphology of the aggregates.

Figure 19 shows an example of the analysis of the supramolecular structure using circular dichroism of xerogels of compounds **47** (Figure 19a), the gelation study using HR-NMR of compound **48** in toluene (Figure 19b) and the predicted structure of the

aggregation of compound **45** using theoretical calculations (Figure 19c). All of them were done in our research group.<sup>30,77</sup>

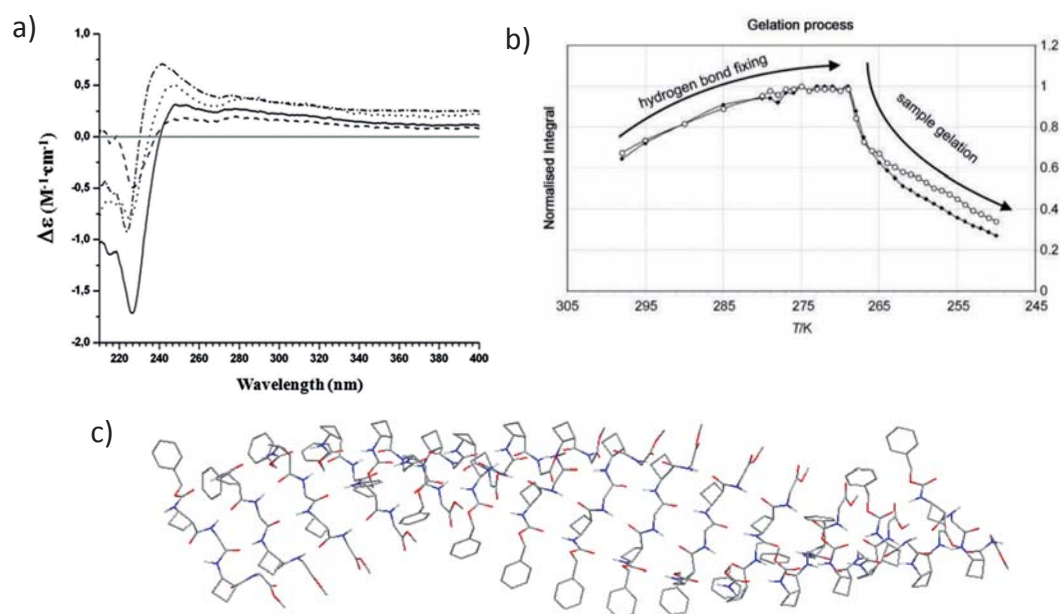


**Figure 19.** a) Circular Dichroism spectra of xerogels from toluene in KBr at 0.03 mmol/g of compounds **47**. b) Stepwise gelation study using HR-NMR of compound **48** at 15 mM in toluene. c) Predicted structure of self-assembled compound **47** using theoretical calculations.

Self-assembly of carbocyclic diamide-based gelators is through hydrogen bond formation, which are directional forces responsible to the morphology of the aggregates, and through van der Waals interactions, which will contribute to the stabilization of the aggregate, as shown in Figure 20.

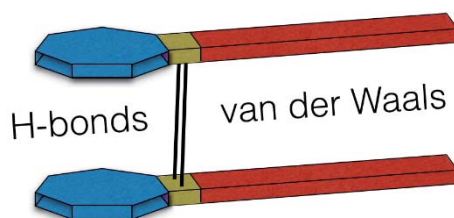


**Figure 20.** Schematic representation of the main forces involved in the self-assembly of carbocyclic diamide-based gelators.





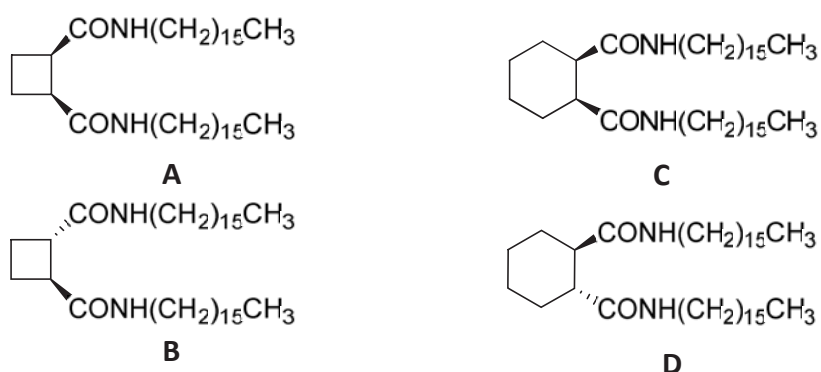
### 5.3 Results and Discussion

In this chapter of the thesis, the study of the properties of different families of carbocyclic diamide-based low molecular weight gelators is described. As said above, these kind of studies give basic information that can be used in the future to design new LMWGs with certain specific properties. The influence of the ring size, the stereochemistry and the substitutions of the ring in diamide-based gelators will be discussed.

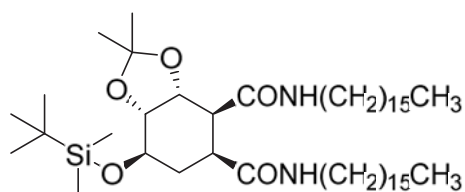
The syntheses of all these LMWGs were carried out for the first time by Dr. Marta Sans (cyclobutane-based **A** and **B**) from our research group and by María Campos (compounds from **C** to **L**) from *Centro de Investigaciones Químicas (CIQUS)* in Santiago de Compostela (Galiza). Moreover, Dr. Marta Sans carried out some preliminar gelation studies of compounds **A-D** with some solvents and also HR-NMR and SEM studies, which are included in this chapter in order to obtain a complete view of all the results and to better discuss them.

Three different families of LMWGs were studied and compared in order to find out differences and to be able to better understand the gelation abilities of these kinds of molecules. Results of this chapter will be presented as three separated studies. The studied families are presented below:

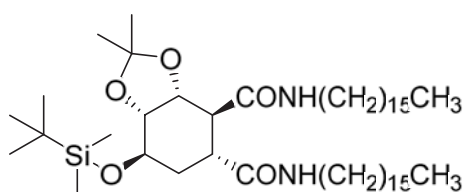
#### Family 1: non-substituted diamide-based carbocycles



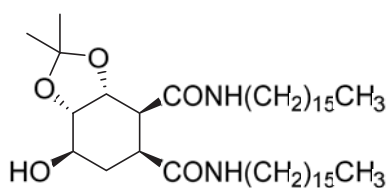
Studying these four molecules, we could determine the influence of the **stereochemistry**, and the **ring size** on the aggregation and on the gelation properties.

Family 2: substituted diamide-based carbocycles

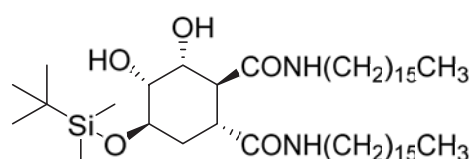
E



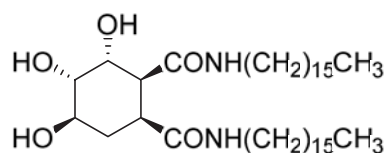
F



G

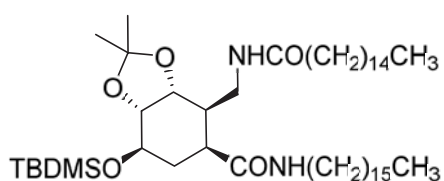


H

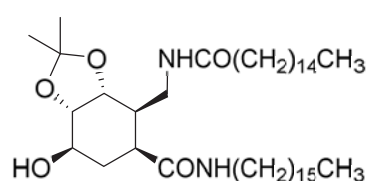


I

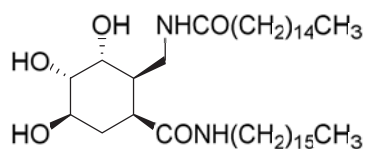
In this case, we have studied the influence of the **stereochemistry** and the different **substitution of the ring** as well as comparing them with the non-substituted ones.

Family 3: substituted diamide-based carbocycles with a spacer

J



K



L

Finally, with this family we have studied the influence of the different **substitutions of the ring** and the influence of the **CH<sub>2</sub> spacer**, which afford a change in the regiochemistry of the amide.

### 5.3.1 Gelation study of Family 1

The gelation ability was studied in 14 common solvents following a well-known procedure described in section 10.8. To determine the presence of a gel, the tube inversion test was used.

Table 8 summarizes the study showing the behaviour of each LMWG in each solvent. The aspect of the gel was classified as clear, translucent or opac. As example, three images of different gels are shown in Figure 22.



**Figure 22.** Examples of clear (left), translucent (middle) and opac (right) gels.

**Table 8.** Gelation behaviour of compounds **A**, **B**, **C** and **D** in common solvents.

Compound	Pentane	1,4-dioxane	Toluene	Et <sub>2</sub> O	CHCl <sub>3</sub>	AcOEt	THF	CH <sub>2</sub> Cl <sub>2</sub>	i-PrOH	Acetone	EtOH	MeOH	CH <sub>3</sub> CN	H <sub>2</sub> O
<b>A</b>	I	I	53 T	I	S	I	I	I	I	I	I	I	I	I
<b>B</b>	I	I	46 T	I	S	I	I	I	I	I	I	I	I	I
<b>C</b>	30 O	51 O	100 O	I	S	I	I	I	I	I	I	I	I	I
<b>D</b>	I	3 T	7 T	I	18 T	I	I	I	I	I	I	I	I	I

Dielectric constant increases from left to right.

C: Clear T: Translucid O: Opac

Minimum gelation concentration in mg/mL.

I: Insoluble, S: Soluble.

These compounds are insoluble in most of these solvents between the ranges of concentration of this study. Compounds **A** and **B** can only gelate toluene with an *mgc* value around 50 mg/mL. We could say that they are bad organogelators because they only can form a gel with toluene, but we could also say that they are toluene-selective organogelators. Both are soluble in chloroform and insoluble in all the other solvents. Thus, there are no significant differences between them and so we could say that between these two compounds stereochemistry has no a significant influence on the behaviour as gelators.

Compounds **C** and **D** are different between them because they can gelate different solvents and with different *mgc* values. Therefore, there is an effect of the stereochemistry on their ability to gelate solvents. Compound **C** can gelate pentane and 1,4-dioxane at 30 and 51 mg/mL respectively. It can gelate toluene but in a high concentration. Finally, compound **D** can gelate 1,4-dioxane, toluene and chloroform at very low concentrations. A good LMWG can gelate a solvent with an *mgc* value lower than 20 mg/mL. Therefore, in this case, we could conclude that compound **D** is a very good organogelator in these three solvents. In this case stereochemistry plays a very important role.

Comparing the ring size, it is shown that cyclobutane-based compounds can only gelate toluene while the cyclohexane-based ones can gelate other solvents. It is clear that there is an interaction between ring size factor and stereochemistry factor, as it is represented in Figure 23.

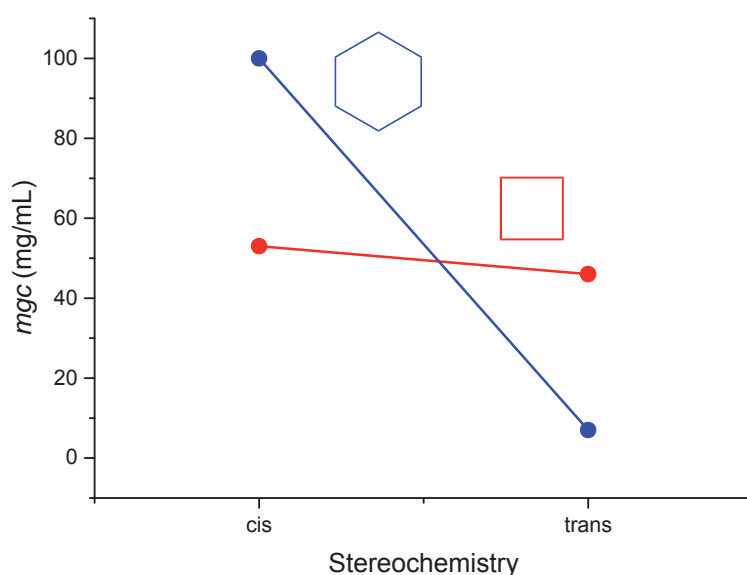


**Figure 23.** Representation of the variation of the *mgc* depending on the stereochemistry.

Gels were stable at room temperature for at least 6 months. To check their thermoreversibility, gels at concentrations equal or higher than *mgc* were heated to just below the boiling temperature and then they were allowed to cool down to room temperature. The heating-cooling cycle was repeated several times, thus providing evidence for the gel formation as the intermolecular bonds could be disrupted upon heating and reformed during cooling. However, sonication was needed in some cases to obtain the gel. All obtained gels were thermoreversible.

In order to better understand the influence of the ring size and the stereochemistry, different supramolecular studies were carried out.

### 5.3.1.1 High-resolution NMR spectroscopy

High-resolution NMR spectroscopy is a technique that is widely used to provide evidence for gel formation and to give information about the secondary structures that are adopted. In liquid-state NMR studies, only the liquid-like fraction of a gel can be observed, and the solid-like part of the gel remains undetected. During the cooling down process, the integral of the signals increase below the temperature of gelation ( $T_{\text{gel}}$ ). Once the  $T_{\text{gel}}$  is reached, the integral of the signals starts to decrease. Signals from protons involved in intermolecular interactions, such as protons from an NH group, can be nicely monitored.

These properties allowed us to prove the existence of intermolecular hydrogen bonds and to determine the gelation temperature for compounds **A**, **B**, **C** and **D**. This study was done in collaboration with Dr. Pau Nolis, from the *Servei de Ressonància Magnètica Nuclear (SeRNM)* from the *Universitat Autònoma de Barcelona*, where high-resolution NMR experiments were carried out.

The gelation process of a solvent, in which the intermolecular interactions are enhanced by some external stimuli, reduces the mobility of the molecules. There are many gelation inductors but change in the temperature is one of the most applied and adaptable to NMR. Therefore, if gelation is slow compared to NMR time scale measurement, this dynamic process can be monitored by variable temperature  $^1\text{H}$ -NMR experiments. By decreasing the temperature, a continuous signal line broadening is observed and finally a

complete signal loss is produced due to the increasing “solid-like” part of the gel, which is NMR invisible.

In this specific study, a controlled cooling down regime was applied to a 17 mM sample of each of the studied compounds in toluene, because all of them are able to gel it.  $^1\text{H}$ -NMR spectra were acquired in 1 K steps, starting from 330 K and lowering to 310 K in the case of *cis*- and *trans*-cyclohexane derivatives (Figure 24). In the case of *cis*- and *trans*-cyclobutane derivatives,  $^1\text{H}$ -NMR spectra were acquired also in 1 K steps, starting from 310 K and lowering to 290 K (Figure 24). Moreover, an equilibration period of three minutes was used in all the compounds as sample thermal equilibration period. The NH proton signals were used to follow the gelation process.

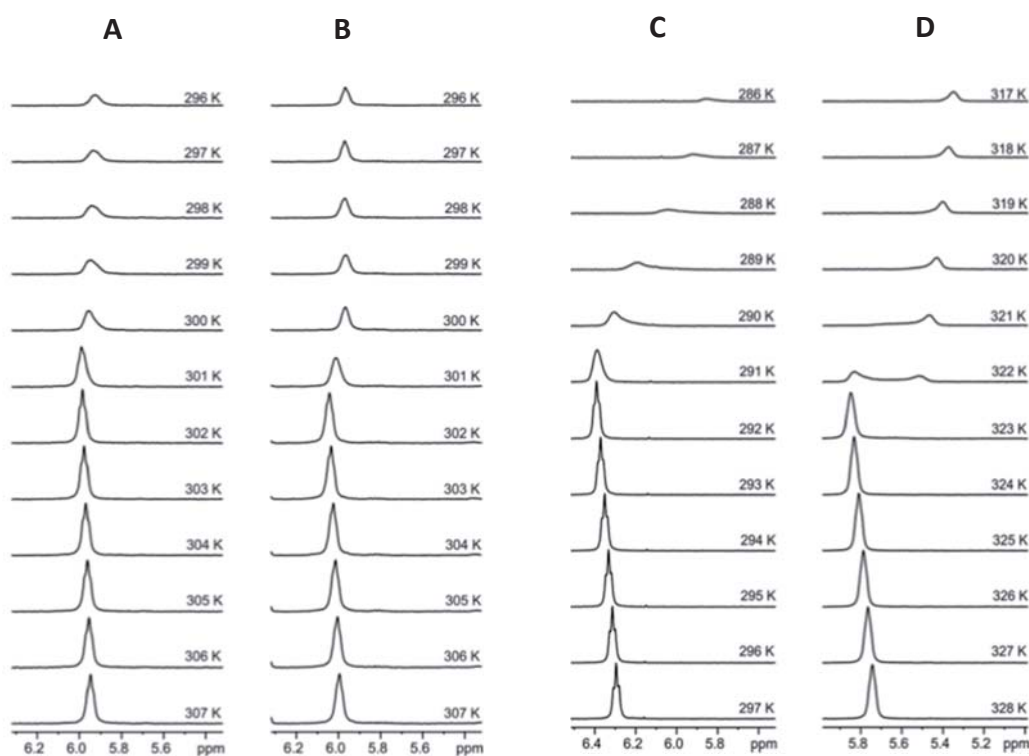


**Figure 24.** Gelation process monitored by variable-temperature  $^1\text{H}$ -NMR spectroscopy experiments in 17 mM solutions gelators **A**, **B**, **C** and **D**. A 400 MHz Bruker Avance III spectrometer equipped with a cooling unit BCU-Xtreme was used.

A continuous increase of the NH proton signal area was observed when cooling the sample. The increase in the signal area during the cooling process suggested that the hydrogen bonds were being fixed increasingly in a well-defined position. The data obtained

for cyclobutane derivatives **A** and **B** reveal that the NH signal for both isomers decays at 303 K and their chemical shift during the gelation process is almost the same, so it seems that the difference in relative configuration does not lead to different gelation processes. On the other hand, there is a significant difference between cyclohexane derivatives **C** and **D**. The NH signal of **C** decays at 291 K whereas the same signal for **D** decays at 323 K. Clearly, in these molecules the *cis/trans* stereochemistry plays a crucial role on their sol-gel transition temperature ( $T_{gel}$ ) and shows that both hydrogen bonding due to the polar amido groups and van der Waals interactions between alkyl chains make *trans* isomer **D** more prone to gelate. Normalization of the NH signals to the highest integral in the spectra series allows visualizing the solution to gel transition graphically (Figure 25).

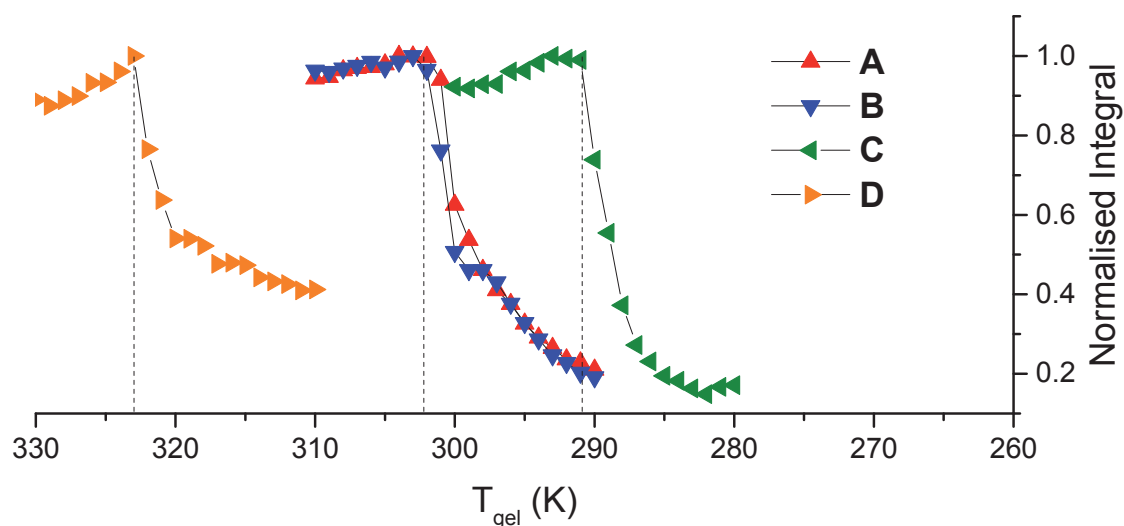


**Figure 25.** Graphical representation of the normalised NH proton integrals during the gelation process (*trans* in blue and *cis* in red) for 17 mM solutions of **A** and **B** (up) and **C** and **D** (down) in toluene- $d_8$ .

Moreover, another feature of both series is the change in the sense of the chemical shift displacement of the NH proton near to the gelation point. This effect was more marked for cyclohexane derivatives **C** and **D** than for cyclobutane compounds **A** and **B**. We observed this trend in the gelation of some dipeptides made with cyclobutane  $\beta$ -amino acids<sup>29</sup> and it was also reported in previous works,<sup>81</sup> being attributed to lipophilic interactions between alkyl groups in the aggregates. In the actual case, a similar effect

could occur involving the  $C_{16}$  alkyl chains suggesting a change in the conformational preference of the molecules that remain in solution as temperature is lowered. This conformational change would mainly affect shielding of the NH proton and would be promoted by the greatly reduced mobility of the molecules in the liquid-like part when the solid-like part of the gel is suddenly formed. In fact, NH proton in **C** is more deshielded than NH proton in **D** (6.4 and 5.9 ppm, respectively). All these facts suggest that hydrogen-bonding is not the only gelation driving intermolecular interaction but van der Waals interactions play also a role. Theoretical calculations were done in order to better study the contribution of each force (see section 5.3.1.3).

The same studies were repeated for less concentrated solutions of the four compounds (4.25 mM and 8.5 mM). Thus, the temperature effects could be separated from the aggregation phenomena. As expected, the  $T_{gel}$  for all compounds was concentration-dependent, being the gel formation easier when increasing the concentration. In Table 9 the  $T_{gel}$  for all the compounds at different concentrations are summarised and they are represented in Figure 26.

The order of the gelation temperatures obtained from HR-NMR studies is in good agreement with the order of *mgc* values in toluene obtained from the gelation studies.

**Table 9.** Concentration dependence of  $T_{gel}$  of **A**, **B**, **C** and **D** in toluene.

Compound	$T_{gel}$ (K)		
	4.25 mM	8.5 mM	17 mM
<b>A</b>	290	296	303
<b>B</b>	289	296	303
<b>C</b>	281	286	291
<b>D</b>	312	318	323



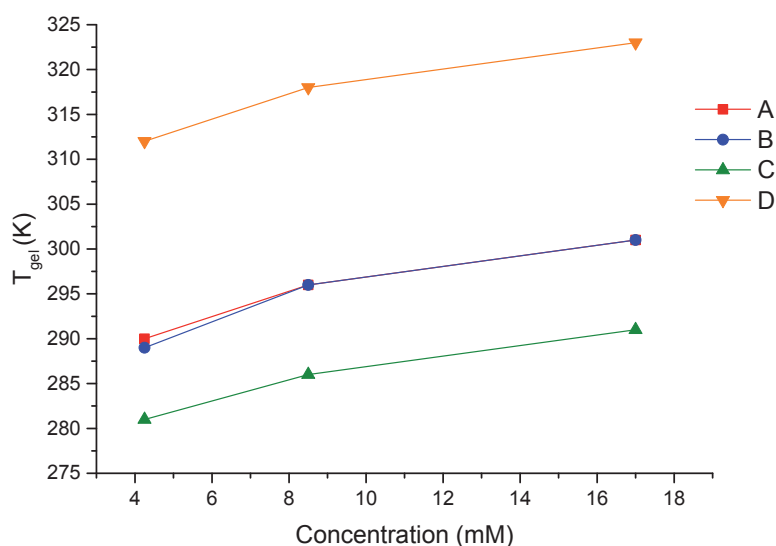


**Figure 26.** Representation of the dependence of the gelation temperature with the concentration of the organogelator.

### 5.3.1.2 Scanning Electron Microscopy (SEM)

In collaboration with Dr. Judith Oró from the *Institut de Ciència de Materials de Barcelona* (ICMAB), SEM experiments were carried out to investigate the morphology of the gels obtained from solutions in toluene. Wet gels were disposed on a carbon-film-coated copper grid and dried by standing for 30 minutes on the grid. The resulting xerogels (dry gels) were then introduced into the microscope chamber working at 70 Pa and 5 kV.

The micrographs were tested at the minimum gelation concentration (*mgc*) for each organogel in toluene. Thus, gel of **A** at 53 mg/mL, gel of **B** at 47 mg/mL, gel of **C** at 100 mg/mL and gel of **D** at 7 mg/mL were used to perform SEM experiments. The same methodology was followed for all compounds in order to avoid external influence on the morphology of the aggregates.<sup>54</sup> The images obtained are shown in Figure 27 and Figure 28.

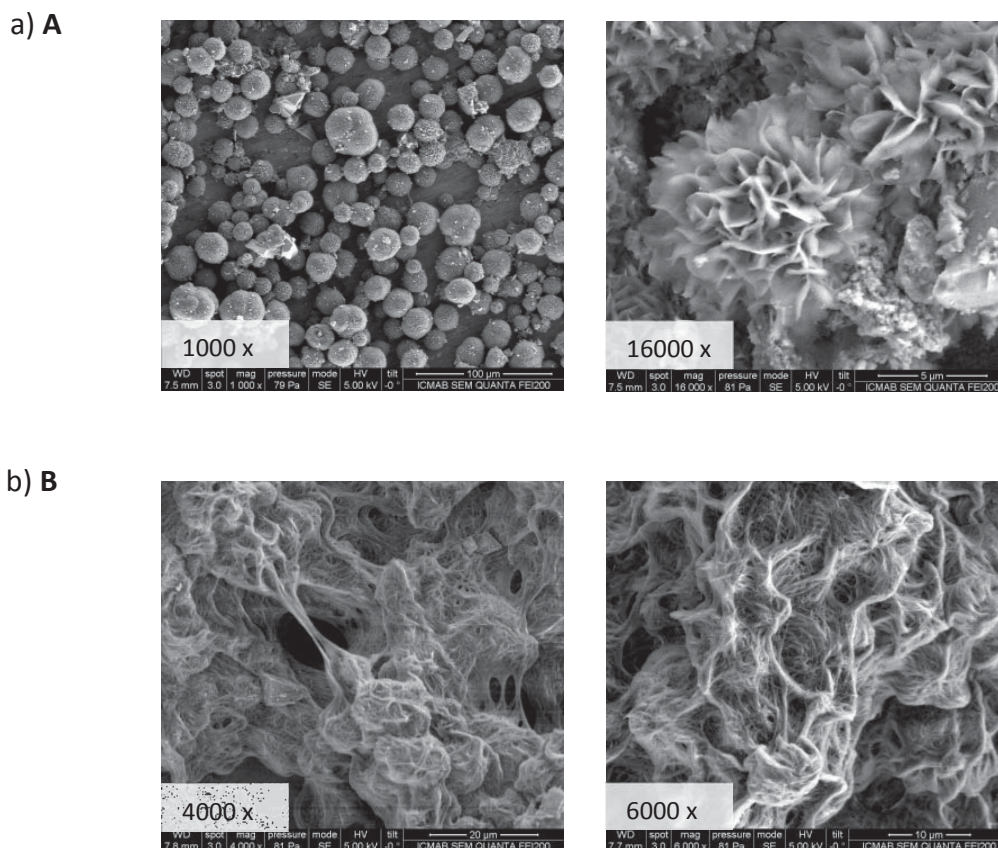


**Figure 27.** SEM images of compounds a) **A** and b) **B** as xerogels (from toluene) on graphite at 80 Pa and at two different magnifications for each sample.

SEM micrographs show that the four compounds adopt different structures. Observing the images for the cyclobutane derivatives, Figure 27a shows that the xerogel from **A** is self-organised in spheres of different sizes between 10 and 20  $\mu\text{m}$ . On the other hand, there are big spheres composed by aggregates of two smaller spheres. At the same time, these spheres are nanostructured in a rose-like shape. Figure 27b shows the images of the xerogel from **B**, it is formed by disordered fibers from lengths of around 40  $\mu\text{m}$ . Compound **B** gives wide and undefined structures although it is possible to appreciate, inside the material, very small fibres that are intertwined with each other. For organogels based on cyclohexane (Figure 28), these topographic images show xerogel from **D** to be composed of fibrillar networks, which consist of intertwined fibres and bundles of variable width. This causes the measured dimensions of these fibres to be highly variable (for example from 5  $\mu\text{m}$  to 100  $\mu\text{m}$ , approximately). In the case of the xerogel from **C**, these

micrographs are composed by small fibers of less than one micrometre of width and similar lengths around 5  $\mu\text{m}$ .

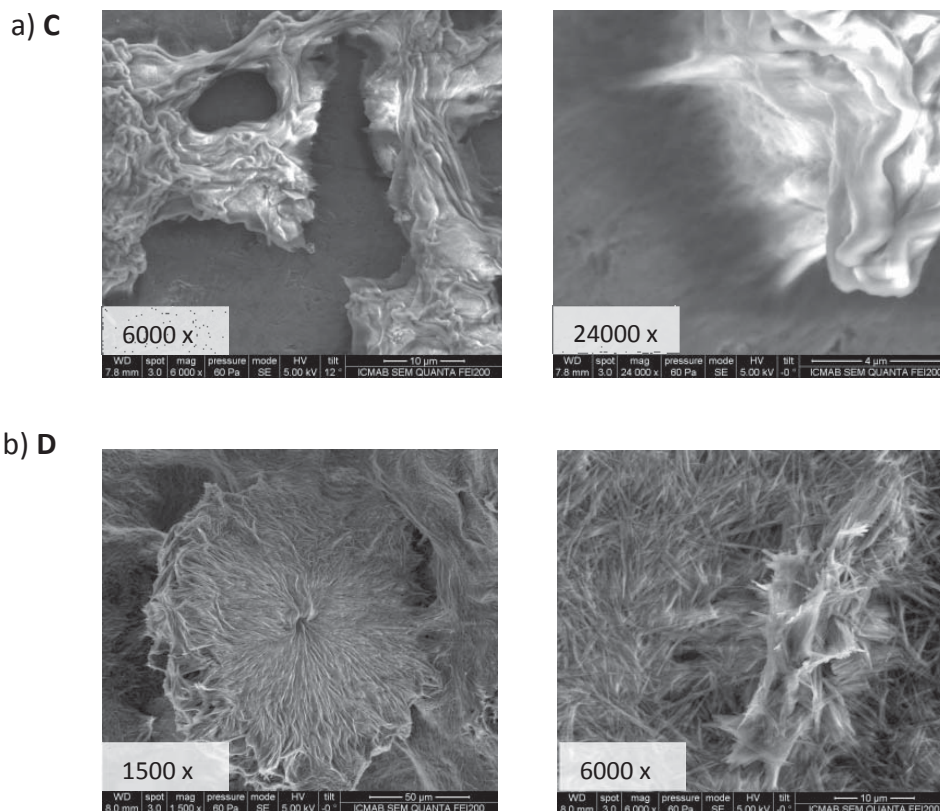


**Figure 28.** SEM images of compounds a) **C** and b) **D** as xerogels (from toluene) on graphite at 60 Pa and at two different magnifications for each sample.

In conclusion, it seems that the *cis/trans* stereochemistry of the compounds has a great influence in the organization of the structures by SEM. Moreover, the size and the rigidity of the ring (cyclobutane vs. cyclohexane) play a significant role in the morphology and dimensions of the structures formed.

### 5.3.1.3 Theoretical Calculations

In order to better understand the structure of the aggregates from the molecular point of view, theoretical calculations were carried out (computational details are shown in section 9.3). The first step to study the structure of the aggregates was to analyse the structure of the monomers. Each molecule has two amide groups and they can be in a *syn* or in an *anti* relative configuration (Figure 29) when they self-assemble. In the case of the

carbocyclic rings, other conformations could be obtained. However, only the conformations, which have as much number of substituents in equatorial positions, were considered.

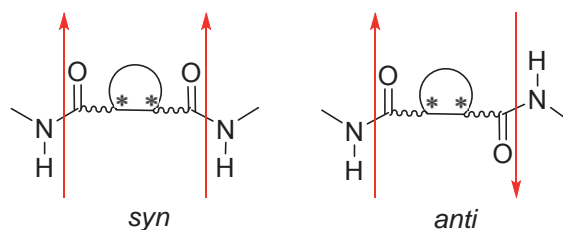


**Figure 29.** Schematic representation of the *syn* and *anti* configuration.

A conformational search using molecular mechanics of the single molecules was done. The structure of the minimum in energy was optimised with quantum mechanics using M06-2X as DFT functional. To study the structure of the dimer, firstly, the tetramer was studied using the same procedure and the *syn* and *anti* configuration were considered. Then, the studied dimer was the internal dimer of the optimized structure of the tetramer. Aggregation energy ( $\Delta E_{\text{agg}}$ ) is the difference in energy of the dimer and two monomers. Distortion energy ( $\Delta E_{\text{dist}}$ ) is the energy required to modify the structure of a single molecule to the structure it adopts when it is aggregated. Aggregation energies of the formation of the dimer and distortion energies are shown in Table 10. Energy values were calculated using two different basis sets: 6-31G(d) and 6-311+G(d,p). The obtained aggregation energy values using 6-311+G(d,p) are 2-5 kcal/mol more negative than using 6-31G(d), as it is observed in values in parentheses from Table 10. That means that using a smaller basis set, the aggregation can be studied with accuracy in a moderate computing time. All shown results of this section were calculated using 6-31G(d) basis set and incorporating the BSSE correction.

As it is shown in Table 10, cyclohexane-based compounds prefer an *anti* configuration of the amide groups when self-assembling while in the case of the cyclobutane-based compounds, they prefer a *syn* configuration in the *cis* isomer while they prefer an *anti* configuration in the *anti* isomer. This could be because of the difference of rigidity between the cyclobutane and the cyclohexane moieties.

**Table 10.** Distortion energies and aggregation energies for the formation of the dimers of the compounds **A**, **B**, **C** and **D**.

Compound	$\Delta E_{\text{dist}}$ (kcal/mol)	$\Delta E_{\text{agg}}$ (kcal/mol) <sup>a</sup>
<b>A</b> <i>syn</i>	5.9	-36.2 (-39.3)
<b>A</b> <i>anti</i>	3.6	-21.2 (-24.3)
<b>B</b> <i>syn</i>	19.5	-4.8 (-8.01)
<b>B</b> <i>anti</i>	14.1	-20.7 (-22.8)
<b>C</b> <i>syn</i>	11.2	-21.6 (-26.9)
<b>C</b> <i>anti</i>	5.7	-34.2 (-39.4)
<b>D</b> <i>syn</i>	24.2	-4.0 (-7.0)
<b>D</b> <i>anti</i>	9.2	-27.8 (-30.7)

<sup>a</sup> Results in parentheses were calculated with the 6-311+G(d,p) basis set.

Once the relative configuration of the amide groups is determined, the structure of the tetramer was studied using the described methodology. After that, the hexamer and the octamer were constructed by taking the structure of the internal dimer of the tetramer. Then a minimization of the energy was followed by a DFT single point calculation of the energy. The structures of the predicted octamers are shown in Figure 30 and Figure 31.

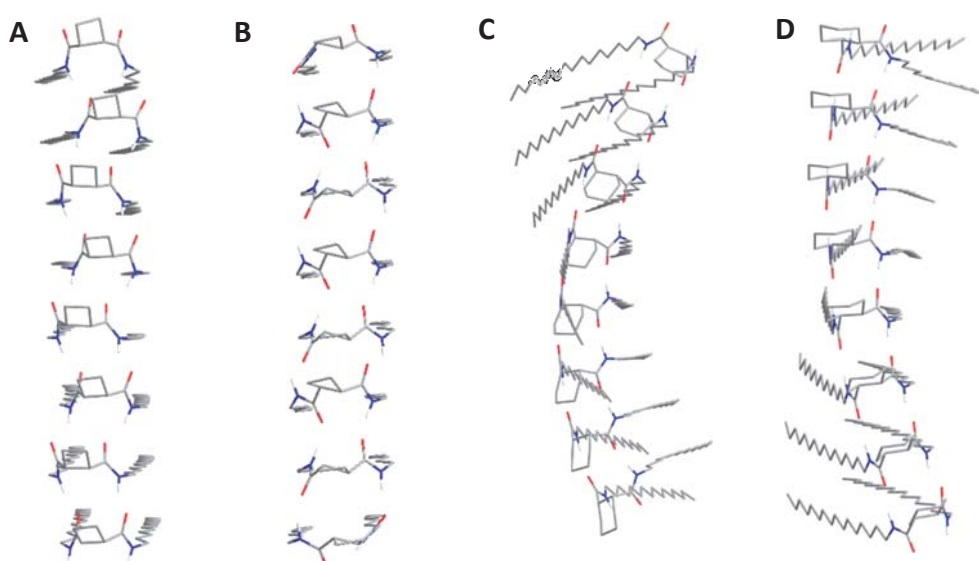


**Figure 30.** Frontal view of the predicted structures of the octameric aggregates of the compounds **A**, **B**, **C** and **D**. Non-polar hydrogens were omitted for clarity.

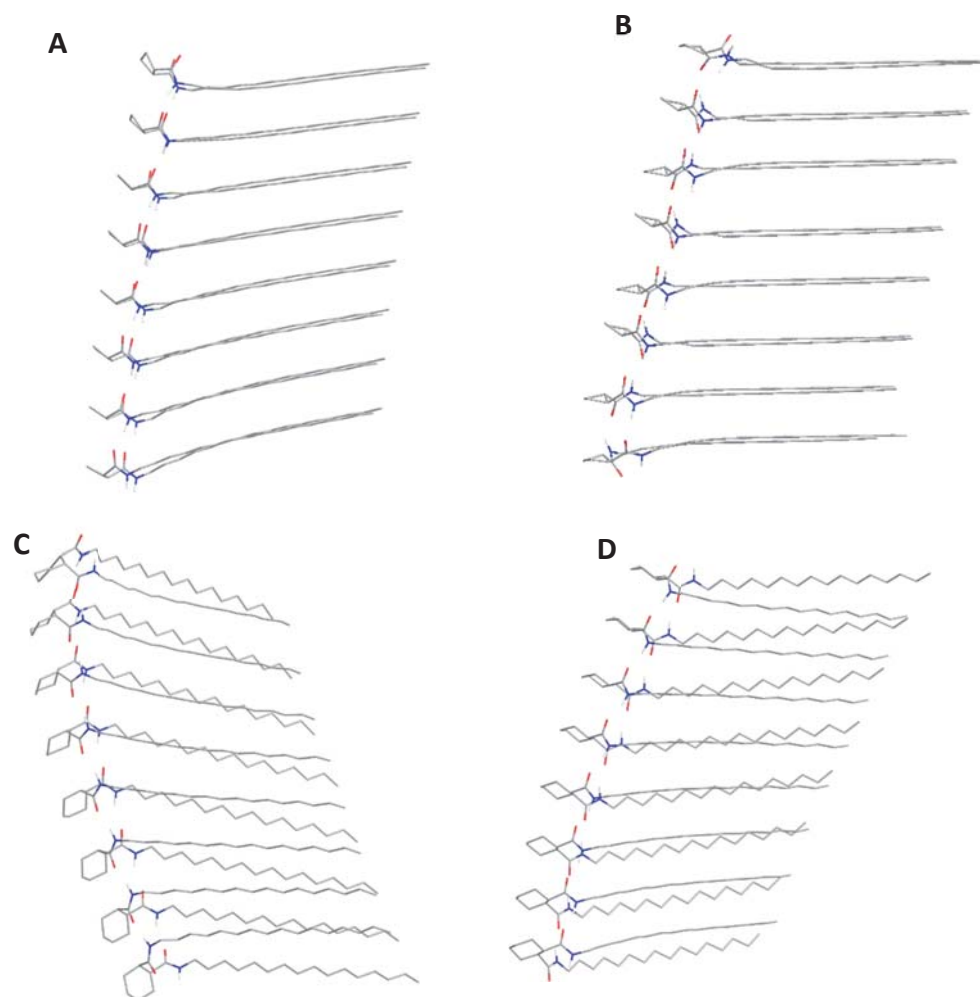


**Figure 31.** Lateral view of the predicted structures of the octameric aggregates of the compounds: a) **A**, b) **B**, c) **C** and d) **D**. Non-polar hydrogens were omitted for clarity.

Predicted structures of the octameric aggregates show that compounds **A** and **B**, which contain a cyclobutane ring, self-assemble forming a zigzag aggregates, the former with a helical-like structure, which means that some asymmetry could be induced during the aggregation process. On the other hand, compounds **C** and **D**, which contain a cyclohexane ring, self-assemble forming a right-handed and a left-handed helical aggregate respectively.

The energies of the formation of each aggregate and the aggregation energies per monomer are shown in Figure 32. Computed aggregation energies include the BSSE correction in order to minimize the influence of the level of theory. To compute the energy

of an aggregate with  $n$  monomers, BSSE was considered  $n-1$  times, one for each interaction.

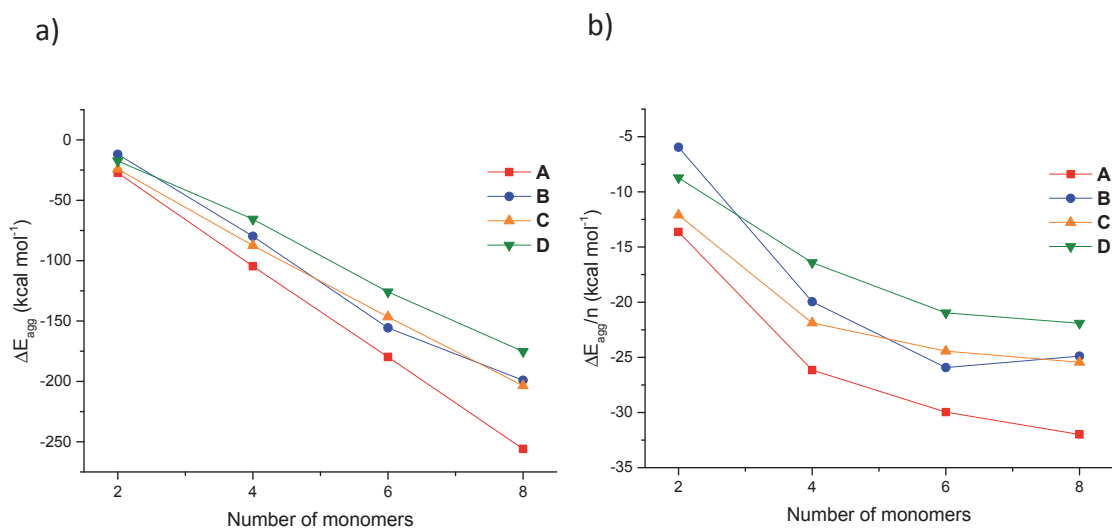


**Figure 32.** Aggregation energies (a) and aggregation energies per monomer (b) of the compounds **A**, **B**, **C** and **D**.

Aggregation energies are favourable when increasing the number of monomers, so self-assembly is favourable. The aggregation energy per monomer gives information about the stabilization due to the introduction of a new molecule in the aggregate. Up to the formation of the hexameric aggregate, the aggregation energy per molecule increases in all cases in absolute value, whereas after that the contribution of a new molecule remains nearly constant. This means that the self-assembly of these compounds is promoted by a cooperative effect in the first steps.<sup>82-85</sup> After that, the addition of new molecules to the external positions has less influence to the whole aggregate.

The main forces involved on the self-assembly process of  $n$  monomers are the hydrogen bonding ( $\Delta E_{HB}$ ) of the amide moieties and the van der Waals interaction of the chains ( $\Delta E_{vdW}$ ). In order to determine the net contribution of each force on the self-assembly, the interaction energy ( $\Delta E_{int}$ ) was calculated using Equations 1 and 2.

$$\Delta E_{agg} = n\Delta E_{dist} + \Delta E_{int} \quad (\text{Equation 1})$$

$$\Delta E_{int} = \Delta E_{HB} + \Delta E_{vdW} \quad (\text{Equation 2})$$

In order to calculate the interaction energy related to the hydrogen bonds, a model tetramer was used. The C16-carbon chain was replaced by a terminal CH<sub>3</sub> group, minimizing the van der Waals interactions. The distortion energy of this moiety was calculated using the previously described methodology. Aggregation energies include the BSSE correction for each interaction. The net contribution of the hydrogen bonds and the van der Waals interactions are shown in Table 11.

**Table 11.** Interaction energy, net forces of the hydrogen bonds and the van der Waals interactions and % of the contribution of each force to the interaction energy. Energies are in kcal mol<sup>-1</sup>.

Compound	$\Delta E_{\text{int}}$	$\Delta E_{\text{H-bond}}$	%E <sub>HB</sub>	$\Delta E_{\text{vdW}}$	%E <sub>vdW</sub>
<b>A</b>	-128.3	-72.6	56.6	-55.7	43.4
<b>B</b>	-131.1	-68.6	52.3	-62.5	47.7
<b>C</b>	-110.5	-70.5	63.8	-40.0	36.2
<b>D</b>	-102.6	-61.6	60.1	-40.9	39.9

Results show that **A** and **B** present larger interaction energies than **C** and **D**. Moreover, for **A** and **B**, the hydrogen bonding is slightly stronger than the van der Waals interactions while for **C** and **D** the difference is more important. This could be in agreement with the fact that in cyclohexane-based gelators, stereochemistry plays a very important role while with cyclobutane-based compounds stereochemistry has no influence. These results are in agreement with the conclusions of Zweep *et al.*<sup>78</sup> These authors investigated the balancing between H-bonding and van der Waals forces during the gelation process.

#### 5.3.1.4 Circular Dichroism

Circular dichroism spectroscopy (CD) is an optical technique based on the difference in the absorption of left-handed circularly polarised light (L-CPL) and right-handed circularly polarised light (R-CPL) at different wavelength, depending on the rotational strength of each molecule. This technique was discovered in 1895 by Aimé



Cotton during his PhD, when he found that some optically active substances presented anomalous rotatory dispersion depending on the wavelength at the region of absorption of the compound.<sup>86,87</sup> In this thesis, this technique was focused on the UV region. CD has numerous advantages respect to other conventional techniques such as rapid data collection or ease of use.<sup>64,88</sup>

Chromophore groups will absorb differently the different circularly polarised light if they are chiral or if they are nearby a chiral group, which induce asymmetry to the chromophore. Non-chiral or non-induced chromophore will absorb both circularly polarised lights at the same intensity and thus, the difference will be zero and no signal on the CD spectrum will be observed.

CD can be studied in solution and in solid state. In our case, the solid state refers to the xerogel phase. The shape of the CD spectrum is determined by the relative position of the electric and magnetic transition dipoles of the chiral chromophore groups, and thus, it gives information about the structure.

In solution, the chirality of single molecules is observed and the signal gives information about the conformation of the chromophores and, in our cases, about the intramolecular amide bonds. In xerogel phase, only chiral aggregates will give a signal on the CD. The signal gives information about the relative position of the chromophore groups and, in our cases, about the intermolecular amide bonds. Depending on the structure of the aggregate, the relative position of the amide groups will vary and thus, the shape of the CD spectrum will also vary.<sup>89,90</sup>

Amides absorb at 200-240 nm due to the  $\pi \rightarrow \pi^*$  and the  $n \rightarrow \pi^*$  transitions.<sup>91</sup> Thus, in our cases these wavelengths will give us information about the interaction between amides and the structure of the aggregates. This region has been extensively studied for determining secondary structures of proteins and it becomes a challenge to study self-assembly due to the limited knowledge and number of publications. In this kind of studies, it is difficult to obtain structural information from the CD spectra alone and other complementary techniques should also be employed.<sup>92</sup> In order to be able to record the spectra at this range, methanol as solvent was used in solution. In xerogel phase, KBr was used as solid "solvent".

Due to the low solubility of organogelators **A-D** in methanol and thus, working under the limit of detection of the technique, the spectra in solution were not recorded.

Xerogels were prepared by removing the solvent of the gel under vacuum at the *mgc* in toluene. Samples for the solid CD were prepared following the procedure explained in section 10.7.2. The spectra in xerogel phase were obtained (Figure 33).

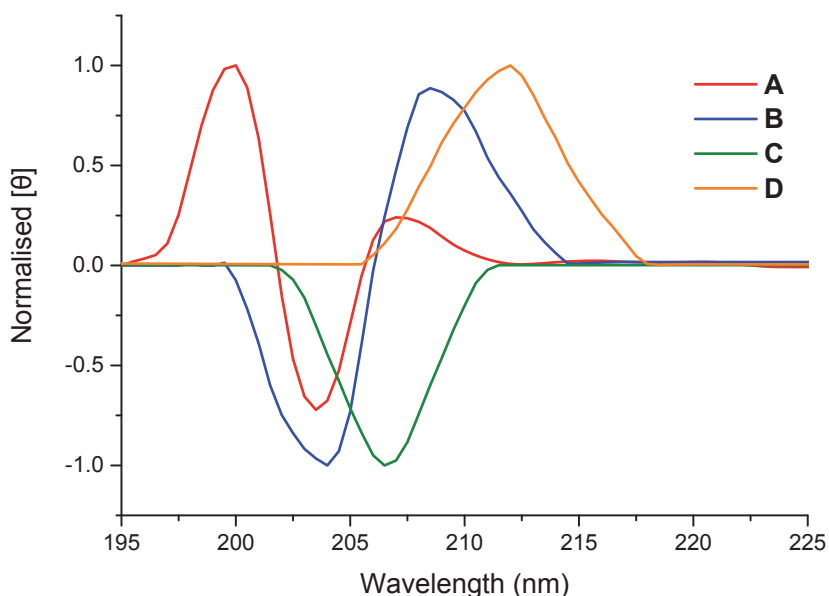


**Figure 33.** Circular Dichroism spectra of organogelators **A**, **B**, **C** and **D** in xerogel phase at 0.024, 0.020, 0.021 and 0.022 mmol/g of KBr respectively at 25 °C.

Unexpected CD signals were obtained. Gelators **A** and **C** are *meso* compounds and as it is shown, they are not silent in the solid state CD, meaning that some asymmetry was induced during the aggregation process forming chiral aggregates. We could say that, at least, there are some molecules that self-assemble in a chiral way. This is in agreement with theoretical calculations, which predict some asymmetry in the aggregate. Nevertheless, different achiral aggregates could be formed (which are CD silent) or even other chiral aggregates. CD spectra show an average of all the asymmetric compounds and aggregates. As explained in the introduction section, there are many other examples of achiral molecules that self-assemble forming chiral aggregates.<sup>61,93,94</sup>

As it is shown, organogelator **A** and **B** show a bisignate Cotton effect while **C** and **D** show a band. Compound **A** show a negative first Cotton effect at 203 nm with a zerocrossing at 201 nm and a small band at 207 nm. Compound **B** shows a positive first

Cotton effect at 208 nm with zero-crossing at 206 nm. Both compounds can self-assemble forming two chiral aggregates. In the case of LMWGs **C** and **D**, it is shown that while the *cis* isomer presents a negative band at 207 nm, the *trans* isomer shows a positive band at 211 nm. They self-assemble forming chiral aggregates.

In order to try to understand why these cyclobutane-based compounds show a bisignate Cotton effect and the cyclohexane-based compounds show a band, the relative position of the chromophore groups on the predicted aggregate was studied (Figure 34).

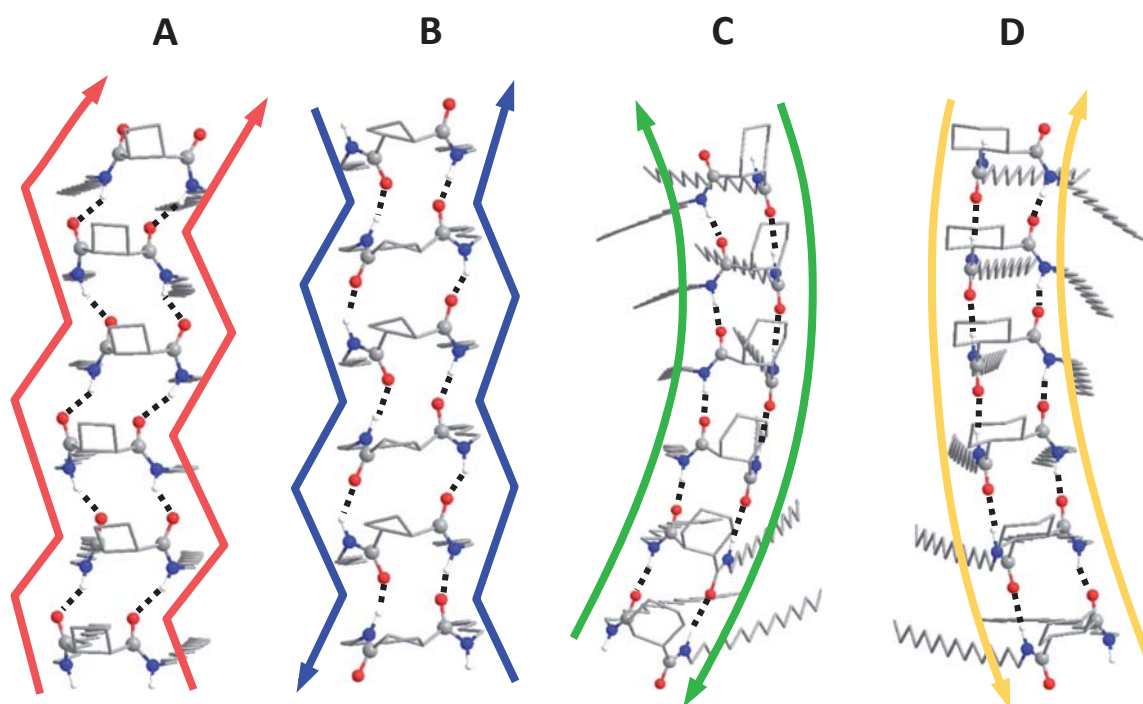


**Figure 34.** Structure of the predicted aggregated which shows the relative position between amide groups forming the backbone of the aggregate. Non-polar hydrogens were omitted for clarity.

First of all, it is important to say that all these four aggregates are chiral because their mirror image is non-superposable. As it is shown, helical aggregates of **C** and **D** show two parallel and uniform skeletons. This could be the reason that why they show a band on the CD and not a bisignate signal. On the other hand, zigzag aggregates of **A** and **B** have two parallel hydrogen bond backbones but with a zigzag structure, which we hypothesise that could be the responsible of the bisignate Cotton effect on the CD due to the different and alternated orientation of the chromophores. Other studies found in the literature show also that a helical aggregate gives a band on the amide region of the CD spectrum

(200-240 nm)<sup>72,95,96</sup> and the zigzag disposition of the chromophores exhibit a characteristic exciton couplet.<sup>97-99</sup>

To predict a CD spectrum in xerogel phase, a certain number of excited states of the molecular orbitals have to be calculated using a good level of theory. However, calculations were only possible using a high number of excitation states with a small basis set or using a large basis set but with few excited states. The CD spectra of a tetrameric aggregate were predicted using CAM-B3LYP/6-31G(d,p) level of theory. Due to the low number of excited states, the predicted CD curve could not be plotted using GaussSum software and therefore, excitation states were plotted using OriginLab. In all cases, predicted spectra did not fit quantitatively the experimental ones due to the low number of calculated excited states in the studied region but the sign of the excited states is in qualitative agreement with the obtained CD spectra (Figure 35). That means that predicted structures could explain properly one of the possible aggregation that these gelators could adopt.

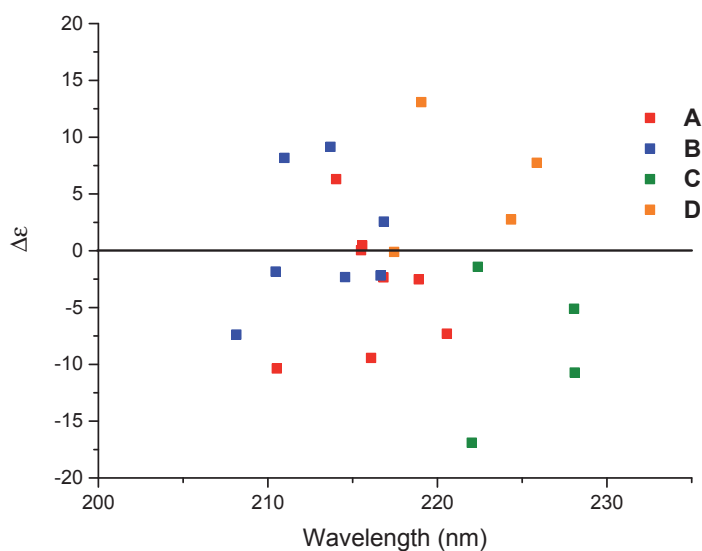


**Figure 35.** Predicted CD spectra of aggregates of **A-D** using CAM-B3LYP/6-31G(d,p) level of theory.

### 5.3.2 Gelation study of Family 2

Family 2, described in page 63, are five substituted diamide-based cycloalkanes. The gelation ability was studied in 14 common solvents following the same procedure as in the former study. To determine the formation of a gel, the tube inversion test is used. Table 12 summarizes the study showing the behaviour of each LMWG in each solvent.

**Table 12.** Gelation behaviour of compounds **E**, **F**, **G**, **H** and **I** in common solvents.

Compound	Pentane	1,4-dioxane	Toluene	Et <sub>2</sub> O	CHCl <sub>3</sub>	EtOAc	THF	CH <sub>2</sub> Cl <sub>2</sub>	iPrOH	Acetone	EtOH	MeOH	CH <sub>3</sub> CN	H <sub>2</sub> O
<b>E</b>	83 C	S	S	S	S	100 O	S	S	100 O	S	21 O	17 O	S	S
<b>F</b>	S	S	S	S	S	S	S	S	S	S	50 T	16 O	S	S
<b>G</b>	I	51 T	102 T	S	S	S	S	S	S	S	S	S	S	S
<b>H</b>	54 O	61 O	64 T	70 O	S	45 O	S	S	S	22 O	56 O	70 O	S	S
<b>I</b>	I	102 O	82 T	I	82 T	I	S	S	I	I	I	I	I	I

Dielectric constant increases from left to right.

C: Clear T: Translucid O: Opac

Minimum gelation concentration in mg/mL.

I: Insoluble, S: Soluble.

The first comment on this table is that this family behaves in a different way compared to Family 1. Thus, substitutions to the ring seem to play an important role, at least, on the solubility.

Comparing diastereoisomers **E** and **F** we could find out the influence of the stereochemistry in this family. As it is shown, both gelators can gel methanol at a very low *mgc* value. In addition, they can gel ethanol at a low value of *mgc*. Moreover, **E** can gel pentane, EtOAc and iPrOH but at very high *mgc* values. Stereochemistry seems to have less importance than in non-substituted cyclohexane-based compounds probably due to the presence of other functional groups in the molecule.

Compound **G** is a very bad organogelator. It can only gel 1,4-dioxane and toluene but at high concentrations. The difference between **E** and **G** is that the former has a TBDMS protection while **G** has not. This result suggests that this protection favours the gelation of ethanol and methanol, unlikely one could expect.

Compound **I** has a completely different behaviour compared to this family. It seems to act as non-substituted cyclohexane-based gelators (**C** and **D**) because it can gel 1,4-dioxane, toluene and chloroform although at higher *mgc* and it is insoluble in all the other solvents. This compound **I** has three free OH groups and it is insoluble in all the alcohols. That means that the OH groups do not interact with the solvent. In other studies described in the literature<sup>100</sup> with a similar molecule with free OH groups that is not soluble in alcohols, the authors hypothesise that the interaction between the free OH groups of different molecules are so strong that they cannot interact with the solvent and thus, they are insoluble.

Finally, compound **H** can gel a large variety of solvents of very different polarities. The difference between **H** and **F** is that **H** has two free OH groups while **F** have a ketal protection. In this case, it has also the TBDMS protection and it can gel also ethanol and methanol.

To summarize some behaviours, **E**, **F** and **H** are the only ones that have a TBDMS protection, and the only ones that can gel alcohols. **G**, **H** and **I** have free OH groups and they are the only ones of this family that can gel toluene and 1,4-dioxane.

**E**, **F**, **G** and **H** are very different from **I**, which resembles more to **A**, **B**, **C** and **D** despite having three free OH groups. To be able to understand these behaviours, some techniques were used.

Gels were stable at room temperature. Moreover, these gels were reversible at the body temperature. By heating the gel with a hand, it became a solution. Once the solution was left to cool down again at room temperature, the gel was formed again showing thermoreversibility. However, in some cases, sonication was needed to obtain the gel.

### 5.3.2.1 Hansen Solubility Parameters

During the years, different attempts to correlate solvent parameters and gelation ability were developed or reused. Some considerations must be taken into account: Can a solvent be considered as a macroscopic continuum characterised by its bulk physical properties? Can some set of solvent parameters predict all the different gelation abilities? Or what solvent parameters are most crucial to predict the gel formation?<sup>101</sup>

The most common parameter to distinguish different solvents is the dielectric constant ( $\epsilon$ ), which was used as the “polarity” of a solvent. The solvents of Table 12 are sorted by the dielectric constant but as it is observed, the rationalization of the gelation study cannot be related only to the dielectric constant.<sup>102</sup> Also, other studies show that it is only useful in some cases and inside the same class of solvents (*e.g.* alcohols of different alkyl chain lengths). Other global physical solvent parameters were used to classify the solvents, such as the refractive index, the octanol/water partition coefficients and Henry’s law,<sup>103</sup> the Reichardt’s  $E_T(30)$  solvent parameter<sup>104–106</sup> or the pyrene fluorescence solvent parameter<sup>107</sup>, but none of them was shown to be good enough to rationalize all the gelation studies.

Hildebrand and Scott,<sup>108</sup> and Scatchard<sup>109</sup> developed in 1949 a series of solubility parameters, known as Hildebrand parameters, which take into account the solubility, van der Waals forces and also the vaporization energy of the solvent. This parameter seems to be useful to discriminate between solutions, gels and precipitates, but only in some cases and using small subsets of solvents.

Considering a solvent as a macroscopic continuum characterised by a single physical constant (*e.g.*, dipole moment, dielectric constant, refractive index, etc.), solvatochromic shift, or Hildebrand solubility parameter is insufficient to predict the gelation behaviour. Next, multi-term solvent parameters are considered, which can distinguish individual types of interactions and were reported as better predictors of gelation.

An improvement of the dielectric constant are the Kamlet-Taft parameters ( $\alpha$ ,  $\beta$  and  $\pi^*$ ), which divide it in three parameters forming a 3D space of polarity ( $\epsilon = f(\alpha, \beta, \pi^*)$ ).<sup>102,110–112</sup>

Kamlet–Taft parameters characterise a solvent through its polarizability  $\pi^*$ , hydrogen bond donating (the acidity parameter,  $\alpha$ ), and hydrogen bond accepting (the basicity parameter,  $\beta$ ) terms. Kamlet-Taft parameters can be used to explain different solubilities and some authors tried to explain the gelation studies but without success because other factors are involved in the gelation process. Different modifications were proposed, such as Catalan’s Solubility Parameters,<sup>113–115</sup> but their use in the gelation studies cannot be standardised.

Hansen solubility parameters (HSPs) were devised to overcome the limitations of the Hildebrand solubility parameter that do not include the effects of specific intermolecular interactions such as polarity and hydrogen-bonding.<sup>116</sup> To derive the HSPs, it is assumed that the energy of vaporization of a species, which is a measure of its total cohesive energy  $E$ , is the sum of three individual energetic components, dispersion interactions ( $E_D$ ), dipole–dipole interactions ( $E_P$ ) and hydrogen-bonding interactions ( $E_H$ ).

$$E = E_D + E_P + E_H \quad (\text{Equation 3})$$

The dispersive component  $E_D$  dominates for simple, low polarity solvents such as saturated hydrocarbons. The second component  $E_P$  accounts for interactions due to polar groups on the solvent. Nitroparaffins, propylene carbonate, and tri-*n*-butyl phosphate are examples of solvents that are polar, but immiscible with water.<sup>116</sup> The third component  $E_H$  arises from hydrogen bonding interactions. Dividing each factor by the molar volume ( $V$ ) gives the square of the total HSP (which is identical to the Hildebrand solubility parameter,  $\delta_T$ ) as the sum of squares of the individual HSP components.

$$\frac{E}{V} = \frac{E_D}{V} + \frac{E_P}{V} + \frac{E_H}{V} \quad (\text{Equation 4})$$

$$\delta_T^2 = \delta_D^2 + \delta_P^2 + \delta_H^2 \quad (\text{Equation 5})$$

HSPs were commonly used to select solvents for dissolving polymers. However, their importance in new fields is rapidly emerging and they were first introduced to the field of molecular gels by Raynal and Bouteiller in 2011.<sup>117</sup>

Plotting the HSPs of each solvent, a new 3D space is generated and the solvents are sorted over the space depending on these three parameters. A specific and expensive software (HSPiP)<sup>118</sup> was developed in 2015 to easy rationalize the HSP space and to find other parameters such as the solubility radius. However, for our purpose, software such



as OriginLab can satisfy our needs. Moreover, the representation of the HSPs was improved in order to represent better them on a 2D surface. Teas parameters are the normalization of the HSPs, and then, the resulting plot is a 2D plot with three coordinates that are dependent from each other forming a triangle.<sup>119–122</sup> In Figure 36 a graphical representation of the Kamlet-Taft parameters, the Hansen Solubility Parameters and the Teas parameters is shown.

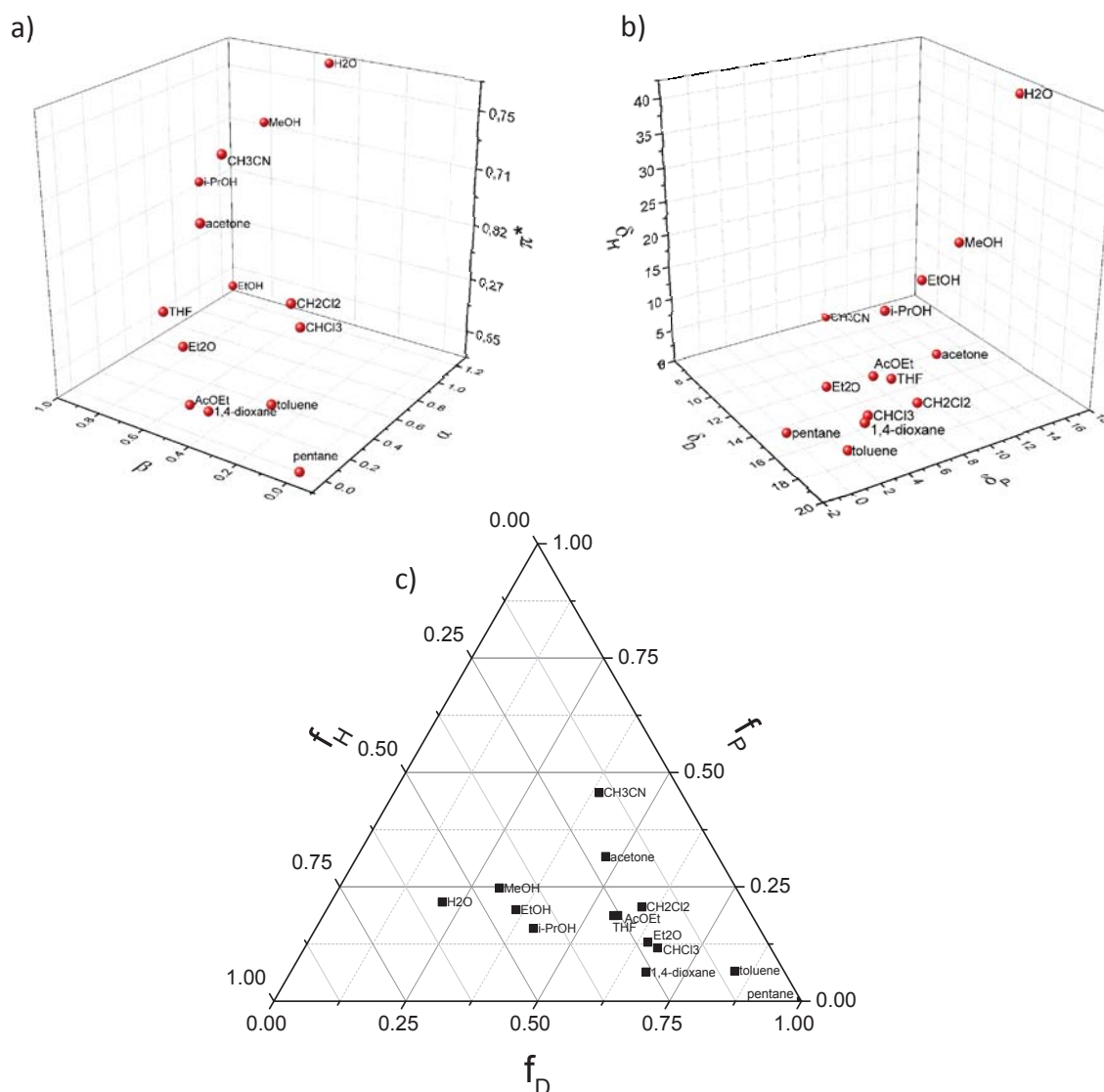


**Figure 36.** Graphical representation of: a) Kamlet-Taft parameters, b) Hansen Solubility parameters and c) Teas parameters. Only the 14 solvents used in this work are represented.

In order to try to explain the gelation behaviour, Kamlet-Taft and Hansen Solubility parameters were used, but as in other gelation studies, only HSPs seems to lead to satisfactory results.

The representation of the HSPs of the behaviour of the organogelator **H** shows that there are two areas of gel solvents. In blue are represented the solvents in which **H** is able to gel and in red are represented the solvents in which it is soluble. In order to better see the two areas, the plane  $\delta_p$ - $\delta_D$  was represented.

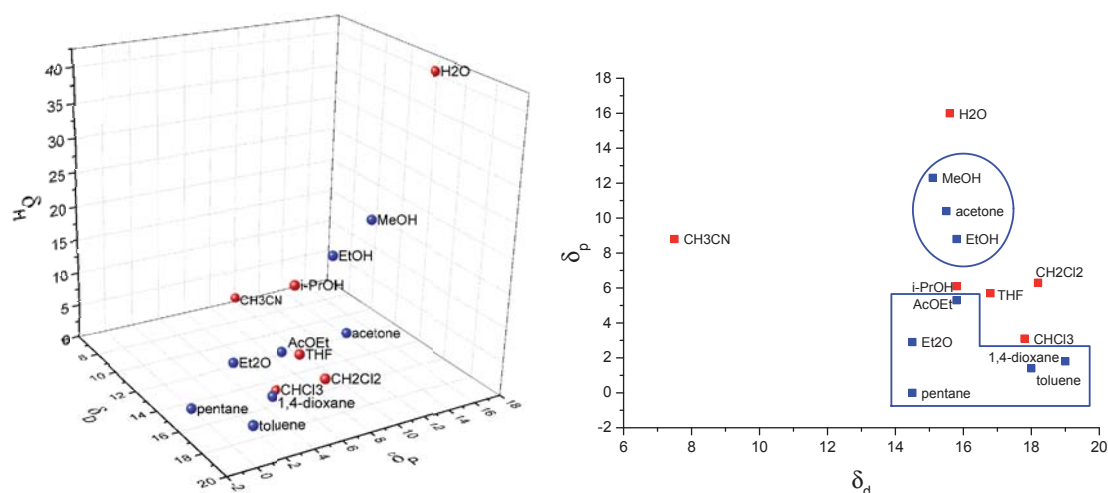


**Figure 37.** HSPs representation and 2D representation of the HSPs of the gelation study of organogelator **H**.

Two different areas of solvents on the HSPs space means two different behaviours of this organogelator, which can be related to two different aggregation patterns.<sup>100</sup> Looking at the structure and comparing it to other studies in the literature, we could hypothesise that **H** interact through the free OH groups forming an aggregate with two different hydrogen bonds, those through the amides and those through the OH groups. In order to confirm this hypothesis, theoretical calculations were carried out (see section 5.3.2.3).

Organogelator **I** has a strange behaviour on the gelation study because despite having three free OH groups, it is insoluble in polar solvents, especially in alcohols and one could expect that the interaction with the free OH groups with the OH groups from the solvent should be favourable. HSPs could help us to understand this behaviour.

As it is shown in Figure 38, compound **I** is only soluble in a region inside the HSPs space, which is represented with a red circle in the 2D representation and it can only gel three solvents that are very close in the HSPs space. In addition, it is observed that depending on the value of  $\delta_D$  it is possible to classify the solvent depending on the

behaviour. In order to better understand the gelation abilities of compound **I**, theoretical calculation were carried out (see section 5.3.2.3).

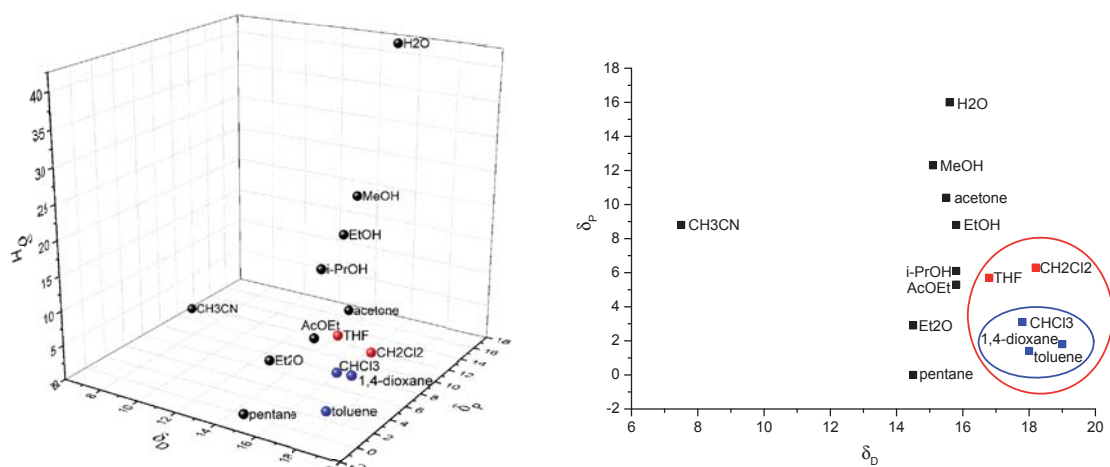


**Figure 38.** HSPs representation of compound **I** and 2D representation of the HSPs.

### 5.3.2.2 Scanning Electron Microscopy (SEM)

Morphology of the gels was studied by SEM of the xerogels obtained from the gels in different solvents at the *mgc* (Figure 39 and Figure 40).

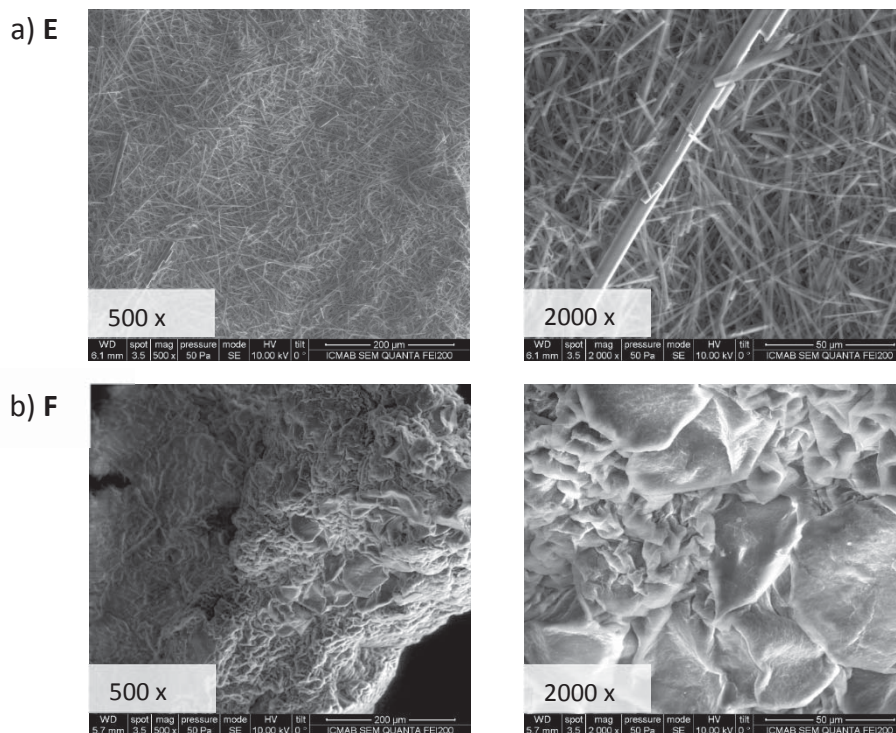
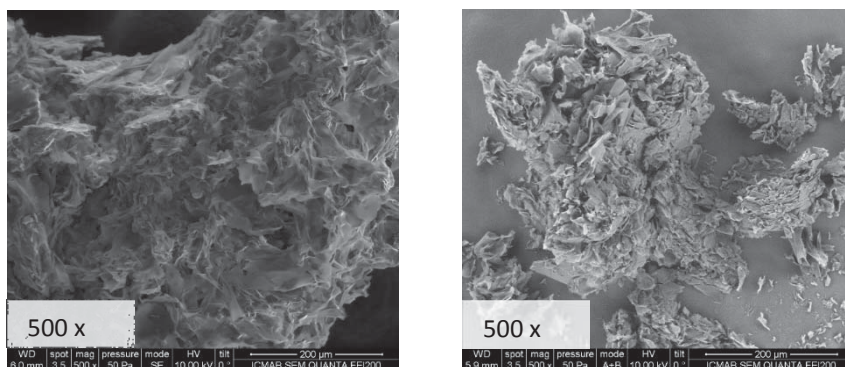


**Figure 39.** SEM images of compounds a) **E** and b) **F** as xerogels (from methanol) on graphite at 50 Pa and at two different magnifications for each sample.

c) **H** in acetone



d) **H** in pentane

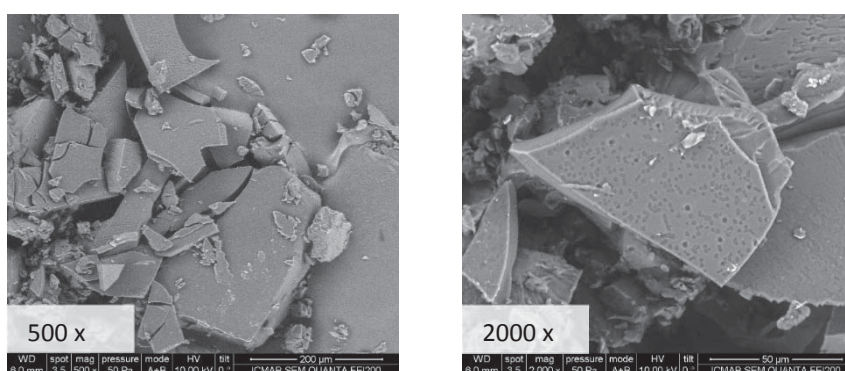


**Figure 40.** SEM images of compound **H** as xerogel from a) acetone and b) pentane on graphite at 50 Pa and at two different magnifications for each sample.

SEM images show that compound **E** and **F** have different morphology despite having the same gelation behaviour. Compound **E** forms fibres from different length, some of them are very large (around 200  $\mu\text{m}$ ). Organogelator **F** forms also big aggregates but in this case, it seems the interior of a cave of rocks. Compound **H** was studied in two different solvents, acetone and pentane, one of each area of solvents from the HSPs space.

### 5.3.2.3 Theoretical Calculations

Theoretical calculations of compounds **E** to **I** were carried out following the procedure explained in section 9.3 using the M06-2X/6-31G(d) level of theory for the optimization of the geometry of the monomer and the tetramer and using minimizations of the energy with molecular mechanics for the structure of the hexamer and the octamer.

Predicted structures of the octamers of compounds **E** and **F** are shown in Figure 41 and Figure 42, respectively.

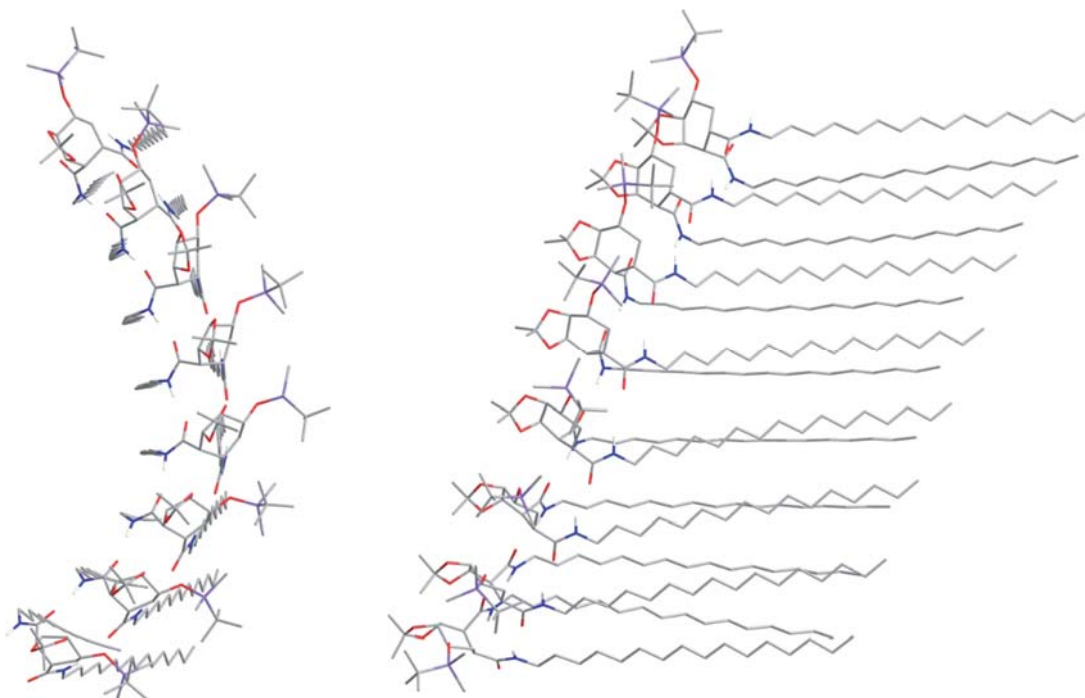


**Figure 41.** Frontal and side view of the predicted structure of the octameric aggregate of compound **E**. Non-polar hydrogen atoms were omitted for clarity.

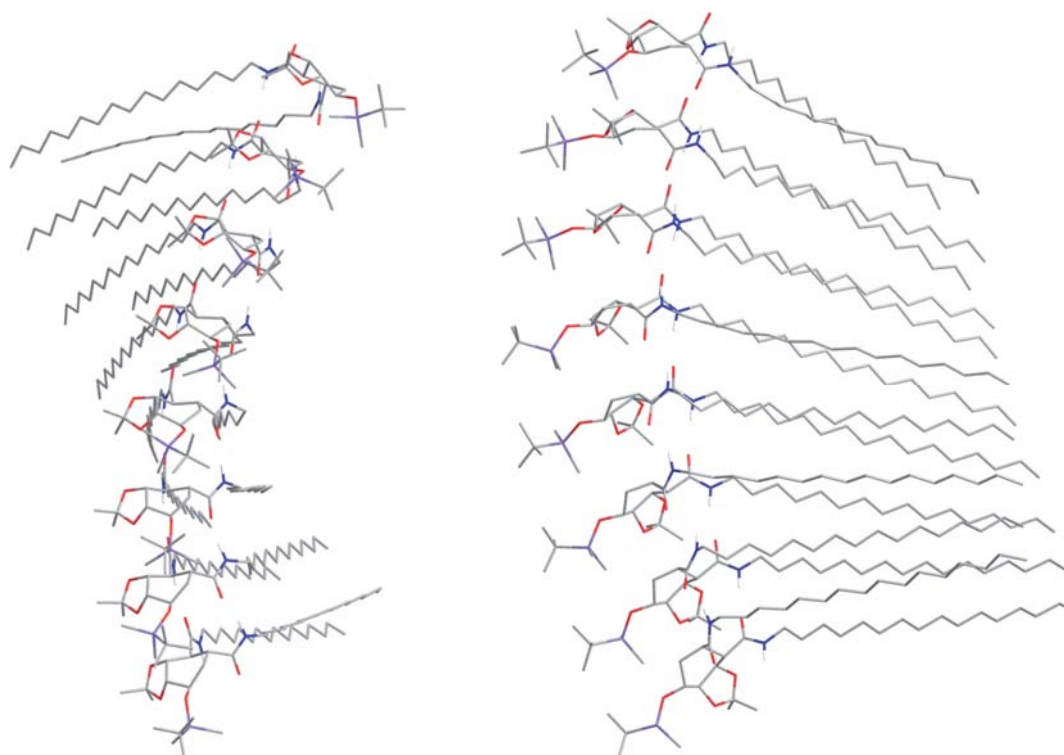


**Figure 42.** Frontal and side view of the predicted structure of the octameric aggregate of compound **F**. Non-polar hydrogen atoms were omitted for clarity.

Due to the presence of the TBDMS protection and the *cis* configuration, compound **E** shows a curved and non-helical aggregate without any rotation of the hydrogen bond skeleton. Otherwise, compound **F** forms a right-handed helical aggregate. In both cases, the chains are placed in a parallel way, maximising the van der Waals interactions. Calculated structure of the aggregate of compound **G** also shows a right-handed helical structure (Figure 43).

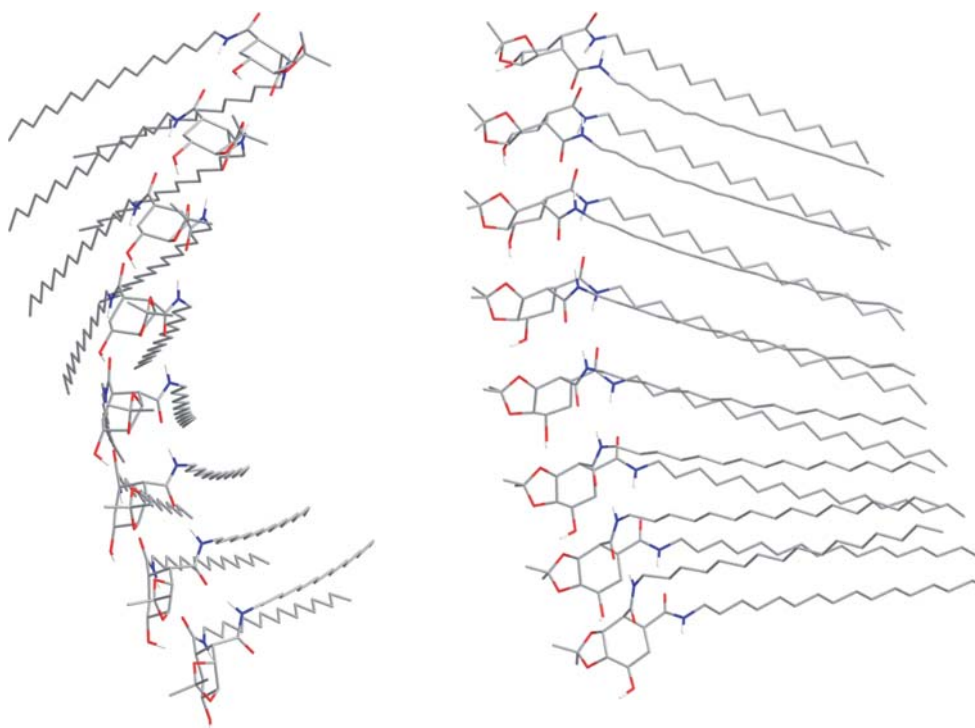


**Figure 43.** Frontal and side view of the predicted structure of the octameric aggregate of compound **G**. Non-polar hydrogen atoms were omitted for clarity.

As we have hypothesised studying the HSPs graphics, compound **H** should have two different aggregation patterns, which are denoted as **H'** and **H''**. Figure 44 shows the predicted structure **H'** of an aggregate of compound **H**. As it is shown, it forms a non-helical aggregate where the molecules are placed in a zigzag disposition. The free OH groups are forming intermolecular hydrogen bonds favouring the aggregation. In addition, we tried to predict a structure where these free OH groups form hydrogen bonds with another molecule placed in front of the other.

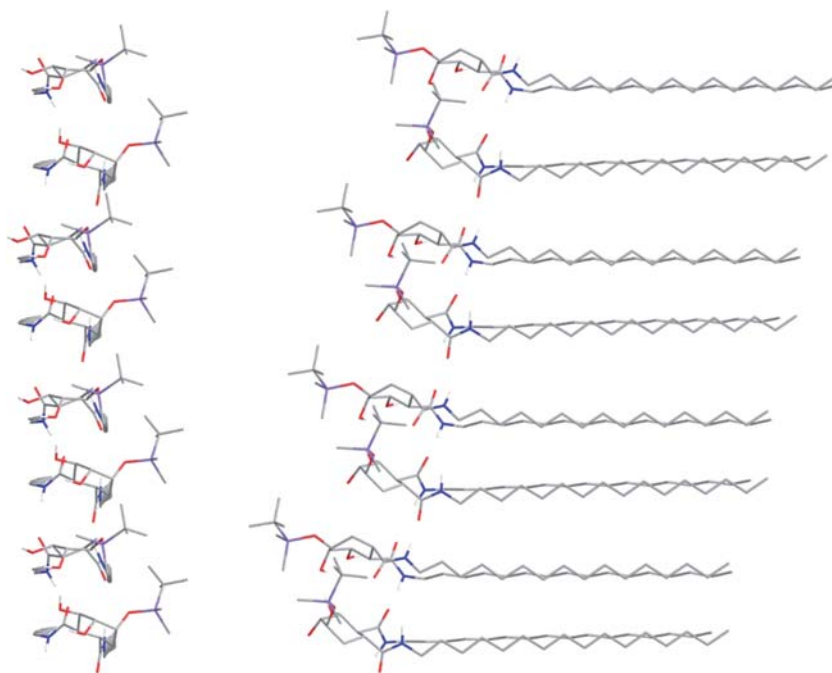


**Figure 44.** Frontal and side view of the predicted structure **H'** of the octameric aggregate of compound **H**. Non-polar hydrogen atoms were omitted for clarity.

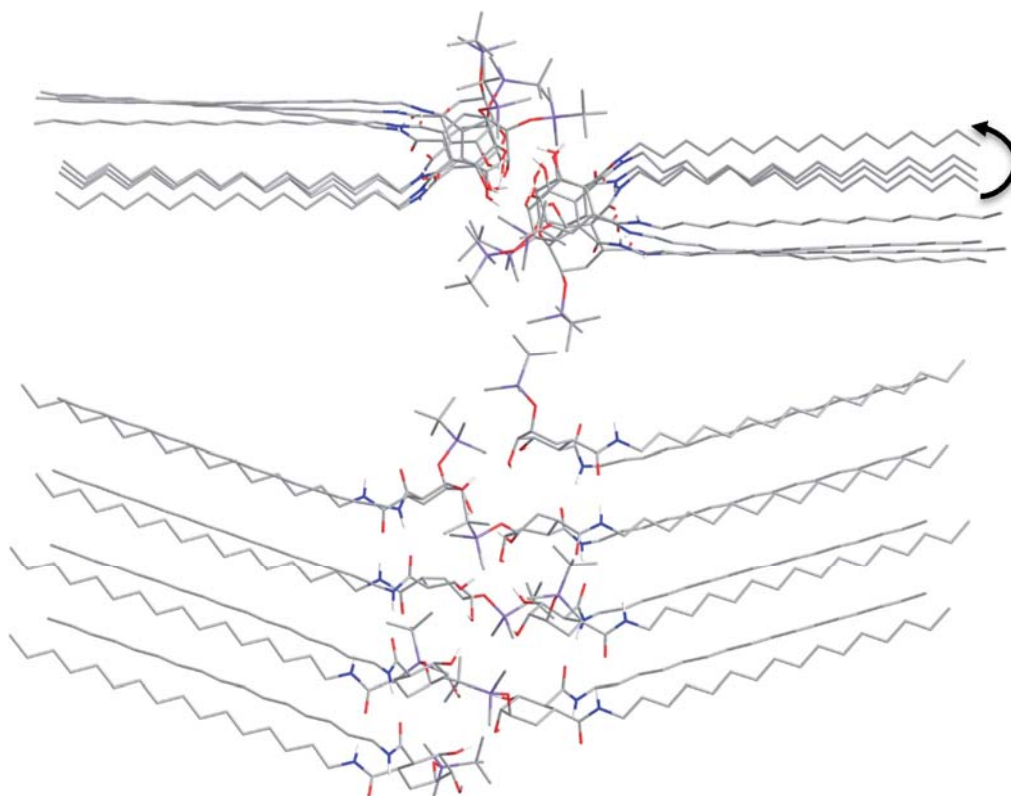


**Figure 45.** Top and side view of the predicted structure **H''** of the octameric aggregate of compound **H**. Non-polar hydrogen atoms were omitted for clarity.

Predicted structure **H''** shows that compound **H** can self-assemble forming hydrogen bonds through the free OH groups, forming an aggregate which shows a torsion that will produce some helicity to the aggregate (right-handed helix). Thus, **H** can adopt two different aggregation patterns. Comparing predicted structure **H'** and predicted structure **H''**, it is shown that while **H'** forms a zigzag orientation of the hydrogen bonds, **H''** has a parallel orientation forming a helical aggregate. Studying the circular dichroism of xerogels of **H** from two different solvents, one of each area from the HSPs space, we could be able to determine which structure corresponds to each one.

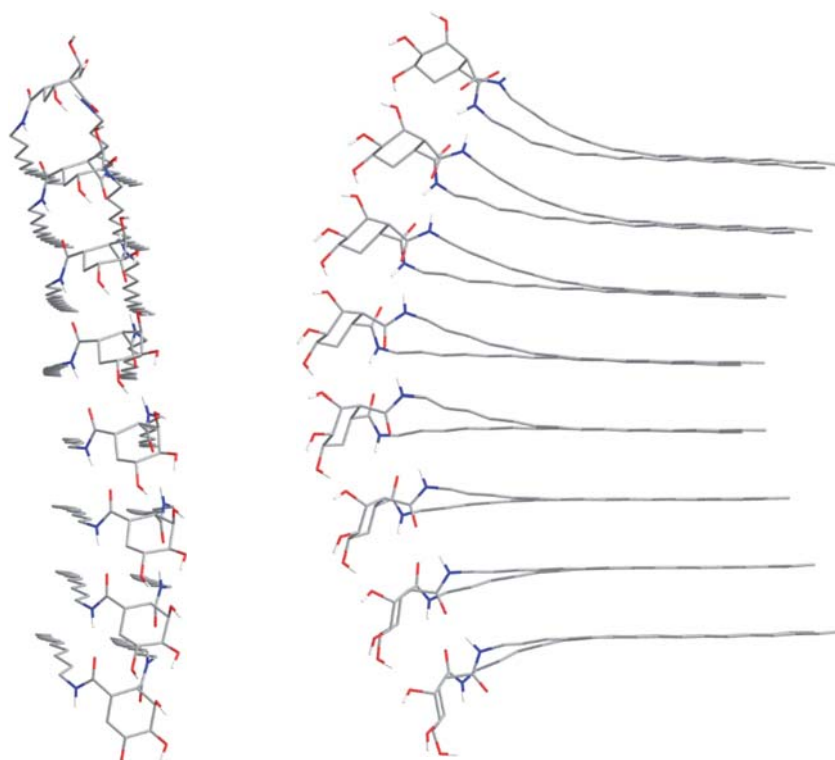


**Figure 46.** Predicted structure **I'** of the octameric aggregate of compound **I**. Non-polar hydrogen atoms were omitted for clarity.

Finally, predicted structure **I'** of compound **I** is shown in Figure 46. Aggregate of compound **I** shows a non-helical aggregation. As it is shown, the distance between chains is shorter than the needed distance to form the intermolecular hydrogen bonds with the free OH groups. Looking at this structure and thinking about its strange behaviour, we have thought the possibility of this compound to form another aggregate through the free OH groups, as compound **H**. In this way, the OH groups of the molecule would be “busy” forming hydrogen bonds and could not interact with the solvent, which could explain why



it is insoluble in alcohols. However, if the polar head of this organogelator is strongly linked to another polar head, then the available part of the molecule could be the amide groups and the long chains, which would explain why it behaves as the non-substituted cyclohexane-based compounds of family A. The predicted structure **I''** of the organogelator **I** is shown in Figure 47.

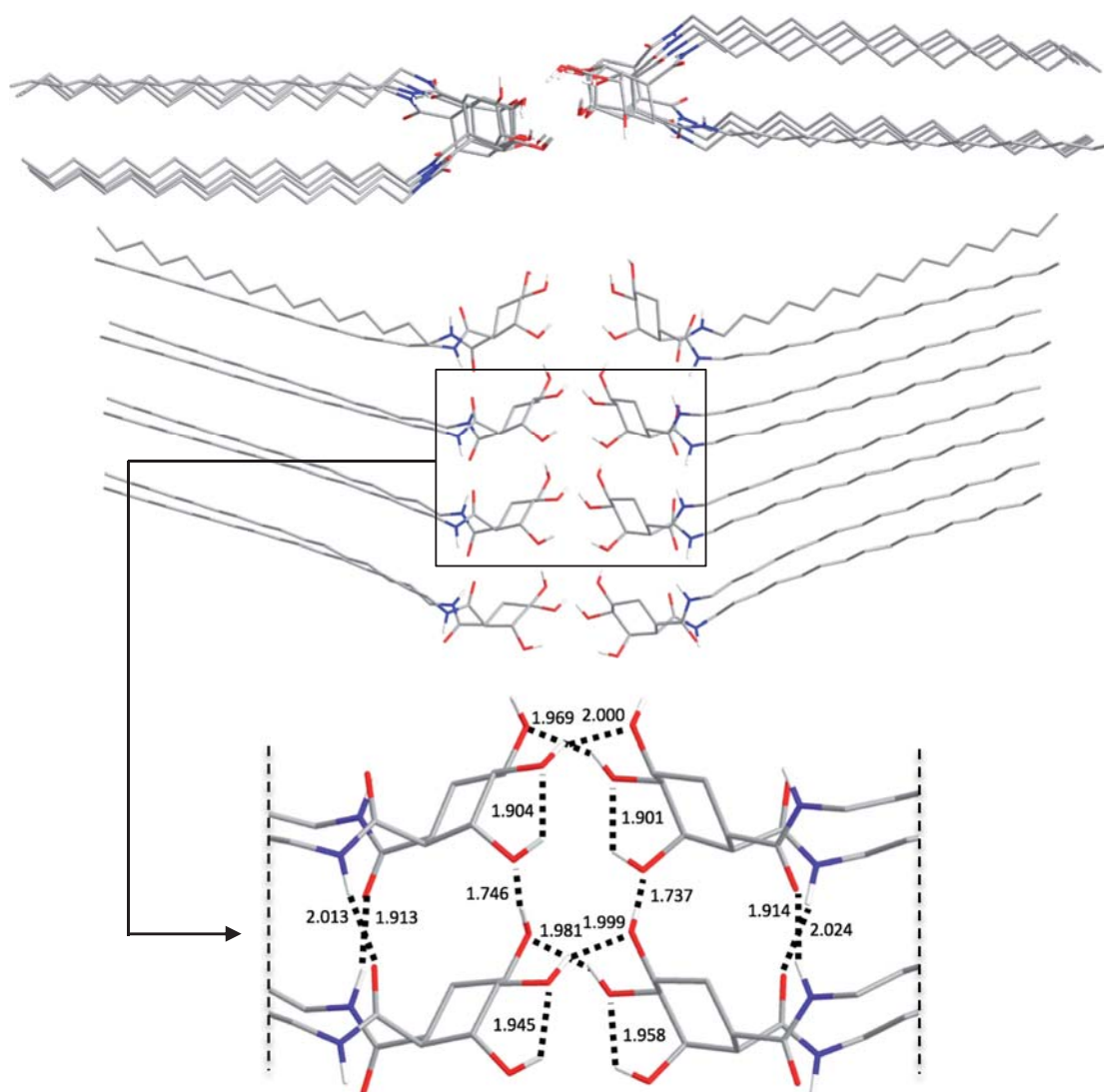


**Figure 47.** Top and side views of the predicted structure **I''** of the octameric aggregate of compound **I**. Non-polar hydrogen atoms were omitted for clarity. Distances are shown in Å.

As it is shown, the free OH groups form a kind of network of intermolecular and intramolecular hydrogen bonds. The predicted aggregate shows that molecules can

interact with another molecule in the same plane and then, this dimer is able to grow up to form the non-helical aggregate.

In order to determine the stability of this predicted structures, the aggregation energy of the formation of the dimer, the tetramer, the hexamer and the octamer was calculated. In addition, the aggregation energy per molecule was calculated with a M06-2X/6-31G(d) level of theory and including the BSSE correction. Aggregation energy ( $\Delta E_{\text{agg}}$ ) and aggregation energy per molecule ( $\Delta E_{\text{agg}}/n$ ) are shown in Figure 48.

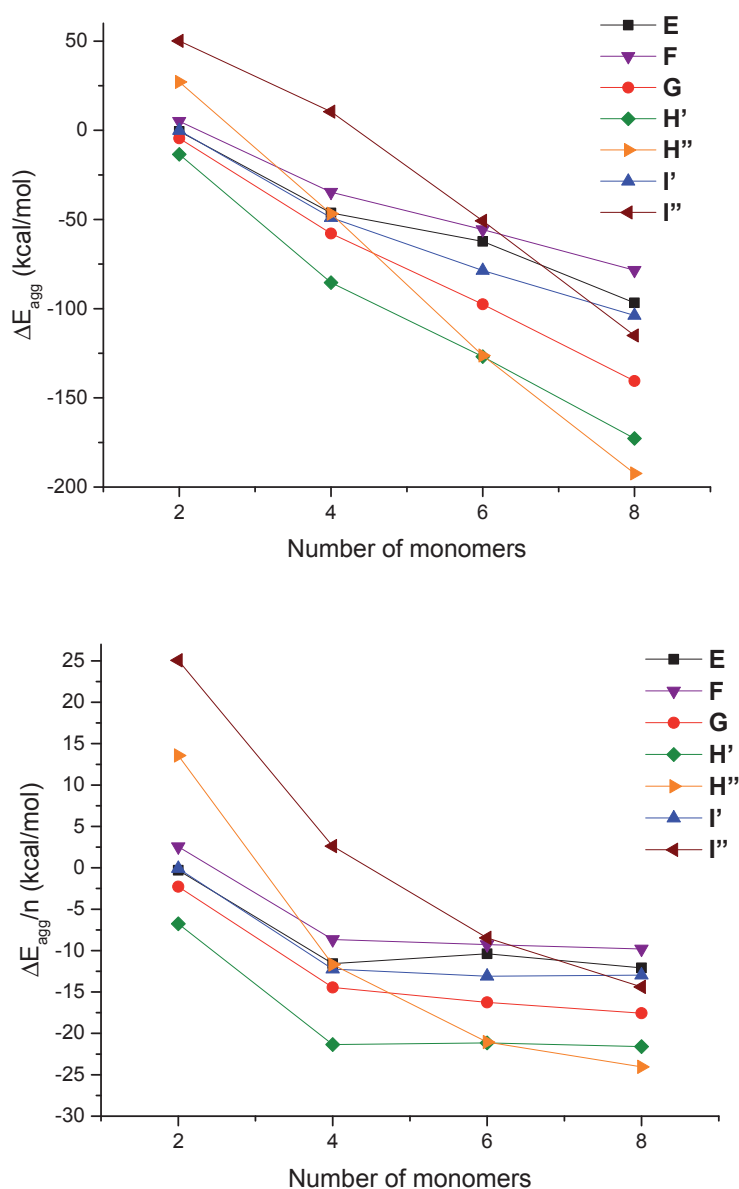


**Figure 48.** Aggregation energies (a) and aggregation energies per monomer (b) of the compounds E, F, G, H and I.

As shown in Figure 48a, the aggregation of all the compounds to form the predicted structures is favourable because the aggregation energy becomes more negative as the number of monomers increases. However, compounds that have two different aggregations (**H** and **I**) show more information. The formation of the dimer through the OH groups is in both cases not favourable because the aggregation energy of the formation is positive, but the formation of the tetramer, the hexamer and the octamer is favourable. This fact means that first of all, the monomer self-assemble through the hydrogen bonds of the amides, and then in a second step, the formation of the aggregate through the OH groups is favourable. In addition, it is shown that the aggregation energy to form the octamer with the predicted structures **H''** and **I''** is more negative (more favourable) than the formation of the octamer with the predicted structure **H'** and **I'**, although it is also favourable, giving the possibility of the coexistence of both structures.

The aggregation energy per monomer show that in these cases, a cooperative effect can only be observed until the formation of the tetramer because then the  $\Delta E/n$  remains nearly constant. However, structures **H''** and **I''** show a strong cooperative effect because the aggregation energy per monomer is still decreasing until the formation of the octamer.

In the case of organogelator **H**, as it was observed using HSPs, each predicted structure has to be correlated with a region in the HSPs space. The next challenge is to determine which structure corresponds to each group of solvents. Other techniques such as circular dichroism could help us to find out the solution.

In the case of organogelator **I**, also the two predicted structures are favourable. However, the network of inter- and intramolecular hydrogen bonds formed by the free OH groups seems to be very strong compared with the predicted structure **H''**. We could suggest that **H''** is formed at least in polar solvents. This could explain why this compound is insoluble in these kind of solvents, because the free OH groups could not interact with the solvent, forming a precipitate. To determine the structure of this compound in apolar solvents, which is able to gel, circular dichroism of the xerogels has to be carried out. Looking at the aggregation energies per monomer, it is shown that as in the case of Family 1, the energy decrease until it reaches a minimum, which means that there is a cooperative effect to start the self-assembly, but once a certain number of molecules are assembled,

the aggregation energy of each monomer remains constant keeping the aggregation favourable.

### 5.3.2.4 Circular Dichroism

Circular dichroism of this family of compounds was carried out in solution and in xerogel phase because they are mostly soluble in methanol. In this way, we could find out if the chirality of a single molecule is retained or if its chirality is lost but a new chirality of the aggregate is induced.

First of all, compounds **E** and **F** were studied (Figure 49). Xerogels were obtained by drying the obtained gels at the *mgc* in methanol.

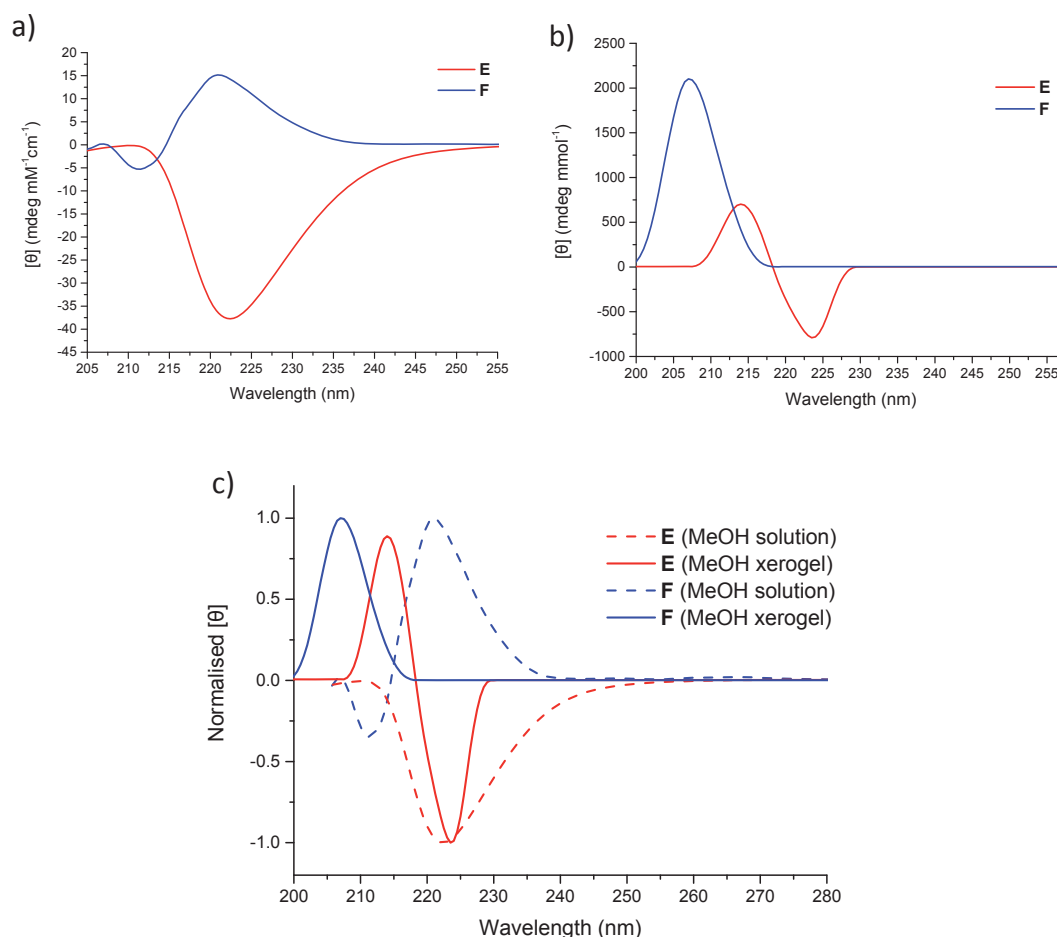


**Figure 49.** a) CD spectra of organogelators **E** and **F** in methanol solution at 2.43 and 2.68 mM respectively at 25 °C. b) CD spectra of organogelators **E** and **F** in xerogel phase (obtained from methanol) at 0.027 and 0.019 mmol/g of KBr respectively at 25 °C. c) Normalised CD spectra in solution and in xerogel phase of compounds **E** and **F** at 25 °C.

In solution **E** presents a negative band with a maximum at 222 nm and **F** a positive band with a maximum at 221 nm and a smaller band at 211 nm which generates a non-symmetrical bisignate signal. This maximum is related to the amide groups, which are the chromophore groups with induced chirality. In xerogel phase, the shape of the CD spectra are different. The signal of compound **F** has shifted and it has a maximum at 207 nm. This blue shift is related to the difference between the intramolecular hydrogen bonds of the amide groups and the intermolecular hydrogen bonds that are formed between molecules. The band of compound **E** has disappeared and now it shows a bisignate signal at 218 nm, also showing a blue shift. In both cases, the chirality of the single molecule in solution is lost in the self-assembly process, forming a chiral aggregate, which demonstrates that the studied solid retains the structure of the gel without the solvent (which means that the xerogel was obtained).

The CD spectra of these organogelators in solution were calculated taking into account 50 excited states (Figure 50) following the methodology of other studies described in the literature.<sup>123,124</sup> Predictions are in good agreement with the experimental spectra showing a negative band for compound **E** and a positive band for compound **F**, which are the main peaks.

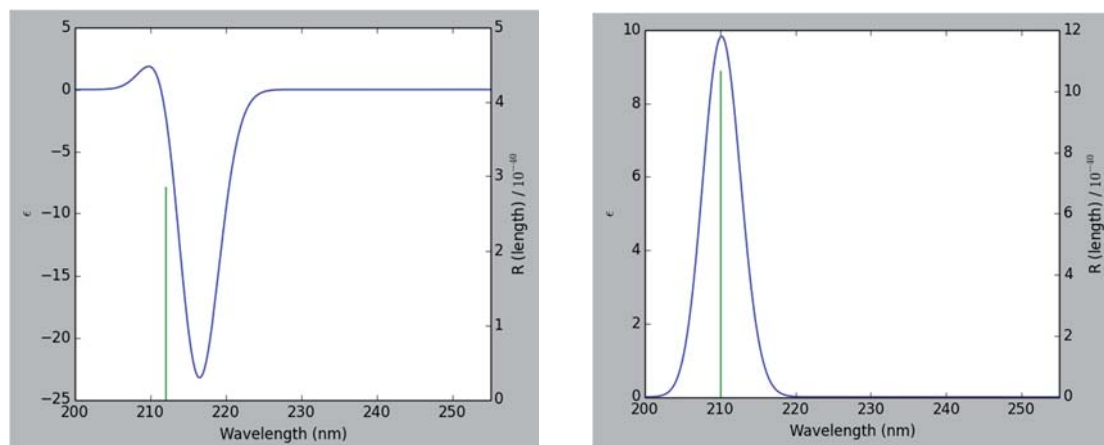


**Figure 50.** Predicted CD spectra of compounds **E** (left) and **F** (right).

Furthermore, the relative intensity of the predicted spectra is in agreement with the experimental values. The intensity of the band of compound **E** is approximately the double than the intensity of the band of compound **F**.

Comparing the CD spectra of the xerogels with the predicted structures, it is important to remark that **F** shows a band and the aggregate shows a helical structure, like **C** and **D**, while **E** shows a bisignate Cotton effect and its aggregate is non-helical with a curvature.

Organogelator **G** shows also a variation in the shape of the CD spectra in solution and in xerogel phase. The xerogel was obtained by drying the obtained gel at the *mgc* in toluene. As shown in Figure 51, it presents a bisignate signal with zerocrossing at 226 nm in solution, whereas it presents a band at 203 nm in xerogel phase, with a significant blue shift. In this case, the predicted structure of this compound has a helical torsion, which would be in agreement with the band in the CD spectra in xerogel phase, as shown in the previous cases.

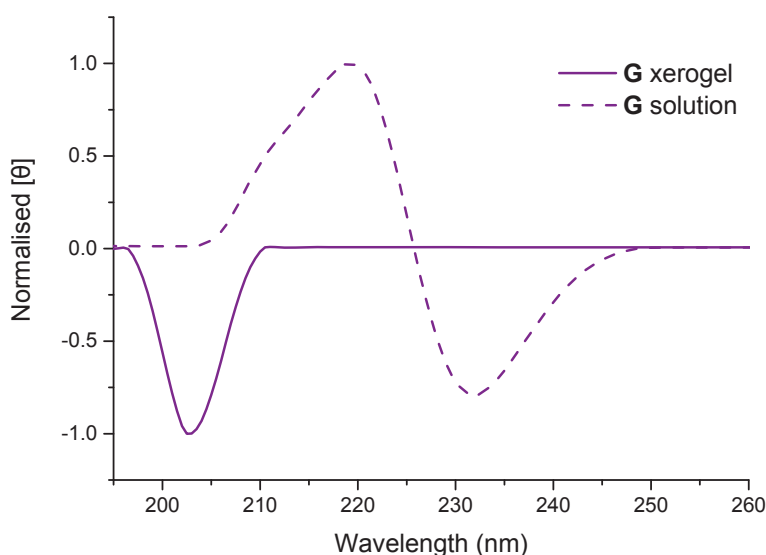


**Figure 51.** Normalised CD spectra of organogelator **G** in methanol solution at 2.47 mM and in xerogel phase at 0.020 mmol/g of KBr at 25 °C.

Studied xerogels of organogelator **H** were obtained from the gels at the *mgc* in pentane and in acetone in order to find out differences between regions of the HSPs space.

In xerogel phase, compound **H** shows different CD shapes depending on the solvent, which is in agreement with other experimental and theoretical evidences (Figure 52). The xerogel obtained from the gel in pentane shows a band at 206 nm, while the xerogel obtained from the gel in acetone shows a bisignate signal with zerocrossing at 204

nm. Predicted structure **H'** shows a zigzag conformation of the hydrogen bonds and forms a non-helical aggregate. Taking into account the acquired knowledge of this kind of compounds, this structure should give a bisignate Cotton effect on the CD spectrum. Thus, we could suggest that compound **H** self-assembles into an aggregate with the predicted structure **H'** in polar solvents such as acetone. Furthermore, predicted structure **H''** shows an aggregate with a torsion that generates a helical structure, which could be related to a band in the CD spectrum. Thus, we could say that compound **H** self-assembles forming an aggregate with a predicted structure **H''** in apolar solvents such as pentane. Therefore, we could be able to determine which structure has each region of solvents from the HSPs space.

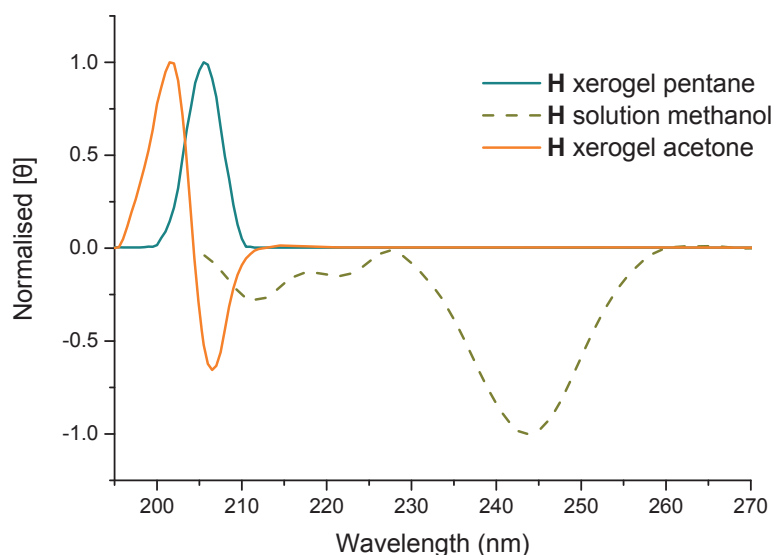


**Figure 52.** Normalised CD spectra of organogelator **H** in methanol solution at 2.56 mM and in xerogels phase from pentane and acetone at 0.021 and 0.020 mmol/g of KBr at 25 °C, respectively.

Due to the low solubility of **I** in methanol, the intensity of the signal is very low and the result in solution cannot be considered as good as in the other cases, but it can be used just to compare it with the CD spectra registered in xerogel phase. The xerogel was obtained by drying the obtained gel at the *mgc* in toluene. Figure 53 shows that while compound **I** shows a band in solution, in xerogel it presents a clear bisignate Cotton effect with a zero-crossing at 205 nm. After different coincidences, we could say that a bisignate signal should correspond to a non-helical aggregate. However, both predicted structures

of the aggregates of **I** present non-helical aggregates, which is in agreement with the other cases but does not allow us to distinguish between the aggregation patterns. At this point, we could suggest that in polar solvents compound **I** self-assembles forming an aggregate like the predicted structure **I''**, but we cannot hypothesise if in apolar solvents the structure is **I'** or **I''**, or even whether it self-assembles or not.

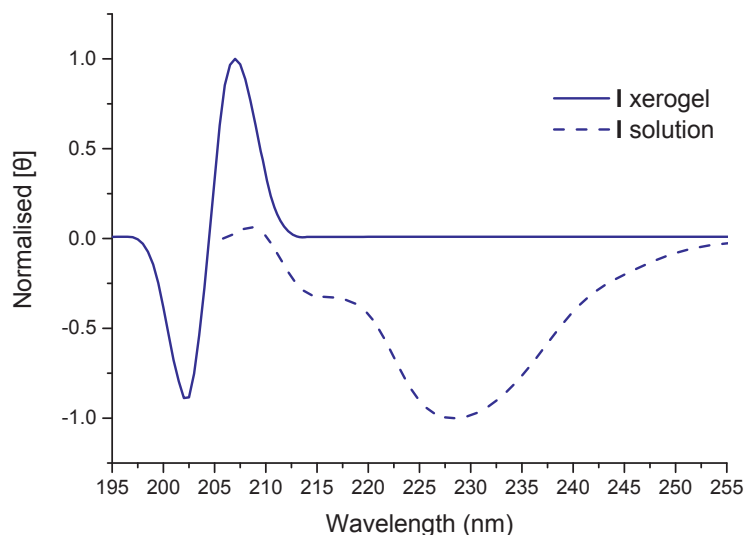


**Figure 53.** Normalised CD spectra of organogelator **I** in methanol solution at 2.17 mM and in xerogel phase (from toluene) at 0.021 mmol/g of KBr at 25 °C.

CD spectrum of **H** in solution shows a negative band at 244 nm, which can be likened to that of compound **I** in solution. As these two molecules are similar and have at least two free OH groups, the spectra are similar and it confirms that the registered spectrum of compound **I** is consistent despite having a low concentration.



### 5.3.3 Gelation study of Family 3

Family 3, described in page 63, are three substituted diamide-based cycloalkanes with a spacer. The gelation ability was studied in 14 common solvents following the same procedure as in Family 1 and 2. To determine the presence of a gel, the tube inversion test is used. Table 13 summarizes the study showing the behaviour of each LMWG in each solvent.

**Table 13.** Gelation behaviour of compounds **J**, **K** and **L** in common solvents.

Compound	Pentane	1,4-dioxane	Toluene	Et <sub>2</sub> O	CHCl <sub>3</sub>	EtOAc	THF	CH <sub>2</sub> Cl <sub>2</sub>	iPrOH	Acetone	EtOH	MeOH	CH <sub>3</sub> CN	H <sub>2</sub> O
<b>J</b>	S	S	S	S	S	S	S	S	S	I	53 <sub>0</sub>	65 <sub>0</sub>	I	I
<b>K</b>	I	S	S	S	S	S	S	S	S	S	S	I	29 <sub>0</sub>	I
<b>L</b>	S	S	S	I	S	I	S	S	S	I	S	S	I	I

Dielectric constant increases from left to right.

C: Clear T: Translucid O: Opac

Minimum gelation concentration in mg/mL.

I: Insoluble, S: Soluble.

Organogelator **J** can gel only ethanol and methanol. To find out the influence of the CH<sub>2</sub> spacer, it can be related to compound **E**, which has the same stereochemistry and the same substitutions. As it is shown, they can gel methanol and ethanol but **J** does at higher *mgc* values than **E**. In addition, **J** is less soluble in polar solvents due to the effect of the spacer and it cannot gel none of the other solvents. Gelation ability was decreased by the presence of the spacer.

Organogelator **K** seems to be an acetonitrile-selective organogelator and with a relatively low *mgc* value. It can be compared with compound **G**, and the behaviour is completely different. In this case, the spacer gives more solubility in apolar solvents while promotes a specific gelation behaviour in acetonitrile.

Finally, compound **L** was not able to gelate any of the solvents considered. Compared with compound **I**, in this case, the spacer solves the problem of the insolubility with alcohols, but then it cannot gelate neither dioxane, toluene nor chloroform. As explained before, **I** has two different aggregations that explain the gelation behaviour. In

this case, the CH<sub>2</sub> spacer disfavours the self-assembly avoiding the aggregates and leading the free OH groups interacting with the OH groups from the hydroxylic solvents. Furthermore, as the spacer disfavours the aggregation, it loses the ability to self-assemble and to gel other solvents. Gels were stable at room temperature and were also reversible body temperature.

In general, the spacer reduces the gelation abilities of these organogelators probably due to the desymmetrisation of the chains.

### 5.3.3.1 Theoretical Calculations

In order to identify visually the effect of the spacer, theoretical calculations following the same procedure as with Family 1 and 2 were carried out.

Predicted structures of the octameric aggregates from **J** and **K** show a left-handed helical aggregation in both cases (Figure 54 and Figure 55, respectively).

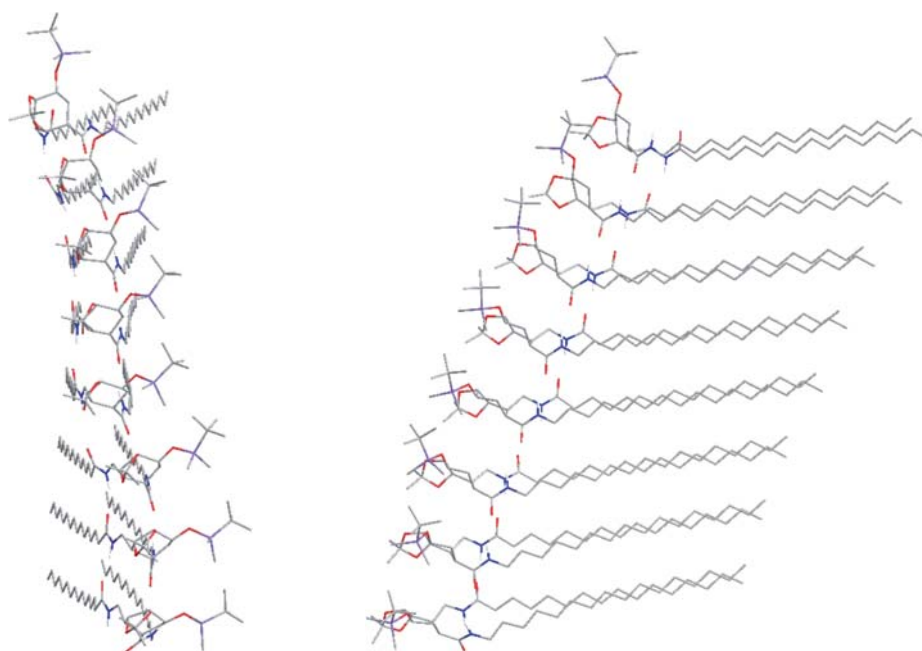


**Figure 54.** Frontal and side views of the predicted structure of the octameric aggregate of compound **J**. Non-polar hydrogen atoms were omitted for clarity.

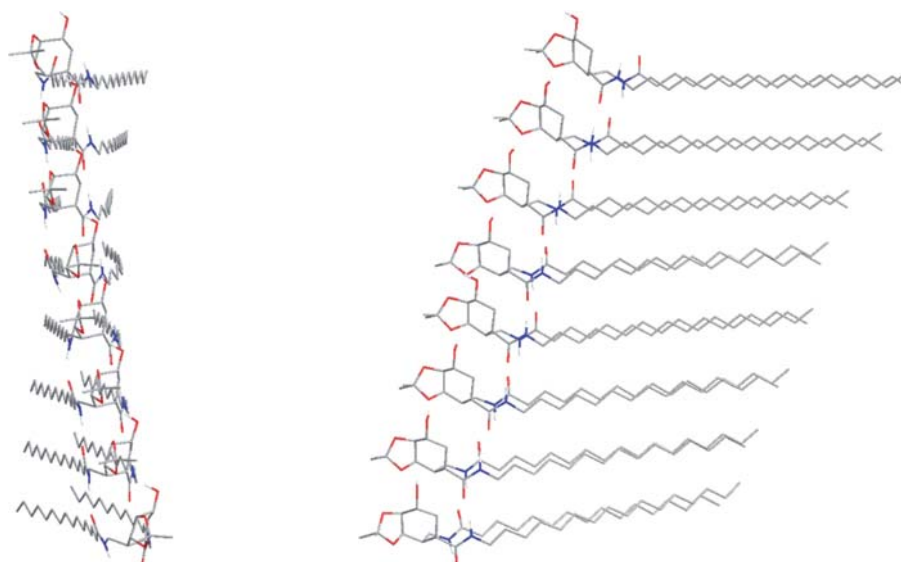


**Figure 55.** Frontal and side views of the predicted structure of the octameric aggregate of compound **K**. Non-polar hydrogen atoms were omitted for clarity.

Aggregation energies and aggregation energies per molecule (Figure 56) were calculated with a M06-2X/6-31G(d) level of theory and including the BSSE correction. They show that the CH<sub>2</sub> spacer disfavours the self-assembly, which is in agreement with the gelation study. The energies of compounds **J** and **K** were compared with compounds **E** and **G** in order to better realise the influence of the spacer. **E** can be directly compared with **J**, and **G** with **K**. Aggregation energies of the formation of the dimers are more favourable for **J** and **K** than for **E** and **G**, while when increasing the number of monomers, the energy values become less favourable.

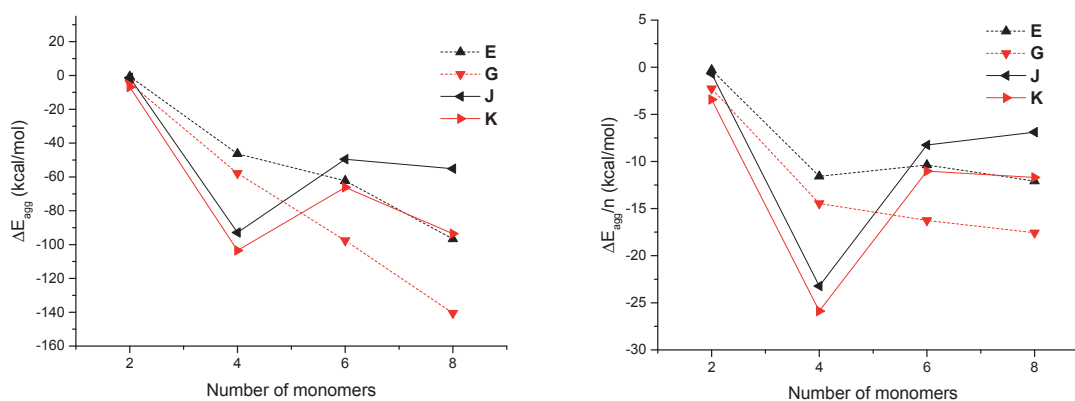


**Figure 56.** Aggregation energies (a) and aggregation energies per monomer (b) of compounds **J** and **K** (solid lines) and **E** and **G** (dash lines).

### 5.3.3.2 Circular Dichroism

Circular dichroism spectra of these organogelators in solution and in xerogel phase were recorded. Xerogels were obtained by drying the gels obtained in methanol for **J** and in acetonitrile for **K** at the *mgc* (Figure 57).

Both compounds show a band in both solution and in the xerogel phase. However, the maximum of these bands has changed and also the sign in the case of compound **K**. In solution, compound **J** and **K** show a positive band at 224 and 221 nm respectively. In xerogel phase, **J** shows a positive band at 213 nm while **K** shows a negative band at 217 nm. This means that the chirality of a single molecule showed in solution is not observed in the xerogel phase and it means that chiral aggregates are formed.

Taking into account the acquired experience in the CD spectra of these kind of compounds, a band in the spectra could be related to the parallel relative orientation of the dipoles of the chromophore groups with induced chirality, which gives to the aggregate a helical structure. In agreement with this knowledge, the predicted structures of the aggregate of these two compounds show a helical aggregate.

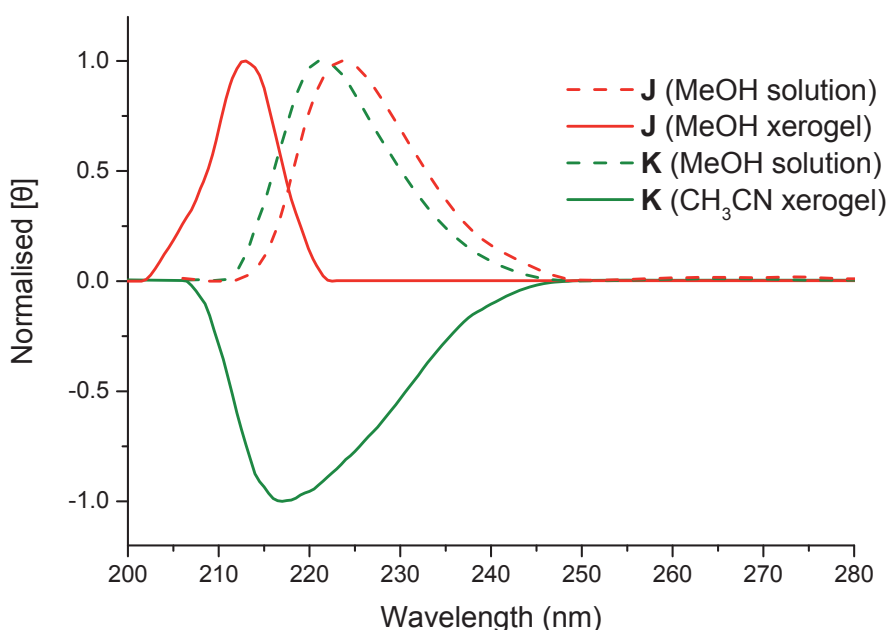


**Figure 57.** Normalised CD spectra of organogelator **J** and **K** in methanol solution at 2.56 and 2.19 mM, respectively, and in xerogel phase of **J** from methanol and of **K** from acetonitrile at 0.020 and 0.021 mmol/g of KBr at 25 °C, respectively.

## 5.4 Summary and Conclusions

In this part of the thesis, the gelation abilities of three different families of carbocyclic diamide-based LMWGs were studied and the *mgc* of the obtained gels was determined. HR-NMR and SEM done by Dr. Marta Sans were included in this chapter to better analyse these gelators. CD and theoretical calculations were done in order to study their supramolecular systems.

Looking at the CD and the theoretical calculations, in all studied cases, predicted non-helical or zigzag aggregates show a bisignate Cotton effect in xerogel phase whereas predicted helical structures show monosignate bands in xerogel phase. In this thesis, we hypothesise that it could be related to the relative position of the amides, which are forming the backbones of the aggregate. With this hypothesis we have tried to rationalise the obtained predicted structures with the obtained CD spectra, which seems to be coherent with other published works.<sup>72,92,95–99,125,126</sup>

Furthermore, in all cases, a blue shift is observed between the CD spectra of the monomers in solution and the CD spectra of the xerogels. A blue shift in  $\pi \rightarrow \pi^*$  transitions is associated to H-type aggregates, in which the absorption is more energetic than the absorption of the monomer suggesting a strong interaction between the amide-groups of the monomers and, thus, the wavelength of the maximum is shifted to lower wavelengths.<sup>125,127</sup> Structure of the predicted aggregates can be related with H-type aggregates,<sup>125</sup> which show that the direction of aggregation of the monomers is roughly perpendicular to the plane of the monomer. Also it is consistent with other studies with similar organogelators.<sup>73</sup>

Stereochemistry and ring size have an influence on the aggregation pattern. Amide groups form the backbone of the aggregate and thus, aggregation structure depends on the relative position of the amide groups. However, in the substituted carbocycles, other hydrogen bonds between monomers are formed and then, stereochemistry has less influence on the final aggregation. The contribution of all the hydrogen bonds has to be considered.

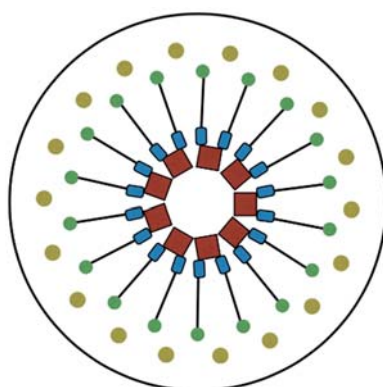
It is observed that while theoretical calculations are in agreement with the experimental circular dichroism of the xerogels, any strong relationship between the

structure of the aggregate and the gelation behaviour was not observed. If there was clear relationship then we could be able to carry out *a priori* predictions of the gelation behaviour of a gel only using theoretical calculations. However, as it is known, the way to find the “Holy Grail” is not so easy.

The effect of having a CH<sub>2</sub> spacer seems not to favour the gelation abilities. Comparing compounds of Family 3 with their homologues from Family 2, the gelation ability is reduced in all cases except with compound **K**, which have an unexpected behaviour gelating selectively acetonitrile in a relatively low *mgc*.

Finally, what plays an important role to the gelation behaviour are the different substitutions of the ring. Compounds having a TBDMS protection are able to gelate alcohols, while compounds with 1 or 2 free OH groups are able to gelate apolar solvents. As it is observed, it seems to be evident that the organogelator does not interact with the solvent using its substitutions. The gelation ability has to be related to the effect that these molecules with these substitutions play inside the solvent, changing the surface tension and increasing the energy of the system.





## **6. Cationic bolaamphiphiles with a cyclobutane scaffold: behaviour as surfactants**

---





## 6. Cationic bolaamphiphiles with a cyclobutane scaffold: behaviour as surfactants

### 6.1 Introduction

Amphiphilic molecules are those that have both hydrophilic and hydrophobic properties. Amphiphilic compounds which are surface-active agents are commonly referred as surfactants.<sup>128–130</sup> Surface active agents mean that these compounds are able to lower the surface tension of a certain liquid-air interface, normally air-water. Surface tension is the energy needed to increase the surface one unit of area. It is a phenomenon promoted by the cohesive forces between liquid molecules. Liquid molecules at the surface interact with themselves and the liquid acquires the minimum possible surface area. They produce foam due to their action at the air-water interface, and they make the grease transfer from dirty hands into the soapy water as a result of its activity at the water-oil (grease) interface.<sup>131</sup>

Due to their amphiphilic behaviour, at low surfactant concentration, molecules are placed at the air-water interface by keeping the hydrophilic part in water and the hydrophobic tail pointing out to the air. When increasing the concentration, molecules are adsorbed at the interface. The presence of hydrophobic chains at the air-water interface causes the decrease of the surface tension of the water molecules. This process can be described using the Gibbs adsorption isotherm (Equation 6), which describes the maximum Gibbs surface excess ( $\Gamma_{max}$ ) and relates the surface tension ( $\gamma$ ) of the aqueous with the concentration of surfactant (C).<sup>132</sup>

$$\Gamma_{max} = \frac{-1}{nRT} \left( \frac{d\gamma}{d \ln C} \right) \quad (\text{Equation 6})$$

At a certain concentration, surfactant molecules start to self-assemble forming aggregates called micelles where the hydrophobic tails are kept at the interior of the aggregate, far from the water. This concentration is called critical micelle concentration (CMC). However, not all surfactants form micelles but they form other aggregates such as vesicles or fibers (Figure 58). Sometimes, CMC is referred as critical aggregation concentration (CAC) in order to try to be more scientifically correct, but CAC is used in other fields like when studying the interaction of surfactants with polymers.<sup>133</sup> Thus, in this

thesis, CMC will be used as most of works to describe the concentration at which surfactants start to self-assemble into aggregates despite having other morphologies.

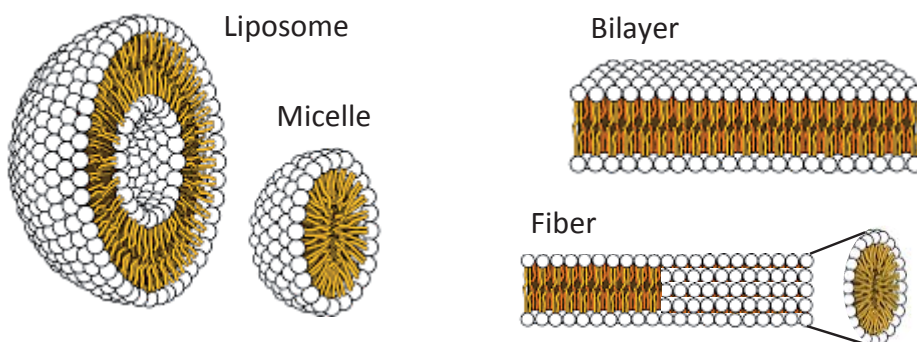


**Figure 58.** Examples of aggregates of amphiphiles.

To determine the CMC, different techniques can be used because many physical properties of these solutions show an abrupt change near the CMC. It is important to remark that CMC is not an exact value but it is a range of concentration at which surfactant molecules start to aggregate. Then, depending on the physical property, the abrupt change can be observed with a certain variation with respect to other methods. Figure 59 shows how different physical properties show an abrupt change at the range of CMC.<sup>134</sup>

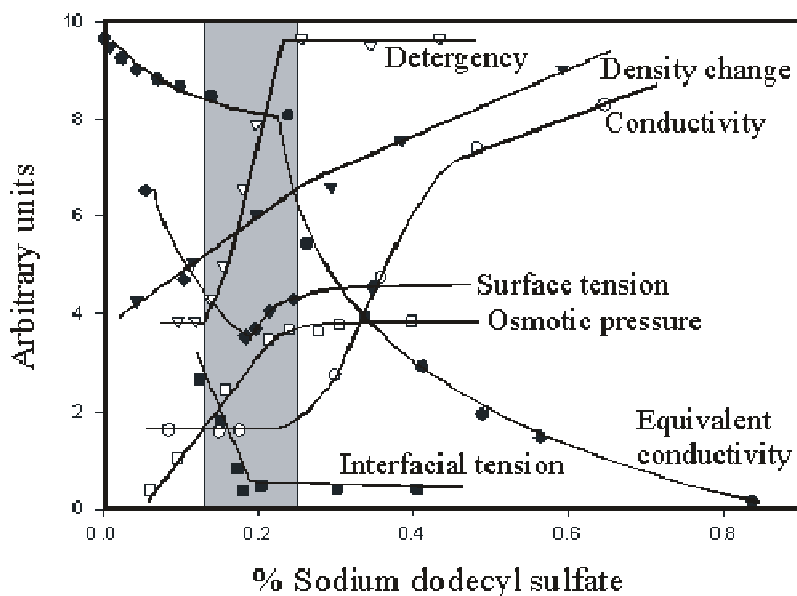


**Figure 59.** Representation of the abrupt changes of different physical properties at the CMC.<sup>134</sup>

One of the most used techniques is based on measuring the surface tension of the water-air interface at different surfactant concentrations. It can be measured using different methods such as Wilhelmy plate,<sup>135</sup> du Noüy ring,<sup>136</sup> drop weight<sup>137</sup> or by volume and shape of the drop.<sup>138,139</sup> The latter is commonly referred as pendant drop method and is the method used in this thesis to determine the CMC.

Pendant drop method consists in fitting the experimental points of the shape of a drop with the Young-Laplace equation, which is a differential equation, and surface tension of the drop can be determined by iteration.

Water has a surface tension around 72 mN/m and due to this high surface tension, it forms drops. Organic solvents have lower surface tension values and for example hexane has a surface tension around 18 mN/m, thus, cohesive forces between hexane molecules are much lower and it is much more difficult to find a drop of hexane. An aqueous solution of a surfactant behaves as an organic solvent due to the reduction of the surface tension.

Surfactants, as discussed earlier, preferentially adsorb at interfaces and in doing so reduce the surface or interfacial tension. However, to better understand this, and to compare different surfactant structures, or different interfaces, it is helpful to quantify the extent to which they lower interfacial tension. This is accomplished by introducing efficiency and effectiveness.

Efficiency defines how much surfactant is required to induce a given decrease in surface tension. Effectiveness refers to the maximum reduction in surface tension that can be achieved for a given surfactant, regardless of concentration.<sup>140</sup>

It is interesting to note that the most effective surfactants are often not the most efficient, and vice versa. Efficiency is primarily determined by thermodynamics. That is how much more preferable it is to have material adsorbed at the interface rather than in the bulk, and so, larger hydrophobic tails tend to increase surfactant efficiency. Effectiveness is mainly related to the optimum surfactant packing at the interface and thus is determined broadly by the chemical structure/molecular shape of the surfactant.<sup>141</sup> Additional intermolecular bonds such as hydrogen bonds increase effectiveness of surfactants due to the strong interaction between them.<sup>142</sup>

The process of surfactant micellization is primarily an entropy-driven process. When surfactants are dissolved in water, the hydrophobic group disrupts the structure of water and therefore increases the Gibbs energy of the system. Surfactant molecules therefore concentrate at interfaces, so that their hydrophobic groups are directed away from the water and the Gibbs energy of the solution is minimised. The distortion of the water structure can also be decreased (and the Gibbs energy of the solution reduced) by the aggregation of surface-active molecules into clusters (micelles) with their hydrophobic groups directed toward the interior of the cluster and their hydrophilic groups directed toward the water. However, the surfactant molecules transferred from the solution to the micelle may experience some loss of freedom from being confined to the micelle. In addition, they may experience an electrostatic repulsion from other similarly charged surfactant molecules in the case of ionic surfactants. These forces increase the Gibbs energy of the system and oppose micellization. Hence, micelle formation depends on the force balance between the factors favouring micellization (van der Waals and hydrophobic forces) and those opposing it (kinetic energy of the molecules and electrostatic repulsion). The explanation for the entropy-dominated association of surfactant molecules is called the "hydrophobic effect" or "hydrophobic bonding".<sup>143</sup>

Surfactants can be classified depending on their polar head group or on their structure.<sup>144</sup>

Regarding the polar head group, surfactants are classified as:

- 1) Cationic: positively-charged head group
- 2) Anionic: negatively-charged head group
- 3) Zwitterionic: one positively-charged head group and one negatively-charged head group
- 4) Non-ionic: no charges

In the industry, anionic surfactants represent more than a 70 % of the production due to their use in different cosmetic products such as different kind of detergents, soaps, shampoos or tanning compounds, in the food industry and as foaming agents. Non-ionic surfactants represent more or less a 23 % of the production of surfactants, also due to their application in cosmetics, in paints and in the farm industry. Finally, cationic surfactants represent a 6 % while zwitterionic ones only 1 % of the market. Cationic

surfactants are commonly used as softeners in cosmetics and in the textile industry, but they find their most important use as biocides. Zwitterionic surfactants are used in some shampoos and other cosmetics as less irritant compounds for delicate skins. In our daily lives, different types of surfactants are in contact with our skins (or they should).<sup>131</sup>

Regarding the structure, surfactants are classified as (Figure 60):

- 1) Single head/single tail
- 2) Bola
- 3) Gemini
- 4) Double and triple chain
- 5) Catanionic

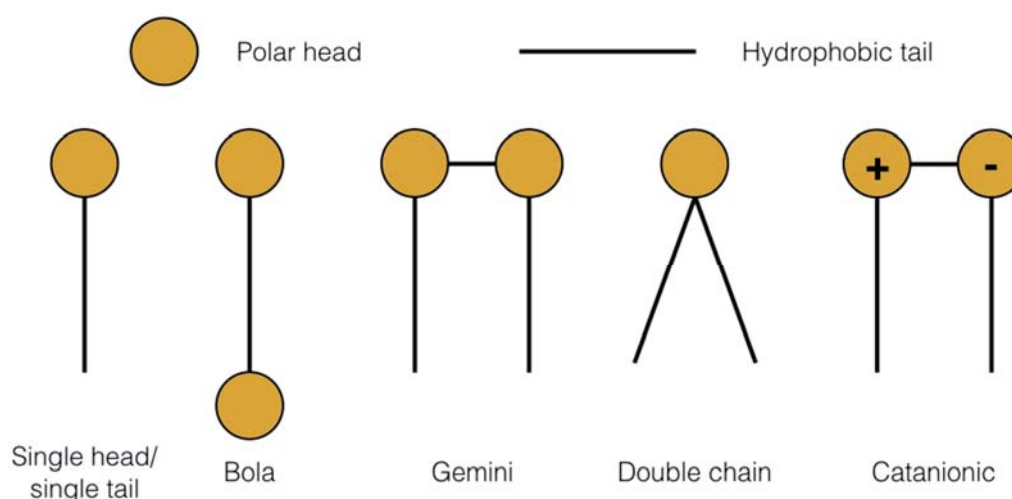


**Figure 60.** Classification of surfactants regarding the structure of the molecule.

Bola-type surfactants are also called bolaamphiphiles, bolaphiles, bola-form electrolytes, bolytes or even only bolas.<sup>145</sup> The name *bola* came from the Argentinian throwing weapon made of weights on the ends interconnected by a cord, designed to capture animals by entangling their legs, as shown in Figure 61.<sup>146,147</sup>

The aggregation morphologies of bolaamphiphiles are as variable as their molecular structures.<sup>148</sup> Nagarajan describes the effect of the polar head and the structure of the amphiphile on the morphology of the aggregate.<sup>149</sup>

Synthetic bolaamphiphiles try to reproduce the structure of a biological membrane and thus, can be used to stabilize a solubilised membrane protein, *Escherichia coli*



**Figure 61.** Argentinian bola weapon to capture animals.<sup>146,147</sup>

diacylglycerol kinase for example. Sanders and co-workers,<sup>150</sup> in 2009, obtained satisfactory results and they observe that certain bolaamphiphiles were considered to be lipid-like by providing activation of the enzyme catalytic activity. This work represented the first documentation of the potential of bolaamphiphiles for use in biochemical and biophysical studies of membrane proteins.<sup>151</sup>

On the other hand, the ability of amphiphiles to form self-organised aggregate structures has been used to template the synthesis of nano- and mesostructured materials. One of the most important cases of templating to synthesise mesoporous materials is that of amphiphile aggregates and silica units interacting in a non-covalent way, which makes the silica organize around the structure-directing agent, in this case the supramolecular aggregate. The silica units then react with each other to generate mesostructured materials. Afterwards, the amphiphile is removed by calcination, which leaves a mesoporous material.<sup>152</sup>

From the supramolecular point of view, bolaamphiphiles show an interesting behaviour. They can adopt different geometries at the air-water interface, depending on their structure. As they have two polar head linked by a hydrophobic tail, the structure at the surface should be folded. However, some studies show that they can form an elongated structure.

In relationship with Chapter 5, Hanabusa and co-workers studied different carbocyclic diamide-based compounds as gelators and as bolaamphiphiles (Figure 62).<sup>72,153,154</sup>

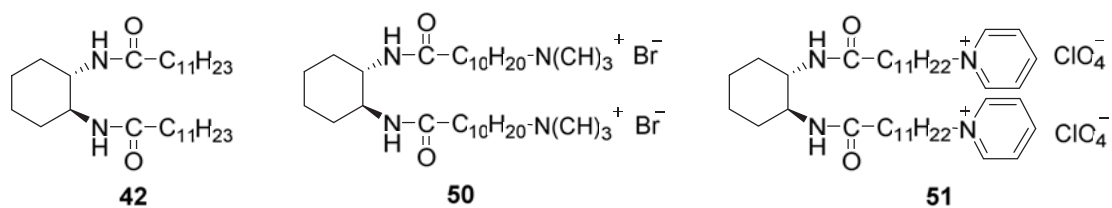


**Figure 62.** Hanabusa studied compounds.

These compounds show interesting supramolecular abilities and show chiral aggregations as can be shown in Figure 63.

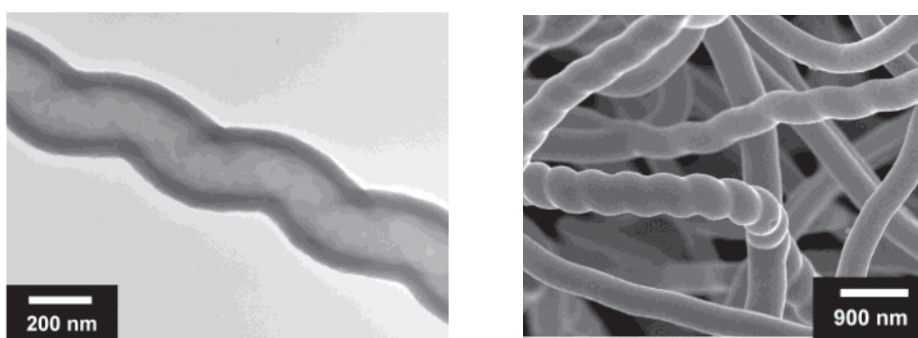


**Figure 63.** a) TEM picture of compound **51**. b) SEM picture of compound **51**.<sup>154</sup>

In our research group, different chiral bisurea-based or bisurea-based carbocyclic compounds were studied as organobridged silesquioxanes (compound **52** of Figure 64)<sup>12</sup> or as organogelators (Chapter 5).

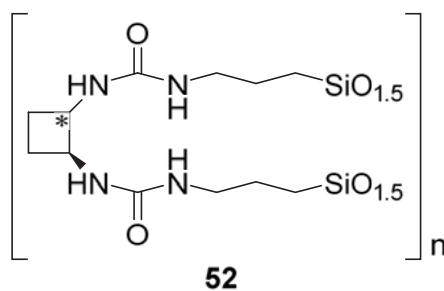


**Figure 64.** Chiral bisurea-based carbocyclic compound studied as organobridged silesquioxanes in our research group.



## 6.2 Objectives

In this part of the thesis, four chiral bolaamphiphiles based on a cyclobutane scaffold with two symmetric chains were studied as surfactants. Special attention was focused on the study of the influence of the relative stereochemistry and the regiochemistry on their aggregation properties. (Figure 65).

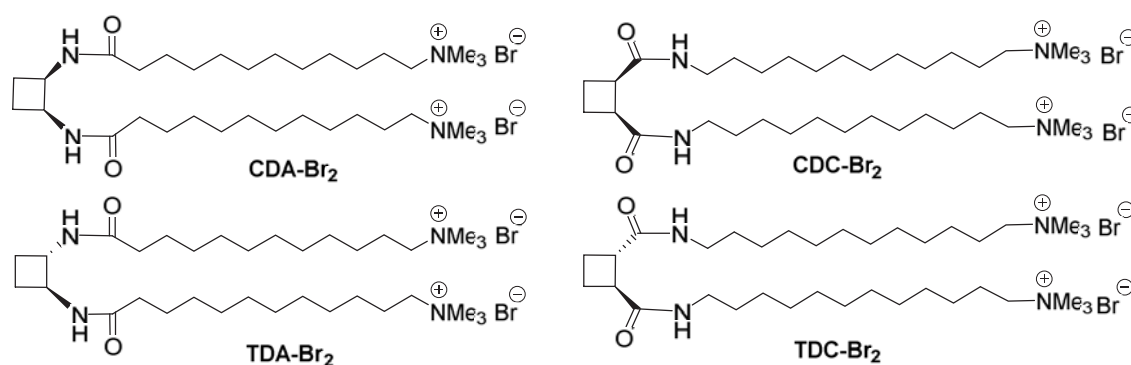


**Figure 65.** Structure of the four studied bolaamphiphiles.

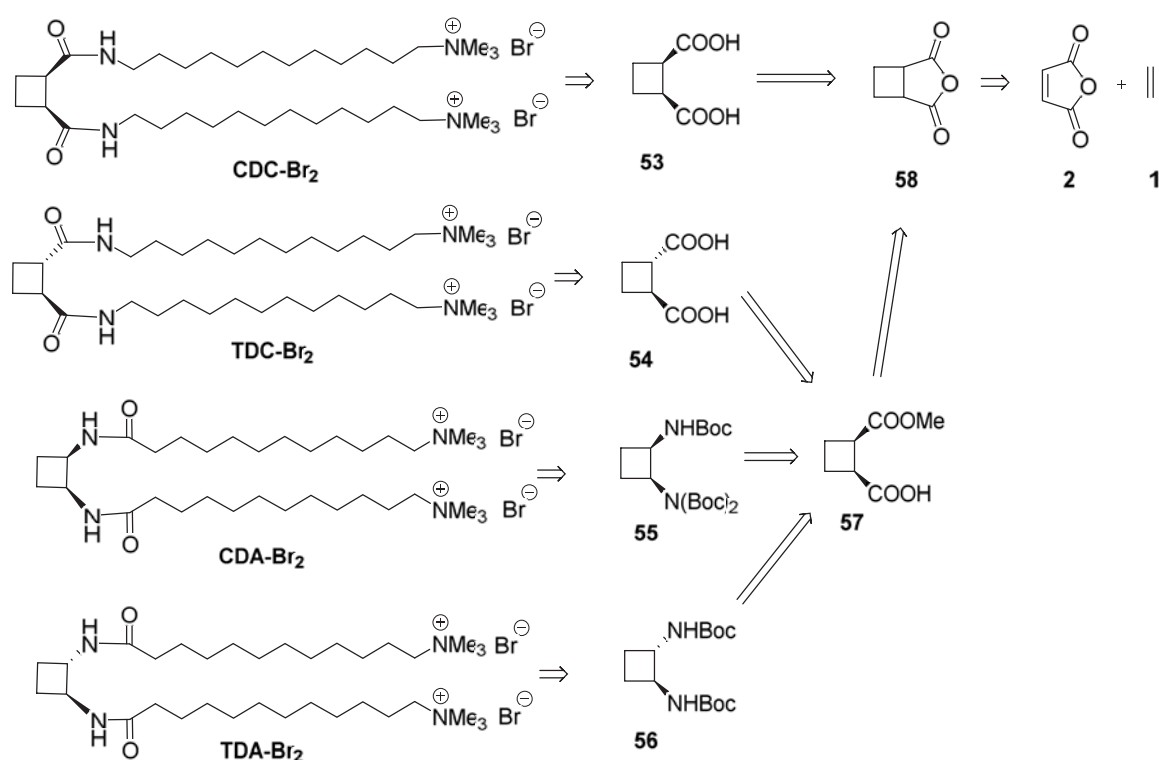
The objectives of this part are:

- 1) Study of the behaviour of this bolaamphiphiles to act as surfactants.
- 2) Study of the influence of the regiochemistry and the stereochemistry on the surfactant behaviour and on the aggregation.
- 3) Contribution of more knowledge to the field of bolaamphiphiles and to better understand the supramolecular self-assembly of chiral cyclobutane-based compounds.

## 6.3 Results and Discussion

### 6.3.1 Synthesis

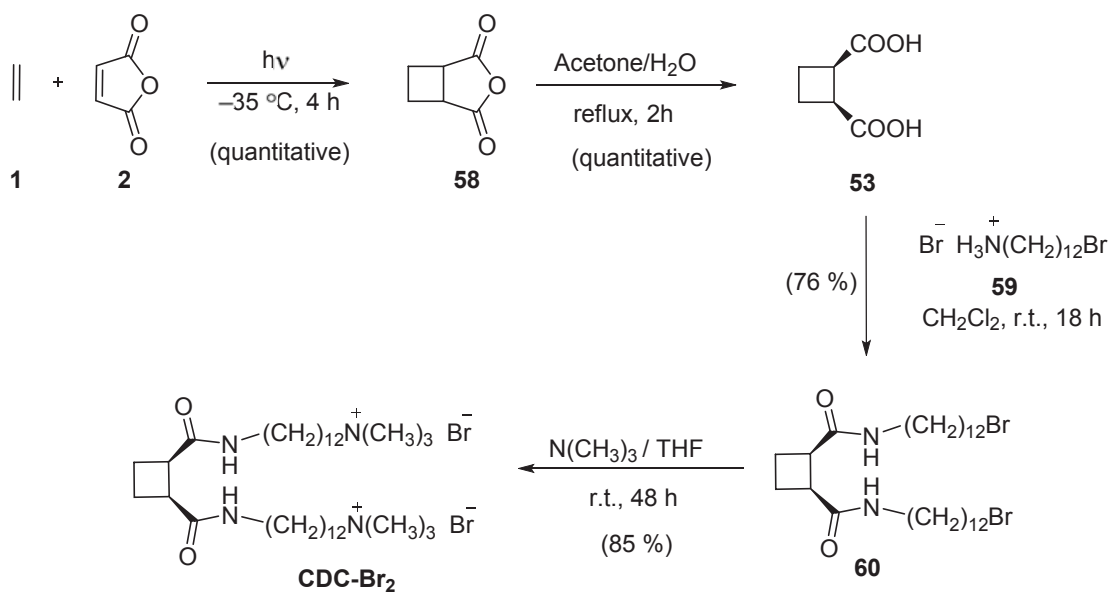
Taking into account the acquired experience in our group preparing enantioselective compounds,<sup>12,155</sup> the studied bolaamphiphiles were synthesised through the following general retrosynthetic pathway (Scheme 5):



**Scheme 6.** General retrosynthetic pathway of the four bolaamphiphiles.

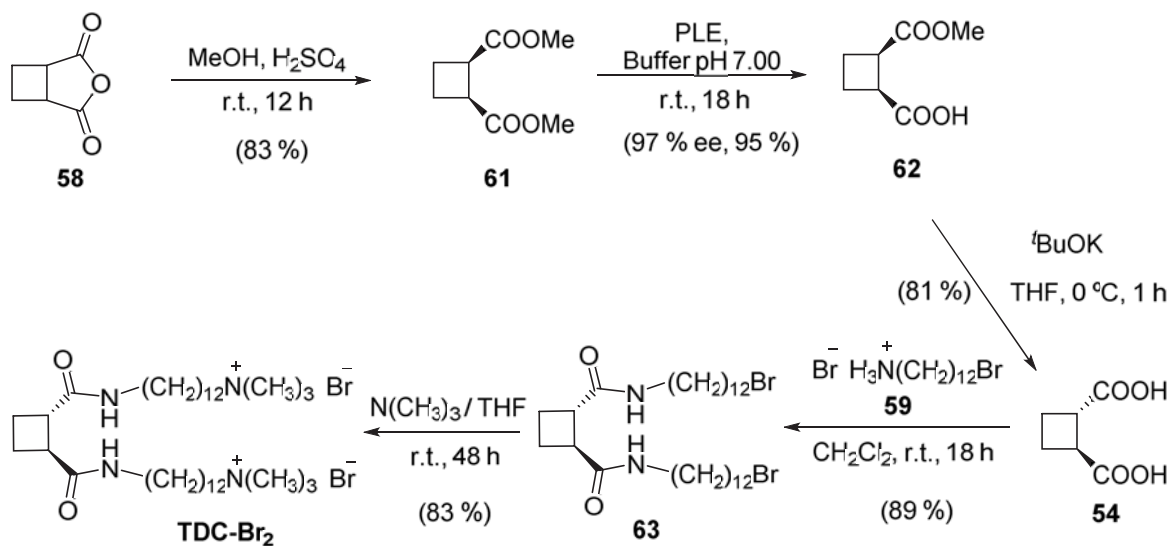
Compounds **CDC-Br<sub>2</sub>** and **TDC-Br<sub>2</sub>** (CO-centered surfactants) were previously synthesised for the first time by Dr. Alessandro Sorrenti and compounds **CDA-Br<sub>2</sub>** and **TDA-Br<sub>2</sub>** (NH-centered surfactants) by Dr. Marta Sans.<sup>155,156</sup> In this thesis, all these surfactants were synthesised again in order to have samples to complete the study of their properties. These syntheses are stereoselective and lead to all surfactants in a completely enantiopure form. The synthetic route of the CO-centered amphiphiles is described in Scheme 7 and Scheme 8.

**Synthesis of CDC-Br<sub>2</sub>:** The synthesis of the *meso* surfactant **CDC-Br<sub>2</sub>** can be achieved in 4 steps in an overall yield of 65 %.



**Scheme 7.** Synthetic route for **CDC-Br<sub>2</sub>**.

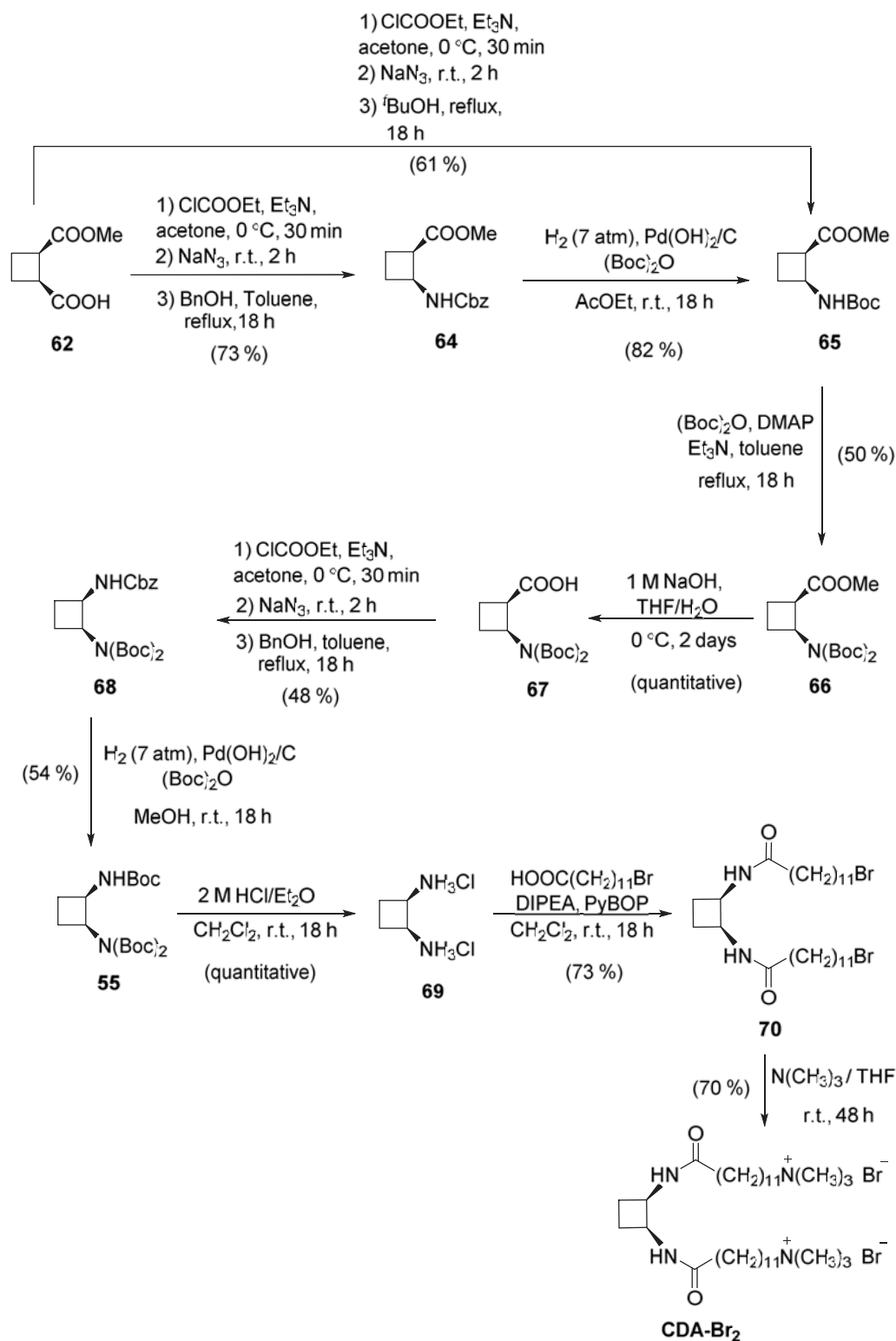
**Synthesis of TDC-Br<sub>2</sub>:** In 6 steps, the **TDC-Br<sub>2</sub>** surfactant can be synthesised in an overall yield of 47 %.



**Scheme 8.** Synthetic route for **TDC-Br<sub>2</sub>**.

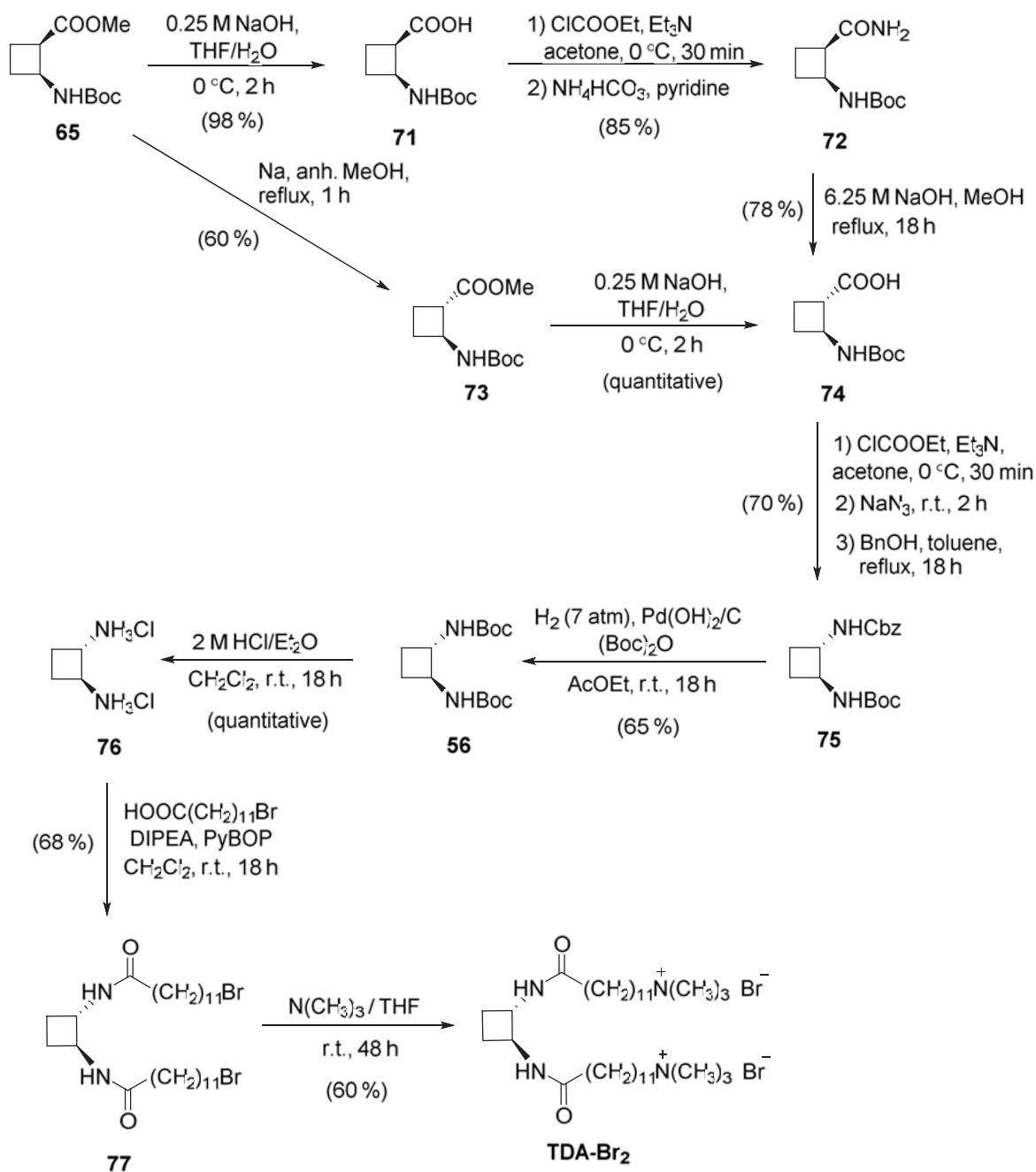
Syntheses of **CDA-Br<sub>2</sub>** and **TDA-Br<sub>2</sub>** are longer and complicated. (Scheme 9 and Scheme 10)

*Synthesis of CDA-Br<sub>2</sub>*: Synthesis of the **CDA-Br<sub>2</sub>** can be achieved through 11-12 steps in an overall yield of 3 %.



**Scheme 9.** Synthetic route for **CDA-Br<sub>2</sub>**.

**Synthesis of TDA-Br<sub>2</sub>:** Synthesis of the **TDA-Br<sub>2</sub>** can be achieved in 12-13 steps in an overall yield of 6 %. Products **65** and **74** can be obtained through two different routes, but both are similar in terms of yield.



**Scheme 10.** Synthetic route for **TDA-Br<sub>2</sub>**.

As it is shown, synthesis of **CDC-Br<sub>2</sub>** and **TDC-Br<sub>2</sub>** are shorter than **CDA-Br<sub>2</sub>** and **TDA-Br<sub>2</sub>**, and the overall yield is significantly higher due to the number of steps.

Once these molecules were synthesised, their physicochemical characterisation was carried out to find out the influence of the stereochemistry and the regiochemistry in the surfactant behaviour.

### 6.3.2 Measurements of the surface tension

The variation of the surface tension depending on the concentration was measured to study the ability of the prepared compounds to act as surfactants. The curve of the surface tension at different concentrations leads us to determine the CMC of each amphiphile. Surface tension was measured using a homemade tensiometer in collaboration with Dr. Ramon Pons from *Institut de Química Avançada de Catalunya (IQAC-CSIC)*. The method known as pendant drop method determines, as explained before, the surface tension of a pendant drop based on the shape of its contour and adjusting it to the Young-Laplace differential equation by iteration.<sup>138,157</sup>

To determine the CMC using the pendant drop method, 16 solutions at different known concentrations of the previously synthesised amphiphiles were prepared using an analytical balance. All the prepared solutions generate foam at concentrations above the CMC. This qualitative fact shows that they seem to act as surfactants. Then, a drop of each solution is located at the end of a tube, avoiding it to fall down. To stabilize the drop and to avoid evaporation of the drop, some deionised water was placed under the sample in order to maintain the humidity at 100 % during all the measurements. Using a camera connected to a program, the contour of each drop can be plotted and its surface tension determined. Measurements were repeated until the value of the measured surface tension reaches the equilibrium (around 3 hours). In Figure 66 and Figure 67, the variation of the surface tension depending on the concentration at 25 °C is represented.

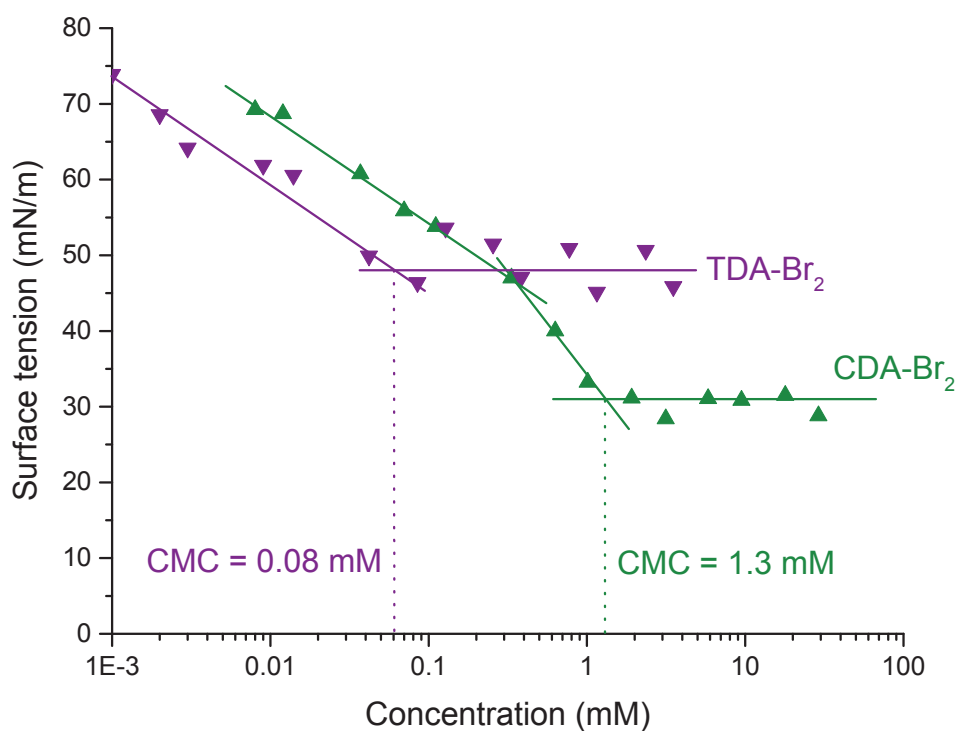


**Figure 66.** Surface tension versus surfactant concentration of **CDA-Br<sub>2</sub>** (green) and **TDA-Br<sub>2</sub>** (purple).

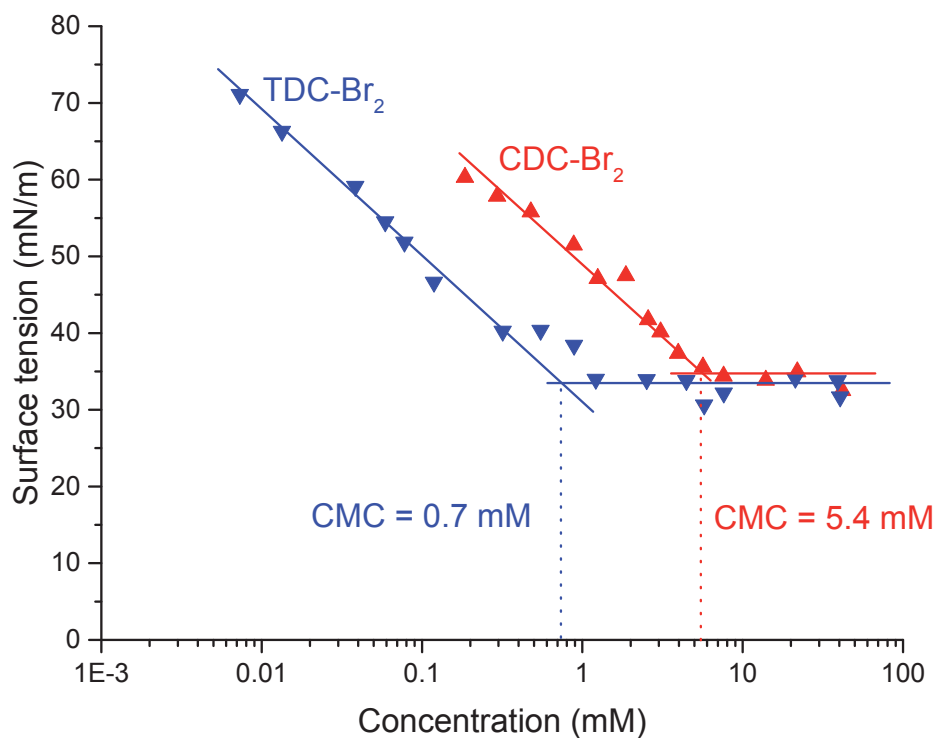


**Figure 67.** Surface tension versus surfactant concentration of **CDC-Br<sub>2</sub>** (red) and **TDC-Br<sub>2</sub>** (blue).

As it is shown, all the studied molecules are able to decrease the surface tension, so all of them have certain surfactant behaviour. However, **TDA-Br<sub>2</sub>** can only decrease the surface tension from 73 to 50 mN/m, thus, it cannot be considered a good surfactant. On the other hand, **CDA-Br<sub>2</sub>**, **CDC-Br<sub>2</sub>** and **TDC-Br<sub>2</sub>** are good surfactants because they can decrease the surface tension under 40 mN/m. If a molecule is not able to reduce  $\gamma$  under 40 mN/m means that this molecule cannot saturate the surface of the water with its hydrophobic tails. If the surface is saturated with hydrophobic tails, then the surface tension should be around 20-40 mN/m depending on the molecule. As a limit situation, the value of the surface tension could be compared with the value of the surface tension of some organic solvents in contact with air. For example, hexane has a surface tension of 18.4 mN/m (at 20 °C), ethanol 22.3 mN/m (at 20 °C), acetone 23.7 mN/m (at 20 °C) and toluene 27.7 mN/m (at 25 °C).<sup>158</sup>

From the slope of the curve just before the CMC, the maximum Gibbs surface excess of the saturated surfactant monolayer at the air/solution interface is obtained, from which the area per molecule at the surface can be calculated (Equation 6 and 7). This area is a thermodynamic value and it depends on the interactions between surfactant molecules, interactions with the solvent and on the conditions of the system such as temperature or ionic strength.<sup>159,160</sup>

$$A_{CMC} = \frac{1}{N_A \Gamma_{max}} \quad (\text{Equation 7})$$

In this equation,  $n$  is the number of species that are absorbed at the surface, and in all our cases  $n = 3$ , the amphiphilic molecule and two bromides.<sup>161</sup> The area per molecule is inversely proportional to the slope of the curve.

In order to quantify the efficiency of these surfactants, the value of  $pC_{20}$  was calculated.  $pC_{20}$  is the  $-\log$  of the concentration needed to decrease 20 mN/m the surface tension of the water-air interface. Effectiveness ( $\Pi_{CMC}$ ) can be calculated by measuring the reduction of the surface tension value, from water to the value at the CMC.

Results of the physicochemical characterisation of the four surfactants are shown in Table 14.



**Table 14.** Table of the physicochemical parameters obtained from the plot of the surface tension versus the surfactant concentration.

Surfactant	Surface Excess $\Gamma_{\max}$ ( $\mu\text{mol}/\text{m}^2$ )	Area $A_{\text{CMC}}$ ( $\text{\AA}^2$ )	Effectiveness $\Pi_{\text{CMC}}$ (mN/m)	Efficiency $p_{\text{C}_{20}}$	CMC (mM)
<b>CDA-Br<sub>2</sub></b>	1.66	100.2 $\pm$ 5.3	41.5	0.853	1.3
<b>TDA-Br<sub>2</sub></b>	0.74	223.5 $\pm$ 21.8	22.9	1.509	0.06
<b>CDC-Br<sub>2</sub></b>	1.18	141.0 $\pm$ 4.0	36.2	0.168	5.4
<b>TDC-Br<sub>2</sub></b>	1.13	147.6 $\pm$ 3.8	38.9	1.108	0.7

As it is shown, the less effective surfactant is **TDA-Br<sub>2</sub>**, as observed before, because it can only reduce 23 mN/m the surface tension while the others can reduce it more than 35 mN/m obtaining a final surface tension value lower than 40 mN/m. It is in agreement with the obtained experimental area at the surface: **TDA-Br<sub>2</sub>** has the largest area on the surface, which avoids that other molecules can aggregate easily and saturation cannot be reached. The more effective surfactant is **CDA-Br<sub>2</sub>**, followed by the two CO-centered surfactants, and finally, **TDA-Br<sub>2</sub>**.

These results are closely related with the obtained experimental areas that these surfactants occupy at the surface. The larger is the area at the surface, the less effective is the surfactant because less molecules can be placed at the surface and thus, less saturated is the surface. In the case of the two CO-centered surfactants, stereochemistry has no influence on the effectiveness while referring to the NH-centered surfactants, stereochemistry plays an important role.

However, as a curiosity, if we compare the slope of the **CDA-Br<sub>2</sub>** curve (Figure 67) at low concentrations, it is shown that is more or less the same than for the **TDA-Br<sub>2</sub>**. It could be related to the possibility that the **CDA-Br<sub>2</sub>** surfactant could adopt different geometries at the surface depending on the amount of surfactant. At low concentrations, the structure of the **CDA-Br<sub>2</sub>** could be very similar to that of **TDA-Br<sub>2</sub>**.

Focusing on the efficiency of these surfactants, the  $pC_{20}$  values can be compared. Efficiency depends, mostly, on the chemical structure of each surfactant. As it is shown, in our cases, stereochemistry seems to be important in the efficiency of the surfactant, and thus, in the CMC. Both *cis* surfactants are more efficient than the *trans* surfactants and thus less amount of them is needed to decrease the surface tension until the limit.

### 6.3.3 Cryogenic Transmission Electron Microscopy (cryoTEM)

The aggregation of these amphiphiles above the CMC was studied by using cryoTEM at  $-200\text{ }^{\circ}\text{C}$ , freezing the sample using liquid ethane to avoid water crystallization and without modifying the structure of the aggregates. CryoTEM images of the aggregation of these molecules is shown in Figures 68-71.

**CDA-Br<sub>2</sub>:**

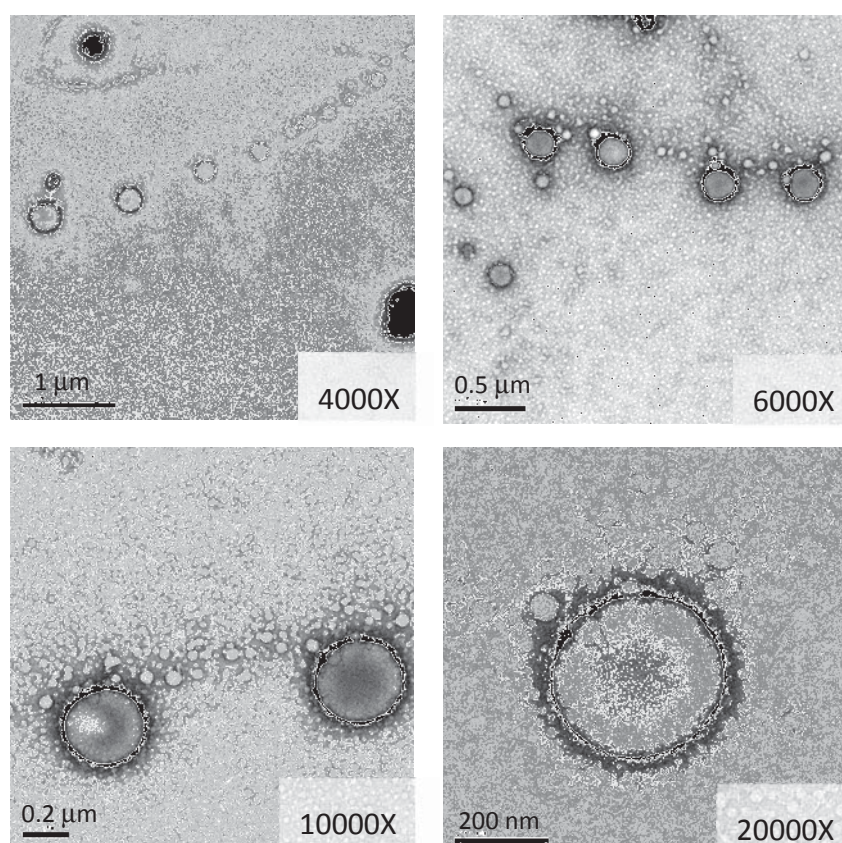


**Figure 68.** Four representative cryoTEM images of the **CDA-Br<sub>2</sub>** above the CMC.

**TDA-Br<sub>2</sub>:**

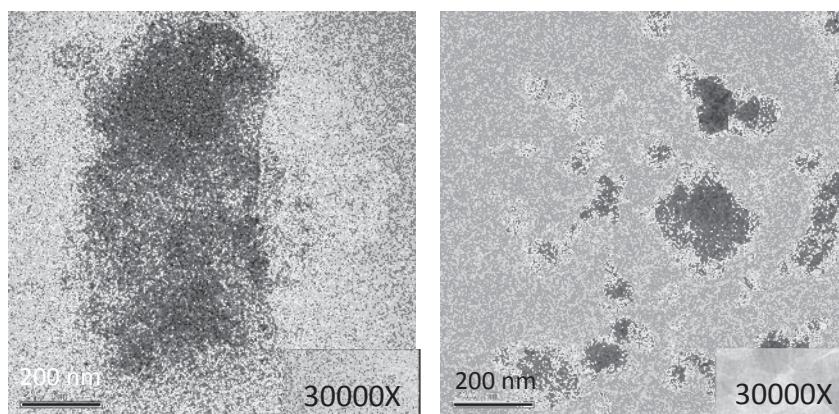


**Figure 69.** Two representative cryoTEM images of the **TDA-Br<sub>2</sub>** above the CMC.

**CDC-Br<sub>2</sub>:**

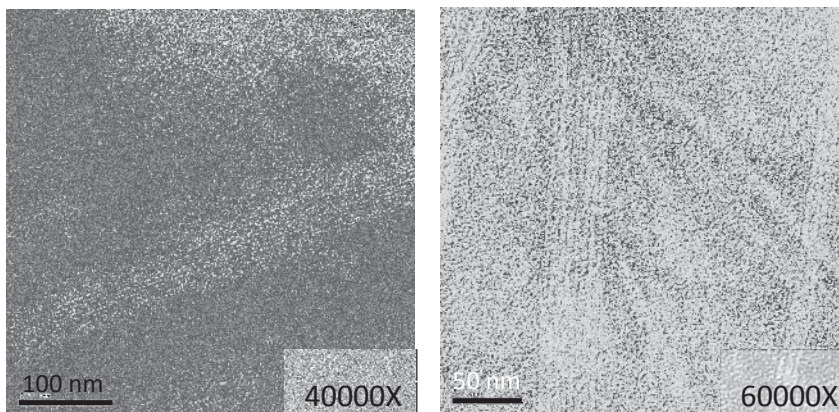


**Figure 70.** Two representative cryoTEM images of the **CDC-Br<sub>2</sub>** above the CMC.

**TDC-Br<sub>2</sub>:**

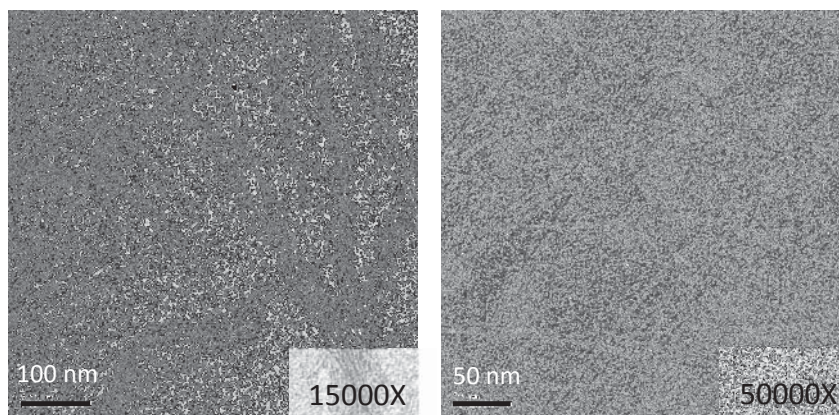


**Figure 71.** Two representative cryoTEM images of the **TDC-Br<sub>2</sub>** above the CMC.

As it is shown, **CDA-Br<sub>2</sub>** form vesicles of different sizes. In these pictures, vesicles from 50 until 250 nm can be seen. The high contrast at the surface is due to the presence of the high electronic density of the bromide ions. **TDA-Br<sub>2</sub>** forms big and irregular aggregates, but also it can form different vesicles and aggregates of fibers. Due to the irregularity of these aggregates, it is difficult to determine a size of these vesicles.

In contrast, both, **CDC-Br<sub>2</sub>** and **TDC-Br<sub>2</sub>**, form long and regular fibers. **CDC-Br<sub>2</sub>** fibers are 5 nm of width and **TDC-Br<sub>2</sub>** of 8 nm. Furthermore, these fibers aggregate between them forming a sheet-like aggregate, especially in the case of **CDC-Br<sub>2</sub>** where 8-10 fibres are self-assembled. In the case of the **TDC-Br<sub>2</sub>**, only some aggregation between 3-4 fibers can be observed in some points, but most of them are alone. Taking into account that the length of one of these studied molecules is around 4 nm, we could say that the fibers from the **CDC-Br<sub>2</sub>** are formed by one molecule of width while the fibers of the **TDC-Br<sub>2</sub>** could be formed by two surfactant molecules of width or a molecule in the extended form.

Observing these pictures, we could conclude that regiochemistry has a direct effect on the shape of the aggregates. While NH-centered surfactants form vesicles, CO-centered surfactants form fibers. These morphologies observed by cryoTEM can be compared with the results from other studies with bolaamphiphiles.<sup>162</sup>

### 6.3.4 Small Angle X-Ray Diffraction (SAXS)

SAXS is a useful technique for determining the size and the shape of the particles that are in solution.<sup>163,164</sup> Using X-Ray light, the scattering due to the differences in the electron density can be detected. Unlike in single crystal X-Ray diffraction, in solution scattered light does not give us information about the exact position but give us information about the average size and shape of the particles that are in solution. Thus, treatment of the obtained data is purely mathematical and could be very complicated. A SAXS spectrum could be understood as the Fourier transform of the variation of the electron density all along the liquid sample during the time.<sup>165</sup> SAXS is a useful technique for measuring surfactant solutions.<sup>166,167</sup>

Samples were prepared at concentrations above the CMC in order to determine the shape and the size of the aggregates,<sup>168</sup> which could be compared with cryoTEM images. SAXS gives us averaged information about the whole sample but mathematical treatments are needed to obtain the information because the phase of the waves is lost and 3D images cannot be obtained. CryoTEM shows only a small part of the sample but with a lot of detail because lens can be used to reconstruct the hologram of the sample. Then, combining both techniques, we could obtain enough information to determine the structure of the aggregates.

X-Ray light were obtained from synchrotron light provided by ALBA Synchrotron.<sup>169</sup> Samples were measured there by courtesy of Dr. Ramon Pons, Dr. Jordi Morros, Jordi Caelles and Imma Carreras.

The scattered angle is represented as  $\phi$  and each angle has an associated reciprocal distance, which is called  $q$  and it expressed in  $\text{nm}^{-1}$  (Equation 8).

$$q = \frac{4\pi}{\lambda} \sin\phi \quad (\text{Equation 8})$$

Reciprocal distance  $q$  can be converted into real distances of the sample ( $d$ ), as shown in Equation 9.<sup>170</sup>

$$d = \frac{2\pi}{q} \quad (\text{Equation 9})$$

Intensity of the scattered light ( $I$ ) is represented against  $q$  values and the function of a system with  $N$  particles can be expressed as shown in Equation 10.

$$I(q) = I_0 \cdot \sum_{i=1}^N (\Delta\rho_i^2 \cdot V_i^2 \cdot P_i(q)) \quad (\text{Equation 10})$$

where  $\Delta\rho$  is the difference of electron density of the particle,  $V$  is its volume and  $P(q)$  is the form factor of each particle. Figure 72 shows the SAXS spectra of compounds **CDC-Br<sub>2</sub>** and **TDC-Br<sub>2</sub>**.

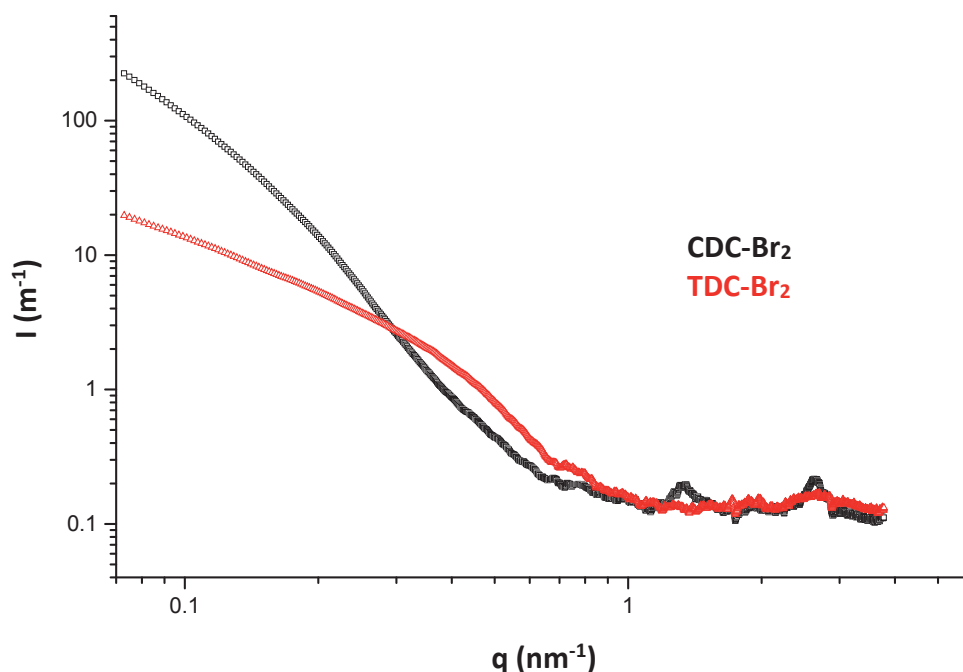


**Figure 72.** SAXS spectra of **CDC-Br<sub>2</sub>** and **TDC-Br<sub>2</sub>** at 1.6 and 3 % in weight respectively.

The first analysis is to determine the slope of the curves at low  $q$  values which is related to the size of the particles. At low  $q$  values, **CDC-Br<sub>2</sub>** show slopes around  $-2.2$  and at  $q$  intermediate value around  $-4$ . A value of  $-2.2$  could be related to a rough lamellar structure which could be formed by different cylinders one next to the other. The slope  $-4$  shows that **CDC-Br<sub>2</sub>** forms big aggregates. On the other hand, **TDC-Br<sub>2</sub>** has a slope of  $-1.3$ , which could be related to separate cylinders.

**TDC-Br<sub>2</sub>** does not show any peak at high  $q$  values, which means that any repetition in the structure of the aggregate is not found. However, **CDC-Br<sub>2</sub>** shows two peaks, at  $q=1.3$  and  $2.6$  nm. This repetition shows that one is the double from the other. In a lamellar structure, peaks follow a repetition following the series  $[1, 2, 3, 4, 5, \dots]$ . In a hexagonal packing, peaks follow a repetition following the series  $[1, \sqrt{3}, 2, \sqrt{7}, 3, \dots]$ . In this case, the repetition peak at  $\sqrt{3}$  is not observed. Thus, we could suggest that aggregation of cylinders is forming a lamellar structure. Taking into account this repetition we could propose that the radius of a single cylinder could be around  $2.4$  nm if considering a lamellar structure and  $2.8$  nm is considering hexagonal packing. This analysis is in agreement with the

cryoTEM images from these surfactants. **CDC-Br<sub>2</sub>** shows aggregated cylinders with a radius around 2.5 nm forming lamellar structures while **TDC-Br<sub>2</sub>** shows separated cylinders.

Surfactants **CDA-Br<sub>2</sub>** and **TDA-Br<sub>2</sub>** were too insoluble and the signal/noise show that poor information could be obtained. SAXS spectra of **CDA-Br<sub>2</sub>** and **TDA-Br<sub>2</sub>** are shown in Figure 73.

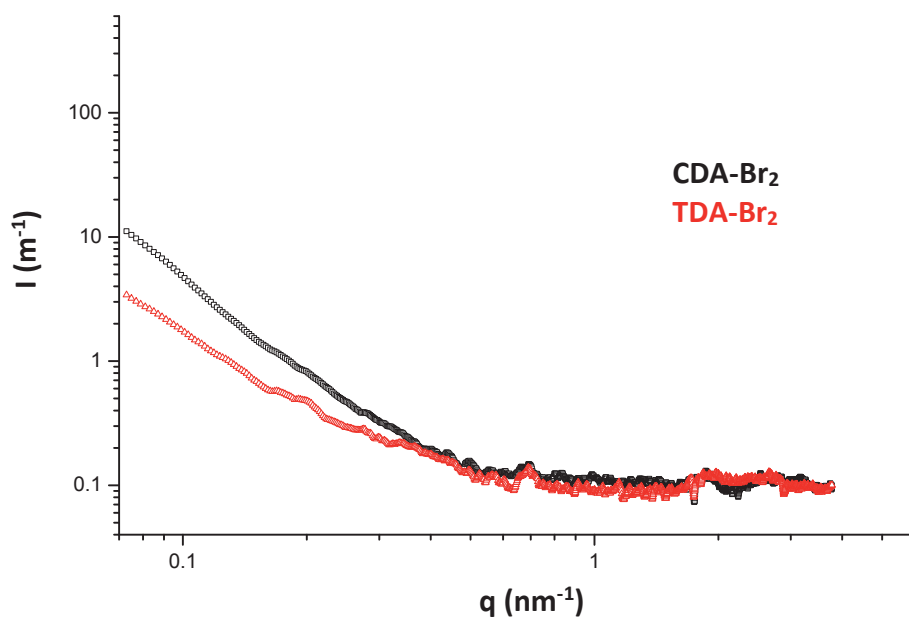


**Figure 73.** SAXS spectra of **CDA-Br<sub>2</sub>** and **TDA-Br<sub>2</sub>** at 1.25 and 0.2 % in weight respectively.

At low  $q$  values, the slope for **TDA-Br<sub>2</sub>** is  $-2.2$  which could be related to rough lamellar structures and from  $-2.6$  to  $-2.9$  for **CDA-Br<sub>2</sub>**, which could be related to a fractal structure. Unfortunately, this information is not enough to understand the structure of the surfactant aggregates. In these cases, only cryoTEM images give us information about the size and shape of the structures.

### 6.3.5 Theoretical calculations

In order to gain insight the structure and the aggregation of these bolaamphiphiles, some theoretical calculations were carried out. First of all, the structure of each molecule in solution was studied. A conformational search in gas phase using molecular mechanics was carried out and the most favourable structure were optimised in water using

quantum mechanics at the M06-2X/6-31G(d) level of theory (see section 9.4 for details). The optimised structures of the surfactants are shown in Figure 74.

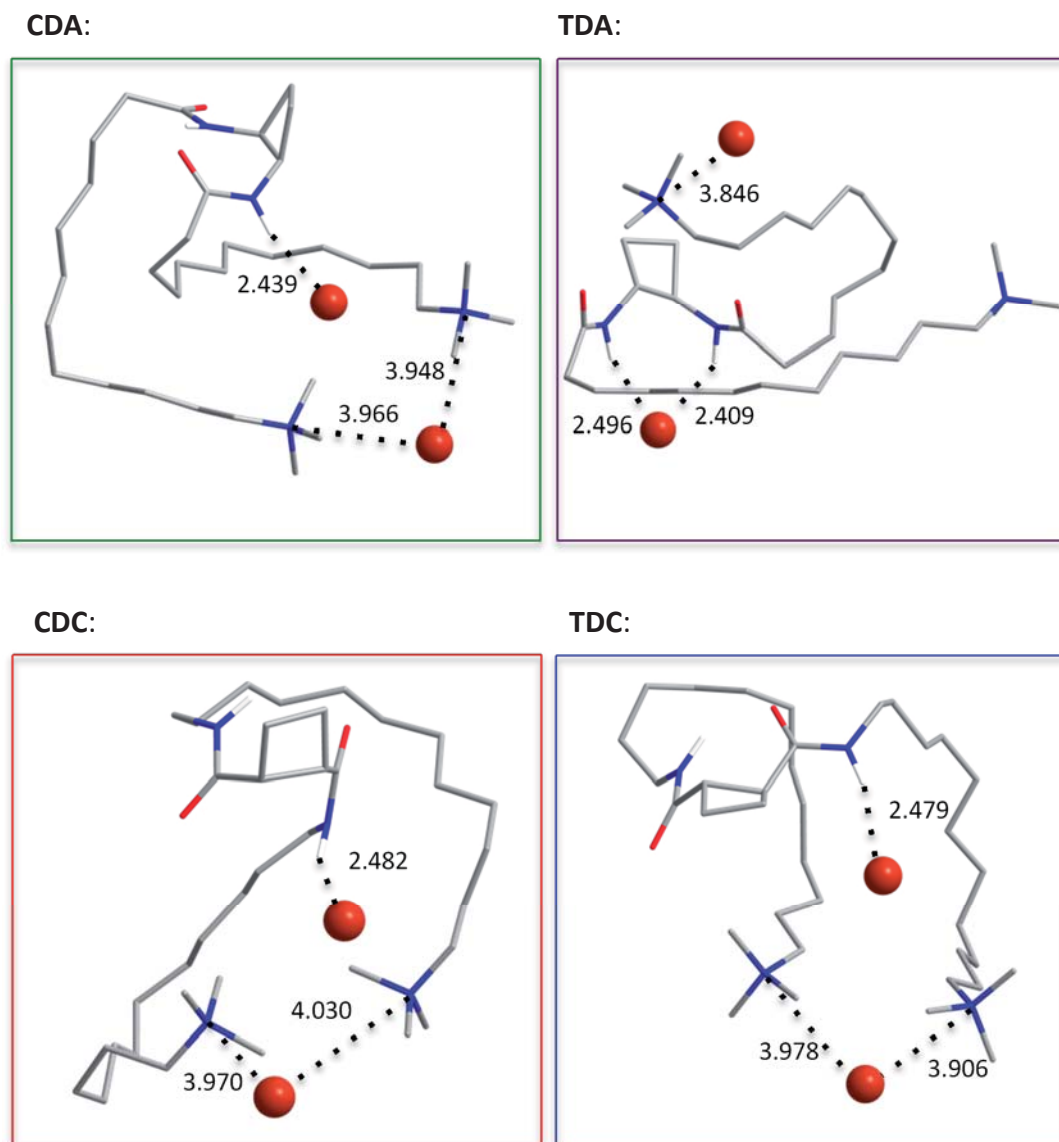


**Figure 74.** Optimised structures of the studied bolaamphiphiles in solution. Non-polar hydrogens were omitted for clarity. Distances are shown in Å.

The chains of these molecules are placed in a random and flexible way. In all cases, one of the bromide ions forms hydrogen bonds with the amide groups and the other is electrostatically interacting with the ammonium tail.

In solution, these molecules have a large number of degrees of freedom and so, this is only one of the possible conformations that they could adopt in solution.



It is known that most of bolaamphiphiles show a “wicket” structure at the surface.<sup>161,171</sup> The word “wicket” comes from the cricket. In Figure 75 is shown a wicket from the cricket and a surfactant with a wicket-like conformation.

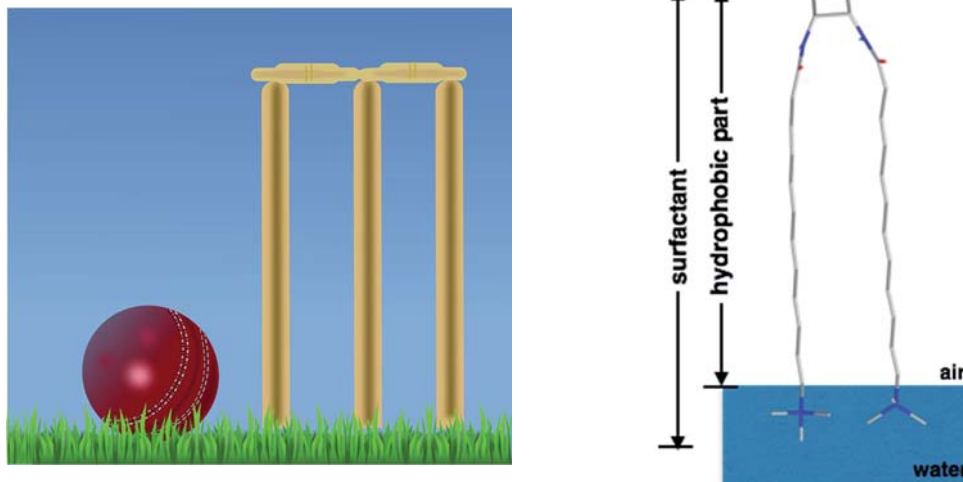


**Figure 75.** a) Wicket. b) Bolaamphiphile on the surface adopting a wicket-like conformation.

Even if they adopt a wicket-like conformation or not, it is known that all the surfactants on the surface have the polar head(s) inside the water and the hydrophobic tail outside the water, in the air, in order to minimize repulsions. It is very difficult to study the interface between two solvents using quantum mechanics and thus, the study the structure of these molecules at the interface becomes a challenge. As the structure of these molecules will depend only on the hydrophobic part, which is outside the water as shown in Figure 75, we have developed a new methodology.

This methodology consists in cutting the hydrophobic part and study itself as a new molecule and replacing the ammonium group by a methyl group. Therefore, the cyclobutane-containing moiety with the two hydrophobic tails were studied.

First of all, a conformational search of the hydrophobic part with the long chains was carried out. The most favourable conformation was optimised using M06-2X as DFT method in gas phase. From the structure of a monomer, the dimer was built up. A conformational search and a DFT optimization of the most favourable structure of dimer was done. Then, the tetramer was built and the process repeated. Once the optimised

structure of the tetramer is obtained, the octamer was built and minimised using molecular mechanics in gas phase. At the end, we suppose that the structure of a monomer inside the aggregate of 8 monomers could be similar to the structure of a real surfactant at the surface. After that, the added methyl group was cut and the polar head was introduced in order to get the final proposed structure of the surfactant at the surface. In the Figure 76 the proposed structure of all the studied bolaamphiphiles is shown.

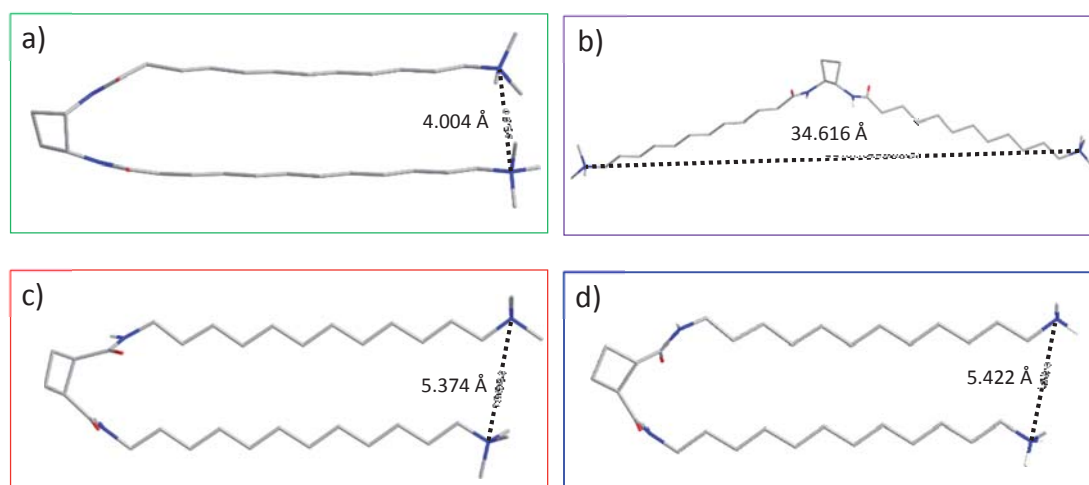


**Figure 76.** Proposed calculated structures of the four studied bolaamphiphiles at the surface. a) **CDA**, b) **TDA**, c) **CDC** and d) **TDC**. Non-polar hydrogens were omitted for clarity. Distances between polar heads ( $d_{NN}$ ) are shown in Å.

As it is shown, three of four amphiphiles have a wicket-like conformation (**CDA**, **CDC** and **TDC**), while **TDA** has an extended configuration. As we have seen, **TDA-Br<sub>2</sub>** is the only bolaamphiphile that is not able to decrease the surface tension under 40 mN/m, so it cannot be considered as surfactant. Due to its structure, it has a big area at the surface (lowest slope of the curve of the surface tension plot), then less molecules can be placed on the surface (lowest density) and finally it will aggregate faster in order to avoid repulsions (lowest CMC).

All the other cases have a wicket-like conformation. It is shown that both CO-centered surfactants have the same distance between polar heads, while **CDA** has a lower distance. This distance could be related to the effectiveness of a surfactant because

the lower is this distance, the number of molecules that can be placed at the surface is larger and hence, the surface tension is reduced. Taking into account this premise, the theoretical calculations are in qualitative agreement with the experimental data.

Once we had the 3D structure of each bolaamphiphile, we could try to calculate the theoretical value of the area per molecule at the surface. This value cannot be compared directly with the experimental data obtained from the surface tension plot because one is a thermodynamic value and the other is completely theoretical without taking into account the interaction between molecules, neither the solvent, nor the thermodynamic parameters of the system. Therefore, these calculated values could be only qualitatively compared with the experimental ones.

If we would go to the microscopic world and we would enter inside a solution of a surfactant in water and would look to the surface, we could see all the polar heads of the molecules pointing down to the solution and some bromide ions to maintain the electroneutrality, as it is shown in Figure 77.

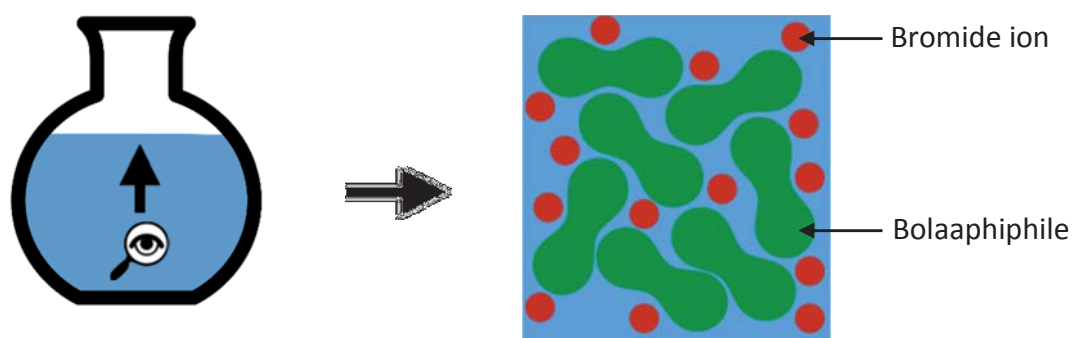


**Figure 77.** Schematic representation of the molecules placed at the surface of the solution seen from the bulk of the solution.

In a limiting situation, the entire surface should be saturated with molecules before the CMC as the absorption Gibbs isotherm describes. Nagarajan described the relationship between the theoretical area of a surfactant (geometrical parameter) and the experimental area (thermodynamic parameter).<sup>172,173</sup>

Therefore, Nagarajan deduced that the obtained experimental area will be always higher than the theoretical area of the polar part of the surfactant. Vidal *et al.* have calculated the area of a non-ionic surfactant at the surface by using a 3D representation of a simulated molecule and calculating a square around it (Figure 78). However, as they explain, it is just an approximation to have an idea about the area value.<sup>174</sup>

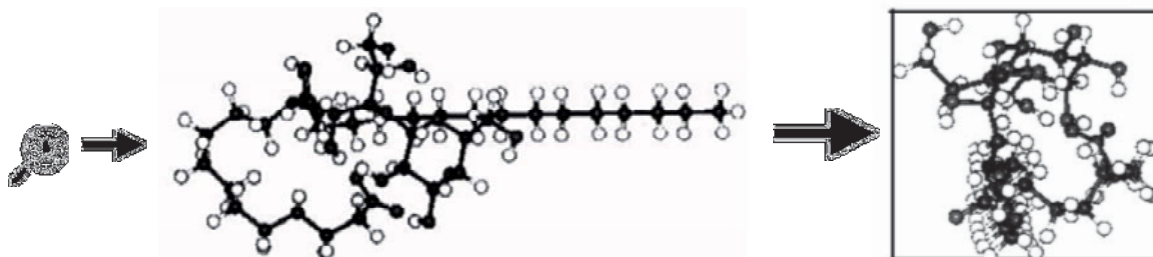


**Figure 78.** Representation of the calculated area of a surfactant at the surface using simulations.

In our case, it is more difficult than in the case of a non-ionic surfactant because it is important not to forget that two bromides per molecule will be also at the surface and they have to be also considered when calculating the area. However, it is difficult to estimate the contribution of the bromide ion at the surface because it can be located freely around the polar head of the surfactant, at the surface or in the solution, reducing the effective area of each bromide at the surface.

The area that a bromide ion occupies at the surface can be calculated taking into account that the ionic radius is  $1.960 \text{ \AA}$ ,<sup>175</sup> and thus, the area per bromide observed from the solution as a circle is  $12.07 \text{ \AA}^2$ . To calculate the area of the polar head of a bolaamphiphile is much more complicated. First of all, we should understand what we are calculating. The area of the cationic part we want to calculate is shown in Figure 79.



**Figure 79.** Schematic representation of the area per molecule at the surface.

To simplify it, we have taken a rectangle as an approximation of the area, as it is shown in Figure 80.



**Figure 80.** Schematic approximation of the area per molecule on the surface, which will be calculated.

Thus, the area of the polar part ( $A_p$ ) can be described as shown in Equation 11.

$$A_p = 2R(2R + d_{N-N}) + 2A_{Br^-} \quad (\text{Equation 11})$$

$R$  is the radius of one of the polar heads,  $d_{N-N}$  is the distance between polar heads and  $A_{Br^-}$  is the area of a bromide.

Nagarajan studied and proposed different methods to calculate  $A_p$ , but nowadays, it is still a non-solved problem because each surfactant behaves differently than the others. At this point, we contacted Nagarajan to deepen into the field and he explained us how his theory has evolved during the years, specially the calculation of the trimethylammonium part. In 1979, he considered that the area of the trimethylammonium should be the same (or practically the same) as the area of trimethylamine. Therefore, taking into account the already known distances of the atoms, he proposed that the area should be around  $17 \text{ \AA}^2$ .<sup>176</sup> In 1987, he improved his theory taking into account that each methyl group of the trimethylammonium head has to be considered as a sphere, and the area of the trimethylammonium group at the surface could be estimated as  $35 \text{ \AA}^2$ .<sup>172</sup> Finally, in 1992, he improved again the theory considering that each methyl group was a cone instead of a sphere. In this way, the polar head of trimethylammonium bromide had an estimated area at the surface of  $54 \text{ \AA}^2$ .<sup>177</sup> However, he recognised that a reasonable approach is that someone in the future perform molecular modelling of the head group using a computational software and then from the generated molecular conformation, estimate the projected area of the molecule at the surface. The use of such standard methodology will make it easier for treating more complex head group structures where the simple geometrical visualizations he did (such as the idea of a cone) may not be easily applied.

Taking into account his studies, we have finished the work he proposed. From the DFT optimization of the surfactant in water, the distances and the angles of the trimethylammonium group can be obtained. These distances and angles are in agreement with a previous study of the ammonium head at 100 K.<sup>178</sup> In Figure 81, the different calculated parameters are shown.

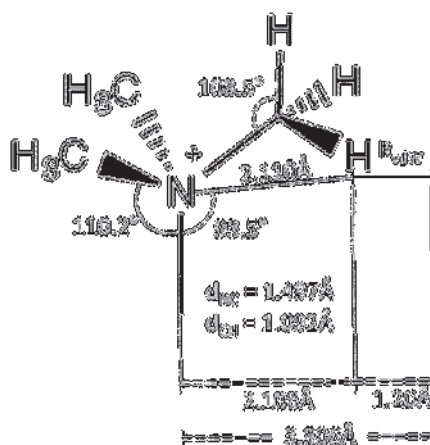


**Figure 81.** Calculated distances and angles of the polar head  $-\text{N}(\text{CH}_3)_3^+$ .

So, the area of the  $-\text{N}(\text{CH}_3)_3^+$  using our approximation is  $34.3 \text{ \AA}^2$  and all the polar head  $-\text{N}(\text{CH}_3)_3\text{Br}$  is  $46.4 \text{ \AA}^2$ . These values can be compared with those provided by Nagarajan (he proposed  $35 \text{ \AA}^2$  for the  $-\text{N}(\text{CH}_3)_3^+$  part and  $54 \text{ \AA}^2$  for  $-\text{N}(\text{CH}_3)_3\text{Br}$ ). The calculated values for  $A_p$  are shown in Table 15.

The order of the calculated areas of the polar part is in qualitative agreement with the order of the experimental areas. The smallest calculated area is that from the **CDA**, followed by the area of the two CO-centered molecules, and finally, the **TDA**. As we are using a rectangle as an approximation of the real polar area from Figure 80, the lower is the distance of the two polar heads, the lower is the committed error. We could say that this approximation is only valid for those surfactants, which has a “wicket” configuration at the surface. Thus, other configuration such as **TDA** cannot be described as a rectangle.

Calculated areas are in agreement with the range of magnitude. Taking into account that the area of a hydrocarbon chain is known to be  $21 \text{ \AA}^2$ ,<sup>172</sup> and that our surfactants have two of them, the area of the surfactants should be, at least, higher than  $42 \text{ \AA}^2$ , and in all cases the value of the area is higher. The influence of the two positive heads forces the separation of the chains and leads to an increase of the area per molecule.

**Table 15.** Experimental area per molecule at the surface and calculated areas of the polar part. Distances are in Å and areas are in Å<sup>2</sup>.

Surfactant	$A_{CMC}$	calculated $A_p'$ (cationic part)	calculated $A_p$
CDA-Br <sub>2</sub>	100.2	70.2	94.3
TDA-Br <sub>2</sub>	223.5	272.6	296.7
CDC-Br <sub>2</sub>	141.0	79.3	103.4
TDC-Br <sub>2</sub>	147.6	79.6	103.7

Our proposed approximation seems to be in very qualitative agreement with the experimental results. However, this new methodology can only be applied to those bola surfactants whose geometry and the distance between polar heads are determined by the hydrophobic tail and they can be studied as separated parts. Nevertheless, this theoretical study has given us some more information about these four bolaamphiphiles which together with the other studies led us to know how they behave in aqueous solution.

## 6.4 Summary and Conclusions

In this chapter, four bolaamphiphiles containing 1,2-chiral cyclobutanes were synthesised. Measurements of the surface tension show that all the amphiphiles are able to decrease the surface tension but **TDA-Br<sub>2</sub>** cannot reduce the surface tension under 40 mN/m, so it cannot be considered as a good surfactant, while the others can. The *trans* bolaamphiphiles are less soluble than the *cis* ones and thus, they have a lower value of CMC. Thus, **stereochemistry** has an effect on the **efficiency** of these surfactants.

CryoTEM images show that NH-centered amphiphiles aggregate forming vesicles while the CO-centered amphiphiles form fibers. **Regiochemistry** has an effect on the **morphology** of the aggregate.

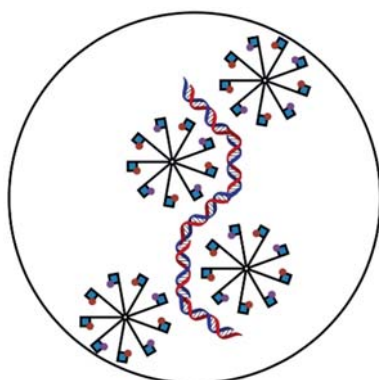
SAXS analysis is in agreement with cryoTEM images showing that **CDC-Br<sub>2</sub>** form self-assembled cylinders while **TDC-Br<sub>2</sub>** show separated cylinders.

A new methodology to calculate the structure of these bolaamphiphiles at the surface was developed and results are in good agreement with the experimental data.

This study gives information to deep in the field of bolaamphiphiles showing that regiochemistry and stereochemistry play an important role to control the surfactant abilities and the aggregation. In addition, this study helps us to better understand the structure of cyclobutane-based compounds.







**7. Chiral pH-dependent  $\beta$ -amino acid-based surfactants: synthesis, study of their properties and study as potential new vectors for gene therapy**

---



## **7. Chiral pH-dependent $\beta$ -amino acid-based surfactants: synthesis, study of their properties and study as potential new vectors for gene therapy**

### **7.1 Introduction**

Gene therapy has gained significant attention over the past two decades as a potential method for treating genetic disorders such as Severe Combined Immunodeficiency,<sup>179</sup> Haemophilia B,<sup>180</sup> cystic fibrosis,<sup>181</sup> Leber's Congenital Amaurosis,<sup>182</sup> and Parkinson's disease,<sup>183</sup> as well as an alternative method to traditional chemotherapy used in treating cancer.<sup>184</sup> It consists on introducing a target gene, which is encoded in a DNA or RNA chain, into a specific cell. Depending on the temperature, the pH or the ionic strength, a single DNA chain in solution could adopt different structures. Vectors are compounds that condense DNA molecules forming DNA-vector complexes in order to protect the information of the chain.<sup>185</sup>

Initial studies showed that viral carriers such as retroviruses and adenoviruses exhibit high efficiency in delivering both DNA and RNA to numerous cell lines. However, fundamental problems associated with viral vector systems, including toxicity, immunogenicity and limitations with respect to scale-up procedures, encouraged the investigation of other potential vectors for introducing the DNA into targeted tissues.<sup>186</sup>

Research efforts are currently focused on designing effective carrier vectors that compact and protect DNA for gene therapy: DNA is rapidly degraded by serum nucleases in the blood when injected intravenously.<sup>187</sup> Additionally, they have to transfect into cells and release the target DNA inside. Finally, vectors have to be metabolised. In this thesis, compaction, protection, decompaction and cell transfection were studied using different techniques (Figure 82).

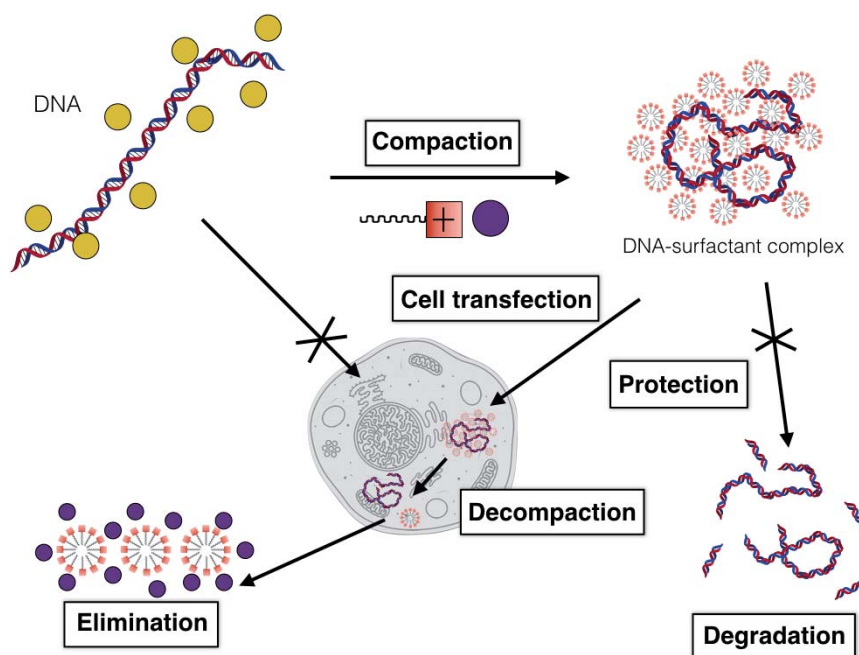


**Figure 82.** Schematic summary of the study of new potential vectors for gene therapy.

The role of chemists in the field of gene therapy is to design and prepare new non-viral vectors, such as cationic lipids (**78**),<sup>188</sup> cationic surfactants (**79**),<sup>189</sup> cationic polymers (**81**),<sup>190</sup> metallic cations (**82**),<sup>191</sup> dendrimers,<sup>192</sup> polypeptides (**80**) and nanoparticles (**83** and **84**), as shown in Figure 83.

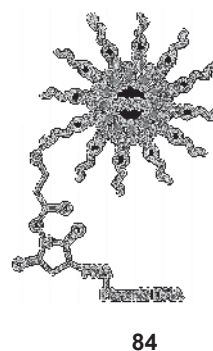
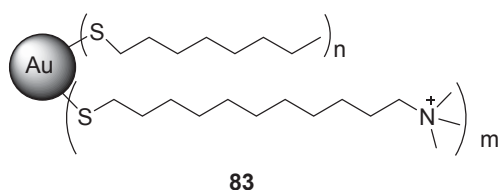
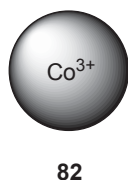
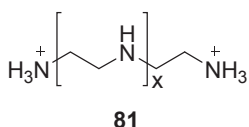
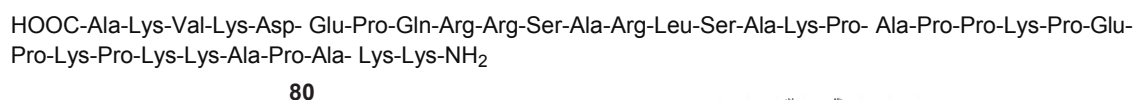
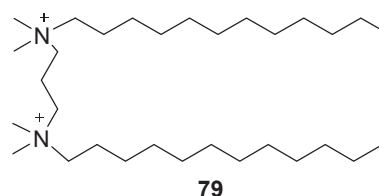
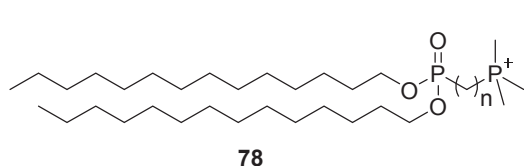


**Figure 83.** Examples of non-viral vectors for gene therapy.

Special attention has been paid to cationic surfactants due to their abilities.<sup>133</sup> Cationic polar heads could interact with negatively charged phosphate groups of the DNA chains while hydrophobic chains could stabilize the aggregates. Gemini surfactants have shown to be very efficient compounds for compacting DNA for biological application such as gene therapy.<sup>193,194</sup> To transfect into cells it is important to control DNA compaction and the neutralization of negative charges.

Binding of cationic surfactants to DNA occurs at concentrations much below the CMC of the DNA-free surfactant solutions. The concentration at which surfactant molecules start to self-assemble in the presence of a polyelectrolyte like DNA is called critical aggregation concentration (CAC) and it could be understood as a CMC where the counterion of the micelle (or the aggregate) is DNA.<sup>195</sup> Binding isotherms of cationic surfactants to DNA show a sigmoidal shape, indicating cooperativity.<sup>196</sup> DNA-surfactant complexes seem to transfect into cells through endocytosis. Once inside the cell, endosome is opened and the DNA is released.<sup>197,198</sup>

The mechanism of the DNA-surfactant complexation is still matter of debate. There are two main lines of thinking, all of them based on experimental evidences. Both suggest that after CAC surfactant aggregates bind cooperatively DNA compacting the elongated chain into DNA-surfactant aggregates. Discussion arises at low concentrations, below the CAC. Bloomfield *et al.*<sup>199</sup> propose that first of all, a single surfactant molecule binds DNA through electrostatic interactions because the selectivity coefficient between sodium ions and surfactants is 0.028 and thus, any preference of one towards the other is not observed. Then, other surfactant molecules self-assemble cooperatively forming aggregates (mechanism A, Figure 84). Different authors have demonstrated this hypothesis by using optical tweezers and determining the strength of the binding of surfactant molecules at the DNA surface<sup>144</sup> or by using different physicochemical methods<sup>145</sup>. On the other side, Zhu and Evans proposed that interaction with surfactant molecules and DNA is purely electrostatic and that there is no preferential binding of surfactant monomers to DNA because the phosphate-sodium environment is very unfavourable for hydrophobic chains. Nevertheless, they suggest that only from a certain concentration (CAC), surfactant start to self-assemble at the DNA surface forming aggregates (mechanism B, Figure 84).<sup>195</sup> Björn Lindman, Rita Dias and other authors reaffirm this theory and it seems to be the most

supported one.<sup>133,202</sup> In this thesis, due to the collaboration with Dr. Dias, mechanism B (Figure 84) of interaction is considered.

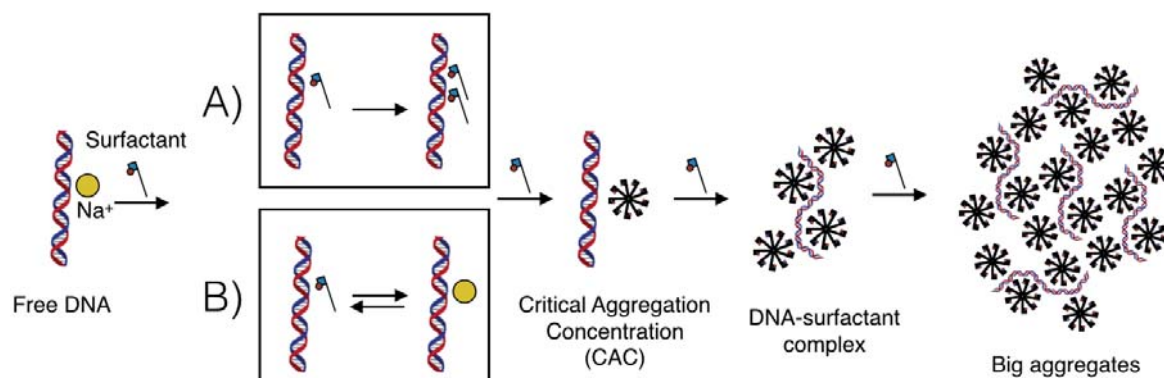


**Figure 84.** Mechanism of binding of surfactants to DNA with the two proposed steps: A and B.

The structure of the surfactant plays a very important role in the DNA compaction. Both polar head and hydrophobic tail are important factors to be taken into account. Modifying the structure of the polar head and the length of the chain compaction of DNA can be modified.<sup>200,203–205</sup> One of the most studied surfactants is CTAB.<sup>202,206</sup> It shows high efficiency compacting DNA compared with other shorter surfactants and it is commercially available. However, trimethylammonium surfactants show cytotoxicity and other surfactants should be synthesised in order to improve compaction and transfection.<sup>207</sup> Different studies comparing it with other compacting agents such as dendrimers were done.<sup>208</sup> In this thesis, CTAB and DTAB (Figure 85) have been studied to compare them with the new synthesised surfactants.



**Figure 85.** Structure of commercial surfactants DTAB and CTAB.

Amino acid-based surfactants are getting importance due to their good levels of biodegradability and biocompatibility.<sup>209–213</sup> The combination of amino acids or peptides with hydrocarbon chains of variable length has given rise to a variety of compounds with an amphiphilic structure and with good surfactant properties. Most of the examples use

natural  $\alpha$ -amino acids. Synthetic amino acid-based surfactants could be pH-sensitive, which provide to the surfactant a great potential for biomedical applications.<sup>166</sup> The presence of amino acids in the structure could lead to have amide groups, which will help self-assembly of surfactants through intermolecular hydrogen bonding.<sup>142</sup> pH-sensitive surfactants show interesting applications in biology because depending on the pH, a mixture of differently charged molecules can be obtained.<sup>214</sup> Figure 86 shows the endocytosis mechanism of DNA-cationic/non-ionic complexes.<sup>215</sup> As it is shown, non-ionic amphiphiles stabilize cationic vesicles by reducing electrostatic repulsions.

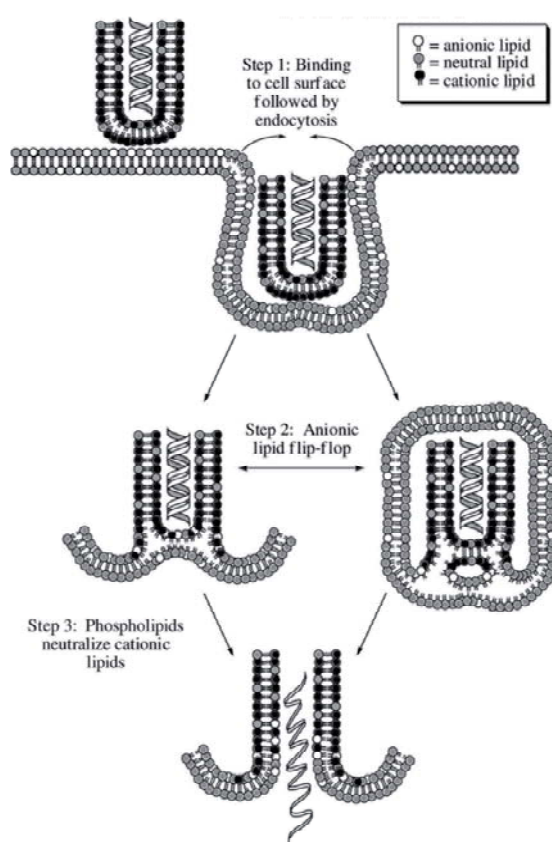


**Figure 86.** Endocytosis mechanism of DNA-cationic/non-ionic surfactant complexes.<sup>291</sup>

In our research group, different cyclobutane-containing amino acid-based surfactants were synthesised and studied. Ospina *et al.* studied different zwitterionic



amino acid-based surfactants.<sup>17</sup> One of them is represented in Figure 87. It shows high efficiency as surfactant due to its low CMC.

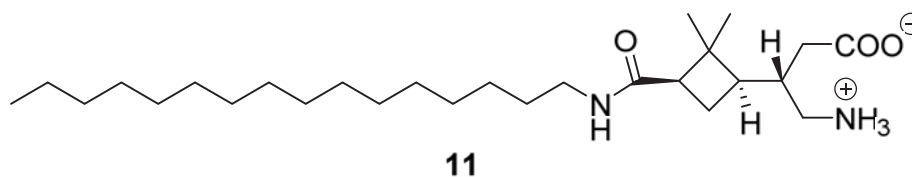


**Figure 87.** Example of zwitterionic amino acid-based surfactant studied by our research group.

Other studied surfactants are based on  $\beta$ -amino acids (Figure 88).<sup>216,217</sup> In this work, the relevance of the relative stereochemistry and of the stereochemical constraints imposed by the cyclobutane ring on the aggregation properties of these compounds at different aggregation states was shown.

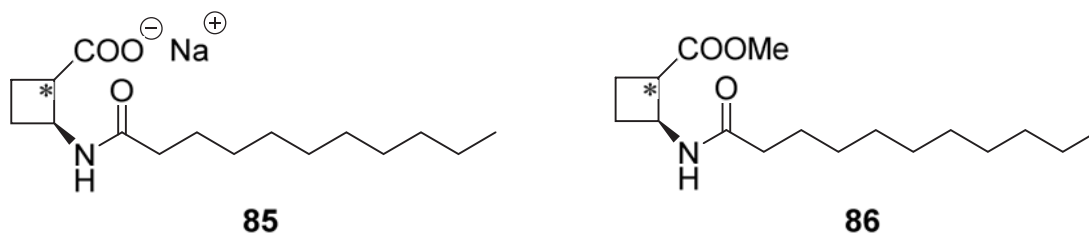


**Figure 88.** Anionic and non-ionic  $\beta$ -amino acid-based surfactants studied in our research group.

## 7.2 Objectives

After the study of non-ionic and anionic  $\beta$ -amino acid-based surfactants, the study of a family of cationic  $\beta$ -amino acid-based surfactants was proposed. Mireia Bouzas synthesised for the first time two new cationic pH-dependent amphiphiles during her Master thesis (Figure 89).<sup>218</sup>

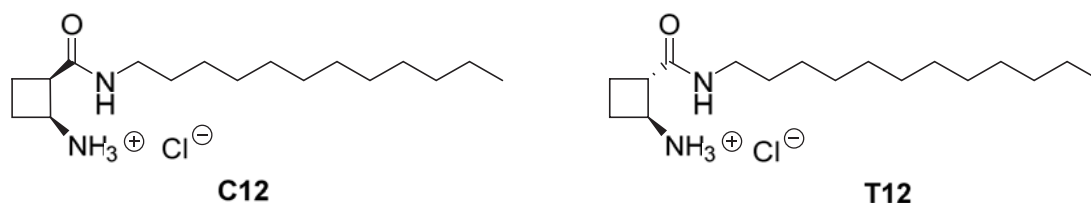


**Figure 89.** Synthesised cationic  $\beta$ -amino acid-based surfactants by our research group.

In this thesis, these two surfactants and two new homologues with a 16-carbon chain length were synthesised and studied as potential new vectors for gene therapy (Figure 90).

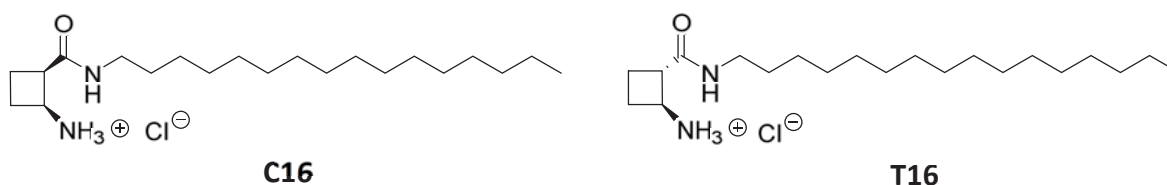


**Figure 90.** Two new pH-dependent  $\beta$ -amino acid-based surfactants synthesised in this thesis for the first time.

The objectives of this work are:

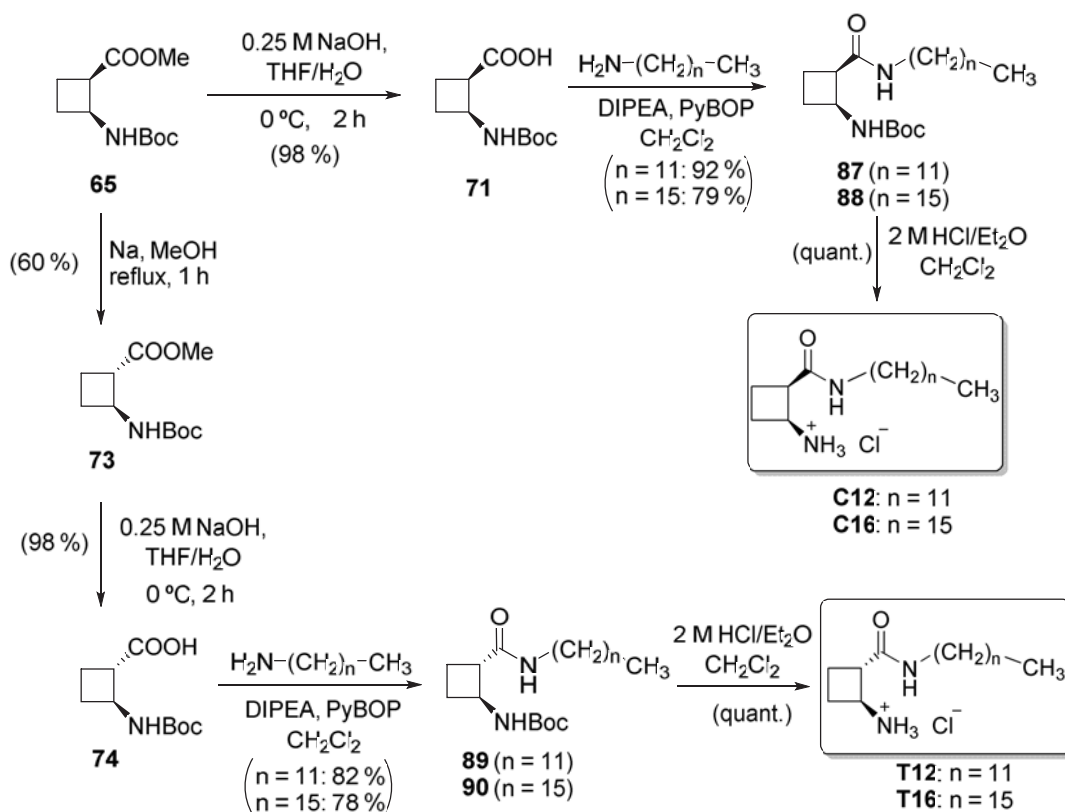
- 1) Synthesis of compounds **C12**, **C16**, **T12** and **T16**.
- 2) Analysis of the supramolecular systems as surfactants.
- 3) Study of their ability to act as vectors for gene therapy by studying the compaction, protection, decompaction and cell transfection of a DNA plasmid.
- 4) Study of the influence of the stereochemistry and the chain length on the properties studied in objectives 2 and 3.

## 7.3 Results and Discussion

Results of this part of the thesis are presented in four parts. First, the synthesis of the four surfactants is described (section 7.3.1). Then, supramolecular analysis (section 7.3.2) and the biophysical study (section 7.3.3) are shown. Finally, results of the biological applications are shown in section 7.3.4. This work was carried out in collaboration with Dr. Ramon Pons from IQAC, with Dr. Rita Dias from NTNU and with Dr. Carme Nogués and Dr. Nerea Gaztelumendi from UAB.

### 7.3.1 Synthesis

The synthetic pathway is shown in Scheme 11.



**Scheme 11.** Synthetic pathway of compounds **C12**, **T12**, **C16** and **T16**.

The synthesis of these four surfactants can be achieved in 7-8 steps in a relative good yield (Table 16). The hydrolysis of the protected monomers **65** and **73** was carried using NaOH in THF/H<sub>2</sub>O in a good yield. The coupling reaction was achieved using PyBOP as coupling agent and the purification of the crude was fast and easy. Final deprotection

was achieved quantitatively and the product was efficiently purified by precipitation in acetone.

**Table 16.** Overall yield of the synthesis of the four prepared surfactants.

Compound	Overall yield (%)
<b>C12</b>	36
<b>T12</b>	19
<b>C16</b>	31
<b>T16</b>	18

It is important to remark that *cis* surfactants are less soluble in water than *trans* surfactants, probably due to the formation of an intramolecular hydrogen bond. **C16** is less soluble than **C12** due to the four additional methylene groups, and it requires sonication to completely dissolve the sample. Once the surfactants were synthesised, their physicochemical characterisation was carried out.

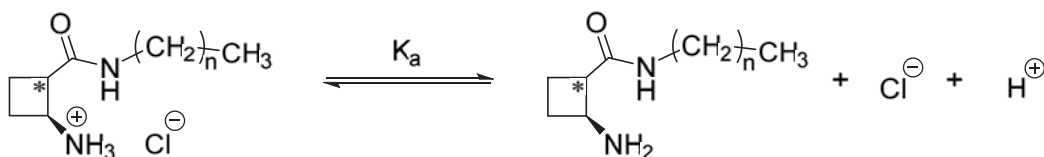
### 7.3.2 Supramolecular analysis

To characterise these pH-dependent surfactants, different techniques were used. First of all, the  $pK_a$  of each surfactant was determined by using a titration of an aqueous solution. In addition, a basic titration followed by an acid retrotitration was carried out to analyse the acid-base character of the amphiphile. Finally, the CMC was determined at three different pH values in order to study their properties in all their states. Other techniques such as circular dichroism, dynamic light scattering, cryoTEM and theoretical calculations were used in order to better understand these supramolecular systems.

#### 7.3.2.1 Determination of the $pK_a$

The compounds studied in this work have a positive charge on the protonated amino group of the  $\beta$ -amino acid. These surfactants present an acid-base equilibrium in aqueous solutions. The dissociation states of these surfactants are shown in Scheme 12. Their  $pK_a$  can be determined using two different techniques.

- Measuring the pH of the solution at different surfactant concentrations
- Carrying out a titration using NaOH and a retrotitration using HCl



**Scheme 12.** Dissociation equilibrium of these surfactants in aqueous solutions. (n=11,15)

However, this reaction is a simplification of the acid-base reaction. Taking into account that other equilibria are present depending on the concentration of surfactant molecules, the acid-base properties vary depending on the concentration. In order to study their acid-base properties, all the following equilibria were taken into account. R-NH<sub>3</sub><sup>+</sup> refers to the cationic form of the amphiphile while R-NH<sub>2</sub> refers to its non-ionic form. Different pK<sub>a</sub> and CMC values are defined in these equilibria. (Figure 91)

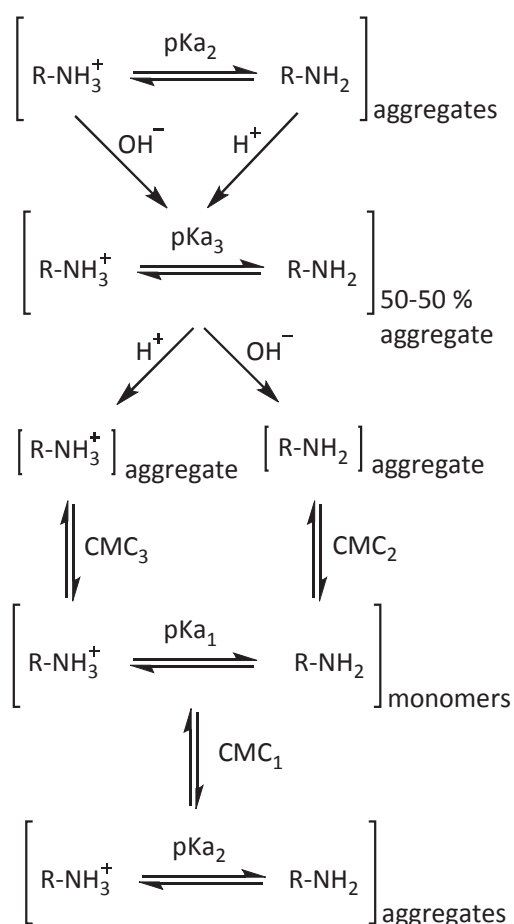


**Figure 91.** Different equilibria that were taken into account.

## 7.3.2.1.1 Dependence of the pH on the concentration of surfactant

Measurements were made at 25 °C and increasing concentrations of surfactant to minimize errors from possible contamination of the electrode. The variation of the pH depending on the surfactant concentration is represented in Figure 92.

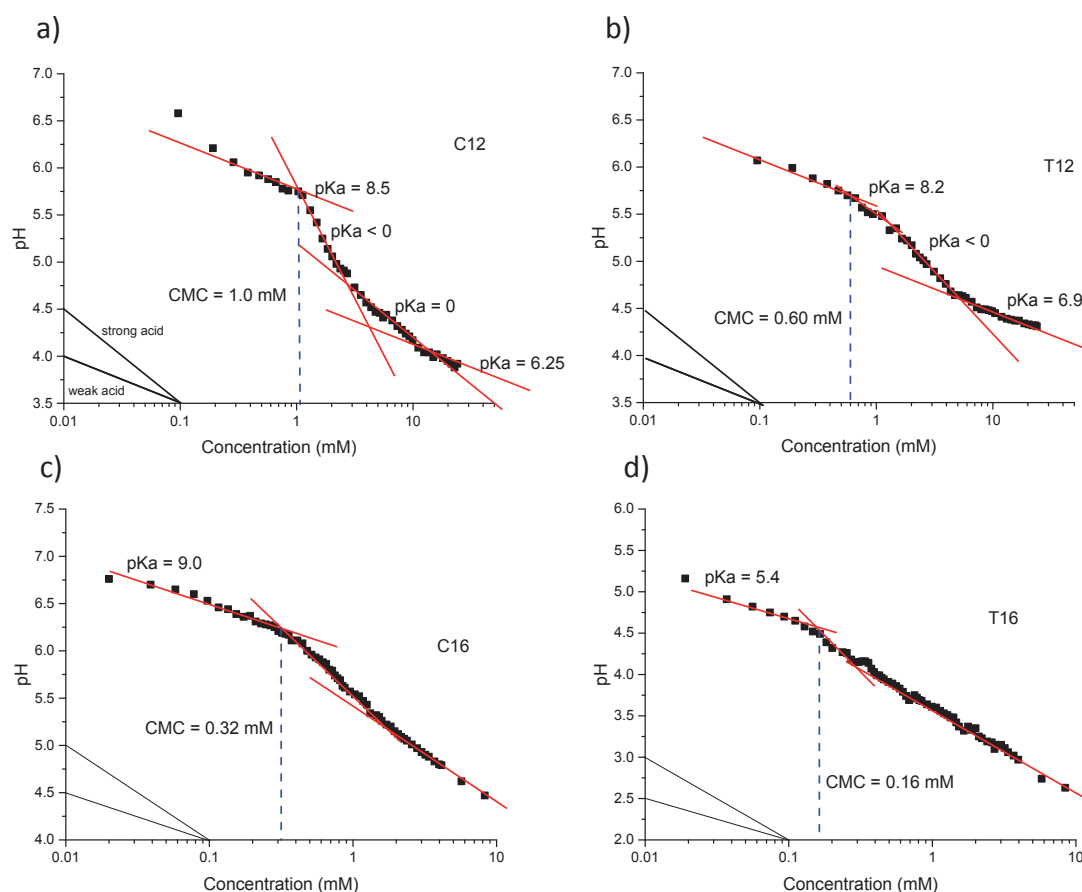


**Figure 92.** pH values at 25 °C versus surfactant concentration. a) C12, b) T12, c) C16 and d) T16.

Once the pH is determined, it is possible to represent the variation of the pKa depending on the concentration of the surfactant according to the following expression (Equation 12).<sup>219</sup> Obtained values are shown in Figure 93.

$$pK_a = -\log \left[ \frac{[H^+]}{C_a \left[ \left( [H^+] - \frac{K_w}{[H^+]} \right)^{-1} \right] - \frac{1}{C_a}} \right] \quad (\text{Equation 12})$$

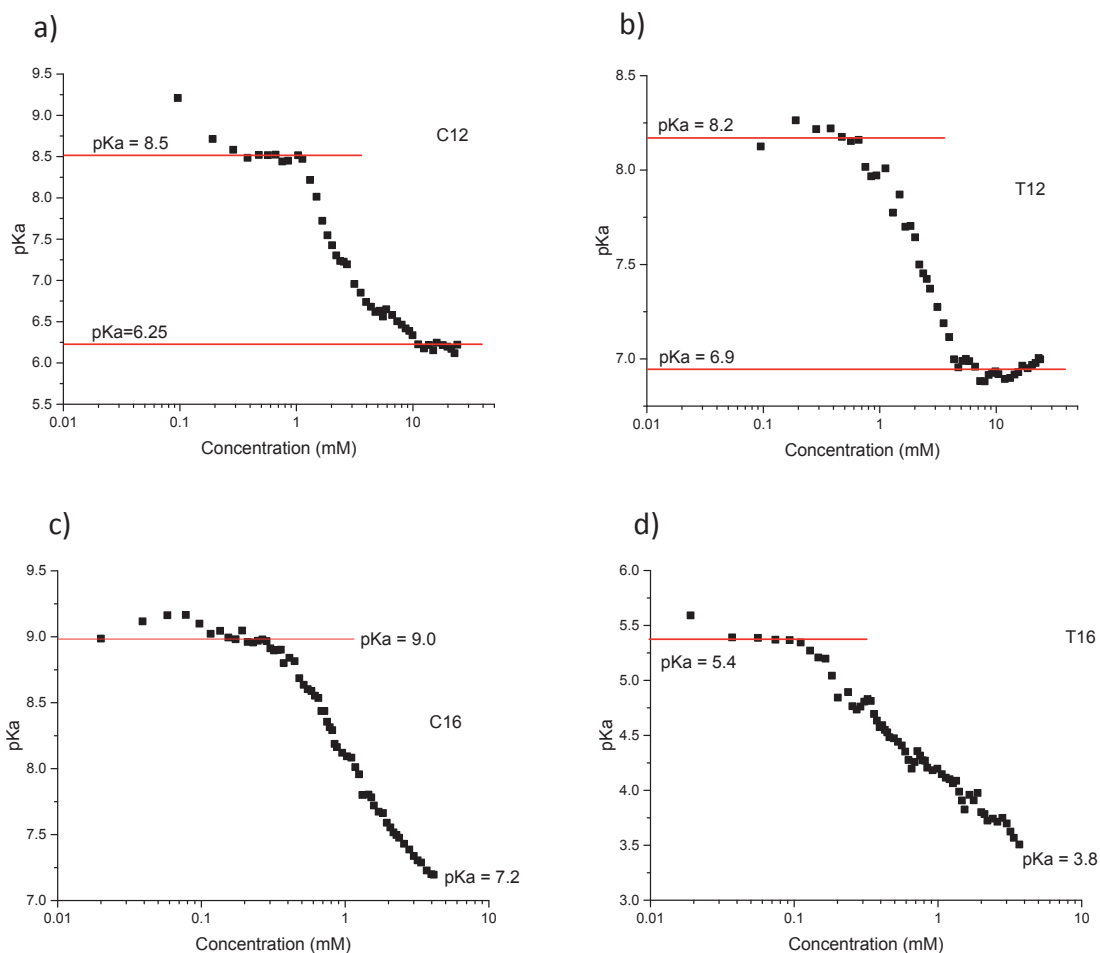


**Figure 93.** Calculated pK<sub>a</sub> values versus surfactant concentration. a) **C12**, b) **T12**, c) **C16** and d) **T16**.

For pH-sensitive amphiphiles, pH measurements as a function of surfactant concentration also provide a simple method for determining the CMC. Referring to the studied molecules, we can observe that at low and high concentrations the pH values follow the expected slope of 1/2 for weak acids, with pK<sub>a</sub> corresponding to the monomers at low concentrations and to the micelles at high concentrations. The onset of micellization will be marked by the first change of slope (at the formation of micelles, a release of protons is produced due to the pK<sub>a</sub> shift of the micelle with respect to the monomer), which corresponds to the CMC. The pK<sub>a</sub> shift of molecules undergoing aggregation has been extensively studied,<sup>220,221</sup> and two main contributions to the pK<sub>a</sub> shift were identified. One contribution comes from the virtual charge effect due to a discontinuity in dielectric constant at the micelle surface<sup>222</sup> and a second contribution comes from the polar head

interaction where some protons are released to the solution in order to stabilize the aggregates.

As it is observed, surfactants with 12-carbon chain length have more or less the same  $pK_a$  before the CMC: 8.5 for **C12** and 8.2 for **T12**. Therefore, in this case, stereochemistry does not play an important role in the acid behaviour of the monomeric molecules. However, the less acid behaviour of the *cis* isomer could be attributed to the strong hydrogen bond formed between the acidic proton from the ammonium group and the carbonyl of the amido group (see section 7.3.2.4) for further information). These values show that these surfactants have weak acidic properties and that their structure will depend on the pH of the solution. However, our surfactants are more acid than dodecylammonium chloride (DAC), which has a  $pK_a$  of 10.63 at 25 °C. Taking into account that the potential application of these surfactants is in the field of the gene therapy and also that the pH of the human blood is around 7.35-7.45, we could see that, at this pH, **C12** and **T12** will be mostly in the acid form, and thus, as cationic surfactants. However, it is important to note that acid-base behaviour could vary in the presence of a polyelectrolyte such as DNA and also with the used buffer solutions.

Looking at the surfactants bearing a 16-carbon chain length, we could observe a non-usual acid character. **C16** shows a  $pK_a$  of 9.0 before the CMC while **T16** shows a very low  $pK_a$  around 5.4. The measurement of the variation of the pH were repeated 4 times preparing again the solutions and even using MiliQ water in order to be sure that there is no influence of external factors. This unexpected behaviour could suggest that, in this case, stereochemistry plays a very important role in the acidity of the proton, in contrast with surfactants with 12-carbon length. Therefore, there would be an interaction between both factors.

A reduction of the apparent  $pK_a$  implies a decrease of the stability of the non-dissociated species (cationic species).<sup>166</sup> If the aggregate of the non-ionic form of the surfactant is formed and it is very stable, it could shift the balance to the non-ionic form that behaves as a pseudo acid, as **T16** does. Thus, this result should not be taken as the real  $pK_a$  of the monomer. During the measurements of **C16**, the solution became turbid, which means that not all the amount of surfactant we are considering is in the solution. Due to the strong hydrogen bond (see section 7.3.2.4) and the long hydrocarbon chain,



the solubility of this compound has an influence on the real concentration in solution and thus, the  $pK_a$  has higher values. For both 16-carbon chain length derivatives, obtained  $pK_a$ 's are not their real values.

A  $pK_a$  shift is observed in all cases. After the CMC, for **C12** the  $pK_a=6.25$  and for **T12**  $pK_a=6.9$ . The variation of  $pK_a$  is higher for **C12** than for **T12**. Thus, these molecules can behave as two different weak acids, before the CMC as monomer molecules and after the CMC as micelles. The  $pK_a$  values after micellization are 7.2 for **C16** and 3.8 for **T16**. However, a weak acid behaviour as micelles was not observed due to the fact that higher concentration cannot be studied because of their low solubility.

As explained before, once molecules start to self-assemble, the pH of the solution starts to decrease with a higher slope. From the intersection of the two lines, the CMC value is obtained. The CMC=1.0 mM for **C12** and CMC=0.60 mM for **T12**. These results can be compared with others from cationic surfactants with same chain length. Dodecylammonium chloride (DAC) has a CMC value at 25 °C of 9 mM at pH 7 and of 15 mM at pH 5.<sup>128</sup> As it is compared, the CMC values of our surfactants are lower than the others. This means that the concentration of aggregation is achieved using less amount of surfactant. Thus, our surfactants are more efficient than others. **C16** has a CMC=0.32 mM and **T16** a CMC=0.16 mM. As it is shown, *cis* surfactants are less efficient than the *trans* ones. Therefore, as in Chapter 6, stereochemistry has an influence on the surfactant efficiency.

Additionally, the relationship between the concentration of the cationic and the non-ionic species can be plotted by just representing  $[H^+]/K_a$  versus the concentration of the surfactant. This relationship gives us information about the total charge of all the surfactants at each point. (Figure 94)

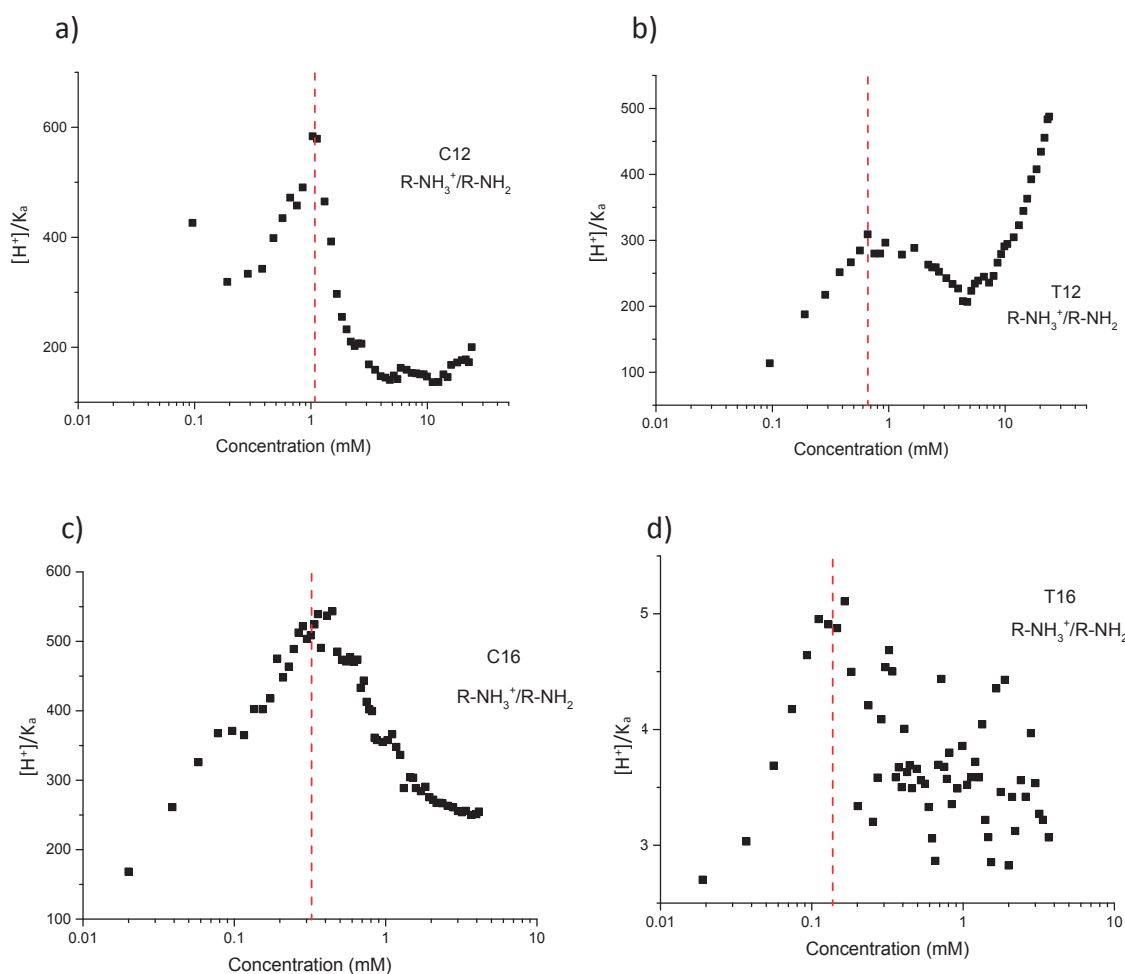


**Figure 94.** Representation of the relationship between the concentration of the cationic and the non-ionic species at each concentration of surfactant. a) **C12**, b) **T12**, c) **C16** and d) **T16**.

These representations help us to understand the behaviour of these surfactants as acids. As it is shown, all of them have a maximum of charge at the CMC point. Before the CMC, each surfactant behaves as a normal weak acid. Once the CMC is reached, the amount of cationic species divided by the amount of non-ionic species starts to decrease in order to stabilize the aggregates and to avoid electrostatic repulsion between surfactants. Once the aggregates are stabilised, the charge starts to increase because the aggregates behave as weak acids again.

Furthermore, looking at the y-axis of these graphs, we could see the order of magnitude of the charge. It shows that, while for the other surfactants the relationship of charge is between 100 and 500, for **T16** is between 3 and 5 showing that the concentration

of the cationic surfactant is only 3-5 times higher than the concentration of the non-ionic surfactant.

The behaviour of these surfactants could be interesting in medicinal chemistry, because changes in the protonation state of pH-titrable headgroups would lead to changes in headgroup area and, as a result, in their aggregation state. Surfactants with this type of behaviour were shown to be efficient vectors for gene therapy because the release of DNA into the cells is improved and, consequently, the level of gene transfection may be increased.<sup>214</sup>

### 7.3.2.1.2 Acid-Base titration of the surfactant aggregates

An aqueous solution at 5 mM (in all cases above the CMC) of our surfactants was prepared. The solution was kept at 25 °C and under nitrogen atmosphere. Then, a previously standardised solution of 5 mM NaOH was added and the pH was measured. Once the titration is finished, a retrotitration using also a previously standardised 5 mM HCl was carried out. In order to determine the equivalence point, the 1<sup>st</sup> and the 2<sup>nd</sup> derivatives were calculated. The  $pK_a$  can be obtained from the pH at the halfequivalence point. This  $pK_a$  will refer to the aggregate, which have the half part of cationic molecules and the half part of non-ionic molecules. In this case, any other effect should not be observed because we are displacing the equilibrium totally.

At the end of the first titration with NaOH, the obtained aggregate consists mostly of non-ionic surfactants, while at the end of the retrotitration with HCl, the aggregate will be mainly made by cationic surfactants.

In order to better analyse the titration curves, the pH versus the recalculated concentration of surfactant at each point were represented. Titration curves are shown in Figure 95.

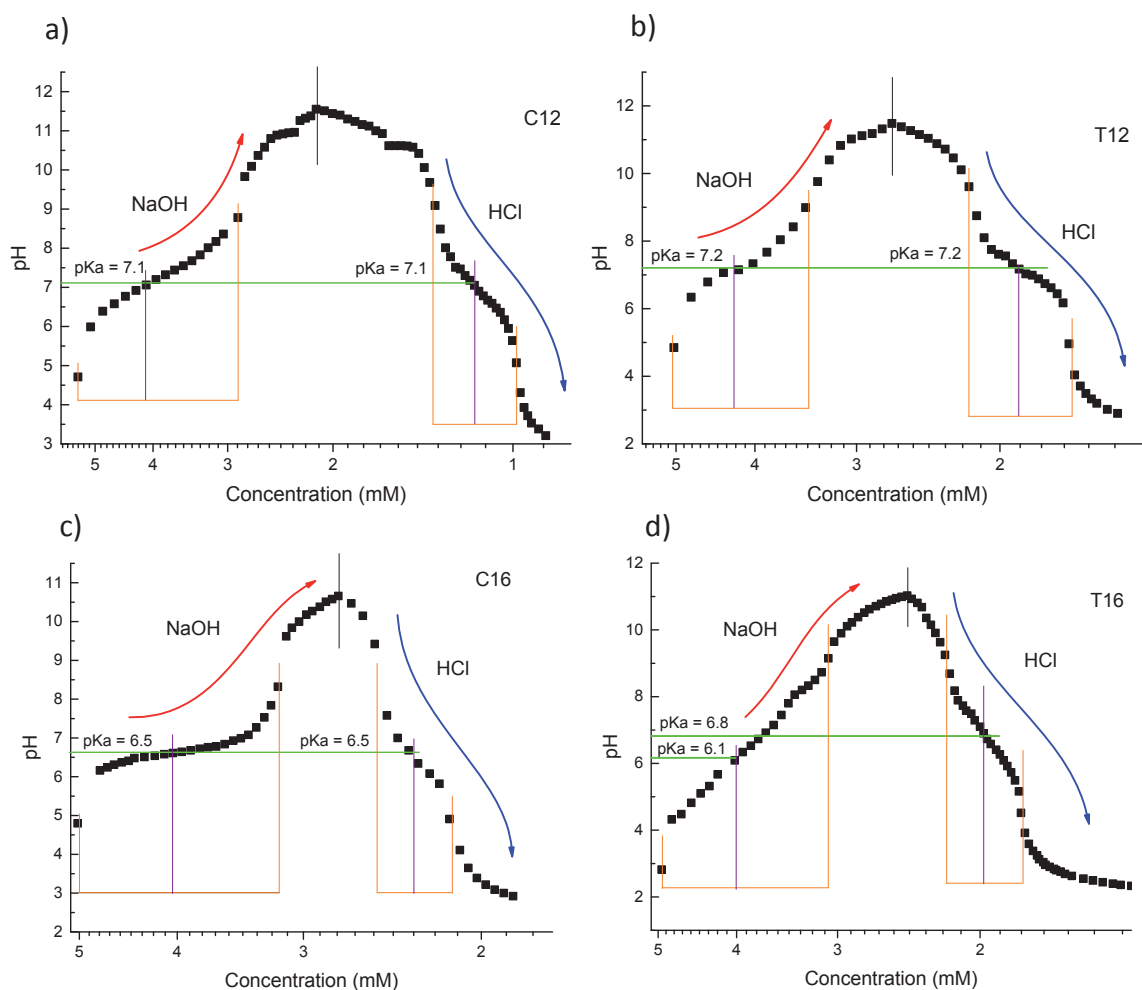


**Figure 95.** Titration curves of 5 mM aqueous solutions of a) **C12**, b) **T12**, c) **C16** and d) **T16** at 25 °C using 5 mM NaOH and 5 mM HCl. In orange are shown the starting points and the equivalence points. In violet are shown the semiequivalence points, and in green are shown the obtained pKa values from the titration curves.

What is shown in these curves is very representative and give us highly significant information. First of all, it is shown that the pK<sub>a</sub> of these aggregates only depends on the length of the chain and not on the stereochemistry. The pK<sub>a</sub> of the half-charged aggregates for the 12-carbon length surfactants is 7.2 while the pK<sub>a</sub> for the 16-carbon length surfactants is around 6.5.

Looking at the profiles of the titration curves, it is shown that for **C12**, **T12** and **C16** there is a clear equivalence point around 3 mM while for **T16** the equivalence point is less clear and it has a homogeneous slope during the NaOH titration. That means that the

starting aggregate is different from the others, as we observed in the first measurements. Our hypothesis seems to be in agreement with this titration. Furthermore, once the non-ionic aggregate is obtained and the retrotitration is carried out, the profile of all the surfactants is more or less the same, showing perfectly the two equivalence points. The first one is related to the remaining base in the medium and the second one refers to our compound. **T16** behaves as the others once the non-ionic aggregate is obtained showing that there is a strong influence of the starting aggregate on the pH measurements.

### 7.3.2.2 Measurements of the surface tension

Once the acid-base behaviour of the four studied compounds was determined, their behaviour as surfactants was studied. Until now, all the studies were carried out in the bulk of the solution. Nevertheless, the pendant drop method measures the variation of the surface tension of the air-water interface and thus, it measures the change of the property at the surface of the solution.

As observed before, these pH sensitive surfactants are not purely cationic surfactants, but they are a mixture of cationic and non-ionic surfactants depending on the pH. Therefore, in order to study their surfactant behaviour, different measurements of the surface tension were carried out at different pH values. The limit behaviour as cationic surfactants can be studied at pH 2, and it can be achieved by preparing all the samples using 5 mM HCl. The limit behaviour as non-ionic surfactants can be studied at pH 12, and it can be achieved by preparing all the samples using 5 mM NaOH. Finally, to investigate the surfactants of mixed natures, a third study was carried out using water as solvent and without modifying the pH. It was called natural pH because the pH will be given by the surfactant itself. Surface tension was measured using the procedure explained in section 10.4. Representation of the surface tension versus surfactant concentration at three different pH's is shown in Figure 96.

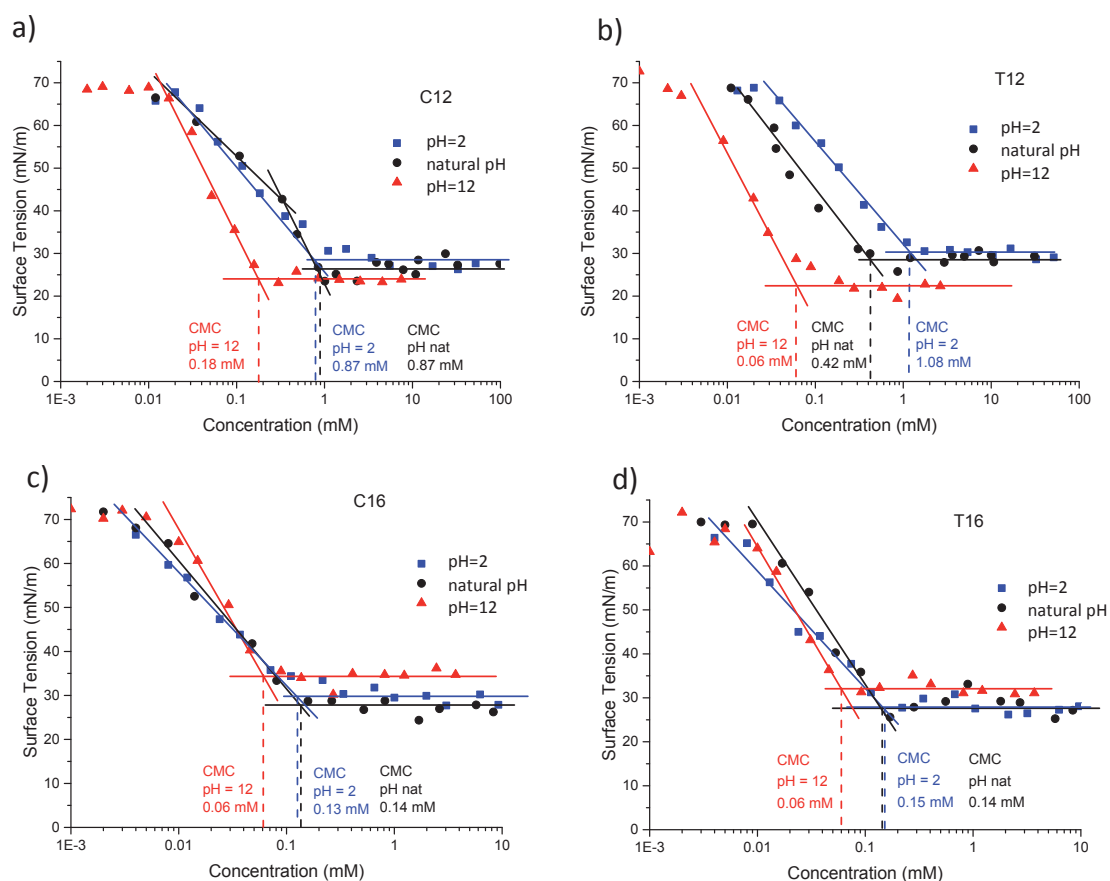


**Figure 96.** Surface tension versus surfactant concentration for a) **C12**, b) **T12**, c) **C16** and d) **T16** at three different pH values (2, natural and 12).

As in the Chapter 6, from these curves, it is possible to obtain different parameters to compare the surfactant behaviour. All these values are summarised in Table 17.

First of all, from the  $\Pi_{CMC}$  values, we can deduce that all the studied compounds behave as surfactants because they can reduce the surface tension of the air-water interface more than 30 mN/m.

Special attention has to be paid to the obtained CMC values, because they will mark the working concentrations for the study of the interaction with the DNA. At pH 2, both *cis* and *trans* surfactants of each chain length have a very similar CMC value: around 1 mM for the 12-carbon length and around 0.15 mM for the 16-carbon length. The behaviour of these cationic surfactants can be compared with other well-known such as DTAB (12-carbon length) and CTAB (16-carbon length). DTAB has a CMC=16 mM at 25 °C<sup>223</sup> and CTAB has a CMC=0.98 mM at 25 °C<sup>224</sup>. As it is shown, the presence of each CH<sub>2</sub> seems to decrease

**Table 17.** Maximum Gibbs surface excess ( $\Gamma_{\max}$ ), area per molecule at the surface, CMC and effectiveness ( $\Pi_{\text{CMC}}$ ) obtained from the plot of the surface tension versus the surfactant concentration of compounds **C12** and **T12**.

Compound	pH	$\Gamma_{\max}$ ( $\mu\text{mol}/\text{m}^2$ )	Area ( $\text{\AA}^2/\text{molec}$ )	CMC <sub>2,1,3</sub> <sup>‡</sup> (mM)	$\Pi_{\text{CMC}}$ (mN/m)
<b>C12</b>	2	4.1	41	0.87	41.5
	nat.	6.7-3.4	25-50	<b>0.87</b>	46.8
	12	7.3	23	0.18	48.0
<b>T12</b>	2	4.2	40	1.08	40.8
	nat.	4.6-2.3	36-72	<b>0.42</b>	44.3
	12	7.6	22	0.08	49.9
<b>C16</b>	2	4.3	39	0.13	44.6
	nat.	5.0-2.5	33-66	<b>0.14</b>	44.6
	12	7.5	22	0.06	37.4
<b>T16</b>	2	4.2	39	0.14	43.6
	nat.	6.2-3.1	27-54	<b>0.15</b>	44.4
	12	7.8	21	0.06	40.2

<sup>‡</sup> 2,1,3 refers to the equilibria shown in Figure 91 (p. 154)

4 times the CMC. However, in our cases, the cyclobutane moiety seems to smooth this effect and the reduction of the CMC is less than 2 times for each CH<sub>2</sub>. That means that these surfactants are more efficient than the commercial ones. At pH 2, having only cationic surfactants, stereochemistry seems not to play any role; however, CMC values for the *trans* isomers are slightly higher.

At pH 12, the CMC values of the compounds seem to be more dependent on the stereochemistry and on the length of the chain. For the non-ionic **C12** surfactant, the CMC value is around 0.18 mM while for the **T12** is around 0.08 mM. The *trans* isomer seems to be more efficient than the *cis* one. However, for both 16-carbon length the CMC is around 0.06 mM, so in this case, the length of the chain has more influence on the solubility and thus on the CMC value than the stereochemistry. Therefore, both **C16** and **T16** behave similarly as non-ionic surfactants.

Finally, at natural pH, where there is a mixture of cationic and non-ionic surfactant, the CMC values seem to have the same behaviour than at pH 12. **C12** has a CMC=0.87 mM while **T12** has a CMC=0.42 mM. Moreover, **C16** and **T16** have CMC values around 0.15 mM. These values can be compared with the obtained ones when measured in the bulk of the solution. The values of CMC for these four surfactants at natural pH are summarised in Table 19.

**Table 18.** Summary of the obtained CMC values in water solution and at the surface.

Surfactant	CMC <sub>1</sub> Solution (mM)	CMC <sub>1</sub> Surface (mM)
<b>C12</b>	1.0	0.89
<b>T12</b>	0.60	0.42
<b>C16</b>	0.32	0.14
<b>T16</b>	0.16	0.15

All the CMC values are between 0.1 and 1 mM. These values are very interesting for biological applications, because only a small amount of each surfactant would be necessary to interact with DNA molecules. As it is shown, there is some discrepancy between CMC values of the same compound but it is, as explained before, because they were obtained by measuring different physical properties. Additionally, one of them is measured in solution and the other at the surface and as there are different equilibria, CMC values can vary from the surface to the solution. Physical properties measured at the surface normally show the change at a lower concentration than physical properties measured in solution. Nevertheless, it could vary depending on the method.<sup>134,216</sup>

Effectiveness and efficiency can easily be calculated as explained in Chapter 6. According to other studies, non-ionic surfactants are more efficient than their cationic homologue due to the solubility. Non-ionic surfactant are less soluble in water than the cationic ones and thus they start to self-assembly earlier in order to decrease the energy of the system.

For **C12** and **T12**, the non-ionic surfactants are more effective than the cationic ones. That means that they can saturate the surface of the solution with their carbon



chains more than the cationic ones. That sounds reasonable because the cationic surfactants have electrostatic repulsion between them and, then, they should not saturate the surface as well as the non-ionic do. However, looking at **C16** and **T16**, the non-ionic surfactants are less effective than the cationic ones. Looking at the literature, there are some examples of surfactants that are less effective as non-ionic than as cationic state, but it is not the usual behaviour.<sup>128</sup>

Finally, the calculation of the area that these surfactants occupy at the surface was calculated. Based on the Gibbs absorption isotherm, the slope of the curve before the CMC is described in Equations 6 and 7 (described in pages 11 and 125, respectively). Working at pH 2 and using HCl, the concentration of  $\text{Cl}^-$  remains practically constant and thus its derivative is zero. Therefore, only the derivative of the concentration of the cationic moiety has to be considered and  $n=1$  at pH 2. At pH 12 there is not any problem to discuss that also  $n=1$  because it is a non-ionic surfactant and thus, it is the only species that is absorbed at the surface. The problem comes when we try to determine how many species are absorbed at the surface at natural pH, where we have a mixture of surfactants and where the concentration of the counterions has to be taken into account. In fact, there will be three types of species absorbed at the surface, but the concentrations of them are not independent because they are in equilibrium. Therefore, what we have done to solve this dilemma is to consider both, 1 and 2, as the number of species absorbed at the surface, and then the real area will be a number between these two calculated values.

Looking at the obtained values of the experimental areas of these surfactants at the surface, we can observe that all of them, when they are in the cationic state, occupy around  $40 \text{ \AA}^2$  while when surfactants are in the non-ionic state they occupy around  $22 \text{ \AA}^2$ , which corresponds to the minimum area that a carbon chain occupies at the surface.<sup>172</sup> This result shows that in all cases they are able to saturate the surface of the solution with their carbon chains. The area per molecule of the cationic surfactants are bigger than the non-ionic surfactants due to the repulsion between the charges.

Finally, it can be observed that the obtained result of the area per molecule at natural pH is between 22 and  $40 \text{ \AA}^2$ . However, this value has no physical sense because it does not refer to any particular molecule but to a mixture of molecules. Taking into

account the surfactant behaviour, all of them are good candidates for being studied as new potential vectors for gene therapy.

### 7.3.2.3 Cryogenic Transmission Electron Microscopy (CryoTEM)

The aggregation of these four surfactants above the CMC at three different pH values (2, natural and 12) was studied by using TEM microscopy at  $-200\text{ }^{\circ}\text{C}$ , freezing the sample using liquid ethane to avoid water crystallization and the modification of the structure of the aggregates. This technique could be useful to determine the morphology of the aggregates at high concentrations, but in order to better understand the system at lower concentrations, this technique has to be accompanied with other techniques such as Dynamic Light Scattering (DLS) or theoretical calculations. A representative cryoTEM image of the aggregation of these molecules is shown in Figure 97 for each compound. All the cryoTEM images are shown in section 12.1.

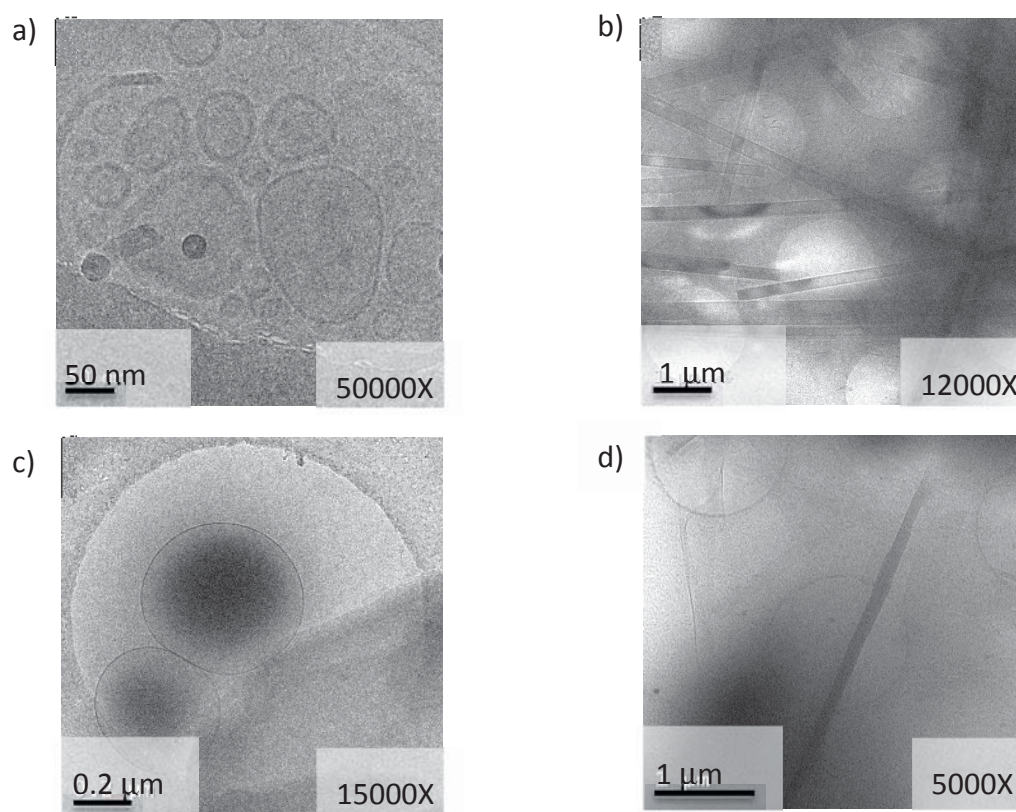


**Figure 97.** Representative cryoTEM images of a) C12, b) T12, c) C16 and d) T16.

Due to the low detection limit of the technique, samples were measured at very high concentration, much higher than the CMC. In this way, the morphology of these surfactants observed by cryoTEM show how they self-assemble at high concentrations. The morphology of the aggregates vary depending on the concentration.<sup>225</sup> Table 19 summarises the obtained morphologies.

**Table 19.** Summary of the cryoTEM images of the studied compounds.

Surfactant	pH 2	pH natural	pH 12
<b>C12</b>	<b>Vesicles</b> of different sizes (20-500 nm $\emptyset$ ). Multilayer vesicles.	<b>Vesicles</b> of different sizes (20-500 nm $\emptyset$ ). Multilayer <b>vesicles</b> (8-10 layers).	Big and irregular aggregates.
<b>T12</b>	Big and irregular aggregates. Some <b>fibers</b> .	Formation of <b>fibers</b> .	Very long <b>fibers</b> (8-11 $\mu\text{m}$ ), 380 nm width. Some <b>vesicles</b> .
<b>C16</b>	<b>Vesicles</b> (400-500 nm $\emptyset$ ). Elongated aggregates (1-2 $\mu\text{m}$ ).	Elongated aggregates (1-4 $\mu\text{m}$ ).	Big and irregular aggregates. Some <b>vesicles</b> .
<b>T16</b>	Big and irregular aggregates. Some branched <b>fibers</b> . Some <b>vesicles</b> .	Long <b>fibers</b> . Large laminar surfaces.	Long <b>fibers</b> (>3 $\mu\text{m}$ ). Irregular aggregates.

As it is shown, stereochemistry has a strong influence on the morphology of the aggregates. As general observation, *cis* surfactants seem to self-assemble forming vesicles, while *trans* surfactants seem to self-assemble forming fibers.

### 7.3.2.4 Theoretical Calculations

In order to find out some relevant information about the structure of the monomers and the aggregates, theoretical calculations were carried out following the procedure described in section 9.5. Predicted structures of the monomers show that a hydrogen bond is formed between the carbonyl group of the amide and a hydrogen of the free amine/ammonium group. In Figure 98, predicted structures of **C12** and **T12** at pH 2 and at pH 12 are shown. Surfactants **C16** and **T16** show the same geometry of the polar head and thus, they are not shown. Table 20 summarises the hydrogen bond distances of each compound as cationic and non-ionic surfactants.

**C12**, cationic:



**C12**, non-ionic:



**T12**, cationic:



**T12**, non-ionic:



**Figure 98.** Predicted structures of **C12** and **T12** as cationic and non-ionic forms. Non-polar hydrogen atoms were omitted for clarity.

As it is shown, *trans* isomers show weak hydrogen bonds and, due to the stereochemistry, its distance is similar in both forms. Cationic *cis* isomers form a hydrogen bond stronger than non-ionic ones. **C16** has not only a strong hydrogen bond but also, a long chain. Both factors could cause the low solubility of this compound. **C12** is more soluble due to the length of the chain, but is less soluble than **T12** and the strength of the hydrogen bond could be the explanation.

**Table 20.** Distances of the hydrogen bonds of the monomers of surfactants **C12**, **T12**, **C16** and **T16**. Distances are shown in Å.

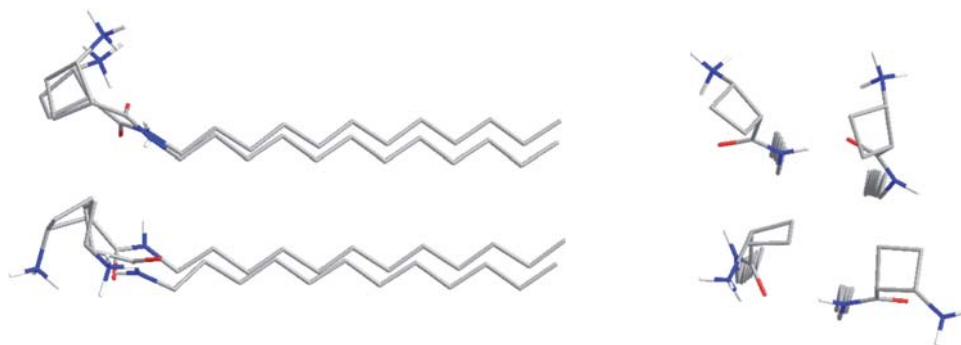
Surfactant	C=O····H-N (Å)	
	cationic	non-ionic
<b>C12</b>	1.979	2.469
<b>T12</b>	2.853	2.863
<b>C16</b>	2.042	2.639
<b>T16</b>	2.858	2.869

Once the structure of the monomers is known, the study of the formation of a tetrameric aggregate in water was done. Predicted structures of **C12** and **T12** in the cationic and non-ionic forms are shown in Figure 99.

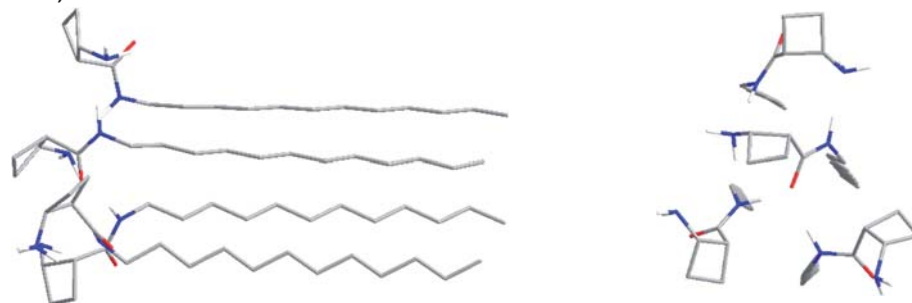
Predicted structures were obtained following the same procedure for all cases and the starting geometry was the same for all the surfactants. However, results show that there is a clear influence of the stereochemistry of the cyclobutane moiety. Both *cis* isomers show aggregation in two dimensions and we could not conclude that there is a preferential direction while *trans* isomers show aggregation in only one dimension. Figure 100 shows the obtained aggregation pattern of these surfactants.

Taking into account only four molecules few information about the final supermolecule can be obtained and, of course, the structure of the whole aggregate cannot be predicted. However, self-assembly in two directions could be associated to surfaces (of a vesicle for example) while self-assembly in one direction could be associated with fibers. These associations could be related to cryoTEM images, in which as a general view *cis* surfactants form vesicles and *trans* surfactants form fibers.

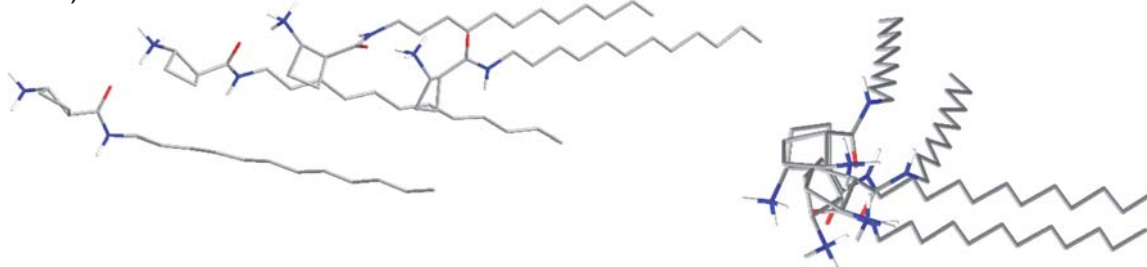
**C12, cationic:**



**C12, non-ionic:**



**T12, cationic:**



**T12, non-ionic:**

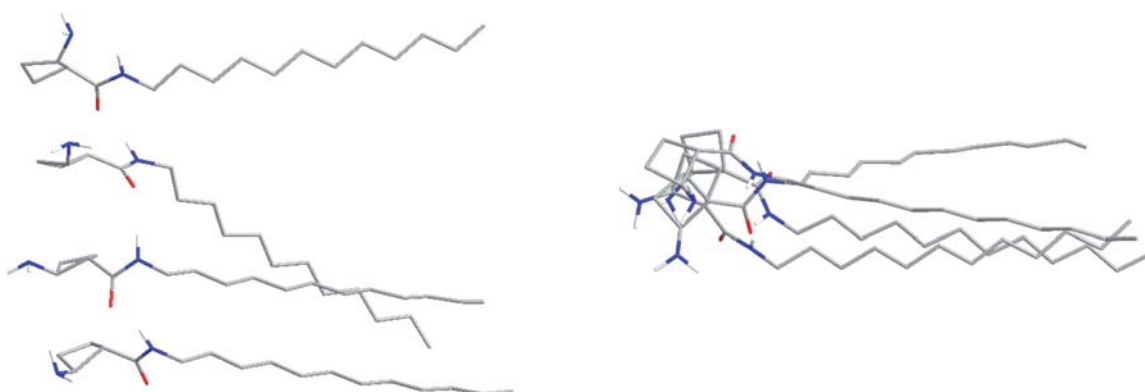


**Figure 99.** Side and top view of the predicted structures of the tetramers of surfactants **C12** and **T12** in the cationic and non-ionic forms.

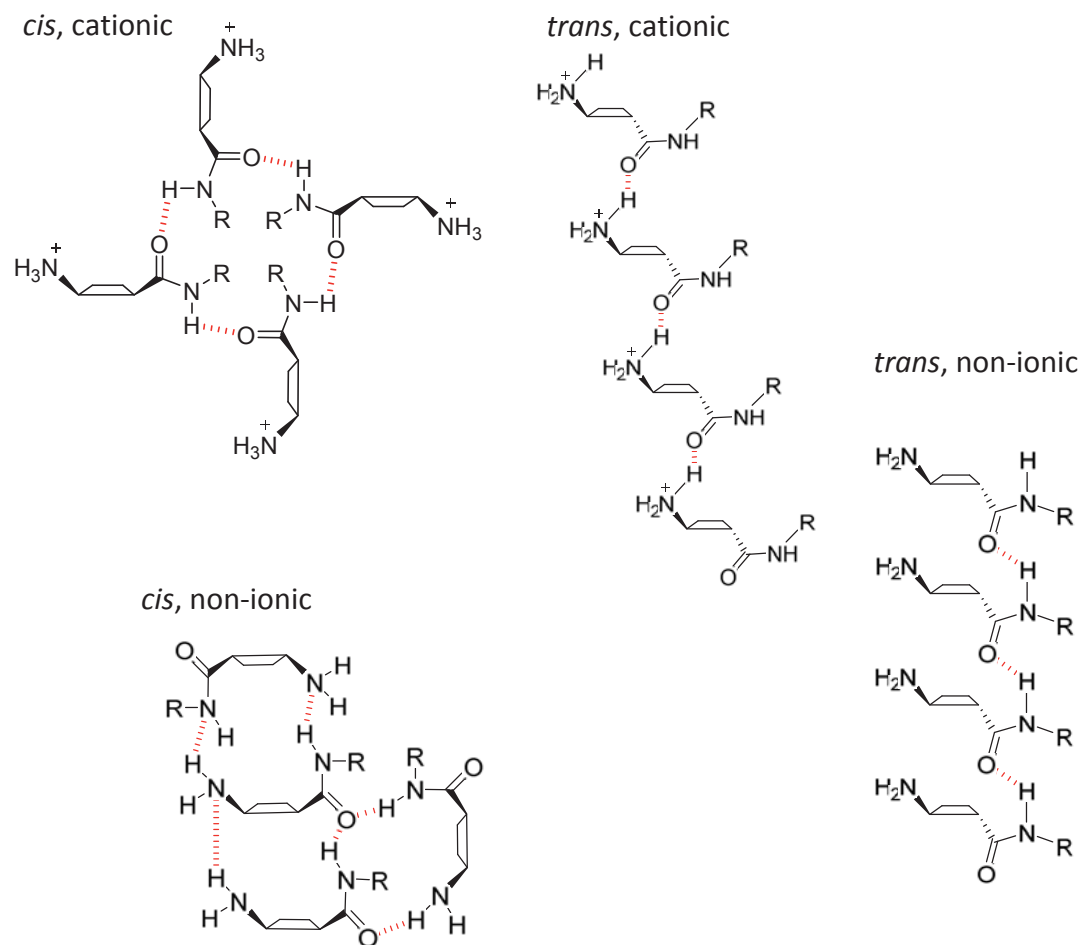


**Figure 100.** Representation of the aggregation patterns of the studied surfactants.

Figure 101 shows the energies of the formation of the tetramers from the monomers.

A clear influence of the stereochemistry can be observed. Aggregation process of *cis* surfactants is more favourable than *trans* surfactants. It could be related to the stability of the monomer in solution. *cis* surfactants are less soluble due to the stronger intramolecular hydrogen bond compared with the *trans* ones. Therefore, *cis* monomers self-assemble into aggregates in order to minimize the energy of the system. Additionally, 16-carbon-long chained surfactants have a lower aggregation energy than the 12-carbon-long surfactants. It could be attributed to the stronger van der Waals interaction due to the presence of four more  $-\text{CH}_2-$  in the chain, which contribute to the stabilization of the aggregate.

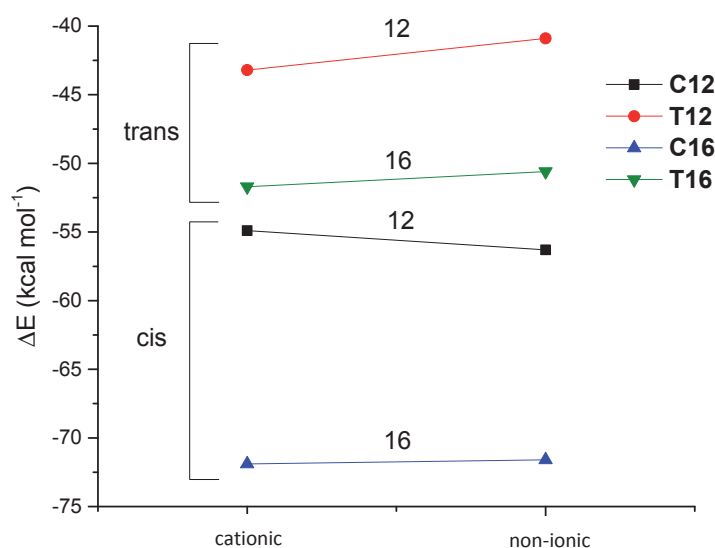


**Figure 101.** Representation of the aggregation energies of the studied surfactants as cationic and non-ionic forms.

### 7.3.2.5 Dynamic Light Scattering (DLS)

Dynamic Light Scattering is a technique based on the scattered light to determine the size of the particles (or aggregates) that are in solution typically in the sub-micron region. It is also referred as Photon Correlation Spectroscopy or Quasi-Elastic Light Scattering.

Particles in solution have a Brownian motion. This movement depends on the size of the particles. The bigger is the particle, the slower will be the Brownian motion. DLS analyses the Brownian motion using scattered light (for further information, see section 10.10).

Samples are irradiated using a laser as light source and the detector is placed at 173 ° or 90 °, depending on the instrument. Depending on the dispersity of the system and the size of the particles (aggregates), different information can be obtained from the scattered light. The ideal system for DLS is a monodisperse system where all the particles have the same size and the same shape. DLS measurements were carried out in the *Department of Biotechnology of the NTNU* in Trondheim (Norway). (See section 10.11 for



details). Samples were prepared at the CMC and at pH 7.4 using 10 mM TrisHCl, in order to obtain information about the first aggregates that are formed at the lowest concentration.

Depending on the size of the particles, correlation function will show an early (small particles) or late (big particles) decay. However, if different sizes are present, different decays or a mixture of all the decays will be observed. For a polydisperse system, correlation function depends on the sum of all the exponential decays and the treatment of the data becomes difficult. Correlation functions of the DLS measurements are shown in section 12.2.

In all cases, the maximum intensity (y-intercept values) is higher than 0.8, so, the signal-to-noise ratio is high and thus, data quality is good. However, only **C12** shows the same decay at the three replicates. That means that at least all the other samples are polydisperse. **C12** could be also polydisperse if the decay is the sum of different exponential decays. Each decay is associated to one translational diffusion coefficient (Brownian motion rate), and using the Stokes-Einstein equation, each diffusion coefficient can be related to a specific hydrodynamic diameter  $d_H$  of a spherical particle. Stokes-Einstein equation (Equation 13).

$$d_H = \frac{k_B T}{3\pi\eta D_t} \quad (\text{Equation 13})$$

In order to determine the size of particles and to verify the dispersity of the samples, the intensity of the scattered beam depending on the size ( $d_H$ ) of the particle was represented in Figure 102.

As it is shown, all these samples show different peaks at different sizes. That means that the aggregates have different sizes. However, in some cases, each measurement shows a different distribution than the others, meaning that the sample is not only polydisperse but also irregular. From these measurements, different parameters could be calculated. One the one hand, the mean of each peak can be obtained with its associated error. The polydisperse factor (PDI) shows the degree of polydispersity of the sample. A sample has to be considered polydisperse if the PDI is higher than 0.4. A monodisperse sample has a value of PDI around 0.0-0.1 and a moderate polydisperse system has a PDI value between 0.1-0.4.<sup>226</sup> All the PDI values shown in Table 21 are higher than 0.4 and thus,

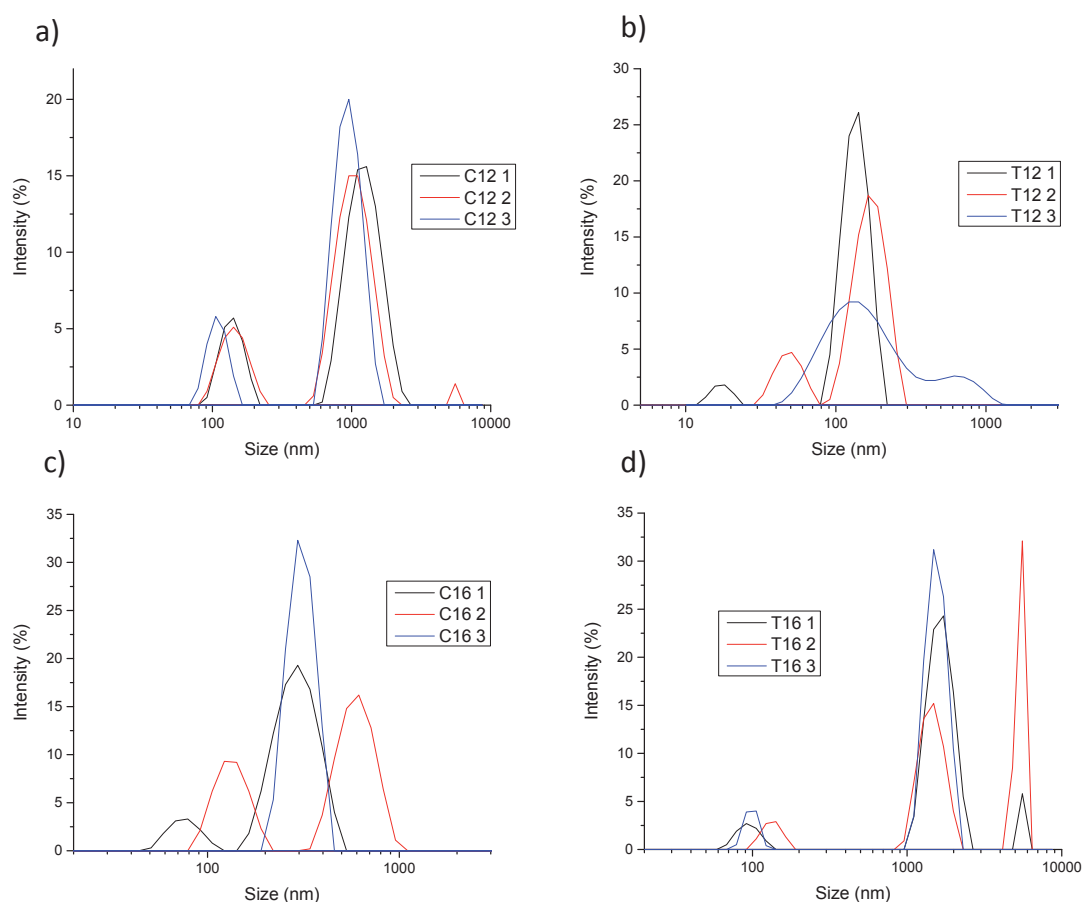


**Figure 102.** Representation of the intensity of the scattered beam at different sizes from the DLS measurements of a) 1.2 M **C12**, b) 0.4 M **T12**, c) 0.2 M **C16** and d) 0.2 M **T16**.

these samples are too polydisperse for a single distribution analysis. The distribution analyses were done taking into account the number of groups of population. The averaged  $\zeta$ -diameter of the particles (aggregates) is calculated taking into account the scattered intensity from the particle and the diameter of each particle and it is expressed as  $D_z$ .<sup>227</sup>  $D_z$  can be understood as the averaged harmonic diameter of the particle taking into account the surface potential, the Stern layer and the  $\zeta$ -potential layer of the aggregates. Values of the  $D_z$  and the translational diffusion coefficient ( $D_t$ ) are also shown in Table 21.

**C12** has two main preferred sizes, around 131 and 1092 nm. On the other hand, **T12** shows a polydisperse system around a size of 155 nm. **C16** shows also different dispersities depending on the measurement, but all the aggregates have a size around 403 nm. Finally, **T16** shows a similar distribution than **C12**, showing, in this case, three preferred sizes, around, 109, 1554 and 5480 nm.

**Table 21.** Size of the aggregates ( $d_H$ ), polydisperse factor (PDI), averaged  $\zeta$ -diameter ( $D_z$ ) and translational diffusion coefficient ( $D_t$ ) obtained from the DLS experiments of surfactants **C12**, **T12**, **C16** and **T16**.

Surfactant	$d_H$ (nm)			PDI	$D_z$ (nm)	$D_t$ ( $10^4 \mu\text{m}^2/\text{s}$ )
	Peak 1	Peak 2	Peak 3			
<b>C12</b>	1092 $\pm$ 206 (80.1) <sup>a</sup>	131 $\pm$ 26 (19.4)	--	0.82	613.4 $\pm$ 25.9	8.0 $\pm$ 0.3
<b>T12</b>	155 $\pm$ 24 (85.6)	238 $\pm$ 482 (12.9)	--	0.41	291.1 $\pm$ 125.6	18.4 $\pm$ 9.7
<b>C16</b>	403 $\pm$ 238 (84.4)	70 $\pm$ 91 (15.6)	--	0.55	42.9 $\pm$ 58.3	10.1 $\pm$ 1.2
<b>T16</b>	1554 $\pm$ 132 (76.2)	109 $\pm$ 30 (19.2)	5480 $\pm$ 187 (4.6)	0.43	314.9 $\pm$ 427.8	1.0 $\pm$ 0.1

<sup>a</sup> Results in parentheses show the percentage of the population that represents each peak.

For **C12**, these sizes could be related to the two different types of vesicles that are observed by CryoTEM (Figure 142). One type shows small vesicles of different sizes and the other shows a multilamellar big vesicles. **T12** shows a very polydisperse system in CryoTEM where the formation of different fibers can be observed (**Figure 143**). CryoTEM images of **C16** show that at high concentration vesicles are formed but also elongated aggregates are found (Figure 144). At the CMC, DLS shows that a polydisperse system is formed by aggregates of diameter between 100 and 1000 nm, which could suggest the formation of vesicles and bigger aggregates. Finally, **T16** forms long fibers and “book-like” aggregates. This polydisperse system is in agreement with the DLS results, which means that at the CMC the system is already polydisperse.

Both DLS and cryoTEM suggest that these surfactants self-assemble forming polydisperse and complex systems at the CMC and at higher concentrations.

### 7.3.2.6 Circular Dichroism

Aggregation of chiral surfactants into non-chiral or chiral aggregates can be followed using circular dichroism.<sup>216,228,229</sup> Measurements before and after the CMC lead us to see whether the chirality of the monomer is transferred to the aggregate, through the formation of intermolecular hydrogen bonds.<sup>154</sup> If the circular dichroism spectra of an

aggregate and of the corresponding monomer match, it would mean that the free rotation of the monomer inside the aggregate is possible.

**C12**, **T12**, **C16** and **T16** have an amide group as chromophore, so analysing the spectra between 200 and 250 nm we could obtain information about the chirality of the system.<sup>88</sup> Taking into account that theoretical calculations show that they self-assemble forming hydrogen bonds, one could expect that the CD spectra before and after the CMC is different because Cotton effects are extremely sensitive to changes in the “chiral environment” close to the chromophore to which they are allied and to interchromophoric interactions in supramolecular aggregates.<sup>125</sup> Samples of **C12** and **T12** were prepared at 5 mM in water and different dilutions were made in order to obtain a range of different concentrations around the CMC. Measurements were done using the methodology described in section 10.7.1. Figure 103 shows the CD spectra of surfactants **C12** and **T12** at different concentrations in water.

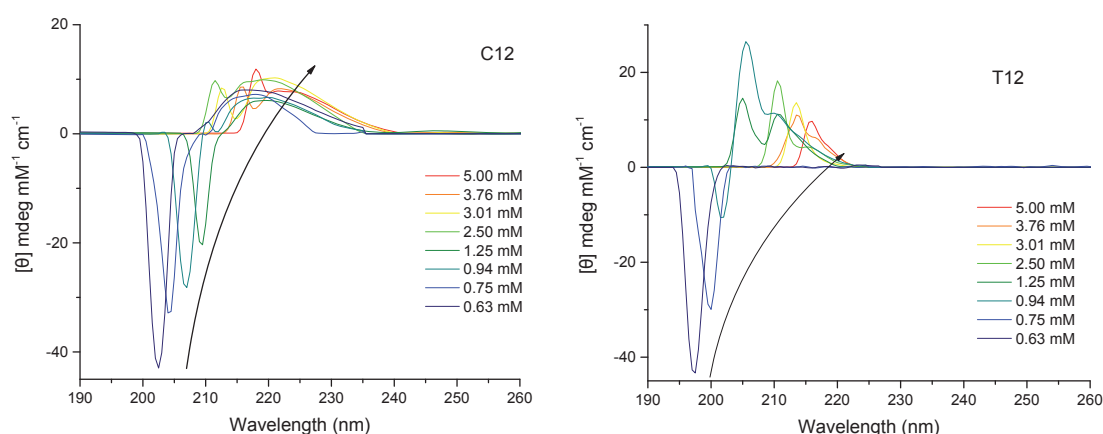


**Figure 103.** Circular Dichroism spectra of surfactants **C12** (left) and **T12** (right) at different concentrations in water.

The theoretical CD spectrum of each monomer was calculated following the methodology described in section 9.5 in order to compare them with the experimental ones. Predicted CD spectra of **C12** and **T12** are shown in Figure 104. In solution, both surfactant monomers show the same shape of the CD signal, which is in agreement with the predicted CD spectra for these surfactants. However, the wavelength of the maximum is not in agreement with the experimental data probably due to limitations of the

calculation and maybe because in this case it is concentration-dependent. **C12** shows a negative band at 202 nm and **T12** shows a negative band at 197 nm.

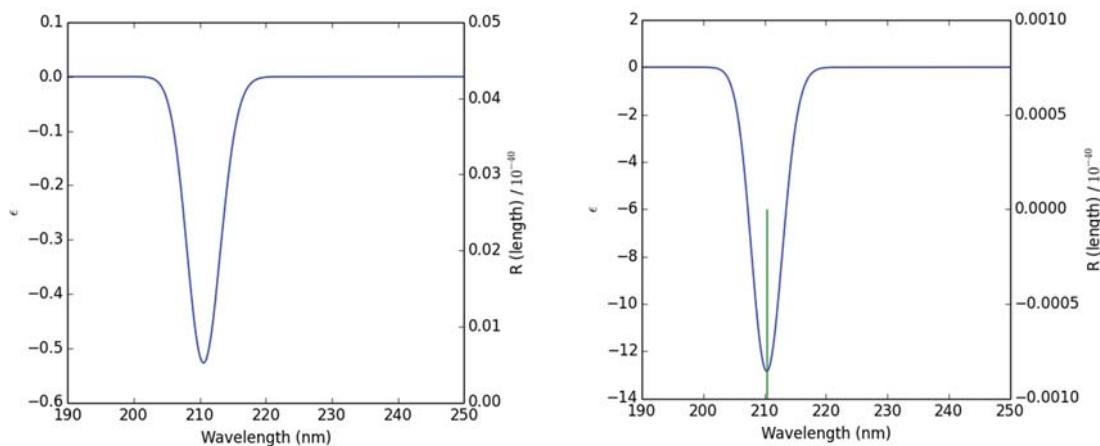


**Figure 104.** Predicted CD of surfactants **C12** (left) and **T12** (right) at M06-2X/6-311++G(2df,2pd) level of theory calculating 30 excited states.

When increasing the concentration of surfactant, the signal of the monomer is shifted to longer wavelengths. In addition, the intensity and the shape of the signals is progressively shifted from the lowest to the highest concentration. This is related to the appearance of chiral aggregates through the formation of intermolecular hydrogen bonds, which is in agreement with the predicted structures obtained using theoretical calculations. The red shift is related to a change in the energy of the transitions of the chromophore group.<sup>125</sup> The monomer has the strongest transition, which is related to the intramolecular hydrogen bond. When increasing the concentration of surfactant, intermolecular hydrogen bonds are formed and they are weaker than intramolecular hydrogens in the monomer. Thus, the red shift could be attributed to the formation of aggregates through the chromophore group. Measurements of the UV-vis absorption of each surfactant solution at different concentrations were carried out in order to verify the obtained CD spectra and also to determine whether a red shift could also be observed (Figure 105).

These compounds absorb UV light from at least 190 until around 230 nm. Thus, obtained CD spectra are fitted in the range of absorption of these compounds.

Furthermore, a slight red shift can be observed from low concentrations to higher concentrations, in agreement with CD results. However, the maximum of absorption of the UV-vis light is not the same as the maximum of absorption of the circularly polarized light.

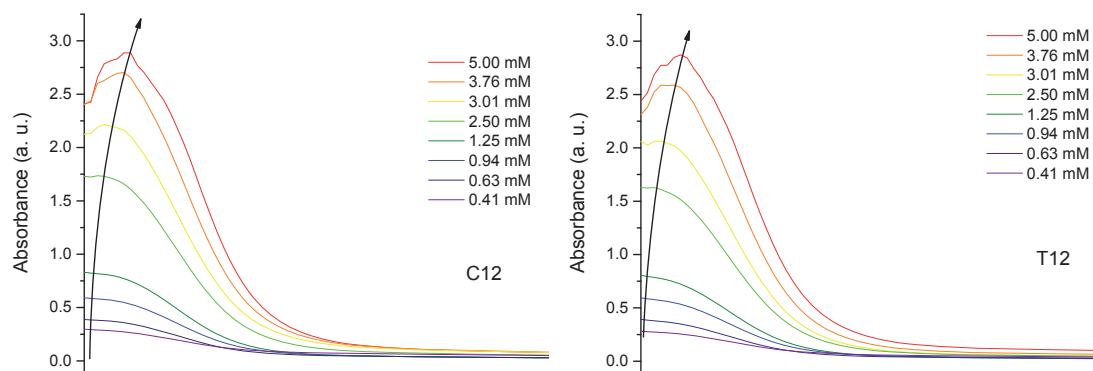


**Figure 105.** UV-vis absorption spectra of surfactants **C12** (left) and **T12** (right) at different concentrations.

The determination of the CMC using absorption of UV-vis light was already reported.<sup>231–234</sup> The change in absorption is related to the formation of aggregates. However, these techniques are based only on the intensity of the absorption and not on the wavelength of the maximum absorption and a clear peak in the spectra should be observed in order to determine the maximum. In 2002, Vijay and Polavarapu studied chiroptical properties of mixtures of surfactants.<sup>235</sup> They analysed the specific optical rotation and the CD spectra of different mixtures of sodium dodecyl sulphate (SDS), which is an achiral surfactant, with a chiral surfactant. A variation of the specific rotation and the circular dichroism was observed. They related this variation to the formation of chiral aggregates. However, also in this case, only peak intensities and band areas were represented.

In our case, the shift of the maximum of absorption is concentration-dependent. Therefore, we decided to represent the wavelength at which the CD spectra show a maximum against the surfactant concentration. In the case of **C12**, only the peak of maximum absorption was considered and in the case of **T12**, the weighted average of each wavelength was calculated to determine the maximum of absorption. Representations of the maximum of absorption depending on the concentration are shown in Figure 106.

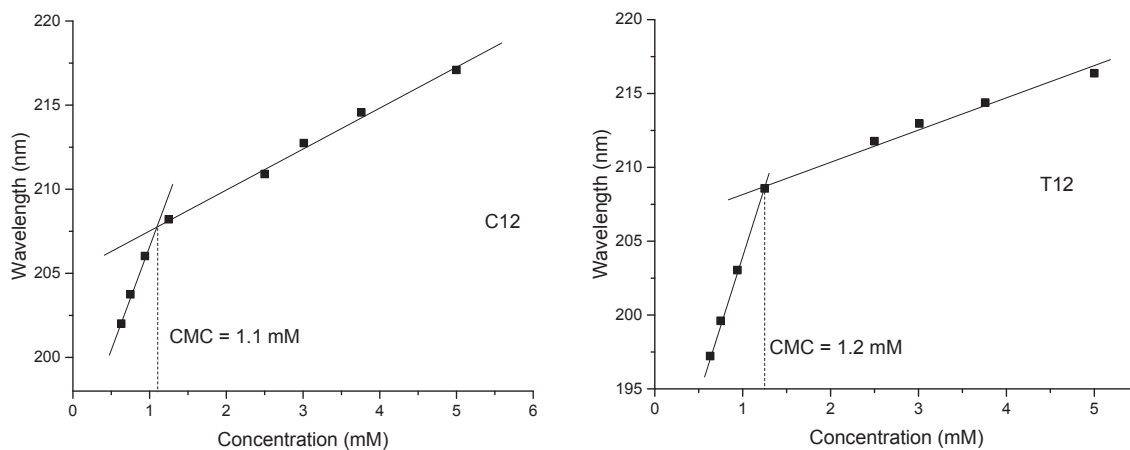


**Figure 106.** Representation of the variation of the maximum of absorption of the circularly polarized light depending on the concentration of surfactant **C12** (left) and **T12** (right).

Both representations show a critical change in the slope of the variation of the maximum of absorption with the concentration. This change could be related to the CMC, which can be compared with the obtained CMC values in solution (see section 7.3.2.1.1). As it is known, CMC is a range of concentrations and depending on the method and also on the measured physical property it can vary up to one order of magnitude.<sup>166,216</sup> Moreover, this method has some restrictions. It should be useful for surfactants with a chiral chromophore (or in a chiral environment) which self-assemble through it. If a chiral surfactant does not self-assemble through the chromophore any shift of the maximum of absorption will not be observed, as it is shown in other studies.<sup>235</sup>

**C16** and **T16** are less soluble in water and have a CMC around 0.1-0.2 mM. The range of concentrations to be studied is decreased due to the limitations of the method. Some solutions show too high turbidity to be measured and some others have not enough material to obtain a reliable signal. Obtained CD spectra of **C16** and **T16** surfactants are shown in Figure 107.

A red shift from lower concentrations to higher concentration can be observed. In addition, the shape of the CD spectra could be related to the shape of the spectra from compounds **C12** and **T12**, which could mean that the pattern of self-assembly depends on the stereochemistry and not on the length on the chain. However, none of the measured samples under the CMC could be analysed and thus, only information about the chirality

of the aggregate can be obtained. In these cases, also, the UV-vis absorption spectra of different surfactant solutions at different concentrations were recorded (Figure 108).

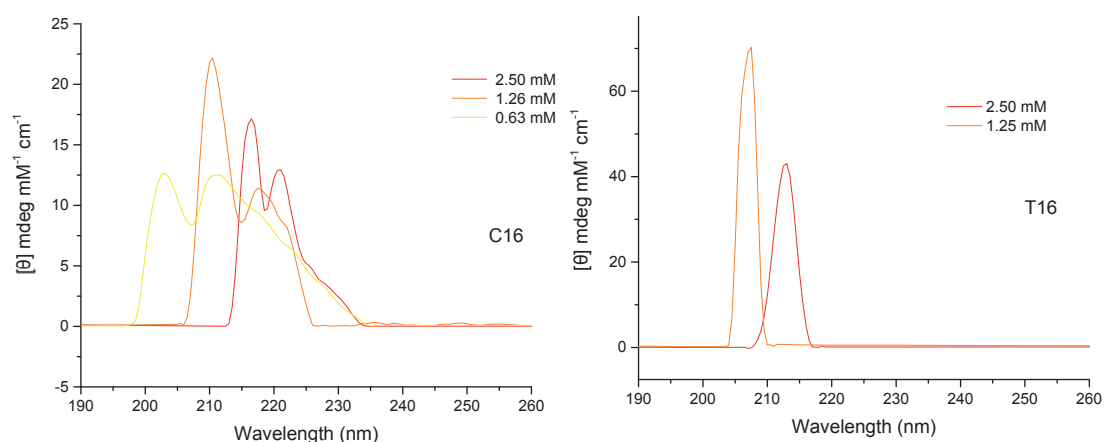


**Figure 107.** Circular Dichroism spectra of surfactants **C16** (left) and **T16** (right) at different concentrations in water.

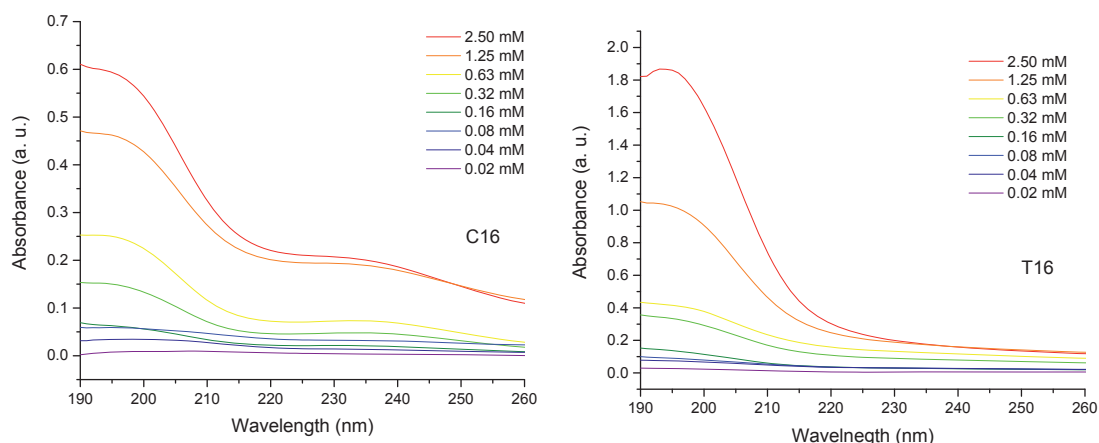


**Figure 108.** UV-vis absorption spectra of surfactants **C16** (left) and **T16** (right) at different concentrations.

Due to limitations of the method, solutions of lower concentration could not be measured and thus, information below the CMC cannot be obtained. Thus, some other restrictions of this method were found. CMC of the studied surfactant should be between 1-5 mM in order to be able to measure a range of concentrations around this value. It is remarkable that CD allowed us to follow the stereochemistry of the surfactants from the



“eyes” of the amide groups during the self-assembly process and has lead to determine the CMC of two surfactants.

### 7.3.3 Biophysical study

Cationic surfactants are potential non-viral vectors for gene therapy, as explained before. In order to assess the suitability of the four new surfactants in this type of applications, a series of biophysical studies looking at their interaction with DNA were conducted.

Studied DNA was a double-chained linear plasmid of 4017 bp (base pairs). The process of obtaining the target DNA from the plasmid is called Polymerase Chain Reaction (PCR) and for each target DNA, a different PCR protocol is required. An useful tool for PCR optimization is using an Experimental Design<sup>236</sup>. Taq Polymerase<sup>237</sup> was chosen for the PCR and the protocol is shown in section 10.12.

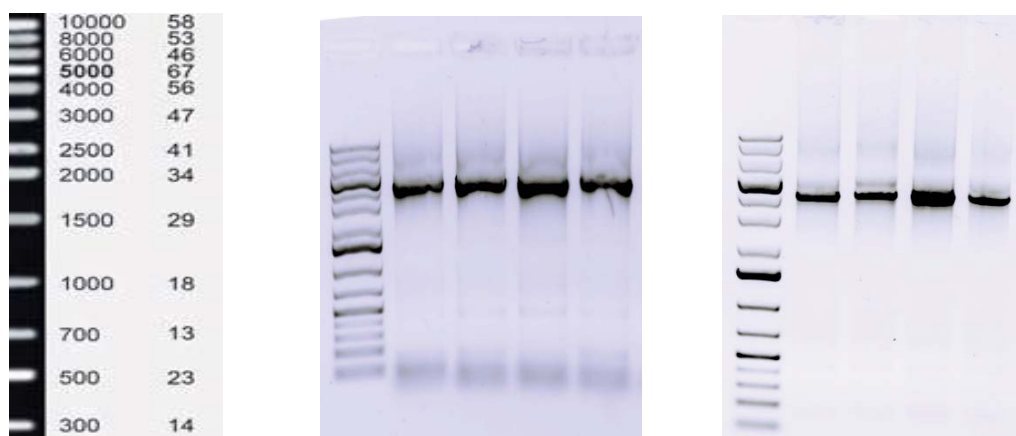


**Figure 109.** Ladder (left), results from the electrophoresis before (middle) and after (right) the purification.

In the middle panel of Figure 109, the majority of the obtained DNA has between 4000 and 5000 bp, which is agreement with our target DNA 4017 bp. After purification, only the band corresponding to 4017 bp is observed, indicating that only the target DNA is in solution. Once the target DNA was obtained, the study of the interaction of our surfactants with it could be started.

### 7.3.3.1 Dye Exclusion Assay (DEA)

In order to study whether these surfactants can bind DNA or not, Dye Exclusion Assay (DEA) was carried out. This technique is useful to determine the amount of accessible DNA in solution. GelStar® is a small unsymmetrical cyanine dye<sup>238</sup> that binds DNA. When it is bound, it absorbs at 492 nm and emits light between 527 and 550 nm, depending on the formed complex. By measuring the intensity at 527-550 nm the accessibility of the DNA molecules can be determined. Control experiments were performed with GelStar® and the largest surfactant concentration used, to check if the dye was incorporated in the surfactant aggregates. We observed no difference between the emission and absorption spectra of the GelStar® in the presence or absence of surfactant alone, and for all different surfactants. In addition, the emission intensity of the DNA-GelStar® complex in the absence of surfactant was used for the normalization of all results.

To prepare the samples, the procedure explained in section 10.14 was followed. Each sample was prepared two or three times in order to obtain the standard deviation and the average of all results. Representative emission spectra of the DNA-GelStar® at different **C12** concentrations are represented in Figure 110. The results of all studied systems are shown in section 12.3. All of them have a maximum of emission at 540 nm and so this wavelength was taken to plot the difference of intensity versus the concentration of surfactant ( $I/I_{\max, \lambda=540}$ ).

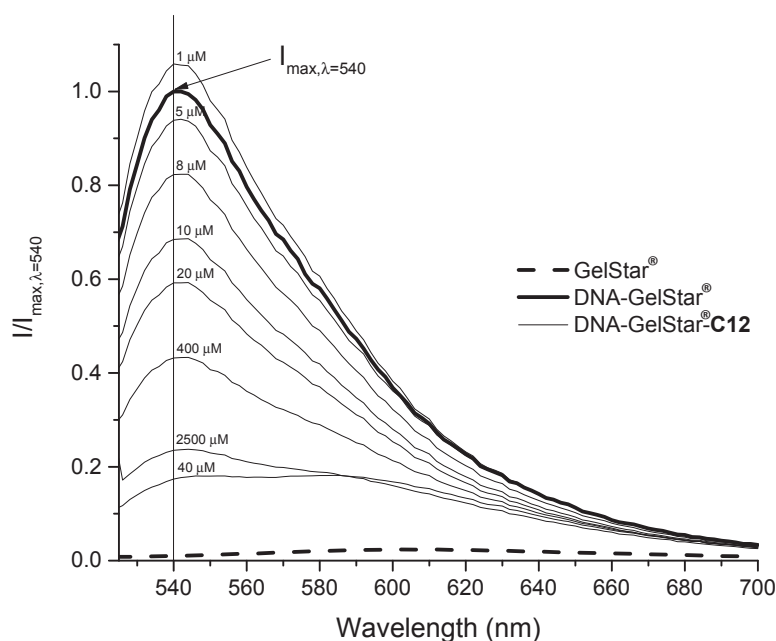


**Figure 110.** Emission spectra of DNA-GelStar® complexes at different **C12** concentrations.

At low concentrations the intensity of the emission spectrum at 540 nm is higher than that of the DNA-GelStar® complex without surfactant because surfactants promote a more extended DNA chain, which is more accessible. After that, intensity of the emitted light is reduced when increasing the surfactant concentration until a certain value at which intensity increases again. Finally, at higher concentrations intensity decreases again. To analyse the results, the intensity of each emission complex at 540 nm normalised with the intensity of the DNA-GelStar® complex is represented versus the surfactant concentration.

In order to compare the results of the synthesised surfactants with some commercial surfactants under the same conditions, we carried out the same experiments using DTAB (12 carbon-long alkyl chain) and CTAB (16 carbon-long alkyl chain). The interaction of these two surfactants with DNA has been studied using several techniques.<sup>206,208,239</sup> Because the concentration of DNA used in different assays was slightly different, and to better compare the data, we show the results also in terms of ratio between the surfactant head group and the phosphate groups. So, results are expressed as function of the surfactant concentration divided by ppm of DNA and also as

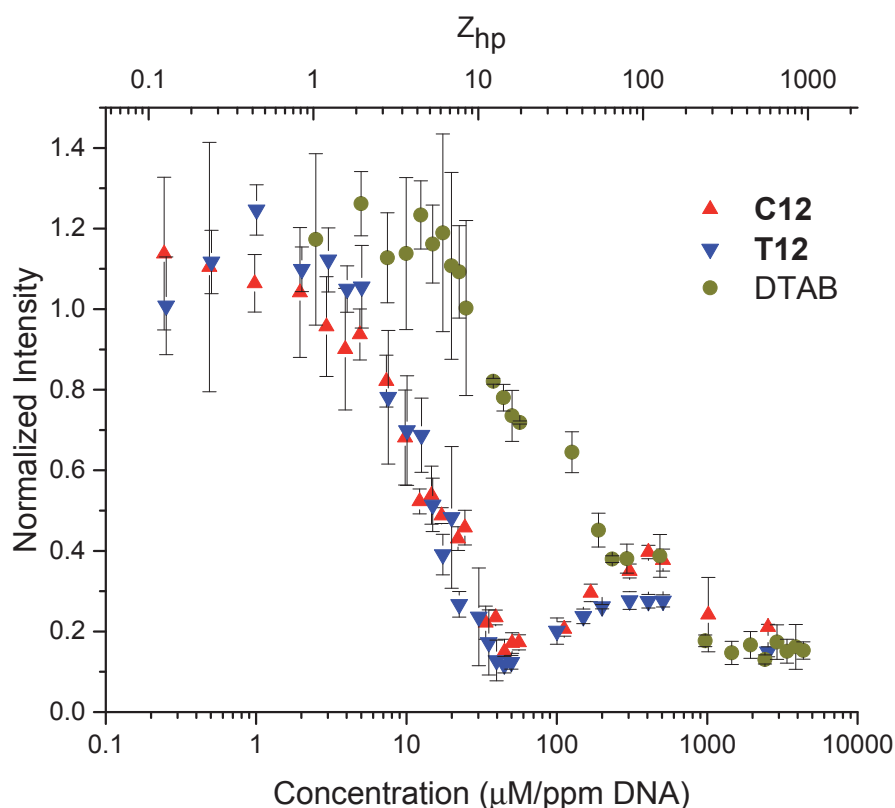


**Figure 111.** Representation of the dye exclusion assay results for the 12-carbon chain length surfactants.

function of the ratio between the number of head groups ( $h$ ) and the number of phosphate groups ( $p$ ) in solution ( $Z_{hp}$ ). Results of the dye exclusion assays of the 12 carbon-long alkyl chain length surfactants are shown in Figure 111.

A first observation of these graphs shows that **C12** and **T12** are very similar and they are much more efficient binding DNA than DTAB because the decrease of intensity occurs at a lower concentration of surfactant. CAC can be determined from the concentration of surfactant at which the intensity starts to decrease. This point is also called  $Z_{hp-1}$  because is the first critical point at a certain charge ratio at which self-assembly starts. A decrease of intensity means that the DNA is less accessible for the GelStar® due to the presence of surfactant aggregates at the surface of the DNA.

In the case of the 16 carbon-long alkyl chain surfactants (Figure 112), it is shown that **T16** behaves similarly than CTAB while **C16** is clearly less efficient. In this case, stereochemistry seems to play a crucial role.

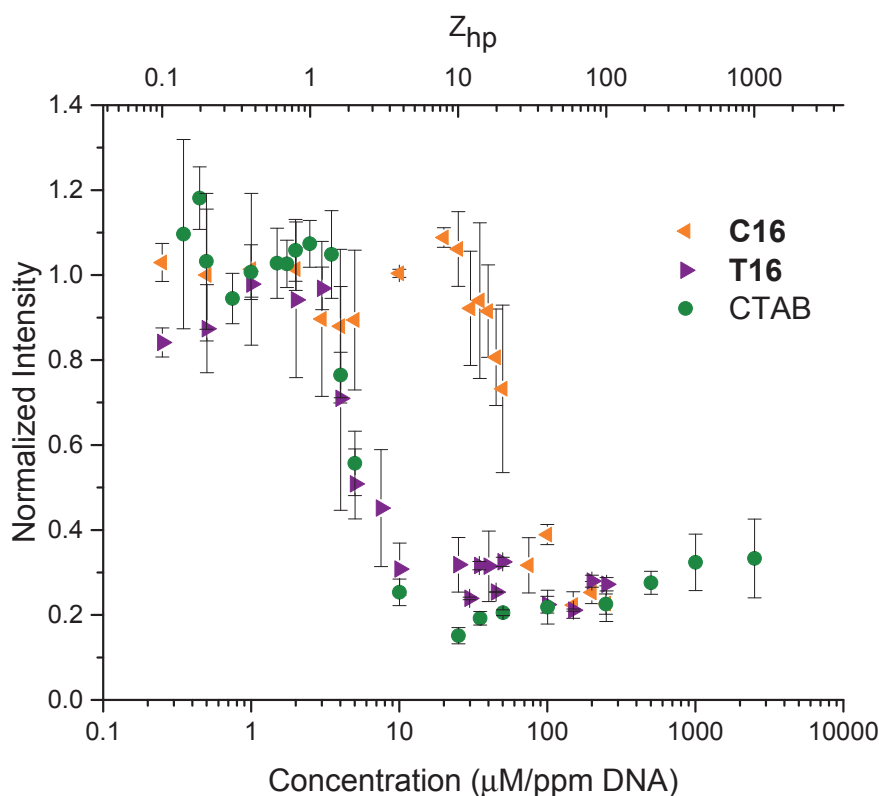


**Figure 112.** Representation of the dye exclusion assay results for the 16-carbon chain length surfactants.

Looking at both graphics we could suggest that stereochemistry and the length of the chain are two important factors when analysing the efficiency of the binding of the DNA and also that both factors are not independent but there is a clear interaction between them on the final behaviour.

In all studied systems, at high intensity values (around 1.0), the errors are higher than at low intensities. In this kind of experiments, the variation is not only attributed to experimental errors but also related to the different species present in solution. At high intensities, DNA is not condensed and has many degrees of freedom, having different morphologies and each one could have different accessibility for the GelStar<sup>®</sup>. In addition, these high errors are due to the cooperative effect of the binding process. The reason for this cooperative binding is the strong attractive ion correlation effect resulting in an alternated positioning of the multivalent surfactant aggregates. Further binding by the compacting agent on the partially compacted DNA is therefore preferred relative to the free DNA molecules, despite contradicting DLVO theory of the stability of colloids and macromolecules in solution, in which attractive van der Waals forces are balanced by repulsive electrostatic interactions.<sup>240</sup> However, it is important to keep in mind that if a cooperative process occurs it does not necessarily imply that the formed aggregates are uniform and thus, the error bars are larger.<sup>133,208</sup> Additionally, sigmoidal curves show that the binding of the surfactant aggregates with the DNA implies a cooperative effect.<sup>208</sup> Once the intensity starts to decrease, surfactant aggregates are starting to lie at the surface of the DNA, losing some degrees of freedom of the DNA, and thus, the diversity of structures in solution is reduced as it can be observed with the error bars.

CAC can be compared with the CMC value of the surfactant. CAC is generally some orders of magnitude lower than the CMC because entropy of the formation of the DNA-surfactant complexes is much more positive than the entropy of micellization, which favours the formation of surfactant aggregates at lower concentrations. In order to compare the results, the curve of the DEA and the variation of the surface tension measured at natural pH in section 7.3.2.2 are represented in the same plot (Figure 113). However, the value of the CMC was taken as a range, according to section 7.3.2 and thus, obtained CMC values in solution are represented also in the same graphic.

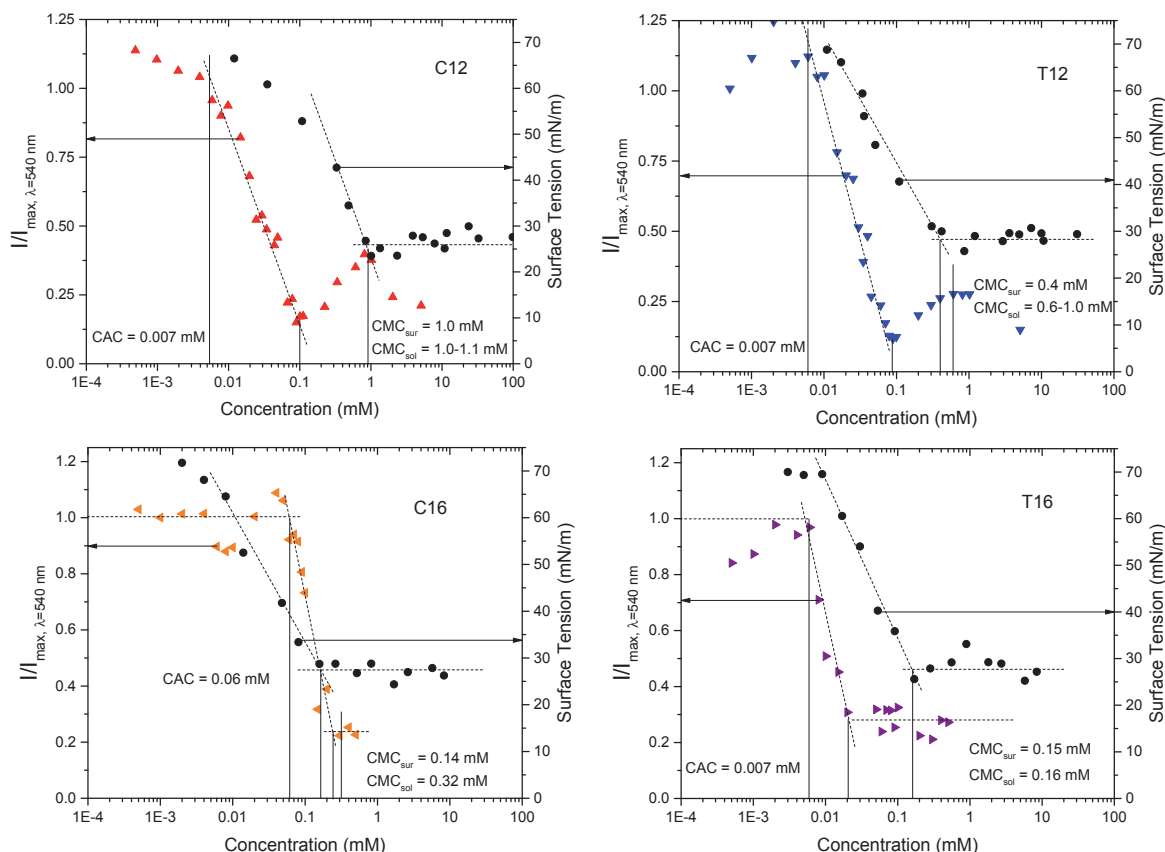


**Figure 113.** Representation of the dye exclusion assay and the pendant drop method results compared with the CMC values.

**C12** and **T12** have a similar behaviour. Both have a CAC around  $7 \mu\text{M}$ , which corresponds at a charge ratio of 1. Furthermore, the shape of the curve is very similar in both cases. At  $7 \mu\text{M}$ , intensity starts to decrease and it reaches its lowest value at around  $90-100 \mu\text{M}$  in both cases. The first point at which the intensity reaches its lowest value is called  $Z_{\text{hp-2}}$  or the concentration of the critical intensity ( $C_{\text{CI}}$ ), and it is the point at which at a certain charge ratio the DNA chain is saturated with surfactants. The “mountain” between  $100 \mu\text{M}$  and the highest concentration is due to the proximity to the CMC. Once the minimum value of intensity is reached, it increases until the concentration of surfactant is the same as the CMC, and then, intensity decreases again. It can be explained by understanding what is happening in the solution.

Above the CAC, surfactant aggregates bind to the surface of DNA. Once the minimum intensity is reached and surfactant concentration is near to the critical micelle concentration, surfactant monomers start to self-assembly in solution. At this point, at the

CMC, micelles or other surfactant aggregates are favourable in solution. Once the DNA-surfactant complexes are formed and the concentration of surfactant is above the CMC, a change in the morphology of the complexes to form big aggregates could lead GelStar® to bind DNA during the process until the final big aggregate of complexes is formed.

**C12** and **T12** are much more efficient than DTAB, not only because they have a very low CMC value compared to DTAB, but also because they have a lower value of CAC (7  $\mu\text{M}$  compared to 50  $\mu\text{M}$ ). Furthermore  $Z_{\text{hp-2}}$  is 100  $\mu\text{M}$  for **C12** and **T12** whereas it is 2000  $\mu\text{M}$  for DTAB. Surfactants **C16** and **T16** show different curves. It is due, basically, to the low solubility of surfactant **C16**. After sonication for 30-45 minutes, samples of highest concentrations seem to be mostly dissolved, but they show some turbidity due to the formation of aggregates.

CAC of **C16** could be estimated as 60  $\mu\text{M}$  and the lower intensity value is achieved at 300  $\mu\text{M}$ . This value corresponds to the CMC of this surfactant. That means that despite of the low solubility, once it is aggregated into micellar aggregates, it can bind DNA as the other surfactants do. Aggregates reduce the energy of the system by keeping the hydrophobic tails out of the water, and thus, solubility is increased.

CMC decreases when increasing the ionic strength because the hydrophobic part of the surfactant is less stable in water and prefers to aggregate earlier. On the other hand, CAC increases when increasing the ionic strength because the entropic factor of releasing the counterions to the medium is reduced and so all the charges are stabilised. There is a value of ionic strength where the CAC reaches the CMC value, which is called the critical ionic strength ( $I_c$ ). From this point, any CAC can no longer be detected.<sup>241</sup> Results for **C16** show that both CAC and CMC of this surfactant are very close. It could be related to the fact that the working ionic strength is near the  $I_c$ . **T16** has a CAC value of 7  $\mu\text{M}$  as CTAB and also the same as **C12** and **T12**. That means that three of the new surfactant are as efficient as CTAB, which is normally used to study compaction of DNA due to its efficiency.  $Z_{\text{hp-2}}$  is 20  $\mu\text{M}$  for **T16** and at 50  $\mu\text{M}$  for CTAB.

Table 22 summarizes the obtained CAC values at  $Z_{\text{hp-1}}$  point, the concentration of the critical intensity, which corresponds to the  $Z_{\text{hp-2}}$  point, the CMC values and the relationship between CAC and CMC. CMC was taken as the mean value between the results obtained at the surface and in the solution. Also  $\Delta Z_{\text{hp}}$  is calculated ( $Z_{\text{hp-2}} - Z_{\text{hp-1}}$ ). This value

is significant to evaluate the cooperativity and strength of the interaction between the DNA chain and the surfactants.

**Table 22.** Summary of the obtained  $Z_{hp}$  values (CAC and  $C_{Cl}$ ), the variation of  $Z_{hp}$  values and the CAC/CMC ratio.

Surfactant	$Z_{hp-1}$ (CAC)	$Z_{hp-2}$ ( $C_{Cl}$ )	$\Delta Z_{hp}$	CAC/CMC
<b>C12</b>	1	15	14	0.003
<b>T12</b>	1	15	14	0.013
<b>DTAB</b>	5	400	395	0.002
<b>C16</b>	10	40	30	0.150
<b>T16</b>	1	3	2	0.010
<b>CTAB</b>	1	4	3	0.004

The ratio of CAC/CMC could also give us an idea about the strength of the interaction between the surfactant aggregates and the DNA chain.<sup>242</sup> However, in the case of DTAB the value is underestimated due to its high CMC. The lower is the relationship, the more favourable is the interaction between the surfactant aggregates and the DNA. As it is shown, this relationship could give us an idea about the strength, but as the factors that influence the CMC are different from those which influence the CAC, these values are only an approximation.

To determine the cooperativity and the strength of the interaction, the variation of  $Z_{hp}$  values has to be calculated. The value of  $\Delta Z_{hp}$  could be understood as a compaction factor. The closer are the  $Z_{hp-1}$  and  $Z_{hp-2}$  points, the higher will be the cooperativity and the strength of the interaction.<sup>239</sup>  $\Delta Z_{hp}$  values show that **T16** binds DNA with more cooperativity and strength than all the other studied surfactants, even CTAB. **C12** and **T12** seem to have the same behaviour, slightly less cooperative than CTAB. Finally, **C16** seems to have a low interaction with DNA but it is still stronger than the interaction of DTAB.

Results of the DEA give us a first idea about the interaction between these surfactants and DNA. However, this technique does not give us information about the degree of compaction of the DNA, only that surfactant aggregates can bind DNA and the



accessibility to the DNA. This technique has to be accompanied with other techniques to be able to understand these systems.

### 7.3.3.2 Electrophoretic Mobility Shift Assay (EMSA)

In electrophoretic experiments, negatively charged DNA chains will move through the agarose gel to the anode. Depending on the size of the DNA chain, it will go faster or slower and it will be possible to determine the size of the DNA chain comparing the mobility with a ladder. However, if the number of negative charges of the DNA chain is reduced, its mobility will be shifted and will not go as far as it should be corresponding to the size of the chain. Positively charged surfactant aggregates will interact with the DNA chain forming a less negatively charged complex, which will be neutral when all the charges were neutralised and even positive if there are more surfactant monomers than phosphate groups. In this way, we could be able to distinguish between DNA chains before and after complexation by analysing the mobility shift in electrophoresis.

Samples of 20  $\mu\text{L}$  were prepared by adding 5  $\mu\text{L}$  of a 20 ng/ $\mu\text{L}$  DNA solution, 5  $\mu\text{L}$  of surfactant solution at different concentrations and 10 mM TrisHCl to keep the pH at 7.4. In order to compare the obtained results with the Dye Exclusion Assay results, the concentration of surfactant will be expressed as concentration of surfactant per ppm of DNA. Results of the EMSA are shown in Figure 114. Bands of the ladder can be compared with Figure 109.

In all cases, EMSA images show that our surfactants can bind DNA forming complexes and thus, the negative charges of DNA are reduced. Looking at these images, it is possible to determine at which concentration there is no free DNA, which could be related to the  $Z_{hp}^2$  value.

The spot of the dsDNA at  $\approx 4000$  bp is observed at low concentrations of surfactant. When increasing the concentration, the intensity of this spot starts to decrease or the spot is shifted. At the same time, a new spot appears at the top part of the gel (well). This spot correspond to the formation of the complex. The shifted spots refers to the transition complexes from the free DNA to the final complex. When reducing the number of negative charges, the mobility of the DNA complex is shifted.

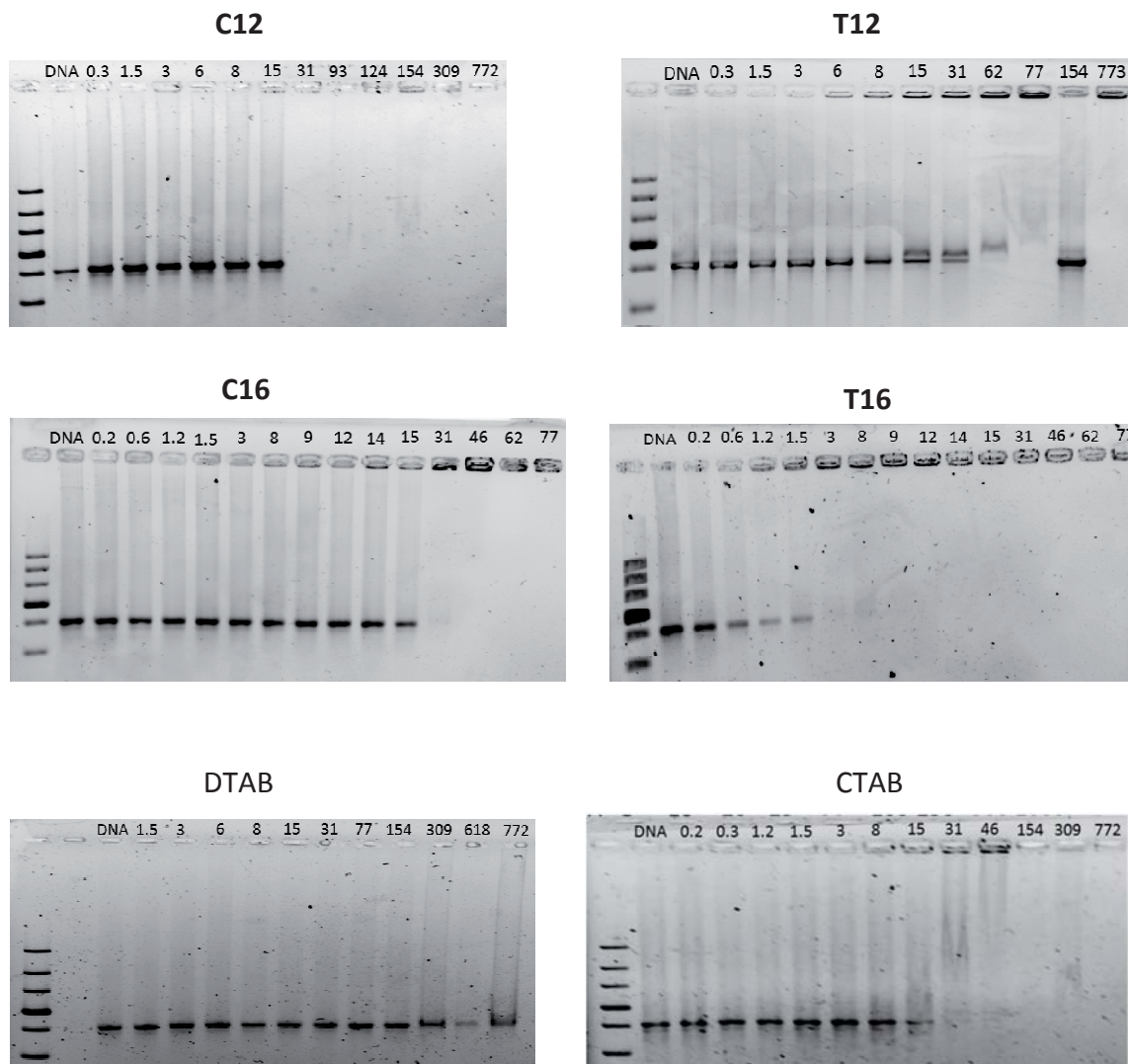


**Figure 114.** EMSA images of **C12**, **T12**, **C16**, **T16**, **DTAB** and **CTAB**. Complexes are shown as ration of charge  $Z_{hp}$ .

In order to quantify the amount of free DNA and the formation of a complex, a measurement of the intensity of the spots of gel of the electrophoresis was done. Measurements of the intensity were done at the retention factor of the free DNA and at the well. The spot that remains at the well during the electrophoresis could be attributed to the non-charged complex because it does not migrate neither to the cathode nor to the anode. Once the non-charged complex is formed, more surfactant aggregates can bind the complex because cooperativity favours self-assembly. Then the non-charged complex becomes a positively charged complex and it migrates to the cathode, decreasing the amount of non-charged complex into the well.

Values of the intensity were taken from the image obtained with the ChemiDoc instrument, which were taken under UV light. *A posteriori* treatment of the images could give us the trend of the intensity, but not the exact number because of the limitations of the instrument. Once the values of the intensity were obtained, a line was drawn in order to see the trend of the variation of the concentrations of the free DNA and the non-charged complex. Obtained graphics are shown in Figure 115. Values were normalised to the maximum obtained intensity values for each compound.

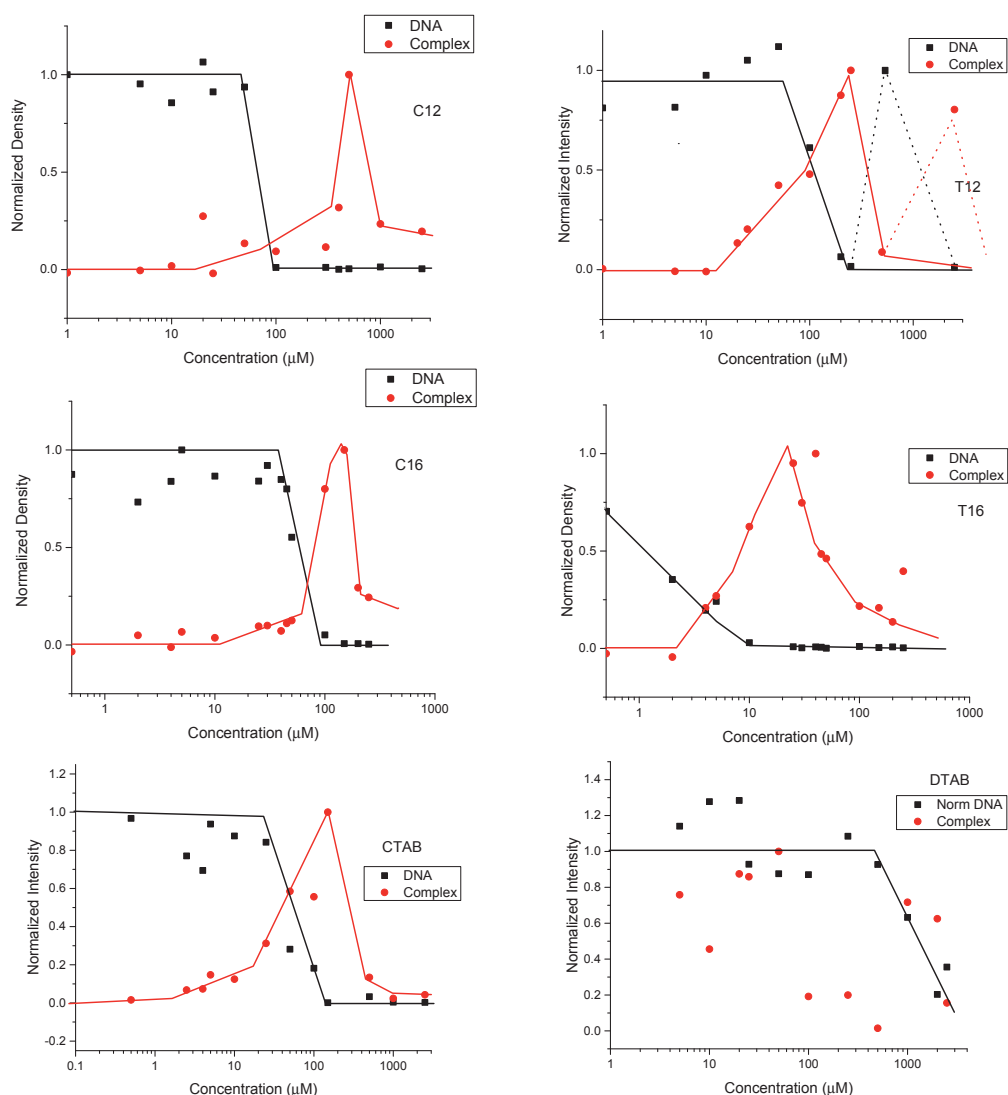


**Figure 115.** Variation of the free DNA and complex concentration during EMSA experiments.

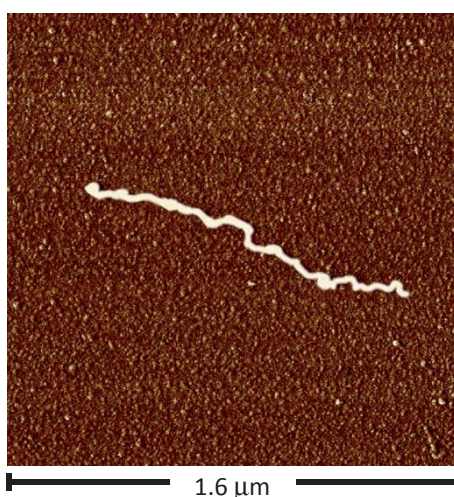
In all cases, concentration of free DNA is reduced from 1 to 0, which means that in all cases free DNA is complexed with surfactant aggregates. DTAB is a special case. Due to

its low efficiency, higher concentration out of the range of this study were required to observe the complete compaction of the free DNA.

The variation of the concentration of the non-charged complex shows a peak. Once the DNA is complexed, the global negative charge of the complex is reduced until it becomes completely non-charged (the maximum of the peak), and then, the concentration of the positively-charged complex starts to increase (this point is referred as  $Z_{hp-3}$ ). However, this peak could be related not only to the formation of the positively charged but also to the precipitation of the complex. Comparison between DEA and EMSA results is shown in section 12.4.

### 7.3.3.3 Atomic Force Microscopy (AFM)

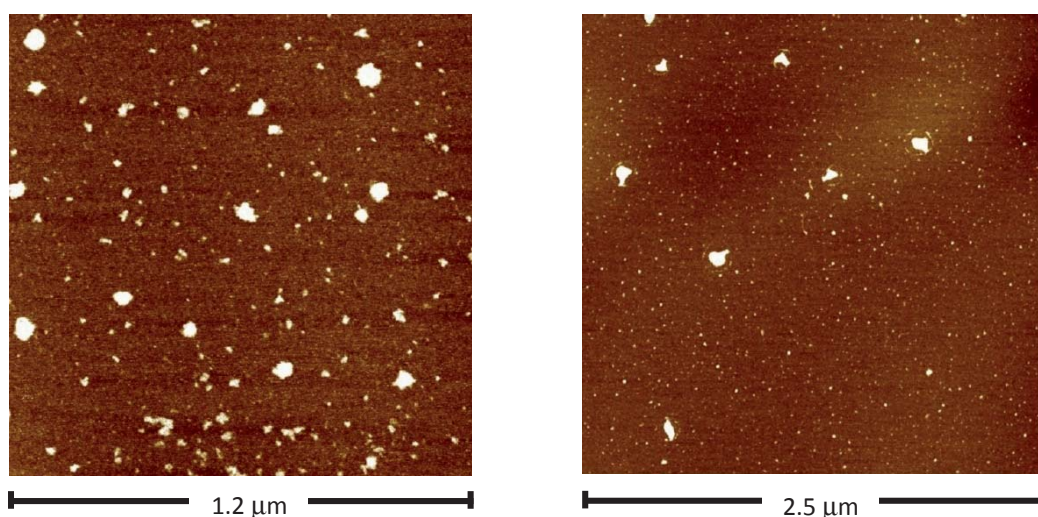
Using techniques such as AFM, we could obtain information about the morphology of the aggregates. In our case, the compaction process was analysed to determine visually whether compaction was achieved or not. Samples were prepared following the methodology described in section 10.6.3. Each sample was measured different times and changing the area in order to obtain a representative result. Figure 116 shows the free DNA, which is about 1.3  $\mu\text{m}$  length.



**Figure 116.** AFM image of the free DNA.

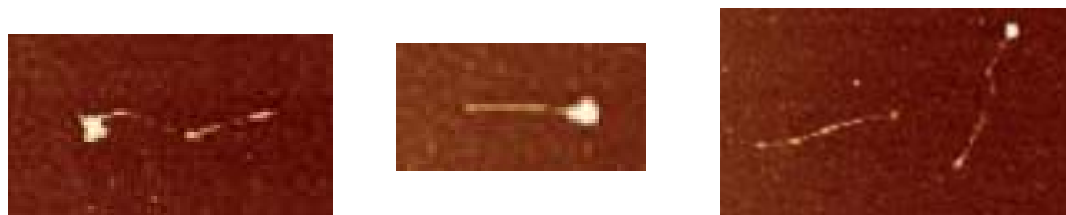
Two different concentrations of **C12** and **T12** were studied. The first one, during the compaction process in order to see the first complexes that are formed. Then, the highest concentration in which the DNA is completely complexed. This way, we could determine if there is a difference in the complex geometry depending on the concentration.

Figure 117 shows the AFM pictures of **C12** and **T12** during the complexation process, at 20  $\mu\text{M/ppm}$ , which corresponds to a ratio of charge around 6. **C12** and **T12** can clearly compact DNA into very small complexes with a diameter lower than 55 nm. Taking into account that the DNA chain is 1.3  $\mu\text{m}$  length, compaction is really effective and suitable for biological studies.



**Figure 117.** AFM images of DNA-**C12** complexes (left) and DNA-**T12** complexes (right) during the compaction process at a  $Z_{hp}$  around 6.

Furthermore, it is important to remark that in the same sample where compacted DNA can be observed, extended DNA chains and partially compacted chains are also present (Figure 118). These pictures are in very good agreement with the DEA where the errors bars were related to the coexistence between different species in solution due to the cooperativity binding.



**Figure 118.** AFM images of extended DNA and partially compacted DNA chains coexisting with compacted DNA.

At higher concentrations, AFM images (Figure 119) show much larger aggregates, which are not suitable for biological studies due to their size. This change of morphology is because studied concentrations are above the CMC and thus, the amount of surfactant is significantly high.

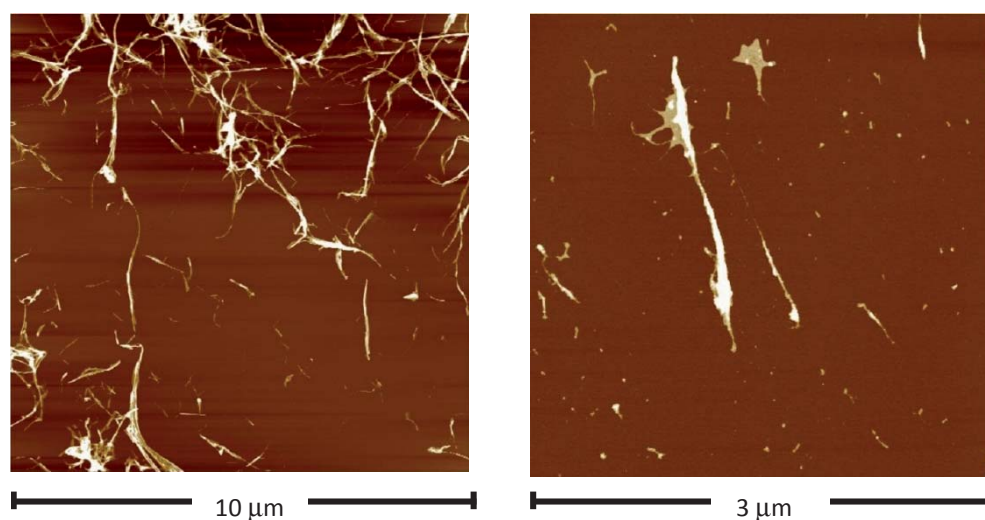


**Figure 119.** AFM images of DNA-C12 complexes (left) and DNA-T12 complexes (right) at high concentration of surfactant which corresponds to a  $Z_{hp}$  around 1545.

#### 7.3.3.4 Compaction using CD

DNA is a chiral molecule and thus, it shows signal to CD depending on the structure of the chain.<sup>88,243</sup> Using CD, the variation of the conformation of the DNA can be monitored during self-assembly process with surfactant aggregates.<sup>228,239,244–246</sup> To carry out CD studies, a high concentration of DNA is needed. Therefore, we selected Salmon Sperm DNA, which has 2000 bp and it is commercially available by Thermofischer in  $10 \text{ mg mL}^{-1}$ .

Figure 120 shows the complexation process of the DNA chain by adding different amounts of surfactant.

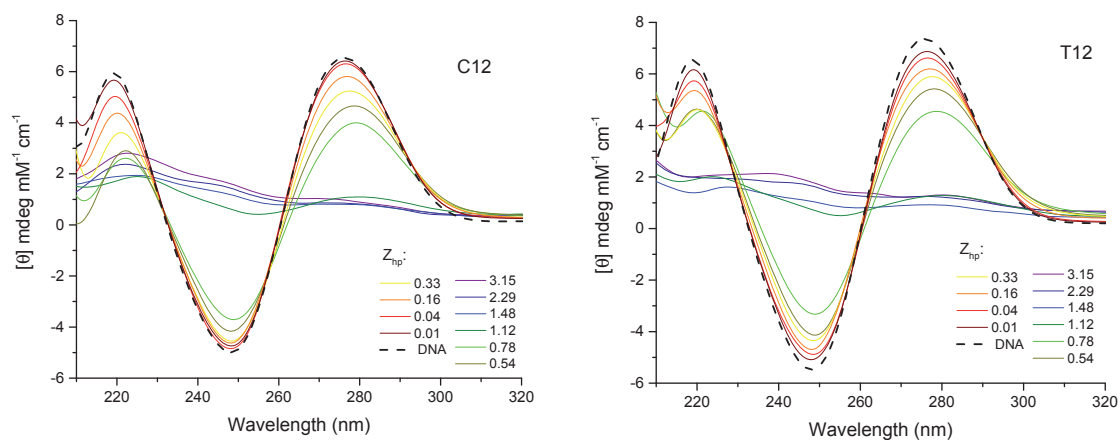


**Figure 120.** CD spectra of DNA-**C12** (left) and DNA-**T12** (right) complexes at different charge ratios.

Sample with the DNA chain (black dashed line) shows a strong bisignate Cotton effect with zero-crossing at 260 nm, which corresponds to a B-form DNA chain.<sup>91</sup> When adding different amounts of surfactant, the signal of the DNA starts to decrease until a ratio of charge around 0.73 and 1.12, which shows a strong change in both signal and intensity. From a  $Z_{hp}$  of 1.12, the signal of the B-form DNA is no longer observed, due to the formation of DNA-surfactant complexes.<sup>244</sup> Both surfactants show the same behaviour, which is in qualitative agreement with DEA and EMSA experiments. Additionally, we could suggest that the obtained CAC values are around a  $Z_{hp}$  of 1, which is in excellent agreement with other techniques, despite studying another DNA chain. That means that the length of the chain has a low influence on the CAC value when comparing a 2 kbp and a 4 kbp DNA chain. Compaction of DNA using surfactants **C16** and **T16** shows interesting results, as shown in Figure 121.

A clear difference between **C16** and **T16** can be observed. **C16** requires higher amounts of surfactant in order to compact a DNA chain compared with **T16**. These results are also in qualitative agreement with DEA and EMSA experiments. In these cases, quantification of the CAC seems to be more difficult because any strong change in intensity cannot be observed. In this way, the normalization of the intensity of the peak at 277 nm and at 248 nm was represented versus the ratio of charge (Figure 122).

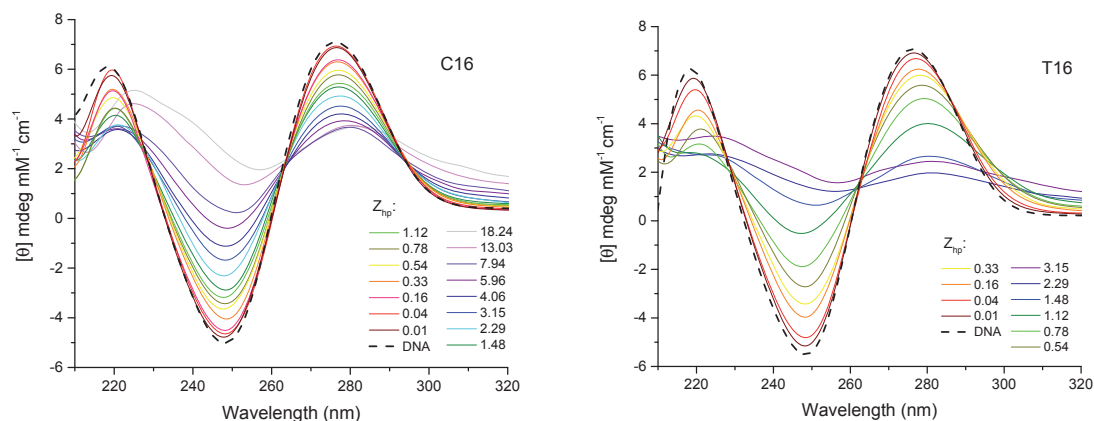


**Figure 121.** CD spectra of DNA-C16 (left) and DNA-T16 (right) complexes at different charge ratios.

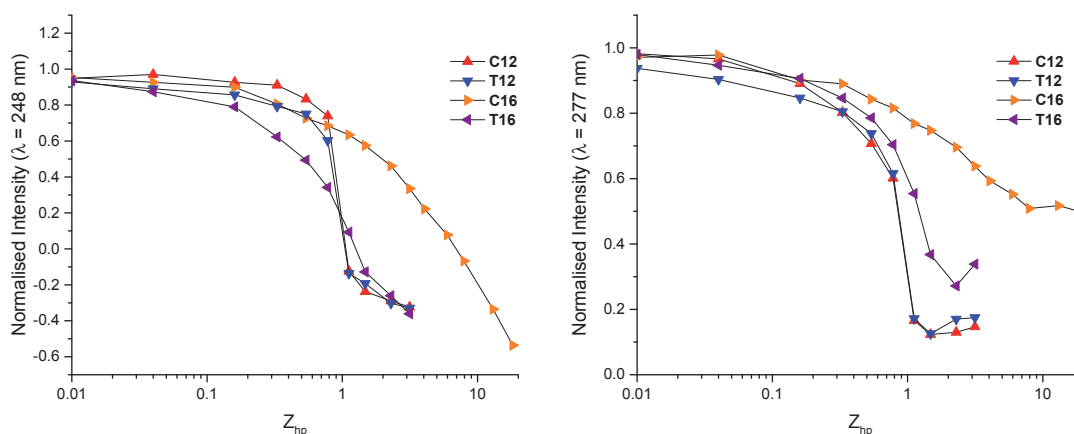


**Figure 122.** Normalised intensity at 248 and 277 nm of the CD spectra of DNA-surfactant complexes.

CAC can be determined by the abrupt change in intensity. As it is shown, **C12**, **T12** and **T16** show a CAC value around a  $Z_{hp}$  of 1, which is in good agreement with DEA and EMSA studies. On the other hand, **C16** shows a higher CAC value that cannot be determined due to the absence of the strong change of intensity but could be estimated around a  $Z_{hp}$  of 8-10, which is also in agreement with previous studies.

Therefore, using circular dichroism, the compaction of a DNA chain (Salmon Sperm DNA in this case) using different surfactants was studied and results are consistent with other studies despite having another DNA chain. That means that there is not any



remarkable influence of the DNA chain on the condensation process (taking into account that we are comparing a 2 kbp DNA chain with a 4 kbp one).

### 7.3.3.5 DNase Foot Printing Assays (DFPA)

DNase Foot Printing Assay is a very used method to study the protein-DNA interactions.<sup>247</sup> DNases cleave a DNA chain into smaller fragments. Some DNases cleaves only a specific region of the chain. If this specific region is protected by a protein (or surfactant aggregates in our case), any fragment of DNA smaller than the starting one should not be observed. Otherwise, if the DNase finds the specific region, it will cleave the DNA into two smaller fragments. This assay can be easily followed by gel electrophoresis.<sup>248</sup>

Three different DNase enzymes were selected: NdeI which cut DNA at a certain region having A and T bases; NruI, which cut DNA at a certain region having G and C bases and a standard DNase, which cut completely the DNA in several smaller fragments. NdeI and NruI were selected because it cleaves selectively at a specific sequence which appears only once in our target dsDNA (Figure 123).



**Figure 123.** Sequence where the enzymes NdeI and NruI act.

*A priori*, we could suggest that surfactants do not bind any specific region of the DNA because they just interact with the phosphate groups, independently of the base of the DNA while proteins or enzymes bind DNA at a selective region depending on the sequence of the base pairs. However, these surfactants form different aggregation morphologies, which could behave different when interacting with certain regions of the DNA. For example, a region with different A and T bases will be more flexible than a region with different C and G bases due to the hydrogen bonds between them. Then, the

mechanical properties of these regions will be slightly different and surfactant aggregates could interact in different ways depending on if they form fibers or vesicles.

What we want to observe is whether the complexed DNA can be cleaved by the enzyme or if it is protected inside the complex. If two different smaller bands were observed in gel electrophoresis after the addition of the enzyme, then, our surfactant would not be able to protect DNA. Otherwise, if our surfactants bind DNA forming a compacted complex, which avoids the enzyme to act, only the band of the complex should be observed. Figure 124 shows the resulting images of the electrophoresis of the NdeI DNase Foot Printing Assays. Images of the Foot Printing Assay for enzymes NruI and the standard DNase show the same results that the images for enzyme NdeI. Resulting images of NruI and standard DNase are shown in section 12.5. Concentrations are shown in  $\mu\text{M}$  of surfactant/ppm of DNA.

The first two samples of each gel are the free DNA (4017 bp) and the two smaller fragments (2612 bp and 1405 bp), respectively. As it is shown, at low concentrations, none of them binds specifically the target region and thus, NdeI DNase cleaves the DNA chains into two smaller fragments.

By increasing the concentration of surfactant, it is observed that the DNA-surfactant complex starts to appear. Also, the spot of free DNA is seen in some cases. At high concentrations, only the spot of the non-charged complex is observed. At this point, DNA is completely compacted. However, only for CTAB and DTAB we could say that the complex contains protected DNA because at the previous concentration only the band of the target DNA is observed. In the cases of our surfactants, we could not say whether the complex contains cleaved DNA or protected DNA. In order to distinguish between both situations, the intensity of the spots in gel of the cleaved DNA has been compared with the intensity of the bands of the free DNA observed during the EMSA study (see Figure 125).

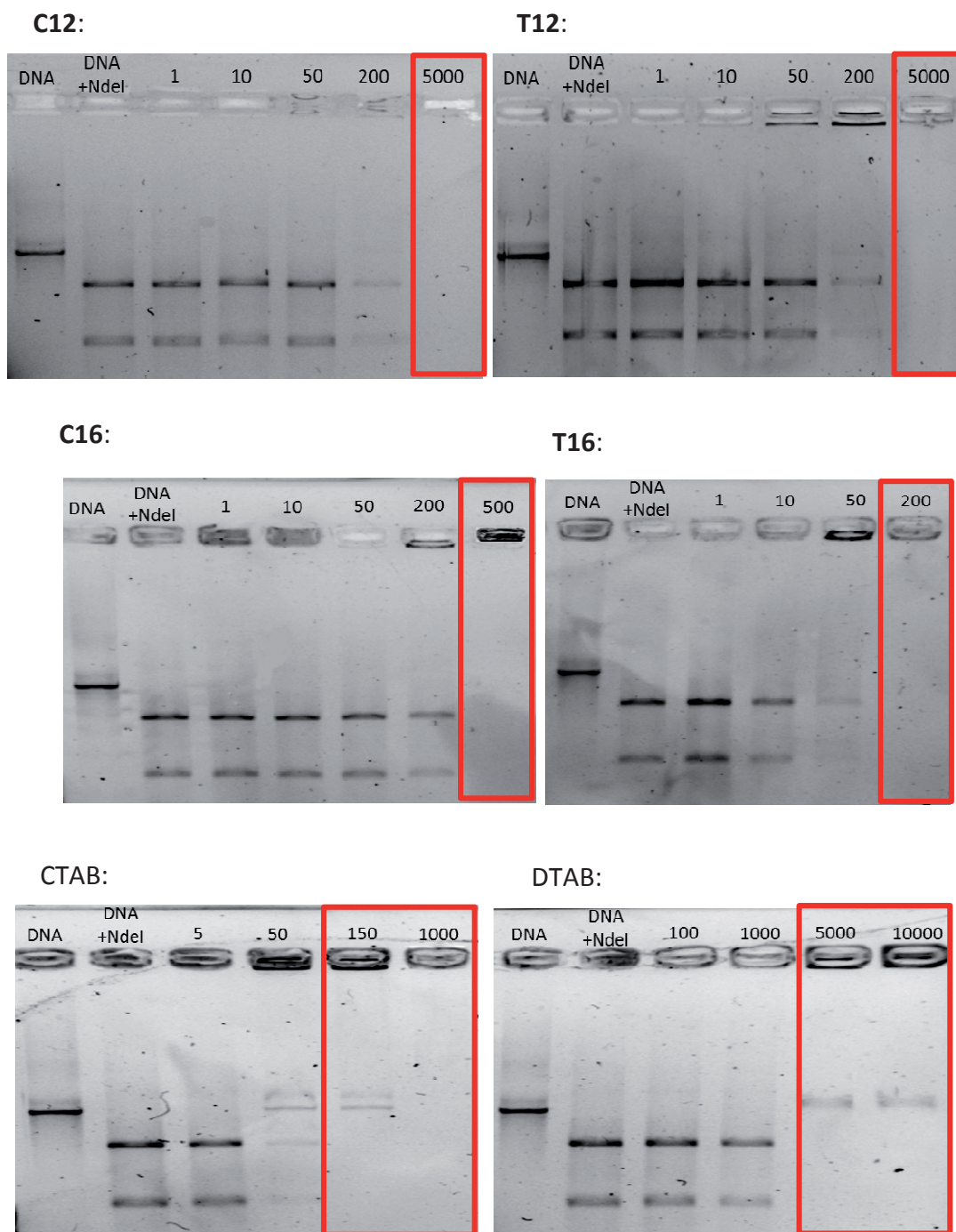


**Figure 124.** Resulting images from the electrophoresis of the NdeI DNase Foot Printing Assays. Concentrations are shown in  $\mu\text{M}$  of surfactant/ppm of DNA.

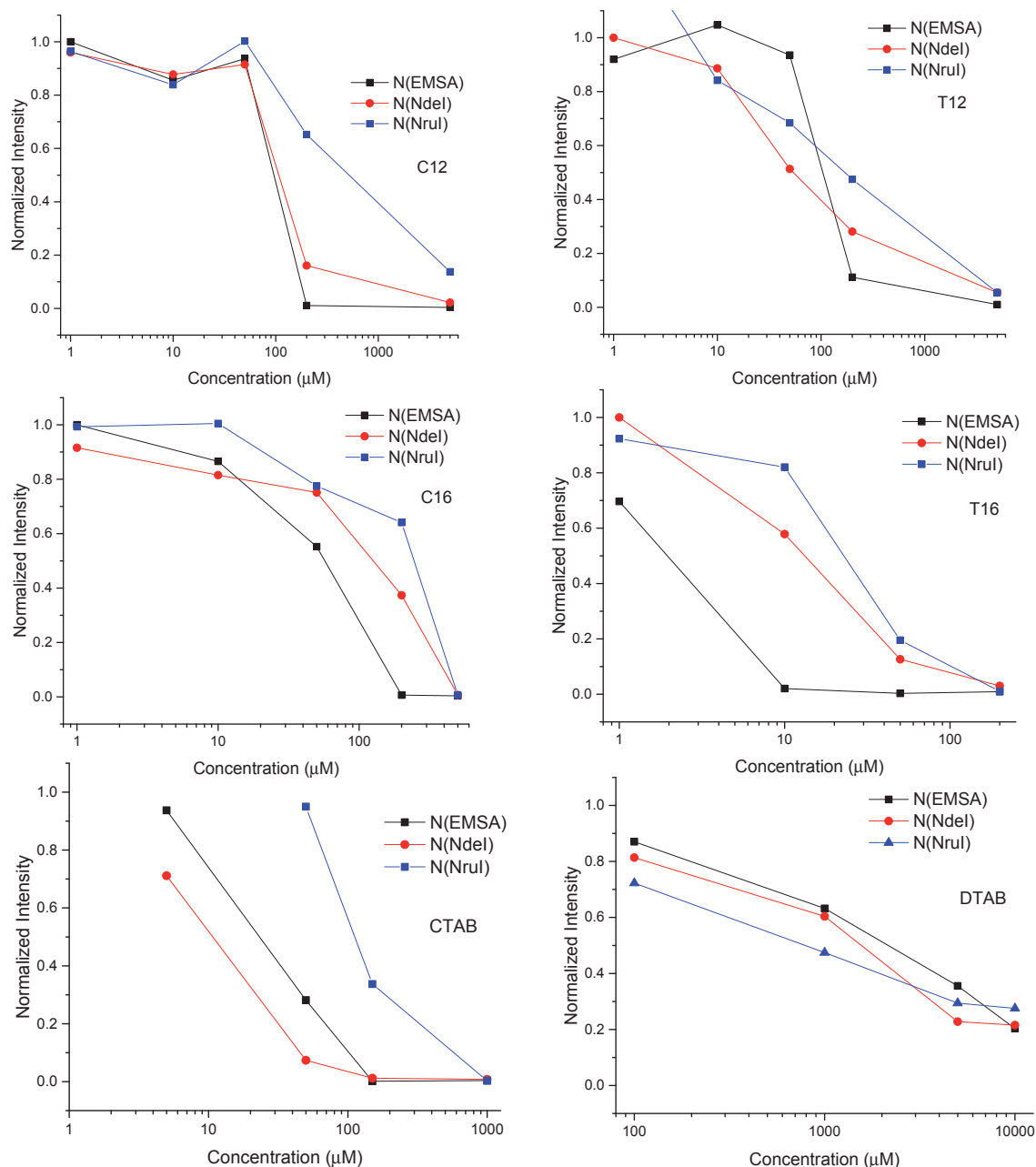


**Figure 125.** Comparison between the amount of free DNA obtained by EMSA and the amount of cleaved DNA obtained by DFPA at different surfactant concentrations. Concentrations are shown in  $\mu\text{M}$  of surfactant/ppm of DNA.

As it is shown, the amount of the cleaved DNA depending on the concentration of surfactant decreases in the same way as the free DNA in the EMSA studies. These results suggest that once the complex is formed, only the free DNA is cleaved and thus we could extrapolate that the complexed DNA is not cleaved and remains protected. However, the

definitive way to be sure that the complexed DNA is protected is to decompact the complexes and to determine the size of the DNA that is inside.

In order to verify the protection of the DNA inside the complex, inactivation of the enzyme and decompaction of the complex should be carried out. Thus, some decompaction studies were done.

### 7.3.3.6 Decompaction and release of the complexed DNA

Decompaction of the complexes inside the cell can only be studied *in situ* because it is not possible to reproduce exactly the cell conditions in the laboratory. Only preliminary studies of the decompaction can be done in order to know if these surfactants have some possibility to release the DNA chain inside the cell by decompacting the complexes. In the present study, decompaction modifying the ionic strength of the medium was carried out.

Despite the apparent importance of the intracellular ionic strength for cells, definitive values of this parameter are lacking in the literature. The value of 0.116 M reported by Motais *et al.*<sup>249</sup> for red cells was obtained from the measured cellular concentrations of only Na<sup>+</sup>, K<sup>+</sup> and Cl<sup>-</sup>, whereas cells contain many other ions which would make significant contributions to intracellular ionic strength because of their concentrations and multivalent states. Usually, in those cases where a simulation of intracellular conditions is desired, a physiological ionic strength is specified, but its adopted values generally lie between 0.11 M and 0.26 M.<sup>250</sup>

Solution of NaCl in MiliQ water at different concentrations were prepared. Then, complexes at the concentration at which the DNA was protected were prepared at pH 7.4 in the presence of GelStar® in order to determine the presence of free DNA using the same technique used in the Dye Exclusion Assays. After that, a titration of solutions of different salt concentrations was carried out. Finally, samples were measured and normalised with the free DNA value in the presence of salt but without surfactant. Results of the decompaction are shown in Figure 126. Complexes were prepared at 5000 µM for **C12** and **T12**, 500 µM for **C16**, 200 µM for **T16**, 1000 µM for CTAB and 10000 µM for DTAB. DNA concentration was 2 µg/mL.

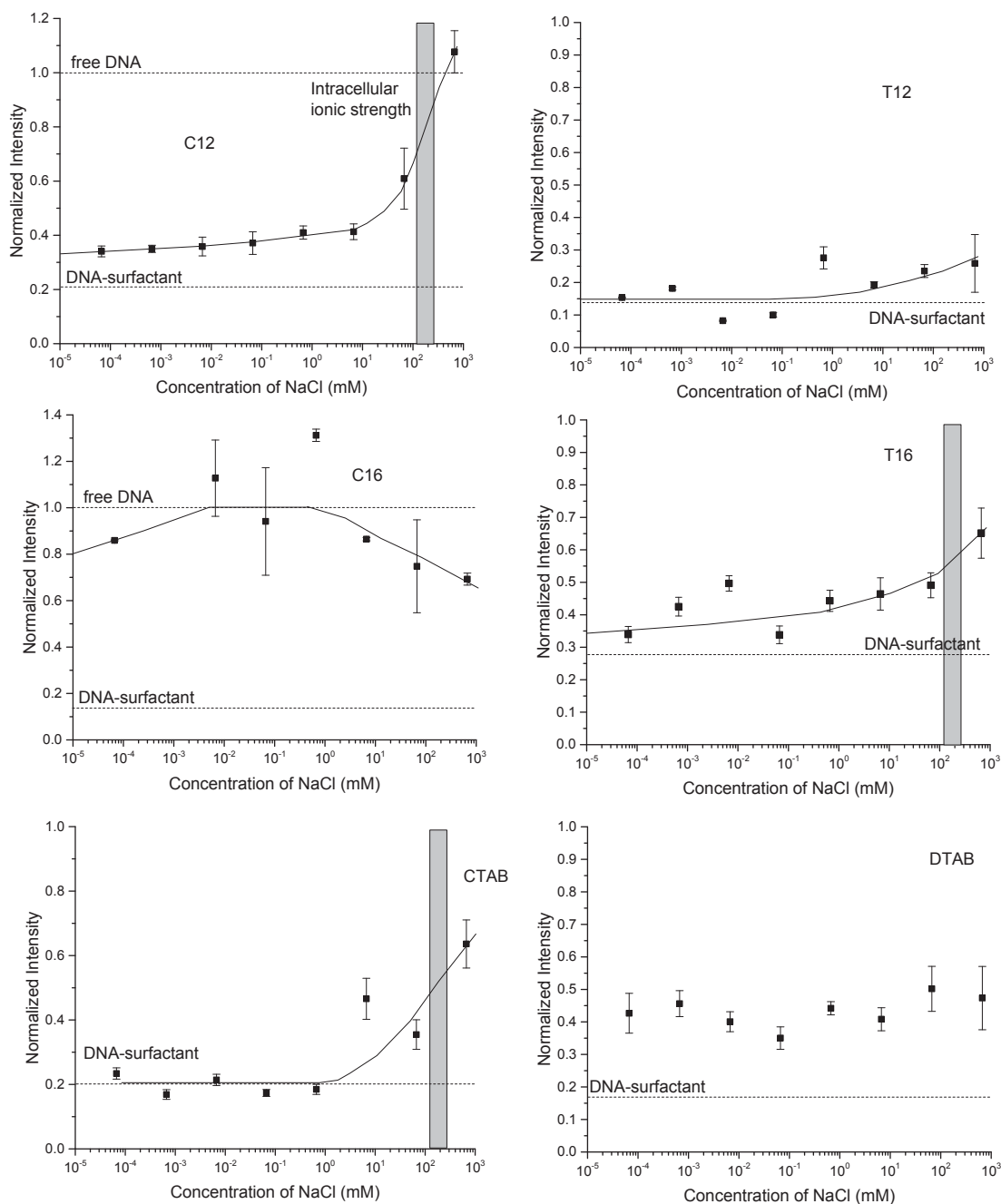


**Figure 126.** Results of the decompaction study modifying the ionic strength using the Dye Exclusion Assay methodology.

Figure 126 shows that **C12**, **T16** and CTAB decompact DNA around the intracellular ionic strength. T12 starts the decompaction but it would require higher ionic strength. DTAB requires also much more amount of salt to decompact completely the DNA.

**C16** is completely decompact at very low ionic strengths. The result for **C16** are in very good agreement with the hypothesis we had looking at the DEA results (section 7.3.3.1). As the CAC is very close to the CMC, it would mean that the working ionic strength

is near the critical ionic strength.<sup>241</sup> As it is shown, increasing a little bit the ionic strength, DNA is completely decompacted, which is a clear evidence that the ionic strength is above the  $I_c$ . In addition, it is shown that a higher ionic strength, intensity starts to decrease. To understand why it is decreasing, first of all we have to understand the phase diagrams of the cationic surfactant (S)/anionic polymer (P) solutions (Figure 127).

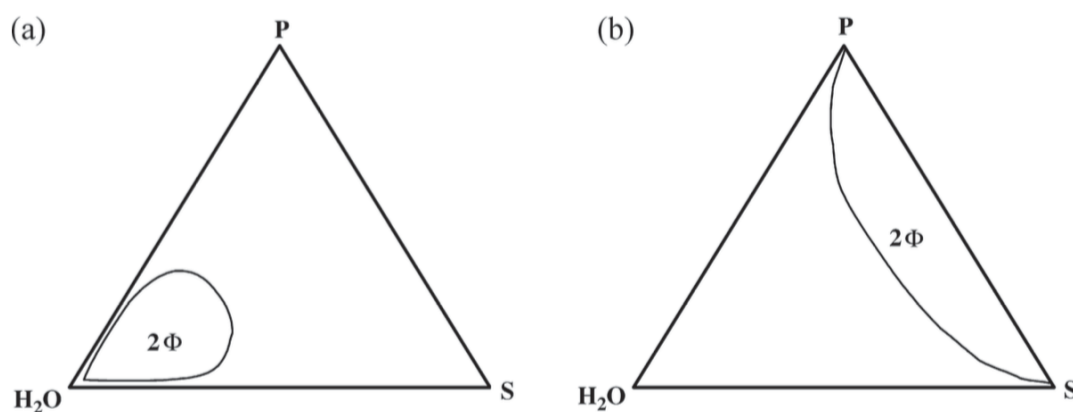


**Figure 127.** Schematic ternary phase diagram showing (a) associative and (b) segregative phase separation in mixed solutions of polymer and surfactant.<sup>133</sup>

At low ionic strength, the associative phase separation is observed ( $2\Phi$ ). Aggregation of oppositely charged compounds is favourable because of the entropic contribution of the counterions. When increasing the ionic strength, the area of the associative phase separation is reduced because the CAC is increased. At the critical ionic strength, any CAC is observed and thus, only one phase is observed. When the ionic strength is further increased, a segregative phase separation is observed ( $2\Phi$ ). At high ionic strength, the entropic factor of the counterions is negligible and thus, dissociation is not relevant. In this way, the polymer with counterions behaves as a non-ionic compound and it starts to precipitate.<sup>133,251,252</sup> We could say that the decrease of intensity at high values of ionic strength is due to the segregative phase separation.

As explained before, once the decompaction conditions of most of the compounds are found, the DNase Foot-Printing Assay is repeated following the steps: 1- formation of the DNA-surfactant complex at the concentration determined by DFPA; 2- digestion reaction using NdeI; 3- inactivation of the enzyme; 4- decompaction of the complex adding

a solution of NaCl; and 5- analysis using gel electrophoresis to know whether the DNA is kept protected or not.

Unexpected results were obtained. Complexes are not decompacted and thus any DNA chain did not migrate to the anode. Only a band in the case of DTAB is observed, but the band is also observed in EMSA studies.

The failed decompaction could be related to the phase separation due to the increase of the ionic strength. The difference between this study and the study of the decompaction using fluorescence is basically, the presence of the enzyme and the CutSmart buffer. Looking at the composition of the CutSmart buffer, we found the explanation of the obtained results (section 7.3.3.3). This buffer is required to carry out the reaction with the enzyme, but it increases a lot the ionic strength.

Once the complex is obtained, increasing the ionic strength, two possible situations appear. The blue line refers to CAC and the area inside the blue line is the range of concentration where the DNA-surfactant complexes are formed. Red line represents the precipitation of the compounds. If the red and the blue line are very close then the complex is not decompacted. Increasing the ionic strength CAC is increased also and solubility is decreased. The ideal conditions for decompaction would be to work under the CAC but out of the precipitation phase (Figure 128).

Expected situation:

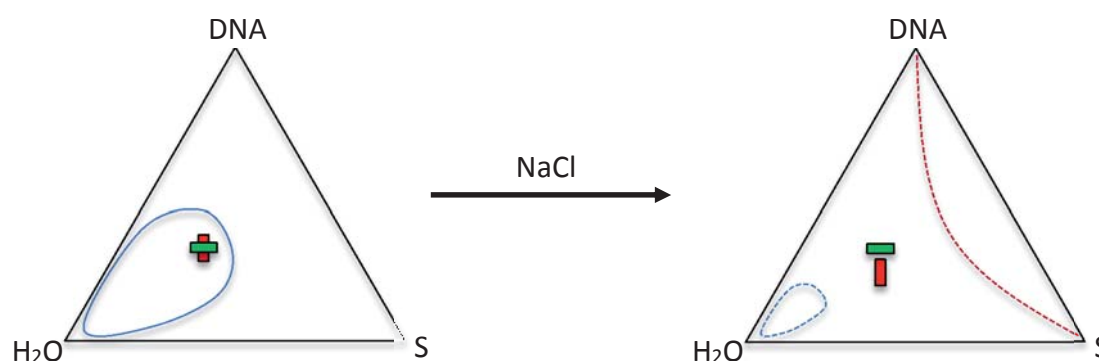


**Figure 128.** Schematic representation of the expected phase separation diagram.

However, as it is observed, the real situation of most of these complexes is shown in Figure 129.



Suggested real situation:

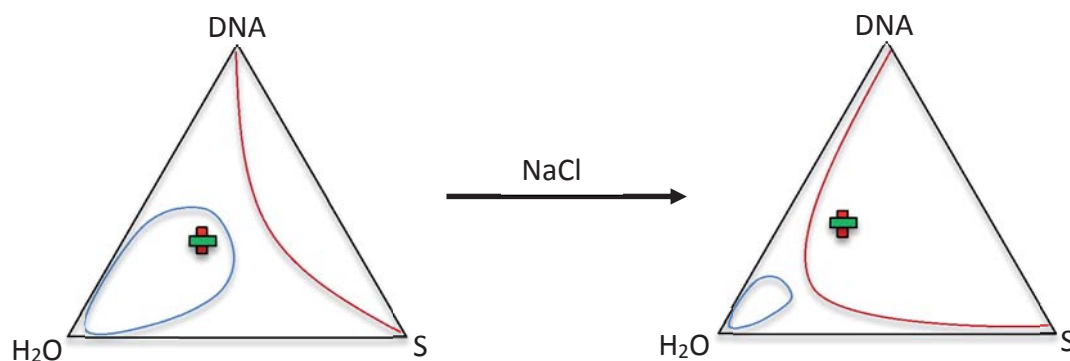


**Figure 129.** Schematic representation of the real phase separation diagram.

The same experiment has been repeated without the buffer needed for the proper activity of the enzyme. As one could expect, the enzyme did not act without the buffer. In addition, decompaction using different salt concentrations was tried but in none of them, any DNA chain does not migrate through the electrophoretic gel.

Decompaction of DNA increasing the ionic strength is dependent on the solubility of the surfactant. Based on the general knowledge, the longer is the hydrocarbon chain the lower will be the solubility in water. Moreover, **C16** is clearly the less soluble surfactant and, based on theoretical calculations, *cis* surfactants form hydrogen bonds with medium strength, which decrease the solubility of the surfactant. But, what happens when combining these two factors? Is it possible to predict the solubility of these surfactants?

Aggregation energies of these surfactants calculated using theoretical calculations in section 7.3.2.4 show that the aggregation of **C16** is more favourable than **C12**, followed by **T16** and finally **T12**. These aggregation energies can be directly related to the stability of a single surfactant in water solution. A low solubility means a low stability in solution and so a tendency to self-assemble into aggregates to reduce the energy of the system.

Other strategies for decompacting DNA-surfactant complexes are related to the formation of mixed aggregates with the surfactant and the decompacting agent. The formation of these new aggregates has to be more favourable than the interaction between surfactant aggregates and the DNA chain.

One of these decompacting agents is heparin, which is widely used as blood thinner. Heparin is a sulphonated polysaccharide polymer and it is shown to decompact DNA-cationic dendrimer complexes very efficiently.<sup>208</sup> Also, heparin is known to form complexes with different surfactants such as anionic<sup>253</sup>, cationic gemini surfactants<sup>254</sup> and also with CTAB<sup>255</sup>. However, in none of them heparin was used as decompacting agent for DNA-surfactant systems. Different heparin concentration were considered.

Additionally, and only as a curiosity, a commercial detergent was studied as decompacting agent. The used detergent was Zalo Plus<sup>®</sup> and it contained two zwitterionic surfactants, cocamidopropyl betaine and alkyldimethyl amine oxide; two non-ionic surfactants, alkylpolyglucoside and a polymer based on alcohol etoxylate; and two anionic surfactants, fatty alcohol ethersulphate and fatty alcohol sulphate. This cocktail of surfactants could interact with our cationic surfactants forming mixed aggregates. This decompaction study was carried out using **C12** and CTAB. Results are shown in Figure 130.

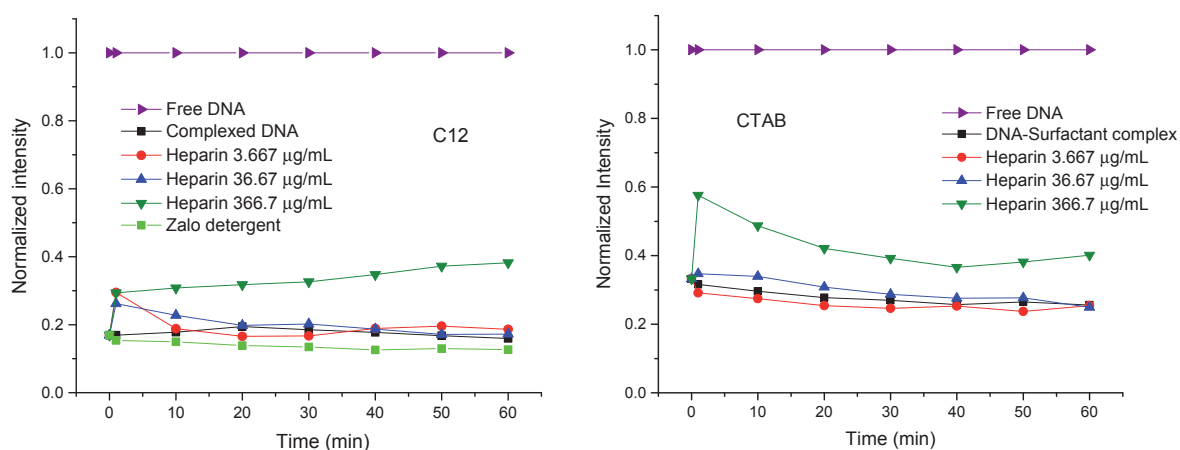


**Figure 130.** Decomposition studies of DNA-**C12** and DNA-CTAB complexes using different concentrations of heparin and Zalo detergent (in the case of DNA-**C12** complexes) during 1 hour.

Results show that these complexes cannot be decompacted using heparin or Zalo detergent. This means that the surfactant-heparin interaction is less favourable than the DNA-surfactant interaction. It also could mean that due to the high concentration of surfactants present in these complexes, they are kinetically entrapped and cannot be decompacted easily.

Looking at all the results of decompaction, it is shown that each surfactant can only be decompacted at a certain ionic strength depending on its solubility. **C16** decompacts at very low ionic strength values, then **C12** followed by **T16** and finally **T12**. This order of decompaction can be directly related to the aggregation energies (section 7.3.2.4). Thus, in our case, using *a priori* theoretical calculations it has been possible to determine the relative solubility of the group of surfactants.

As explained above, these decompaction results show that by modifying the ionic strength these systems could be reversible. With these results, we could start to carry out some cell transfection studies in order to study two different steps of the gene therapy, the cell penetration of these complexes and the decompaction of them inside the cell.

### 7.3.4 Biological application

Once the interaction of **C12**, **T12**, **C16** and **T16** with DNA was studied, some preliminary biological studies were done to determine their cytotoxicity and also to know whether the obtained DNA-surfactant complexes could transfect into cells by themselves or if they would require an external transfecting agent. All biological studies were done in collaboration with Dr. Nerea Gaztelumendi and Dr. Carme Nogués at the Department of Cellular Biology (UAB).

#### 7.3.4.1 Cytotoxicity – MTT assay

To study the toxicity of the surfactants, a well-know procedure called MTT assay was used. This method consists in introducing a soluble dye called 3-(4,5-dimethylthiazol-2-yl)-2,5-diphenyltetrazolium bromide, also known as MTT, into the cell-containing well. Depending on the cell metabolic activity, a certain amount of reductase enzymes will reduce the MTT to formazan (Scheme 13), which is insoluble in water and it is purple. Then, the medium is removed and formazan is dissolved in an organic solvent and the absorbance is determined, which will be proportional to number of living cells.



Commercial surfactants CTAB and DTAB are clearly very toxic because only less than 10 % of the cells were alive after the experiment, whereas **C12**, **T12**, **C16** and **T16** are non toxic because the number of cells was the same than in the control.

#### 7.3.4.2 Cell Transfection

Transfection assays were done using plasmid pEGFP-Peroxi as target DNA. This DNA is 4.7 kbp length and it contains the gene that codifies the Green Fluorescent Protein (GFP). Once the DNA is transfected into a cell, the gene is translated into a messenger RNA chain, which is subsequently converted into GFP by the ribosome and other agents. Using a fluorescence microscope, transfected cells can be detected. HeLa cells were used as target cells due to the well-known procedure to work with them. Lipofectamine® 2000 reagent, which is a mixture of commercial surfactants (1:3, DOPE:DOSPA),<sup>256</sup> was used as positive control, as in other works studying the transfection of DNA-surfactant complexes.<sup>257–260</sup> Four different charge ratios of the DNA-surfactant mixtures were studied in order to find the optimal conditions for transfection and decompaction (1:1, 1:5, 1:10 and 1:50).

Results show that none of the studied DNA-surfactant complexes can transfect into cells and release the DNA inside while the control experiment shows clearly high transfection (Figure 132). None of the studied DNA:surfactants ratios does not show any transfected cells. Images of the cells after the transfection study with the six different surfactant at different  $Z_{hp}$  are shown in section 12.6. Transfection study was repeated by increasing 5 and 7 times the amount of DNA and surfactant (keeping the desired ratios) in order to know whether the negative result was due to the low detection. Same results were obtained indicating that any cell was not transfected.

Thus, these surfactants will require an external transfecting agent in order to carry out the cell uptake. Some preliminar studies were done using polyethylenimine (PEI) as transfecting agent. The DNA-surfactant complexes were prepared as in the previous transfection studies but in this case, before adding the mixture to the cells-containing well, PEI was added to the mixture. First results show that cell uptake was achieved, as it is

shown in Figure 132. However, other studies must be carried out in order to know whether the DNA-surfactant complexes is inside the cell or only the DNA-PEI system.

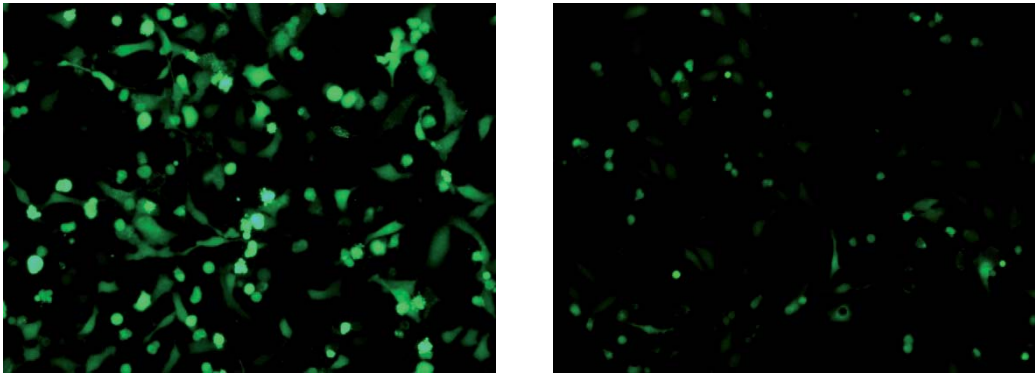


**Figure 132.** Fluorescence microscopy images of the transfected HeLa cells by Lipofectamine 2000 (left) and by using (1:10 DNA:T16)-PEI complexes (right).

These results encourage us to keep studying the use of external transfecting agents to transfect the DNA-surfactant complexes into cells.

## 7.4 Summary and Conclusions

In this chapter, four new pH-dependent  $\beta$ -amino acid-based cationic surfactants have been synthesised and characterised. Stereochemistry and chain length play an important role on the behaviour as surfactants. All of them are more efficient than commercial surfactants CTAB and DTAB because they have a lower CMC value. These four surfactants showed interesting behaviour for biological applications due to their pH-dependence. Weak acid behaviour as aggregates could stabilize DNA-complexes in solution.

A new method for determining the CMC in solution using circular dichroism has been found. Despite this method have some restrictions, it could be used for chiral surfactants, which self-assemble through the chromophore group. Theoretical calculations are in good agreement with circular dichroism studies and with cryoTEM images, suggesting that stereochemistry plays an important role on the morphology of the aggregates. *cis* Isomers form mainly vesicles while *trans* isomers form fibers. However, this complex systems are polydisperse, according to DLS analysis.

Using different techniques, compaction of DNA has been studied. Stereochemistry and the chain length are very important factors and they are not dependent one of each other. While **C12** and **T12** show the same behaviour and are much more efficient than DTAB, **C16** and **T16** behave completely different. **T16** is efficient or even more efficient than CTAB compacting DNA while **C16** is not. All these surfactants form DNA-surfactant complexes, which seem to protect the DNA chain against three different enzymes.

Finally, decompaction of the complexes has been achieved by modifying the ionic strength of the medium. This preliminary result show that these complexes can be decompacted by modifying the amount of salt in the solution.

Biological assays show interesting properties of surfactants **C12**, **T12**, **C16** and **T16**, which are not toxic while CTAB and DTAB are very toxic. However, external transfecting agents are required in order to carry out the cell uptake.

## **8. General Conclusions**

---





## 8. General Conclusions

The study of four different supramolecular systems containing chiral cycloalkane-based molecules has been carried out during this thesis. Different synthetic routes have been used to prepare the molecules and, then, many different techniques have been used to study the systems. Obtained conclusions of the studied systems were divided in four chapters:

- **Tripodal anion receptors:** Theoretical calculations have provided information on the structure of the complexes and have helped in the rationalisation of the thermodynamics of these systems. The presence of cyclobutane moieties in the receptor branches seems to provide preorganization to the receptor favouring the binding of fluoride instead of other anions.
- **Organogelators:** Different cycloalkane diamide-based compounds have been studied. Gelation ability can be modified by tuning the structural factors of the molecule such as the ring size, stereochemistry and substitutions of the ring. Despite the obtained knowledge about these families of compounds using a wide range of techniques, only few influences of these factors on the final behaviour have been found. Moreover, chiral aggregates were obtained from all compounds, despite two of them were *meso* compounds.
- **Bolaamphiphiles:** Stereochemistry of the studied compounds plays an important role on the efficiency as surfactants. Regiochemistry has an influence on the morphology of the aggregates. The structure of four bolaamphiphiles at the air-water interface has been predicted using theoretical calculations.
- **pH-Dependent surfactants:** Modifying the stereochemistry and the length of the chain of this family of amphiphiles, their surfactant and DNA-complexation abilities can be tuned. These surfactants show suitable features as potential new vectors for gene therapy due to their low toxicity and efficiency in compacting a DNA chain. However, external transfecting agents are required to achieve the cell transfection.



## **9. Computational Details**

---



## 9. Computational Details

### 9.1 General methodology

A conformational search of each system was carried out using a mixed low mode/torsional sampling<sup>261</sup> with the OPLS-2005<sup>262</sup> force field implemented in the MacroModel<sup>263</sup> program in order to find and select an approximation of the most stable conformers.

The geometries of the lowest energy conformers of each system were optimised using Density Functional Theory (DFT)<sup>264</sup> with the Gaussian09<sup>265</sup> program. In particular we have used the M06-2X<sup>266</sup> functional with the 6-31G(d) basis set. This is a hybrid meta-GGA functional that includes a 54% of exact exchange and that was shown to describe correctly non covalent interactions.<sup>267</sup>

### 9.2 Tripodal anion receptors

For each structure, we have computed the harmonic vibrational frequencies to verify that they correspond to energy minimum with the same level of theory than the optimization.

Once the structure of the minimum is achieved, we have carried out a DFT single point energy calculation in gas phase and in solution at the M06-2X/6-311++G(2df,2pd) level of theory.

Diffuse functions represent accurately the tail portion of the electron density, which are distant from the atomic nuclei. These additional basis functions are necessary when considering anions. In order to study the effect of the diffusion functions in the molecular geometry of our systems, we have carried out all the DFT optimizations and frequencies calculations also at the M06-2X/6-31+G(d) level of theory to compare the results. Diffuse functions are represented by “+”.

Finally, a calculation of the Basis Set Superposition Error (BSSE) have carried out at the M06-2X/6-311++G(2df,2pd) level of theory using the counterpoise method<sup>268</sup>. Basis set superposition error<sup>269</sup> is a spurious stabilizing contribution arising from the improved

## 9. Computational Details

description of a fragment in a complex due to the assistance of the basis sets of the other fragments. BSSE leads to too large binding energies. This correction can only be calculated in the gas phase due to limitations of the Gaussian09 program.

Transferred charges from the anion to the receptor were calculated using the Natural Bond Orbital analysis (NBO)<sup>270</sup> at the M06-2X/6-311+G(d,p) level of theory.

Energy in solution was calculated using the using two different methods, SMD,<sup>271</sup> which is a Solvation Model based on solute electron Density and C-PCM,<sup>272</sup> which is a Conductor-like Polarizable Continuum Model. These methods describe the solvent as a continuous polarizable medium.<sup>273</sup> The used solvent was DMSO. Finally, all the results of this work were achieved using SMD method because it fits the best with the experimental data.

Gibbs energies in gas phase were calculated assuming gas ideal behaviour at 1 atm as standard state (denoted by the superscript “<sup>o</sup>”). Molecularity correction<sup>274</sup> is needed to convert Gibbs energies to a standard state of 1 mol L<sup>-1</sup> (denoted by the superscript “<sup>\*</sup>”). Assuming ideal gas behaviour, this correction can be calculated using Equation 15.

$$\Delta G^{o \rightarrow *} = RT \ln \left( \frac{Q^*}{Q^o} \right) \quad (\text{Equation 15})$$

where Q is the reaction quotient evaluating all the species in their concentration at standard state. If we consider that all the species from the standard state “<sup>o</sup>” are in gas phase at 1 atm and 298,15 K, concentration of these species is 1/24.46 mol L<sup>-1</sup>, and if we consider that all the species from the state “<sup>\*</sup>” are solutions at 1 mol L<sup>-1</sup> and at 298.15 K, then, molecularity correction can be calculated as Equation 16 wherein  $\Delta n$  is the increment of the number of mols of the reaction.<sup>275,276</sup>

$$\Delta G^{o \rightarrow *} = \Delta n RT \ln(24.46) \quad (\text{Equation 16})$$

All the results of binding energy ( $\Delta E$ ) and Gibbs energy in solution ( $\Delta G$ ) incorporate this counterpoise correction.<sup>277</sup>  $\Delta G$  in solution were calculated using Equation 17.

$$\Delta G_{(solution)} = \Delta G_{(gas)} - \Delta E_{(gas)} + \Delta E_{(solution)} + \Delta G^{o \rightarrow *} + \Delta E_{BSSE} \quad (\text{Equation 17})$$

### 9.3 Organogelators

For all the studied molecules, once the geometry in gas phase is obtained, the dimer is built up and the procedure is repeated. Then, the procedure is repeated again with the tetramer. From the structure of the tetramer optimised with DFT, the internal dimer of the aggregate is selected to be the model of aggregation to build up the hexamer and the octamer with the OPLS\_2005 force field. A minimization of the energy using molecular mechanics of the hexamer and the octamer is carried out. Finally, a single point energy calculation in gas phase at the M06-2X/6-31G(d) level of theory is carried out to get the energy of each system. Aggregation energies of the formation of the dimers in *syn* and *anti* configuration were computed using 6-31G(d) and 6-311+G(d,p) basis sets. Aggregation and interaction energies were calculated including BSSE correction which is assumed to be additive for the formation of an aggregate of  $n$  monomers.<sup>278</sup>

Circular dichroism spectra were calculated by taking the optimised structure of the monomer in methanol solution and calculating 50 excited states with Gaussian09 using the TDDFT method<sup>279–281</sup> with the M06-2X/6-311+G(d,p) level of theory. Prediction of the CD spectra of the tetramer aggregates was carried out from the geometry of the internal tetramer of the octameric aggregate studying 20 excited states with the CAM-B3LYP<sup>282</sup>/6-31G(d,p) level of theory. Representation of the predicted circular dichroism spectra were done using GaussSum software<sup>283</sup>.

### 9.4 Bolaamphiphiles

The optimised structure of the monomers in gas phase was optimised with DFT again in water solution and also taking into account the presence of the two bromide ions.

Then, to study the geometry of the surfactants on the surface, the ammonium head was replaced by a methyl group. The structure of the aggregates from the dimer to the octamer was studied following the procedure described in section 9.3. Once the structure of the octamer is obtained, a monomer was selected and the surfactant is built up again by replacing the added methyl group by the ammonium head. The geometry of the ammonium head was obtained from the optimised monomers with DFT in water solution.



## 9.5 pH-Dependent surfactants

The structure of these molecules and their tetramers in solution was optimised with DFT in water solution using M06-2X and 6-31G(d) level of theory. Finally, aggregation energy in water was calculated using M06-2X and 6-311+G(d,p) level of theory and adding the counterpoise correction of the BSSE. Circular dichroism spectra were calculated by taking the optimised structure of the monomer in water solution and calculating different excited states with Gaussian09 using the TDDFT method<sup>279–281</sup> with the M06-2X/6-311++G(2df,2pd) level of theory.

## **10. Experimental Details**

---



## 10. Experimental Details

### 10.1 Spectroscopy and spectrometry

$^1\text{H}$ -NMR (250, 360, 400 or 600 MHz) and  $^{13}\text{C}$ -NMR (62.5, 90, 100 or 150 MHz) were recorded at *Servei de Ressonància Magnètica Nuclear* from the *Universitat Autònoma de Barcelona (SeRMN)*.

The spectrometers used were:

- AC 250 Bruker for  $^1\text{H}$  at 250 MHz and  $^{13}\text{C}$  at 62.5 MHz.
- AVANCE 360 Bruker for  $^1\text{H}$  at 360 MHz and  $^{13}\text{C}$  at 90 MHz.
- ARX 400 Bruker for  $^1\text{H}$  at 400 MHz and  $^{13}\text{C}$  at 100 MHz.
- AV 600 Bruker for  $^1\text{H}$  at 600 MHz and  $^{13}\text{C}$  at 150 MHz.

Chemical shifts of signals are given in ppm, using as reference the following values:

- $\text{CDCl}_3$ :  $\delta$  7.28 and 77.16 for  $^1\text{H}$  and  $^{13}\text{C}$ , respectively.
- $\text{MeOD-d}_4$ :  $\delta$  3.31 (4.87) and 49.00 for  $^1\text{H}$  and  $^{13}\text{C}$ , respectively.

### 10.2 Infrared spectroscopy (IR)

IR spectra in solid state were recorded on a Sapphire-ATR spectrophotometer and peaks are reported in  $\text{cm}^{-1}$ . Infrared spectra (FT-IR) in solution were recorded on a Perkin Elmer, Spectrum One FT-IR spectrometer, being the signal an average of 16 scans.

### 10.3 High Resolution Mass Spectra (HRMS)

HRMS were recorded at *Servei d'Ànlisi Química* from the *Universitat Autònoma de Barcelona* in a Bruker Squire 3000 micrOTOFQ spectrometer using ESI-MS (QTOF).

### 10.4 Measurements of the surface tension

In collaboration with Dr. Ramon Pons from IQAC-CSIC, a homemade pendant drop tensiometer was employed (Figure 133). A surfactant solution drop is created at the end of a straight-cut Teflon tube having known internal and external diameters. At the same

10. Experimental Details

time, 8 drops from 8 different concentrations can be studied.

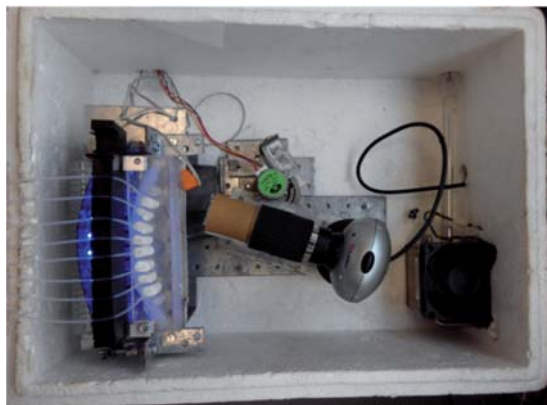


**Figure 133.** Homemade tensiometer used to carry out the measurements of the surface tension.

The drop shape was recorded with a camera and its image was corrected for spherical aberration. The background was subtracted and the resulting droplet contour fitted in a Young–Laplace equation, with a homemade golden section search algorithm (Figure 2). This method is known as pendant drop method.<sup>138,284</sup> Measurement of the surface tension is repeated until the value remains constant (depending on the surfactant, it could be between 1-6 h). Temperature was kept at  $25.0 \pm 0.5$  °C.

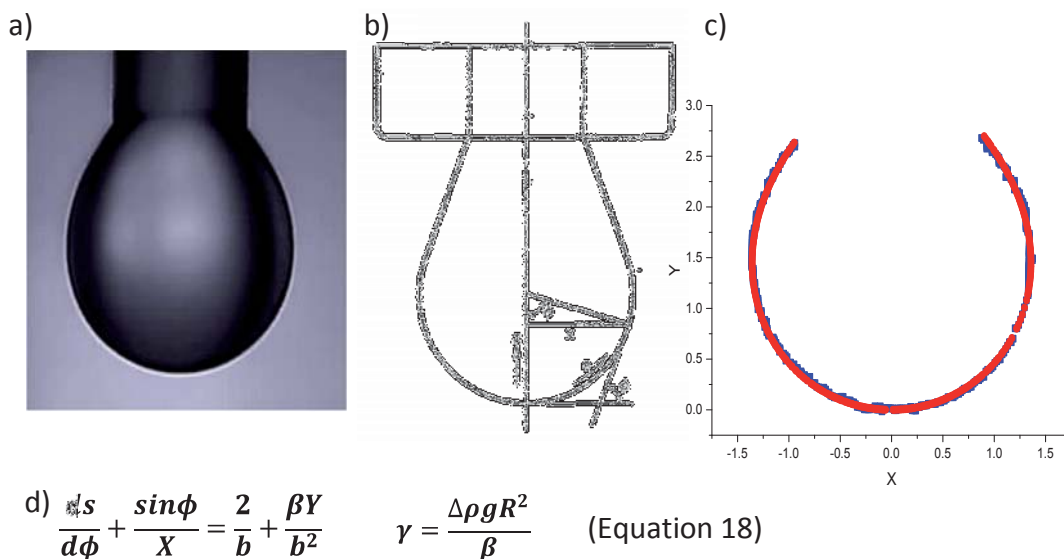


**Figure 134.** a) Image of the contour of the drop captured with a camera. b) Theoretical parameters of the contour of a drop. c) Experimental values from the contour (blue) and the fitted values (red). d) Young-Laplace differential equation.

The experimental surface tension values drastically change in slope at a point corresponding to the critical micelle concentration. The critical concentration, the intersection between two straight lines, is related to the excess of the surfactant(s) at the air/water interface,  $\Gamma_i$ , according to the Gibbs absorption isotherm (Equation 6).

Here  $R$  is the universal gas constant,  $T$  is the temperature,  $\gamma$  is the surface tension, and  $C$  is the concentration. The value of  $n$  is associated with the number of ions (i.e. 3 for bolaamphiphiles, 2 for monovalent ionic surfactants in water and 1 in the presence of electrolytes in strong excess or for non-ionic surfactants). From  $\Gamma_i$  the area per head group,  $A_m$ , was determined.

## 10.5 Measurements of the proton activity of the surfactants

### 10.5.1 pKa measurements

The  $pK_a$  values were determined from the potentiometric titration of 1 mL of 5 mM aqueous surfactant solutions with 5 mM NaOH aqueous solutions. The pH electrode was an ORION 8103SC semimicro and the potentiometer was a Thermo Orion model 720A+. All titrations were conducted at  $25 \pm 0.1$  °C and under nitrogen gas atmosphere and magnetic stirring.  $pK_a$  Was determined as the pH of the corresponding semi equivalence point. Once the titration is finished, a new titration with 5 mM HCl is done to determine the reversibility.

### 10.5.2 pH-Surfactant Concentration Measurements

The pH values of different concentrations of surfactant water solutions under nitrogen were measured using a pH electrode (model ORION 8103SC Ross Semimicro) as shown in Figure 135. Measurements were made at increasing concentrations of surfactant to minimize errors from possible contamination from the electrode.

The acid–base equilibrium was modelled by the next equation for a weak base, assuming dilute ideal behaviour and complete salt dissociation. Equation 19 was obtained taking into account the equilibrium constant definition, mass and charge balances, and ionic water product. 0.5 mL of a 5 mM solution of surfactant in deionised water was prepared and it was added to a 0.5 mL of deionised water using a 50  $\mu$ L Hamilton syringe.

## 10. Experimental Details

$$C_b = (K_a + [H^+]) \left( \frac{K_w}{[H^+]^2} - 1 \right) \quad (\text{Equation 19})$$

The  $pK_a$  values both below the CMC (surfactant as monomer) and above the CMC (apparent  $pK_a$ ) were evaluated by using this equation.

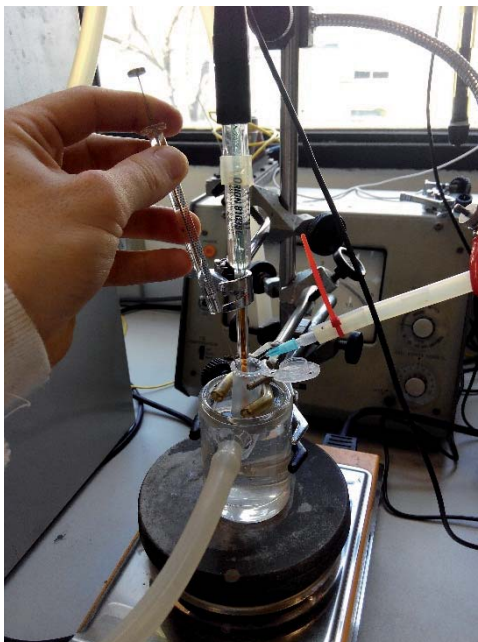


**Figure 135.** Equipment used for titrations of surfactant solutions.

## 10.6 Microscopy

### 10.6.1 Cryogenic Transmission Electron Microscopy (CryoTEM)

A drop of a solution with a known concentration of the surfactant in water is added on carbon-film-coated grids. Then, the sample is frozen at 10000 °C/s using liquid ethane and the sample is kept at  $-180$  °C during the imaging using liquid nitrogen. The electron beam was of 200 kV and around 100  $\mu$ A. Pressure during the experiments was  $10^{-2} \cdot 10^{-6}$  Pa. Images were acquired with Hitachi H-7000 microscope in the *Servei de Microscòpia de la Universitat Autònoma de Barcelona* in collaboration with Dr. Pablo Castro.

### 10.6.2 Scanning Electron Microscopy (SEM)

SEM images were acquired with Quanta 200 ESEM FEG apparatus equipped with a field-emission gun (FEG) in the *Institut de Ciència de Materials de Barcelona (ICMAB)* in collaboration with Dr. Ana Esther Carrillo and Dr. Judith Oró. Wet gels were disposed on a carbon-film-coated copper grid and dried by standing for 30 minutes on the grid. The resulting xerogels (dry gels) were then introduced into the microscope chamber working at 50-70 Pa and 5 kV. In the SEM/EDX analyses, the same apparatus equipped with an Energy Dispersive X-ray (EDX) system for chemical analysis was used.

### 10.6.3 Atomic Force Microscopy (AFM)

Atomic Force Microscopy was used to determine the morphology of the DNA-surfactant complexes. The microscope used was a Multimode 8 from Bruker in the *Norwegian University of Science and Technology (NTNU)* in collaboration with Gjertrud Maurstad.

Samples were prepared for AFM imaging by transferring a 10  $\mu\text{L}$  aliquot to a freshly cleaved 5 mm diameter mica disk, and after 5 min of incubation. Then, the sample surface was rinsed rapidly with pure water (Milli Q) to obtain a clean surface and then dried in a stream of  $\text{N}_2$  followed by vacuum-drying at a pressure of  $1.3 \times 10^{-4}$  Pa for 5 hours.<sup>285</sup> The imaging was done using ScanAsyst mode in air, employing ScanAsyst-air cantilevers with nominal spring constants of 0.4 N/m.

## 10.7 Circular dichroism (CD)

### 10.7.1 CD in solution

A solution about 0.5-5 mM of a sample is prepared in MeOH or in water (it depends on the sample and on the obtained signal) and it is measured in a 1 cm width quartz cuvette. CD spectra were recorded with JASCO-715 spectropolarimeter and were processed using Spectra Manager Software. Table 23 shows the experimental conditions used for the analysis. A systematic treatment of the obtained data was done using the mentioned software.



## 10. Experimental Details

**Table 23.** Experimental conditions for the CD analysis.

Parameter	Value
Range	190-500 nm
Data pitch	0.5 nm
Scanning mode	continuous
Scanning speed	50-100 nm/min
Response	2 sec.
Band width	2-5 nm
Accumulation	1-4

### 10.7.2 Solid state CD of the xerogels

A gel at the *mgc* is prepared in the desired solvent. Then the solvent of the gel is removed under vacuum to get a xerogel. Samples were prepared by mixing the xerogels at around 0.020-0.025 mmol/g of KBr (1.2-1.6 wt. %) in an agate mortar and pressing the mixture for 10 minutes.<sup>286</sup> Homogeneous translucent disks were obtained and the CD spectra were recorded using a JASCO-715 spectropolarimeter and were processed using the associated software. Smoothing and noise elimination were applied in order to obtain proper spectra following a systematic treatment.

Table 23 shows the experimental conditions used for the analysis. Data recording was repeated 3 times rotating the thin film 120 ° in each one to obtain representative data and to avoid macroscopic influences.

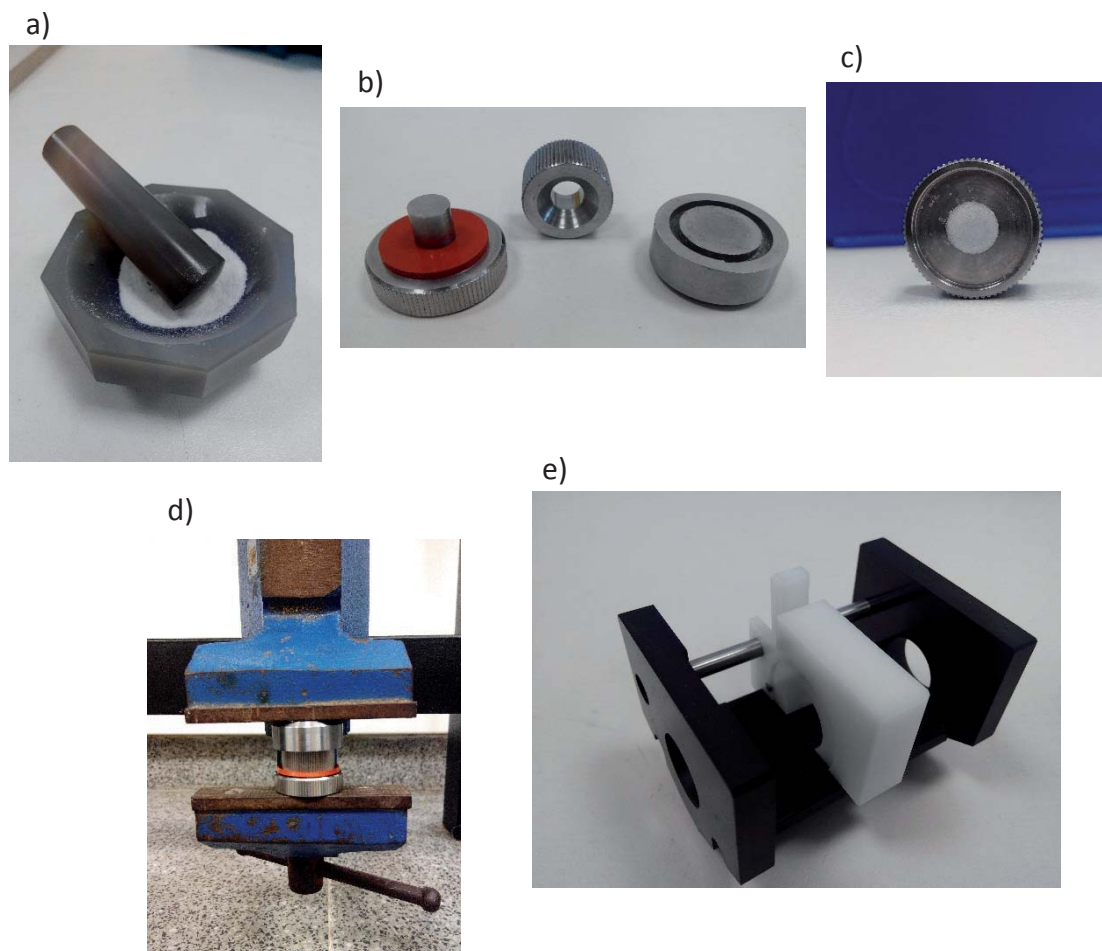


**Figure 136.** a) Mixing agate mortar. b) Metal pieces of the film mold. c) Film already pressed. d) Press. e) Spectropolarimeter accessory to fix the film with the mold.

### 10.7.3 CD of DNA-containing samples

Complexation of a DNA chain has been studied following the steps:

- preparation of 350  $\mu\text{L}$  of solution 0.333  $\mu\text{M}$  (1 mg/mL) of Salmon Sperm DNA (obtained from Thermofischer, stock solution of 10 mg/mL).
- measurement of the CD spectra of the DNA solution in a 1 mm cuvette using the parameters described in Table 24.
- DNA solution is transferred into a glass vial. Then a known volume of a known solution of a surfactant is added. Samples is then mixed and is left for two minutes. After that, the solution is measured and the process is repeated.

**Table 24.** Experimental conditions for the CD analysis using DNA-containing samples.

Parameter	Value
Range	200-350 nm
Data pitch	0.5 nm
Scanning mode	continuous
Scanning speed	200 nm/min
Response	2 sec.
Band width	5 nm
Accumulation	2

## 10.8 Gelation studies

The preparation of the gels was achieved by the following procedure:

A small amount ( $5.0 \pm 0.1$  mg) of LMWG is weighted in a 2 mL transparent-glass vial with septum screw-on cap. Then, a certain volume of solvent to be tested is added and the vial closed. The minimum volume added is 0.05 mL. Then the mixture is heated under the boiling point of the solvent using a balloon system in order to avoid solvent pressure and, once a solution is obtained, the mixture is sonicated for 1 to 5 minutes. For high concentrations and in some solvents, previous sonication is needed for a good solubilisation during heating and sonication time is usually shorter than for diluted gels. Then, the mixture is left to stabilize and to reach room temperature.

To state that the mixture is a gel the tube inversion test is done just by turning the vial upside down. If the sample is a gel it does not drop. The mixtures can also be stated as solutions or insoluble systems. In order to determine the minimum gelation concentration (*mgc*), a new volume of solvent is added to the gel and the process is repeated until no gel is formed: the last volume added determines the *mgc*.

## 10.9 Flash chromatography

Column chromatography was always performed with Scharlau™ silica gel for flash chromatography (mean pore: 60 Å; particle size: 0.04-0.06 mm, 230-400 mesh ASTM), using nitrogen as driving gas.

All reactions were monitored by thin-layer chromatography (TLC) using ALUGRAM™ SILG/UV<sub>254</sub> pre-coated aluminium sheets. Layers of 0.20 mm of thickness covered with silica gel 60 with fluorescent indicator UV<sub>254</sub>.

Several methods were used to visualise the spots:

- Irradiation under a LED UV-light (UV<sub>254</sub>), using a VILBER LOURMAT™ lamp, VL-4LC model.
- Staining thin-layers under acid solution of vanillin in ethanol 96%.
- Staining thin-layers under basic solution of KMnO<sub>4</sub> in water.
- Staining thin-layers under Hanessian solution.

## 10.10 Dynamic Light Scattering (DLS)

Dynamic Light Scattering experiments were carried out in the Department of Biotechnology from the NTNU in Trondheim (Norway).

The instrument used was a Zetasizer Nano ZS (Figure 137). Laser source was He-Ne at 633 nm. The angle of the measurements was 173 degrees. This angle was selected based on the optimization of the instrument and the knowledge they have over this instrument.

Samples were measured 3 times, and each time the samples were analysed 11 times. So, at the end, a mean value of 33 measurements is obtained. All the measurements were carried out at 25 °C.

Correlation function compares the intensity at a time  $t$  with the intensity at a very short time after  $(t + \partial t)$ . Correlation function is represented as  $G(\partial t) = \langle I(t) \cdot I(t + \partial t) \rangle$  and the solution can be expressed as  $G(t) = A(1 + Be^{-2\Gamma\partial t})$  where  $\Gamma = D_t q^2$ ;  $D_t$  is the translational diffusion coefficient of a spherical particle with the same size that the analysed particles and  $q = \frac{4\pi n}{\lambda_0} \sin\left(\frac{\theta}{2}\right)$ . In our case,  $\lambda_0$  is 633 nm,  $\theta$  is 173 ° and

## 10. Experimental Details

$n$  is the refractive index of the dispersant which was taken as the same value as CTAB, 1.435.<sup>287,288</sup> This expression is only valid for a monodisperse system.

Associated software is Zetasizer Software 7.11 and obtained data was treated using OriginLab.



**Figure 137.** Zetasizer Nano ZS used for the DLS experiments.

### 10.11 Polymerase Chain Reaction (PCR protocol)

Plasmid pSB-E1g (8117 bp) was expressed in bulk amounts and purified from DH $\alpha$ 5 *E.Coli*. The procedure for its preparation was optimised by Sravani Ramisetty and Dr. Rita Dias from *Norwegian University of Science and Technology (Norges teknisk-naturvitenskapelige universitet - NTNU)* from Trondheim (Norway). The study of the interaction of these surfactants with DNA was carried out in Trondheim during a three-months stay.

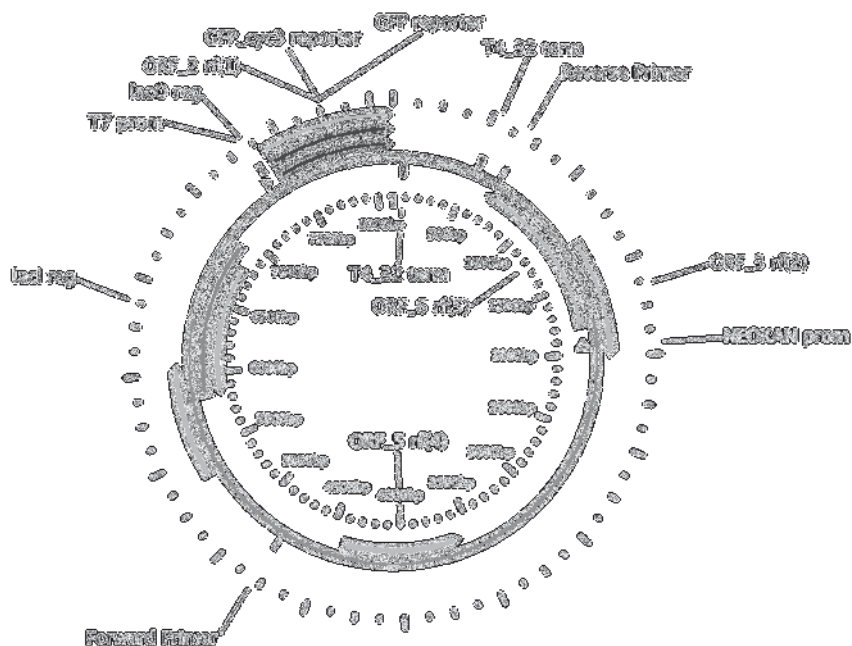


**Figure 138.** Plasmid pSB-E1g (8117 bp). The target fragment is located from the forward primer until the reverse primer in clockwise sense.

Sequence of the used primers is shown in Table 25, and their positions are indicated on the plasmid map in Figure 138.

**Table 25.** Specifics of the primer pair used in PCR protocol.

Primer	Sequence	Position	Annealing T.
Forward	5' GCTGGCCGATAAGCTCTAAG 3'	4779	55 °C
Reverse	5' GGTGCATTGCAAACGCTAGG 3'	679	55 °C

To carry out the PCR, all components should be mixed and spun down prior to pipetting. These recommendations serve as a starting point. PCRs were carried out in an Eppendorf Mastercycle gradient shown in Figure 139.

Procedure for the PCR:

1. Prepare the following 50  $\mu$ l reaction in a 0.5 ml PCR tube on ice:

## 10. Experimental Details

Component	50 $\mu$ l reaction	Final Concentration
10X Standard Taq Reaction Buffer	5 $\mu$ l	1X
10 mM dNTPs	1 $\mu$ l	200 $\mu$ M
10 $\mu$ M Forward Primer	1 $\mu$ l	0.2 $\mu$ M (0.05–1 $\mu$ M)
10 $\mu$ M Reverse Primer	1 $\mu$ l	0.2 $\mu$ M (0.05–1 $\mu$ M)
Template DNA	1 $\mu$ l	<1,000 ng
Taq DNA Polymerase	0.25 $\mu$ l	1.25 units/50 $\mu$ l PCR
Nuclease-free water	to 50 $\mu$ l (40.8 $\mu$ l)	

- Gently mix the reaction and spin down in microcentrifuge. If the thermocycler does not have a heated cover, add one drop of mineral oil to the reaction tube to prevent evaporation.
- Cycling Conditions for a Routine PCR:

Cycle Step	Temperature	Time	Cycles
Initial Denaturation	95 °C	30 seconds	1
Denaturation	95 °C	25 seconds	35
Annealing	55 °C	20 seconds	
Extension	68 °C	4 minutes	
Final Extension	68 °C	5 minutes	1
Hold	4 °C	$\infty$	



**Figure 139.** PCR eppendorf Mastercycle gradient.

**Purification of the target linear dsDNA:**

1. In a 1.5 mL microcentrifuge tube, add 2-7 volumes of DNA Binding Buffer to each volume of DNA sample. Mix briefly by vortexing.
2. Transfer mixture to a provided Zymo-Spin™ Column in a Collection Tube.
3. Centrifuge for 30 seconds. Discard the flow-through.
4. Add 200 µL DNA Wash Buffer to the column. Centrifuge for 30 seconds. Repeat the washing step.
5. Add  $\geq 25$  µL DNA Elution Buffer (10 mM Tris-HCl, pH 8.5, 0.1 mM EDTA) directly to the column matrix and incubate at room temperature for one minute. Transfer the column to a 1.5 mL microcentrifuge tube and centrifuge at for 30 seconds to elute the DNA.

All the used solutions for the purifications were provided by Zymo Research.

Ultra-pure DNA is now ready for use. However, a gel electrophoresis has to be carried out to verify the purity of the sample. Also, NanoDrop measurements were carried out to determine the purity and the concentration of the sample.

**10.12 Gel electrophoresis**

To carry out the gel electrophoresis, 0.8 % Agarose gel (GelRed) was used as medium. Once the solution of GelRed is added, it is needed to wait 15 minutes to let the solution to cool down and to form a gel.

Samples were prepared using 7 mL of MiliQ water, 1.5 mL of a dye and 1 mL of the DNA-containing solution. Samples were loaded to the gel and a voltage of 100-120 V (depending on the size of the gel) was applied. After 20-30 minutes, the voltage was switched off and the gel was placed in a ChemiDoc™ XRS+ Molecular Imager from BioRad. (Figure 140)



## 10. Experimental Details



**Figure 140.** Gel electrophoresis equipment (left). ChemiDoc™ imager (right).

### 10.13 NanoDrop Measurements

A drop of the DNA solution is placed in the pedestal of the ND-1000 NanoDrop® Spectrophotometer (Figure 141). Measurements of the absorption spectra were done from 220 to 350 nm (DNA absorbs at 260 nm). Measurement of the 260/230 and 260/280 absorption ratios are given to determine the purity. Concentration of the sample is also given.

**260/280:** The ratio of absorbance at 260 nm and 280 nm is used to assess the purity of DNA and RNA. A ratio of  $\approx 1.8$  is generally accepted as “pure” for DNA.

**260/230:** This ratio is used as a secondary measure of nucleic acid purity. The 260/230 values for “pure” nucleic acid are often higher than the respective 260/280 values. Expected 260/230 values are commonly in the range of 2.0-2.2. If the ratio is appreciably lower than expected, it may indicate the presence of contaminants which absorb at 230 nm.



**Figure 141.** NanoDrop spectrophotometer.

### 10.14 Dye Exclusion Assay

Dye Exclusion Assay is a technique to determine the amount of accessible DNA in solution. Samples were prepared three times each one following this procedure:

- 1) 5  $\mu\text{L}$  of 20  $\text{ng}/\mu\text{L}$  DNA were mixed with 5  $\mu\text{L}$  of 100X GelStar, prepared from GelStar (10000, 0X) from Lonza. Mixtures were left 15 min of incubation.
- 2) After that, 5  $\mu\text{L}$  of each surfactant solution is added to the corresponding mixture.
- 3) Finally, 35 mL of 10 mM TrisHCl were added to the samples. Samples were left 1 h of incubation.

At the same time, a sample having only DNA and GelStar was prepared. This sample was used as maximum intensity and all the obtained values were normalised with this sample. Each experiment has to be accompanied with this sample in order to be sure that the results are consistent. Also, a sample having surfactant and GelStar is prepared in order to control that the mixture does not give any signal.

After 1 h, samples were measured using an Infinite M200 Pro Tecan Spectrophotometer. The emission spectra was measured from 500 to 700 nm. The experimental parameters are shown in Table 26.

## 10. Experimental Details

**Table 26.** Experimental parameters of the measurements of the emission spectra of the DNA-GelStar-surfactant mixtures.

Parameter	Value
Emission Wavelength Start	500 nm
Emission Wavelength End	700 nm
Emission Wavelength Step Size	2 nm
Emission Scan Number	101
Excitation Wavelength	493 nm
Number of Flashes	15

Each measurement was repeated 4 times at different parts of the sample to get an averaged result and to be sure that the sample is homogeneous.

### 10.15 DNase Foot Printing Assay

Each enzyme requires a specific buffer for its optimal use. NdeI requires CutSmart® Buffer (50 mM Potassium Acetate, 20 mM Tris-acetate, 10 mM magnesium acetate, 100 µg/ml BSA, pH 7.9), and NruI requires 3.1 Buffer® (100 mM sodium chloride, 50 mM Tris-HCl, 10 mM MgCl<sub>2</sub>, 100 µg/ml BSA, pH 7.9). NdeI, NruI, Standard DNase, CutSmart® Buffer and 3.1 Buffer® were provided by New England BioLabs® Inc. The optimal reaction conditions are at 37 °C. It has to be taken into account that using these buffers the ionic strength is increased.

### 10.16 Biological assays

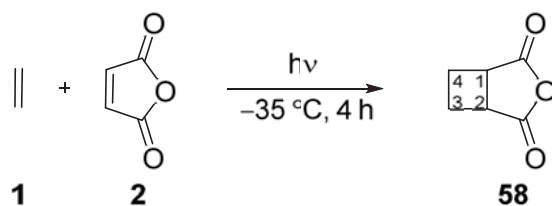
First, solutions of 2.5 mM of surfactant were prepared. 50 µL of each solution was mixed with 50 µL of an aqueous buffer which is commonly used to work with cells. The mixture is then added to the cells-containing solutions.

### 10.17 General tools

- **Optical rotations,  $[\alpha]_D$** , were measured using an automatic polarimeter PROPOL™, Dr. Wolfgang Kernchen model, at  $22 \pm 2$  °C and using a JASCO-715 spectropolarimeter and determined by the associated software. Moreover, some measurements were done using a PERKINELMER™ Polarimeter 341 using a 1 dm cuvette in the IQAC-CSIC.
- **Melting points** were determined on a hot stage using a Kofler apparatus, REICHERT AUSTRIA™ model.
- **UV-vis absorption** was measured in a Hewlett Packard 8453 spectrophotometer in aqueous solutions in a range between 180 and 500 nm.
- **Micro-distillations** were carried out in a BÜCHI™ distiller, GKR-51 model.
- **Lyophilization** of samples were done using a POLYSCIENCE™ lyophilisator, KR-80A model and a TELSTAR™ lyophilisator, model LyoQuest-85.
- **Hydrogenations** were carried out in an autoclave hydrogenation T-reactor Swagelok™, with a pressure capacity from 1 to 20 atm.
- **Photochemical reactions** were performed in a pyrex T-shaped photochemical reactor from TRALLERO&SCHLEE™. Irradiation was emitted from a mercury lamp of 125 W medium pressure PHILLIPS™ and a mercury lamp of 400 W medium pressure ELECTRO DH™. Refrigeration at  $-40$  °C came from a C40P TERMO SCIENTIFIC™ refrigerator, Phoenix II model.
- **Reagents** were used directly from commercial sources and **Solvents** were directly used due to their high quality. If necessary, reagents were conveniently purified and the solvents were distilled under nitrogen atmosphere using standard procedures described at Vogel's, Textbook of practical Organic Chemistry, Ed. Logman Scientific and Technical, UK, 1989.
- **Deuterated solvents** were used directly from commercial source Eurisotop™.

## 10.18 Synthetic procedures

### 3-Oxabicyclo [3.2.0] heptane-2,4-dione, **58**



A solution of maleic anhydride (1.52 g, 15.3 mmol) in acetone (500 mL) was cooled down to  $-35\text{ }^\circ\text{C}$ . The solution was saturated with ethylene bubbling during 10 minutes and the system was irradiated through a Pyrex filter for 30 minutes using a mercury-vapor lamp. After that, the system is cooled down again and the procedure was repeated three times. The solvent was removed under vacuum to afford pure compound **58** as a pale solid (1.93 g, 15.3 mmol, quantitative yield).

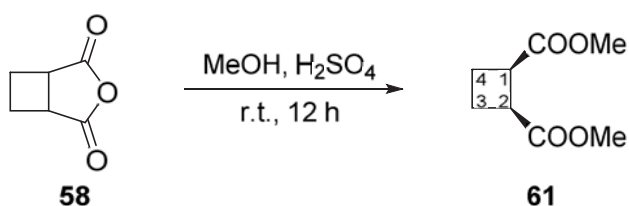
#### Spectroscopic data for compound **58**:

$^1\text{H NMR}$  (250 MHz,  $\text{CDCl}_3$ ):  $\delta$  2.35 (c.a., 2H), 2.74 (c.a., 2H), 3.52 (c.a., 2H,  $\text{H}_1$ ,  $\text{H}_2$ ).

Spectroscopic data are consistent with those reported in reference:

Tufariello, J. J.; Milowsky, A. S.; Al-Nuri, M.; Goldstein, S. *Tetrahedron Lett.*, **1987**, *28*, 267.

### Dimethyl (1*R*,2*S*)-cyclobutane-1,2-dicarboxylate, **61**



A solution of **58** (1.92 g, 15.1 mmol) and concentrated  $\text{H}_2\text{SO}_4$  (1.0 mL) in methanol (50 mL) was stirred at room temperature for 12 h. Dichloromethane (100 mL) was added to the organic phase and it was successively washed with water (2 x 50 mL) and brine (1 x 50 mL). The organic layer was then dried over  $\text{MgSO}_4$ , filtered off and concentrated in order to provide the corresponding crude as yellowish oil (2.15 g, 12.5 mmol, 83% yield).

Generally, the product is obtained pure enough to carry on the next step of the synthesis. However, it can be distilled under vacuum at 150 °C.

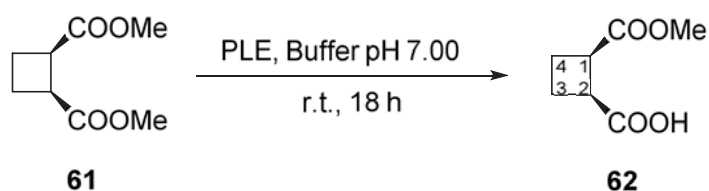
**Spectroscopic data for compound 61:**

$^1\text{H NMR}$  (250 MHz,  $\text{CDCl}_3$ ):  $\delta$  2.10 (c.a., 2H), 2.29 (c.a., 2H), 3.31 (c.a., 2H,  $\text{H}_1$ ,  $\text{H}_2$ ), 3.58 (s, 6H, Me).

Spectroscopic data are consistent with those reported in reference:

Sabbioni, G.; Jones, J. B. *J. Org. Chem.* **1987**, *52*, 4565.

**(1*R*,2*S*)-2-Methoxycarbonylcyclobutane-1-carboxylic acid, 62**



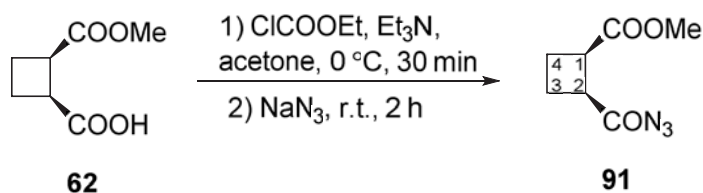
Diester **61** (3.61 g, 21.0 mmol) was dissolved in 250 mL of a buffer previously prepared from 0.1 M  $\text{KH}_2\text{PO}_4$  at pH 7.00. Pig liver esterase (PLE) (98 mg) was added to the solution and the mixture was stirred at room temperature for 18 h. The reaction was kept at pH 7.00 by adding a 1 M solution of NaOH. Then, the reaction mixture was washed with diethyl ether (2 x 100 mL), and 5 % HCl was added to reach pH 2-3. The acid solution was extracted with ethyl acetate (4 x 150 mL) and the organic extracts were dried over magnesium sulfate. The solvent was evaporated under vacuum to dryness obtaining half-ester (*R,S*)-**62** as an orangish oil (3.15 g, 19.9 mmol, 95 % yield, 97 % ee).

**Spectroscopic data for compound (*R,S*)-62:**

<sup>1</sup>H NMR (250 MHz, CDCl<sub>3</sub>): δ 2.23 (c.a., 2H), 2.41 (c.a., 2H), 3.43 (c.a., 2H, H<sub>1</sub>, H<sub>2</sub>), 3.69 (s, 3H, Me).

Spectroscopic data are consistent with those reported in reference:

Sabbioni, G.; Jones, J. B. *J. Org. Chem.* **1987**, *52*, 4565.

**Methyl (1*R*,2*S*)-2-azidocarbonylcyclobutane-1-carboxylate, 91**

To an ice-cooled solution of half-ester (*R,S*)-**62** (5.73 g, 36.2 mmol) in anhydrous acetone (80 mL), triethylamine (6.5 mL, 47.1 mmol, 1.3 eq) and ethyl chloroformate (4.5 mL, 47.1 mmol, 1.3 eq) were subsequently added. The mixture was stirred at 0 °C for 30 minutes. Then, sodium azide (5.9 g, 90.6 mmol, 2.5 eq) in 100 mL of water was added and the resultant solution was stirred at room temperature for 1.5 h. The reaction mixture was extracted with dichloromethane (4 x 100 mL), and the organic extracts were dried over magnesium sulfate. Solvents were removed under reduced pressure to give acyl azide (*R,S*)-**91** as a colourless oil (5.18 g, 28.3 mmol, 78 % yield), which was used in the next step without further purification. **WARNING:** This product should be carefully manipulated because of its explosive nature.

**Spectroscopic data for compound (*R,S*)-91:**

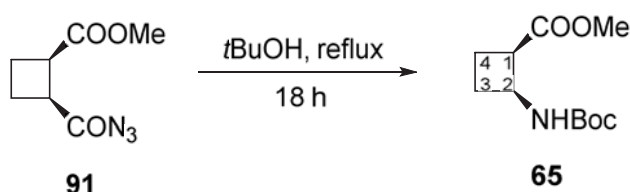
<sup>1</sup>H RMN (250 MHz, acetone-*d*<sub>6</sub>): δ 2.27 (c.a., 4H, H<sub>3</sub>, H<sub>4</sub>), 3,54 (m, 2H, H<sub>1</sub>, H<sub>2</sub>), 3.68 (s, 3H, Me).

Spectroscopic data are consistent with those reported in reference:

Martín-Vilà, M.; Muray, E; P. Aguado, G.; Álvarez-Larena, A.; Branchadell, V.; Minguillón, C.; Giralt, E.; Ortuño, R. M. *Tetrahedron: Asymmetry*, **2000**, *11*, 3569.

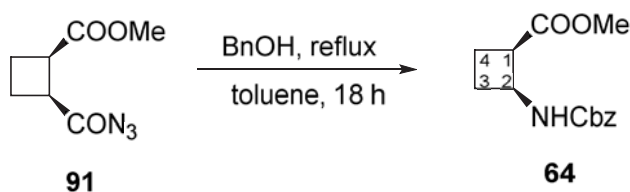
**Methyl (1*R*,2*S*)-2-(*tert*-butoxycarbonylamino)cyclobutane-1-carboxylate, 65**

METHOD A:



To acyl azide (*R,S*)-**91** (5.18 g, 28.3 mmol), 30 mL of *tert*-butanol were added as the solvent and the reagent. The mixture was heated to reflux and stirred for 18 h. Then, the solvent was evaporated under vacuum, and the residue was purified by column chromatography (9:1 hexane-EtOAc as eluent) affording diprotected aminoacid (*R,S*)-**65** as a white solid (4.21 g, 18.4 mmol, 65 % yield).

METHOD B:

**Step 1: Methyl (1*R*,2*S*)-2-(benzyloxycarbonylamino)cyclobutane-1-carboxylate, 64**

A solution of (*R,S*)-**91** (2.54 g, 13.8 mmol) and benzyl alcohol (1.43 mL, 16.6 mmol, 1.2 eq) in toluene (50 mL) was heated to reflux for 18 hours. Toluene was removed under



## 10. Experimental Details

reduced pressure and then the excess of benzyl alcohol was eliminated by lyophilisation or by distillation under vacuum at 150 °C. The residue was chromatographed on silica gel (dichloromethane as eluent) to afford carbamate (*R,S*)-**64** as a dense oil (3.39 g, 12.8 mmol, 92 % yield).

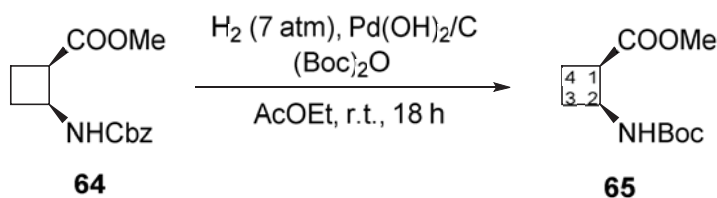
### Spectroscopic data for compound (*R,S*)-**64**:

<sup>1</sup>H NMR (250 MHz, CDCl<sub>3</sub>): δ 1.97 (c.a., 2H), 2.18-2.43 (c.a., 2H), 3.39 (m, 1H, H<sub>1</sub>), 3.66 (s, 3H, Me), 4.46 (m, 1H, H<sub>2</sub>), 5.08 (s, 2H, CH<sub>2</sub>-Ph), 5.64 (broad s., 1H, NH), 7.34 (m, 5H, H<sub>ar</sub>).

Spectroscopic data are consistent with those reported in reference:

Martín-Vilà, M.; Muray, E; P. Aguado, G.; Álvarez-Larena, A.; Branchadell, V.; Minguillón, C.; Giralt, E.; Ortuño, R. M. *Tetrahedron: Asymmetry*, **2000**, *11*, 3569.

### Step 2: Methyl (1*R*,2*S*)-2-(*tert*-butoxycarbonylamino)cyclobutane-1-carboxylate, **65**



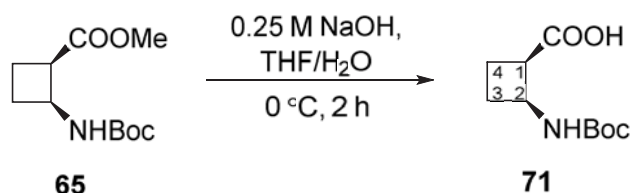
Carbamate (*R,S*)-**64** (3.04 g, 11.5 mmol) in ethyl acetate (15 mL) was hydrogenated under 7 atmospheres of pressure in the presence of 20 % Pd(OH)<sub>2</sub>/C (0.35 g) and Boc<sub>2</sub>O (3.2 mL, 13.9 mmol, 1.2 eq) overnight. The reaction mixture was filtered through Celite® and solvent was removed under vacuum and the residue was purified by column chromatography (dichloromethane as eluent) affording carbamate (*R,S*)-**65** as a white solid (2.17 g, 9.5 mmol, 82 % yield).

**Spectroscopic data for compound (R,S)-65:**

$^1\text{H NMR}$  (250 MHz,  $\text{CDCl}_3$ ):  $\delta$  1.38 (s, 9H, tBu), 1.87-1.97 (c.a., 2H), 2.25 (c.a., 2H), 3.35 (m, 1H, H<sub>1</sub>), 3.67 (s, 3H, Me), 4.41 (m, 1H, H<sub>2</sub>), 5.33 (br. s., 1H, NH).

Spectroscopic data are consistent with those reported in reference:

Izquierdo, S.; Rúa, F.; Sbai, A.; Parella, T.; Álvarez-Larena, A.; Branchadell, V.; Ortuño, R. *M. J. Org. Chem.*, **2005**, *70*, 7963.

**(1R,2S)-2-(tert-Butoxycarbonylamino)cyclobutane-1-carboxylic acid, 71**

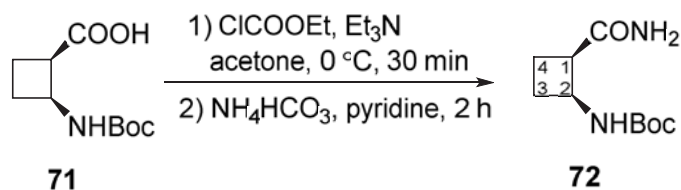
To an ice-cooled solution of ester (R,S)-**65** (790 mg, 3.4 mmol) in a 1:10 THF-water mixture (55 mL), 0.25 M sodium hydroxide aqueous solution (34 mL, 8.6 mmol, 2.5 eq) was added and the resultant mixture was stirred for 2 h. (Reaction progress was monitored by TLC). The reaction mixture was washed with dichloromethane (20 mL), and 5 % HCl aqueous solution was added to the aqueous phase to reach pH 2. The acid solution was extracted with ethyl acetate (4 x 50 mL) and dried over magnesium sulfate. Solvent was removed at reduced pressure to afford crude (R,S)-**71** as a white crystalline solid (720 mg, 3.34 mmol, 98 % yield) without need of further purification.

**Spectroscopic data for compound (R,S)-71:**

$^1\text{H NMR}$  (250 MHz,  $\text{CDCl}_3$ ):  $\delta$  1.45 (s, 9H, tBu), 1.70-2.35 (c.a., 4H, H<sub>3</sub>, H<sub>4</sub>), 3.36 (m, 1H, H<sub>1</sub>), 4.35 (m, 1H, H<sub>2</sub>), 5.57 (broad s, 1H, NH).

Spectroscopic data are consistent with those reported in reference:

Izquierdo, S.; Rúa, F.; Sbai, A.; Parella, T.; Álvarez-Larena, A.; Branchadell, V.; Ortuño, R. *M. J. Org. Chem.*, **2005**, *70*, 7963.

***tert*-Butyl (1*R*,2*S*)-2-carbamoylcyclobutanecarbamate, 72**

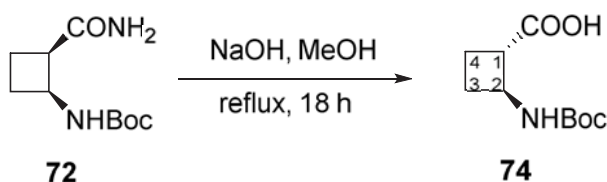
A mixture containing the free acid (*R,S*)-**71** (2.01 g, 9.34 mmol) in anhydrous acetone (50 mL), ethyl chloroformate (1.8 mL, 10.5 mmol) and triethylamine (0.19 mL, 1.4 mmol) was stirred at 0 °C and under a nitrogen atmosphere for 30 minutes. Then, ammonium bicarbonate (2.21 g, 28.01 mmol, 3.0 eq) and pyridine (1.9 mL, 23.34 mmol, 2.5 eq) were added and the mixture was stirred at room temperature for 2 h. EtOAc was added and the solution was washed with water (4 × 15 mL) and then dried under vacuum to give the desired product. Flash chromatography (3:2 EtOAc-hexane) provided the free amide (*R,S*)-**72** as a white powder (1.70 g, 7.94 mmol, 85 % yield).

**Spectroscopic data for compound (*S,R*)-**72**:**

<sup>1</sup>H NMR (250 MHz, CDCl<sub>3</sub>): δ 1.42 (s, 9H, *t*Bu), 1.83-2.41 (c.a., 4H), 3.49 (m, 1H, H<sub>1</sub>), 4.41 (m, 1H, H<sub>2</sub>), 5.33 (br. s., 2H, NH<sub>2</sub>), 5.53 (br. s., 1H, NH).

Spectroscopic data are consistent with those reported in reference:

Fernandes, C.; Pereira, E.; Faure, S.; Aitken, D. J., *J. Org. Chem.* **2009**, *74*, 3217.

**(1*S*,2*S*)-2-(*tert*-Butoxycarbonylamino)cyclobutane-1-carboxylic acid, 74**

A solution of (*R,S*)-**72** (140 mg, 0.65 mmol) in MeOH (15 mL) was treated with 6.25 M NaOH aqueous solution (5.2 mL) and the mixture was heated to reflux overnight. Methanol was then removed by careful evaporation under reduced pressure and the residual aqueous phase was washed with EtOAc (3 × 20 mL). The aqueous phase was then

cooled at 0 °C, while concentrated HCl was added slowly until pH 2. The aqueous phase was then extracted with EtOAc (3 × 60 mL) and the combined organic extracts were dried with MgSO<sub>4</sub> and concentrated under vacuum. After flash chromatography (EtOAc as eluent) the free acid (*S,S*)-**74** was obtained as a white powder (110 mg, 0.51 mmol, 78 % yield).

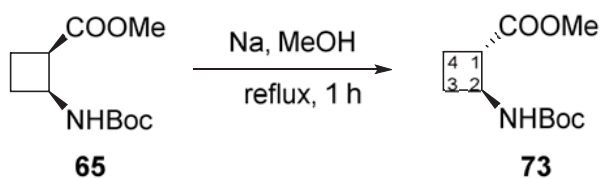
**Spectroscopic data and physical constants for compound (*S,S*)-**74**:**

<sup>1</sup>H NMR (250 MHz, CDCl<sub>3</sub>): δ 1.44 (s, 9H, *t*Bu), 1.88-2.22 (c.a., 4H, H<sub>3</sub>, H<sub>4</sub>), 3.10 (m, 1H, H<sub>1</sub>), 4.14 (m, 1H, H<sub>2</sub>), 6.28 (broad s, 1H, NH).

Spectroscopic data are consistent with those reported in reference:

Fernandes, C.; Pereira, E.; Faure, S.; Aitken, D. J. *J. Org. Chem.* **2009**, *74*, 3217.

**Methyl (1*S*,2*S*)-2-((*tert*-butoxycarbonyl)amino)cyclobutane-1-carboxylate, **73****



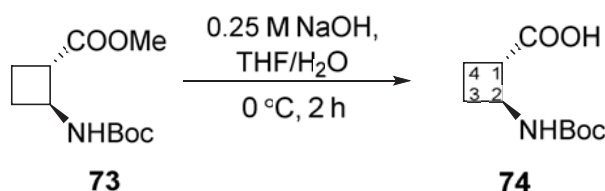
Na (190 mg, 8.26 mmol) was dissolved in anhydrous MeOH (85 mL) at room temperature under nitrogen. Compound **65** (420 mg, 1.83 mmol) was added to the resulting solution and the mixture was stirred at reflux for 1 h. After cooling in an ice bath, the reaction was quenched by addition of 1 M HCl (17 mL). Excess of MeOH was evaporated under reduced pressure and the aqueous layer was extracted with EtOAc (3 × 40 mL). The combined organic layers were dried (MgSO<sub>4</sub>), filtered and evaporated to give a white solid that was purified by chromatography (cyclohexane-EtOAc, 90:10) to afford starting material **65** recovered as a white powder (50 mg, 12 %) and **73** as a white powder (250 mg, 60 %).

**Spectroscopic data and physical constants for compound (S,S)-73:**

<sup>1</sup>H NMR (250 MHz, CDCl<sub>3</sub>): δ 1.43 (s, 9 H, tBu), 1.93 (m, 3H, H<sub>3-4</sub>), 2.25 (qd, J = 8,2 Hz, 1H, H<sub>3</sub>), 2.98 (m, 1 H, H<sub>1</sub>), 3.67 (s, 3H, CH<sub>3</sub>), 4.21 (m, 1 H, H<sub>2</sub>), 4.77 (br s, 1H, NH).

Spectroscopic data are consistent with those reported in reference:

Fernandes, C.; Gauzy, C. ; Yang, Y. ; Roy, O. ; Pereira, E.; Faure, S.; Aitken, D. J. *Synthesis* **2007**, *14*, 2222.

**(1S,2S)-2-(tert-Butoxycarbonylamino)cyclobutane-1-carboxylic acid, 74**

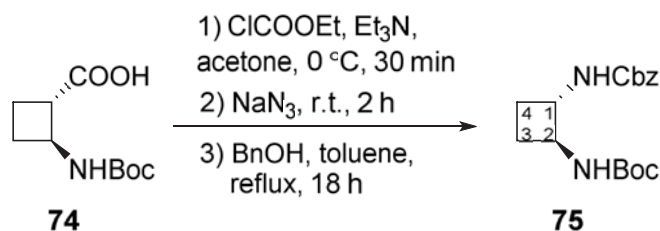
To an ice-cooled solution of ester (S,S)-**73** (790 mg, 3.4 mmol) in a 1:10 THF-water mixture (55 mL), 0.25 M sodium hydroxide aqueous solution (34 mL, 8.6 mmol, 2.5 eq) was added and the resultant mixture was stirred for 2 h. (Reaction progress was monitored by TLC). The reaction mixture was washed with dichloromethane (20 mL), and 5 % HCl aqueous solution was added to the aqueous phase to reach pH 2. The acid solution was extracted with ethyl acetate (4 x 50 mL) and dried over MgSO<sub>4</sub>. Solvent was removed at reduced pressure to afford crude (S,S)-**74** as a white crystalline solid (720 mg, 3.34 mmol, 98 % yield) without need of further purification.

**Spectroscopic data and physical constants for compound (S,S)-74:**

<sup>1</sup>H NMR (250 MHz, CDCl<sub>3</sub>): δ 1.44 (s, 9H, tBu), 1.88-2.22 (c.a., 4H, H<sub>3</sub>, H<sub>4</sub>), 3.10 (m, 1H, H<sub>1</sub>), 4.14 (m, 1H, H<sub>2</sub>), 6.28 (broad s, 1H, NH).

Spectroscopic data are consistent with those reported in reference:

Fernandes, C.; Pereira, E.; Faure, S.; Aitken, D. J. *J. Org. Chem.* **2009**, *74*, 3217.

**Benzyl *tert*-butyl ((1*S*,2*S*)-cyclobutane-1,2-diyl)dicarbamate, 75**

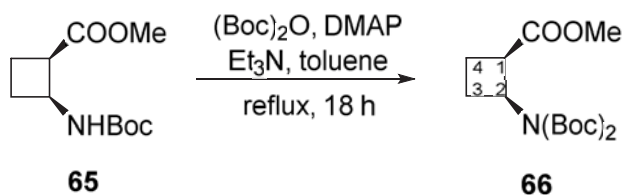
Carboxylic acid (*S,S*)-**74** (400 mg, 1.9 mmol) was dissolved in anhydrous acetone (40 mL). Then, ethyl chloroformate (0.2 mL, 2.1 mmol) and triethylamine (0.26 mL, 1.9 mmol) were added. The system was stirred at 0 °C under nitrogen atmosphere for 30 minutes. Then, NaN<sub>3</sub> (0.19 g, 1.6 eq, 3.0 mmol) dissolved in water (5 mL) was added. The system was stirred at room temperature for 2 hours. After that, water (15 mL) was added and extractions with CH<sub>2</sub>Cl<sub>2</sub> were done (3 x 30 mL). The organic layer was dried with anhydrous MgSO<sub>4</sub> and the solvent was evaporated. 0.36 g (1.5 mmol, 80 % yield) of the acyl azide were obtained as a yellow oil which was used directly in the following step. Acyl azide (0.36 g, 1.5 mmol) was dissolved in anhydrous toluene (80 mL). Then, 0.4 mL (3.9 mmol) of benzyl alcohol were added. The mixture was refluxed for 18 hours. After that, the solvent was evaporated under vacuum and the excess of benzyl alcohol was lyophilised. The reaction crude was purified by column chromatography using silica gel (EtOAc-hexane; 1:3) to obtain (*S,S*)-**75** (410 mg, 1.3 mmol, 70 % yield) as a yellow oil. **WARNING:** Acyl azide intermediate should be carefully manipulated because of its explosive nature.

**Spectroscopic data and physical constants for compound (*S,S*)-75:**

<sup>1</sup>H NMR (CDCl<sub>3</sub>, 250 MHz): δ 1.45 (s, 9H, *t*Bu), 1.50 (c.a., 2H), 2.16 (c.a., 2H), 3.88 (m, 2H, H<sub>1</sub>, H<sub>2</sub>), 4.93 (broad s., 1H, NH), 5.10 (s, 2H, CH<sub>2</sub>-Ph), 5.83 (broad s., 1H, NH), 7.37 (m, 5H, H<sub>ar</sub>).

Spectroscopic data are consistent with those reported in reference:

Sans, M., Illa, O., Ortuño, R. M. *Org. Letters* **2012**, *14*, 10, 2431-2433.

**Methyl 2-bis(*tert*-butoxycarbonylamino)-(1*R*,2*S*)-cyclobutan-1-carboxylate, 66**

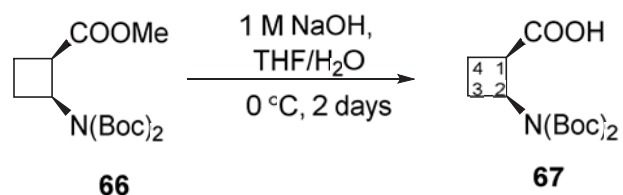
Carbamate (*R,S*)-**65** (600 mg, 1.58 mmol) was dissolved in anhydrous toluene (60 mL) under a nitrogen atmosphere. Then, DMAP (110 mg, 0.9 mmol) and triethylamine (0.5 mL, 3.6 mmol) were added. Then, di-*tert*butyl dicarbonate (0.8 g, 3.67 mmol) was added. The mixture was refluxed for 18 hours. After that, the solvent was evaporated under vacuum and the crude was purified by column chromatography on silica gel using a mixture of hexane-ethyl acetate 4:1 to afford pure (*R,S*)-**66** (260 mg, 0.8 mmol, 50 % yield) as a colorless oil.

**Spectroscopic data and physical constants for compound (*R,S*)-66:**

<sup>1</sup>H NMR (CDCl<sub>3</sub>, 250 MHz): δ 1.44 (s, 18H, *t*Bu), 1.87 (m, 1H), 2.21 (m, 2H), 2.57 (m, 1H), 3.35 (m, 1H, H<sub>1</sub>), 3.61 (s, 3H, Me), 4.56 (q, *J*=12.5 Hz, 1H, H<sub>2</sub>).

Spectroscopic data are consistent with those reported in reference:

Sans, M., Illa, O., Ortuño, R. M. *Org. Letters* **2012**, *14*, 10, 2431-2433.

**(1*R*,2*S*)-2-bis(*tert*-Butoxycarbonylamino)cyclobutane-1-carboxylic acid, 67**

Methyl ester (*R,S*)-**66** (200 mg, 0.61 mmol) was dissolved in a 1:10 THF-water mixture (20 mL). Then, 1 M NaOH (6.1 mL, 10 mmol) was added. The mixture was stirred at 0 °C for 2 days. After that, the solution was acidified to pH 2 with 2 M HCl. Then, the mixture was extracted with CH<sub>2</sub>Cl<sub>2</sub> (3 x 15 mL). The organic layers were combined and dried with anhydrous MgSO<sub>4</sub>. The solvent was evaporated and (*R,S*)-**67** (190 mg, 0.61 mmol, quantitative yield) was obtained as a white solid.

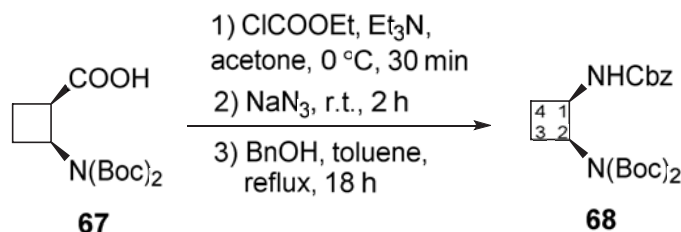
**Spectroscopic data and physical constants for compound (R,S)-67:**

$^1\text{H NMR}$  ( $\text{CDCl}_3$ , 250 MHz):  $\delta$  1.46 (s, 18H, *t*Bu), 1.97 (m, 1H), 2.21 (c.a., 1H), 2.31(c.a., 1H), 2.62 (m, 1H), 3.42 (m, 1H,  $\text{H}_1$ ), 4.58 (q,  $J=14$  Hz, 1H,  $\text{H}_2$ ).

Spectroscopic data are consistent with those reported in reference:

Sans, M., Illa, O., Ortuño, R. M. *Org. Letters* **2012**, *14*, 10, 2431-2433.

***tert*-Butyl ((1*R*,2*S*)-2-(benzyloxycarbonylamino)cyclobutane)(*tert*-butoxy-carbonyl)carbamate, 68**



Carboxylic acid (*R,S*)-**67** (160 mg, 0.5 mmol) was dissolved in anhydrous acetone (20 mL). Then, ethyl chloroformate (0.05 mL, 0.55 mmol) and triethylamine (0.07 mL, 0.50 mmol) were added. The system was stirred at  $0\text{ }^\circ\text{C}$  under a nitrogen atmosphere for 30 minutes. Then, of  $\text{NaN}_3$  (0.05 g, 1.6 eq, 0.79 mmol) dissolved in water (5 mL) was added. The system was stirred at room temperature for 2 hours. After that, water (10 mL) was added and extractions with  $\text{CH}_2\text{Cl}_2$  were done (3 x 15 mL). The organic layer was dried with anhydrous  $\text{MgSO}_4$  and the solvent was evaporated. The corresponding acyl azide (100 mg, 0.4 mmol, 80 % yield) was obtained as a yellow oil and it was used directly in the following step. **WARNING:** This product should be carefully manipulated because of its explosive nature.

Acyl azide (100 mg, 0.4 mmol) was dissolved in anhydrous toluene (50 mL). Then, benzyl alcohol (0.1 mL, 1.03 mmol) was added. The mixture was refluxed for 18 hours. After that, the solvent was evaporated under vacuum and the excess of benzyl alcohol was lyophilised. The reaction crude was purified by column chromatography using silica gel



## 10. Experimental Details

(Ethyl acetate-hexane; 1:2) to afford (*R,S*)-**68** (100 mg, 0.24 mmol, 60 % yield) as a yellowish oil.

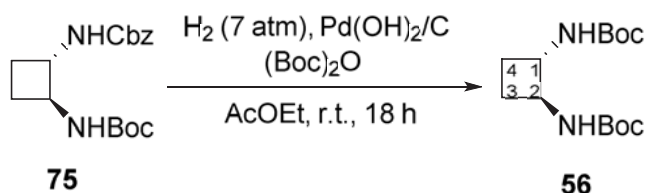
### Spectroscopic data and physical constants for compound (*R,S*)-**68**:

$^1\text{H NMR}$  ( $\text{CDCl}_3$ , 250 MHz):  $\delta$  1.48 (s, 18H, *t*Bu), 1.96 (c.a., 1H), 2.24 (c.a., 3H), 4.47 (c.a., 1H,  $\text{H}_2$ ), 4.75 (c.a., 1H,  $\text{H}_1$ ), 5.08 (broad s., 2H,  $\text{CH}_2$ -Ph), 6.12 (broad s., 1H, NH), 7.34 (m, 5H,  $\text{H}_{\text{ar}}$ ).

Spectroscopic data are consistent with those reported in reference:

Sans, M., Illa, O., Ortuño, R. M. *Org. Letters* **2012**, *14*, 10, 2431-2433.

### *tert*-Butyl (1*S*,2*S*)-cyclobutane-1,2-diylidicarbamate, **56**



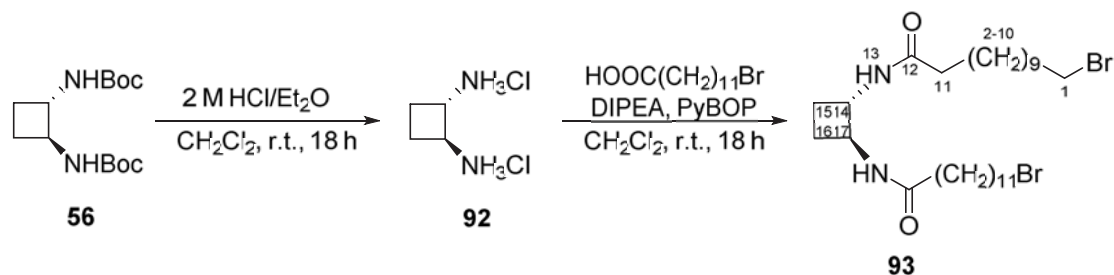
Diamine (*S,S*)-**75** (170 mg, 0.53 mmol) in ethyl acetate (15 mL) was hydrogenated under 7 atmospheres of pressure in the presence of 30 %  $\text{Pd}(\text{OH})_2/\text{C}$  (6 mg) and  $\text{Boc}_2\text{O}$  (0.12 mL, 0.55 mmol, 1.2 eq) overnight. The reaction mixture was filtered through Celite<sup>®</sup> and solvent was removed under vacuum and the residue was purified by column chromatography (1:2 ethyl acetate-hexane as eluent) affording the desired diamine (*S,S*)-**56** as a white solid (100 mg, 0.35 mmol, 65 % of yield).

### Spectroscopic data and physical constants for compound (*S,S*)-**56**:

$^1\text{H NMR}$  (250 MHz,  $\text{CDCl}_3$ ):  $\delta$  1.45 (c.a., 18 H, *t*Bu), 2.04-2.23 (c.a., 2H,  $\text{H}_3$ ,  $\text{H}_4$ ), 3.83 (broad s, 2H,  $\text{H}_1$ ,  $\text{H}_2$ ), 5.05 (broad s, 2H, NH).

Spectroscopic data are consistent with those reported in reference:

Sans, M., Illa, O., Ortuño, R. M. *Org. Letters* **2012**, *14*, 10, 2431-2433.

**C<sub>12</sub>-NH-Centered-bromoalkyl, 93**

Diamine (*S,S*)-**56** (100 mg, 0.4 mmol) was dissolved in CH<sub>2</sub>Cl<sub>2</sub> (5 mL). Then, a 2 M HCl solution in diethyl ether (4 mL, 8 mmol) was added. The reaction was stirred at room temperature overnight. After that, the solvent was evaporated under vacuum. 65 mg (0.40 mmol, quantitative yield) of an intermediate diamine in the form of a chloride salt were obtained as a brown oil. This compound was used in next step without further purification. Diamine (*S,S*)-**92** (50 mg, 0.31 mmol) was dissolved in anhydrous dichloromethane (12 mL) and bromododecanoic acid (150 mg, 0.54 mmol), DIPEA (0.4 mL, 2.30 mmol) and PyBOP (409 mg, 7.86 mmol) were subsequently added. The mixture was stirred at room temperature under nitrogen atmosphere overnight. Afterwards, the mixture was washed with sodium bicarbonate and the organic phase was dried over magnesium sulfate. Solvent was removed and the residue was chromatographed on silica gel using EtOAc as eluent. Bromo derivative (*S,S*)-**93** (165 mg, 0.27 mmol, 68 % yield) was obtained as a white solid that can be crystallised in dichloromethane.

**Spectroscopic data and physical constants for compound (*S,S*)-93:**

$[\alpha]_D^{20}$ : -15 (*c* 1, MeOH)

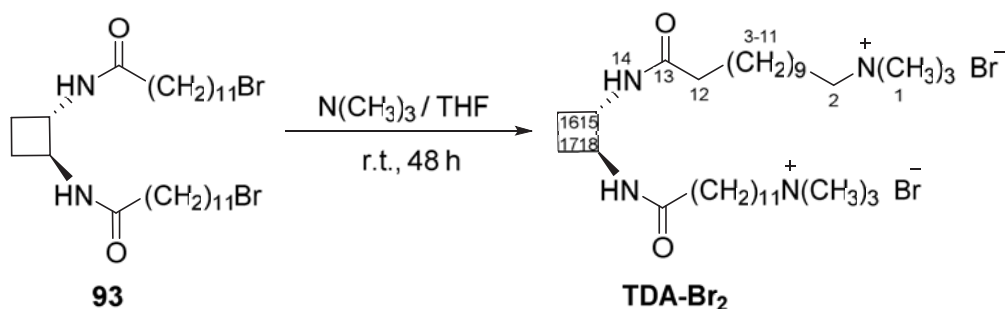
**M. p.:** 180-184 °C (CH<sub>2</sub>Cl<sub>2</sub>)

**IR (ATR):**  $\nu$  3296, 2919, 2851, 1641, 1542 cm<sup>-1</sup>

**<sup>1</sup>H NMR** (250 MHz, CDCl<sub>3</sub>):  $\delta$  1.30 (broad s., CH<sub>2</sub>, 14H, H<sub>2-10</sub>), 1.39-1.48 (c.a., 2H), 1.54-1.68 (c. a., 2H), 1.73-1.92 (c.a., 2H), 2.10-2.32 (c.a., 2H, H<sub>11</sub>), 3.45 (t, *J*=7.39 MHz, 2H<sub>1</sub>), 4.04 (broad s., 1H, H<sub>14</sub>), 6.08 (broad s., 2H, NH<sub>13</sub>).

**<sup>13</sup>C NMR** (62.5 MHz, CDCl<sub>3</sub>):  $\delta$  23.8, 25.6, 28.2, 28.8, 29.2, 29.3, 29.4, 29.5 (CH<sub>2</sub>), 32.8 (C<sub>2</sub>), 34.1 (C<sub>1</sub>), 36.9 (C<sub>6</sub>), 52.1 (C<sub>14</sub>), 173.4 (C<sub>12</sub>).

**MS** calculated for [M + Na]<sup>+</sup>: 631.27. Found: 631.23.

**Bolaamphiphile TDA**

A solution of (*S,S*)-**93** (30 mg, 0.05 mmol) in anhydrous THF (3 mL) was saturated with trimethylamine and the reaction was stirred at room temperature for 48 hours. Then, the solvent was evaporated under vacuo to afford **TDA-Br<sub>2</sub>** (25 mg, 0.03 mmol, 60 % yield) as a white solid that can be crystallised in a mixture of MeOH-diethyl ether.

**Spectroscopic data and physical constants for compound TDA-Br<sub>2</sub>:**

$[\alpha]_D^{20}$ : -20.7 (*c* 1.3, MeOH)

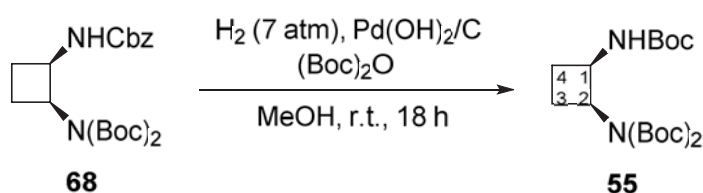
**M. p.:** 115-117 °C (MeOH)

**IR** (ATR):  $\nu$  3296, 2919, 2851, 1641, 1542  $\text{cm}^{-1}$

**<sup>1</sup>H NMR** (360 MHz, MeOD-*d*<sub>4</sub>):  $\delta$  1.32 (broad s., CH<sub>2</sub>, 18H), 1.52-1.87 (c.a., 2H), 2.05-2.20 (c.a., 2H), 3.14 (broad s., 9H, H<sub>1</sub>), 3.32 (c.a., 2H, H<sub>12</sub>), 4.20 (broad s, 2H, H<sub>15</sub>, NH<sub>4</sub>).

**<sup>13</sup>C NMR** (90 MHz, MeOD-*d*<sub>4</sub>):  $\delta$  22.5, 22.6, 25.6, 25.9, 28.8, 28.8, 29.0, 29.1, 29.2 (C<sub>3</sub>-C<sub>11</sub>), 35.7 (C<sub>12</sub>), 51.1 (C<sub>2</sub>), 52.1 (C<sub>1</sub>), 66.5 (C<sub>15</sub>), 174.2 (C<sub>13</sub>).

**HRMS** Calculated for [M - Br]<sup>+</sup>: 645.4677. Found: 645.4673.

***tert*-Butyl(*tert*-butoxycarbonyl)((*1R,2S*)-2-(*tert*-butoxycarbonylamino)cyclobutane) carbamate, **55****

Diamine (*R,S*)-**68** (200 mg, 0.48 mmol) was dissolved in the minimum amount of methanol. Then, di-*tert*-butyl dicarbonate (200 mg, 0.92 mmol) and Pd(OH)<sub>2</sub>/C (100 mg, 50 % weight) were added. The mixture was hydrogenated under 7 atm of pressure during 12 h. Then, the crude was filtered through Celite™ and washed with methanol. The solvent was evaporated under vacuum. The crude was purified by column chromatography with silica gel (hexane-ethyl acetate; 9:1) to afford (*R,S*)-**55** (100 mg, 0.26 mmol, 54 % of yield) as white solid.

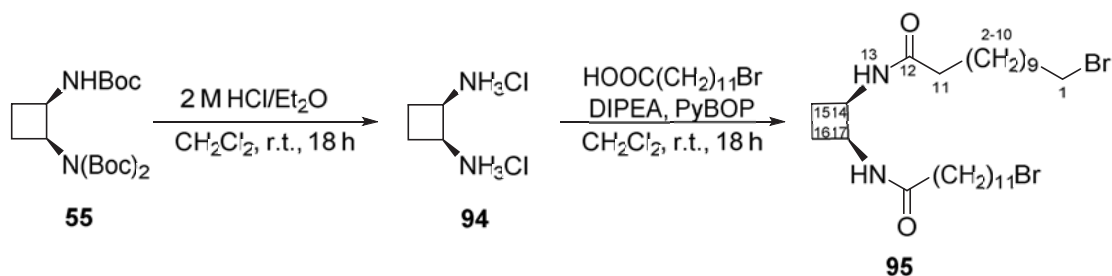
**Spectroscopic data and physical constants for compound (*R,S*)-55:**

<sup>1</sup>H NMR (360 MHz, CDCl<sub>3</sub>): δ 1.43 (s., 9H, *t*Bu), 1.51 (s., 18H, 2*t*Bu), 1.86-2.00 (c.a., 1H), 2.12-2.40 (c.a., 3H), 4.40 (broad s., 1H, H<sub>2</sub>), 4.71 (q, *J*=12.6 Hz, 1H, H<sub>1</sub>), 5.71 (broad s., 1H, NH).

Spectroscopic data are consistent with those reported in reference:

Sans, M., Illa, O., Ortuño, R. M. *Tetrahedron* **2016**, 72, 2913-2919.

**((14*R*,17*S*)-Cyclobutane-14,1-diyl)bis(1,1'-bromododecanamide), 95**



(*R,S*)-**55** (90 mg, 0.23 mmol) was dissolved in CH<sub>2</sub>Cl<sub>2</sub> (5 mL). Then, a 2 M HCl solution in diethyl ether (3 mL, 8 mmol) was added. The reaction was stirred at room temperature overnight. After that, the solvent was evaporated under vacuum. (*R,S*)-**94** (35 mg, 0.23 mmol, quantitative yield) was obtained as a white solid. This compound was used in next step without further purification. Diamine (*R,S*)-**94** (20 mg, 0.13 mmol) was dissolved in anhydrous CH<sub>2</sub>Cl<sub>2</sub> (10 mL). Then, bromododecanoic acid (100 mg, 0.36 mmol), DIPEA (0.4 mL, 2.30 mmol) and PyBOP (120 mg, 0.31 mmol) were subsequently added. The mixture was stirred at room temperature under nitrogen atmosphere overnight. Afterwards, the mixture was washed with sodium bicarbonate and the organic phase was dried over

## 10. Experimental Details

magnesium sulfate. Solvent was removed, and the residue was chromatographed on silica gel (EtOAc) to achieve compound (*R,S*)-**95** (60 mg, 0.095 mmol, 73 % yield) as a white solid.

### Spectroscopic data and physical constants for compound (*R,S*)-**95**:

**M. p.:** 94-95 °C (MeOH)

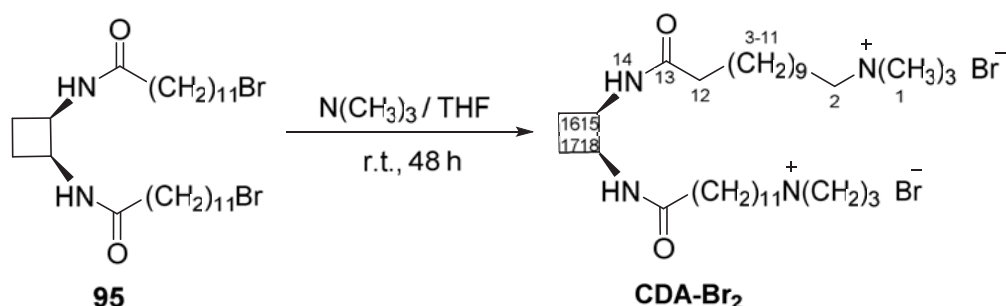
**IR (ATR):**  $\nu$  3290, 2918, 2850, 1641, 1546  $\text{cm}^{-1}$

**$^1\text{H}$  NMR** (250 MHz,  $\text{CDCl}_3$ ):  $\delta$  1.30 (broad s., 14H), 1.38-1.51 (c.a., 2H), 1.58-1.70 (c.a., 2H), 1.80-1.98 (c.a., 2H), 2.15-2.24 (c.a., 2H,  $\text{H}_{11}$ ), 3.43 (t,  $J=7.5$  Hz, 2H,  $\text{H}_1$ ), 4.38 (broad s., 1H,  $\text{H}_{14}$ ), 6.28 (broad s., 1H,  $\text{NH}$ ).

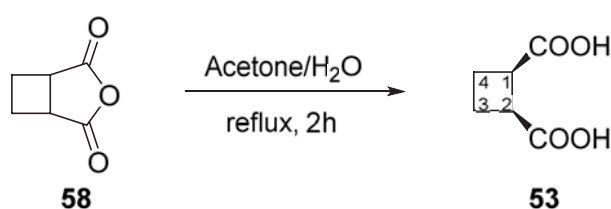
**$^{13}\text{C}$  NMR** (62.5 MHz,  $\text{CDCl}_3$ ):  $\delta$  25.8 ( $\text{C}_{16}$ ), 26.2, 28.6, 29.2, 29.7, 29.8, 29.8, 29.9, 29.9 ( $\text{C}_{10}\text{-C}_3$ ), 33.2 ( $\text{C}_2$ ), 34.5 ( $\text{C}_1$ ), 37.2 ( $\text{C}_{11}$ ), 50.1 ( $\text{C}_{14}$ ), 174.8 ( $\text{C}_{12}$ ).

**HRMS** Calculated for  $[\text{M} + \text{Na}]^+$ : 631.2269. Found: 631.2268.

### Bolaamphiphile **CDA-Br<sub>2</sub>**



Amide (*R,S*)-**95** (80 mg, 0.13 mmol) was dissolved in anhydrous THF (5 mL). Then, the solution was saturated with trimethylamine and the reaction was stirred at room temperature for 48 hours. Surfactant **CDA-Br<sub>2</sub>** (65 mg, 0.09 mmol, 70 % yield) was obtained as a white solid, which can be crystallised in methanol.

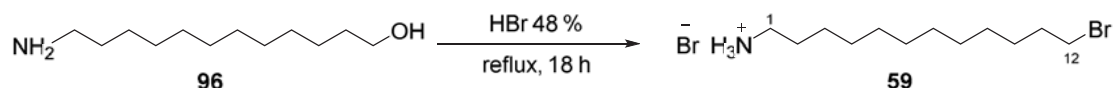
**Spectroscopic data and physical constants for compound CDA-Br<sub>2</sub>:****M. p.:** 104–105 °C (MeOH)**IR (ATR):**  $\nu$  3295, 2917, 2850, 1648, 1537 cm<sup>-1</sup>**<sup>1</sup>H NMR** (250 MHz, MeOD-*d*<sub>4</sub>):  $\delta$  1.35 (broad s., 16H), 1.58-1.72 (c.a., 2H), 1.94-2.06 (c.a., 2H), 2.16-2.34 (c.a., 2H, H<sub>12</sub>), 3.15 (s, 9H, H<sub>1</sub>), 3.40 (c.a., 2H, H<sub>2</sub>), 4.52 (broad s., 1H, H<sub>14</sub>).**<sup>13</sup>C NMR** (62.5 MHz, MeOD-*d*<sub>4</sub>):  $\delta$  21.1 (C<sub>15</sub>), 22.7, 24.1, 24.4, 27.2, 27.4, 27.6 (C<sub>4</sub>-C<sub>10</sub>), 34.1 (C<sub>3</sub>), 49.8 (C<sub>11</sub>), 51.1 (C<sub>14</sub>), 65.4 (C<sub>2</sub>), 173.1 (C<sub>12</sub>).**HRMS** Calculated for [M – Br]<sup>+</sup>: 645.4677. Found: 645.4680.**(1*R*,2*S*)-Cyclobutane-1,2-dicarboxylic acid, 53**

A solution of cycloadduct **58** (3.9 g, 31 mmol) and H<sub>2</sub>O (6 mL, 10 eq) in acetone (100 mL) was refluxed for 2 h. After that, acetone was evaporated under reduced pressure and the residual water was lyophilised to give 4.6 g of (*R,S*)-**53** (quantitative yield) as a white solid.

**Spectroscopic data for compound (*R,S*)-53:****<sup>1</sup>H NMR** (360 MHz, MeOD-*d*<sub>4</sub>):  $\delta$  2.08 (s., 2H, H<sub>3</sub>, H<sub>4</sub>), 3.45 (s., 2H, H<sub>1</sub>, H<sub>2</sub>).**<sup>13</sup>C NMR** (90 MHz, MeOD-*d*<sub>4</sub>):  $\delta$  20.9 (C<sub>1</sub>, C<sub>2</sub>), 40.21 (C<sub>3</sub>, C<sub>4</sub>), 158.31 (CO).

## 10. Experimental Details

### 12-Bromododecan-1-aminium bromide, **59**

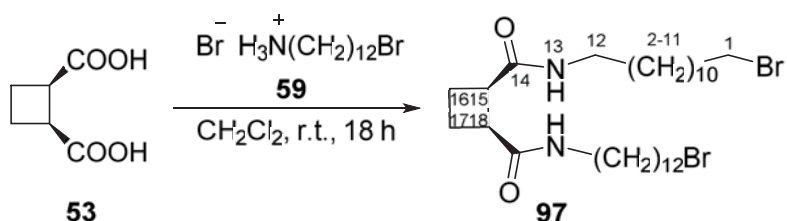


A solution of 12-aminododecanol **96** (200 mg, 1.0 mmol) was dissolved in aqueous HBr 48% (2 mL) and the solution refluxed overnight. Then, this solution was evaporated and the orange solid residue was dissolved in water (5 mL) and extracted with CH<sub>2</sub>Cl<sub>2</sub> (4 x 15 mL). The combined organic extracts were washed with brine dried over MgSO<sub>4</sub> and rotary evaporated to give **59** (300 mg, 94 % yield) as a white crystalline solid.

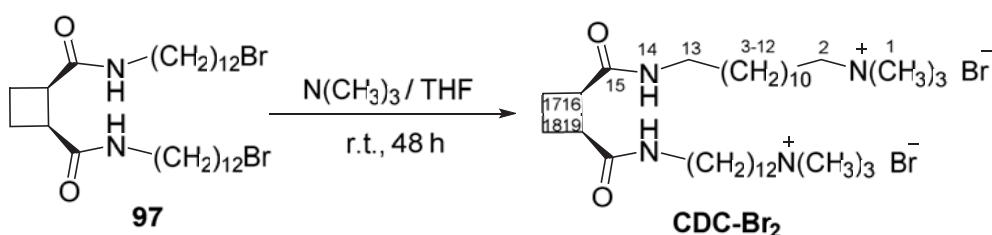
#### Spectroscopic data for compound **59**:

<sup>1</sup>H NMR (250 MHz, CDCl<sub>3</sub>):  $\delta$  1.15-1.54 (m, 16H, H<sub>3</sub>, H<sub>10</sub>, 1.71-1.94 (m, 4H, H<sub>11</sub>, H<sub>2</sub>), 3.02 (broad s, s, 2H, H<sub>1</sub>), 3.43 (t, 2H, H<sub>12</sub>), 8.19 (broad s, 3H, NH<sub>3</sub><sup>+</sup>).

### (15*R*,18*S*)-*N*<sup>1</sup>,*N*<sup>2</sup>-Bis(1-bromododecyl)cyclobutane-15,18-dicarboxamide, **97**



To a stirred solution of (*R,S*)-**53** (100 mg, 0.69 mmol) in a mixture of dry CH<sub>2</sub>Cl<sub>2</sub> (10 mL) and DMF (0.7 mL), DIPEA (0.9 mL, 5.32 mmol) and FDPP (0.583 mg, 1.52 mmol) were added. After 10 minutes 12-bromododecan-1-aminium bromide **59** (595 mg, 1.73 mmol, 2.5 eq) was added as a solid and the mixture was left under stirring overnight. After that, more CH<sub>2</sub>Cl<sub>2</sub> was added and the organic phase was washed with NaHCO<sub>3</sub> and brine, dried on MgSO<sub>4</sub> and concentrated to give a yellow solid. Purification by flash chromatography (EtOAc/MeOH; from 10:0 to 9:1) afforded (*R,S*)-**97** (340 mg, 0.53 mmol, 76 % yield) as a pale yellow solid that can be crystallised with CH<sub>3</sub>CN.

**Spectroscopic data and physical constants for compound (R,S)-97:****M. p.:** 75-76 °C (CH<sub>3</sub>CN)**IR (ATR):**  $\nu$  3297, 2915, 2848, 1649, 1547 cm<sup>-1</sup>**<sup>1</sup>H NMR** (360 MHz, CDCl<sub>3</sub>):  $\delta$  1.27 (broad s., 28H), 1.37-1.52 (c.a., 8H), 1.86 (c.a., 4H, H<sub>1</sub>, H<sub>2</sub>), 2.15 (c.a., 2H), 2.34 (c.a., 2H), 3.21 (c.a., 4H, H<sub>12</sub>), 3.32 (broad s., 2H, H<sub>15</sub>, H<sub>18</sub>), 3.42 (c.a., 4H, H<sub>1</sub>), 6.11 (broad s., 2H, NH)**<sup>13</sup>C NMR** (90 MHz, CDCl<sub>3</sub>):  $\delta$  22.4 (C<sub>16</sub>), 26.9, 28.1, 28.8, 29.3, 29.5, 32.8, 34.1 (C<sub>1</sub>), 39.7 (C<sub>12</sub>), 43.2 (C<sub>15</sub>) 172.5 (CO).**HRMS** Calculated for [M + Na]<sup>+</sup>: 659.2583. Found: 659.2596.**Bolaamphiphile CDC-Br<sub>2</sub>**

Compound (R,S)-**97** (220 mg, 0.337 mmol) was dissolved in 4 mL of THF. Then 15 mL of DMF were added (the solid is insoluble in pure DMF) and the solution was bubbled 10 min with gaseous trimethylamine. The mixture was left one week under stirring, afterwards it was freeze dried to give a glass like solid, which was dissolved in the minimum amount of MeOH and reprecipitated from Et<sub>2</sub>O, affording surfactant **CDC-Br<sub>2</sub>** as a white solid (190 mg, 85 % yield).

**Spectroscopic data and physical constants for compound CDC-Br<sub>2</sub>:****M. p.:** 168-170 °C (MeOH)**IR (ATR):** 3292, 2920, 2851, 1649, 1545, 1466, 1358, 1246, 965, 910 cm<sup>-1</sup>**<sup>1</sup>H NMR** (360 MHz, MeOD):  $\delta$  1.28 (broad s., 28H), 1.76-1.90 (c.a., 3H), 2.10-2.20 (c.a., 2H), 2.29-2.37 (c.a., 2H), 3.17 (broad s., 18H, H<sub>1</sub>), 3.31-3.42 (a.c., 4H).

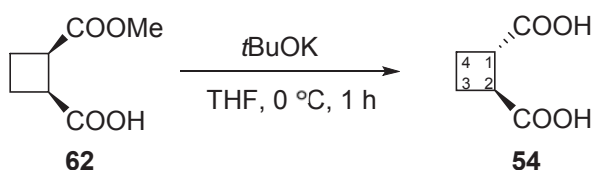


## 10. Experimental Details

**<sup>13</sup>C NMR** (90 MHz, MeOD):  $\delta$  21.8, 23.0, 26.4, 27.1, 29.2, 29.5, 29.5, 29.6, 29.6, 29.7, 39.5, 42.6 (C<sub>13</sub>), 52.6 (C<sub>1</sub>), 66.9 (C<sub>2</sub>), 174.3 (CO).

**HRMS** Calculated for [M – Br]<sup>+</sup>: 675.4972. Found: 675.4963.

### (1*S*,2*S*)-Cyclobutane-1,2-dicarboxylic acid, **54**

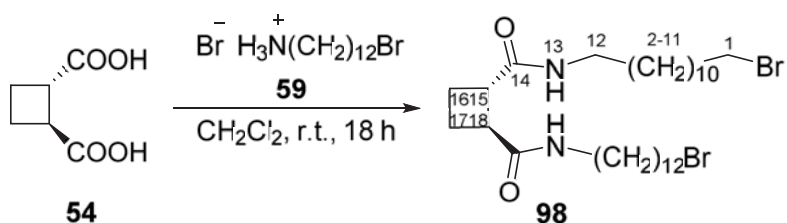


To a stirred solution of *t*-BuOK (850 mg, 7.5 mmol) in 25 mL of THF at 0 °C, hemiester (*R,S*)-**62** (0.596 g, 3.77 mmol) dissolved in 5 mL THF was added. The solution was stirred 1 h at 0 °C after that it was acidified by HCl 1M and more water was added to dissolve the formed salts. The resultant pale yellow solution was dried to give a yellowish solid. The solid was dissolved in water and the resultant solution extracted with EtOAc (x 4). The organic phase was dried on MgSO<sub>4</sub> and concentrated to give (*S,S*)-**54** as a white solid (440 mg, 81 % yield).

#### Spectroscopic data for compound (*S,S*)-**54**:

**<sup>1</sup>H NMR** (250 MHz, CDCl<sub>3</sub>):  $\delta$  2.11 (broad s., 4H, H<sub>3-4</sub>), 3.40 (m., 2H, H<sub>1-2</sub>).

### (1*S*,18*S*)-*N*<sup>1</sup>,*N*<sup>2</sup>-Bis(1-bromododecyl)cyclobutane-15,18-dicarboxamide, **98**



To a stirred solution of enantiopure (*S,S*)-**54** (100 mg, 0.69 mmol) in dry CH<sub>2</sub>Cl<sub>2</sub> (12 mL), DIPEA (0.72 mL, 5.32 mmol) and FDPP (580 mg, 1.5 mmol) were added. After 10 min

the ammonium salt **59** (595 mg, 1.73 mmol, 2.5 eq) was added as a solid and the mixture left stirring overnight. After that, more CH<sub>2</sub>Cl<sub>2</sub> was added and the organic phase was washed with NaHCO<sub>3</sub>, brine, dried on MgSO<sub>4</sub> and concentrated to give a yellow solid. Purification by flash chromatography using CH<sub>2</sub>Cl<sub>2</sub>/MeOH as eluent (gradient from 10:0 to 9:1), followed by crystallization from EtOAc, afforded (*S,S*)-**98** (400 mg, 89 % yield) as a white solid.

#### Spectroscopic data and physical constants for compound (*S,S*)-**98**:

$[\alpha]_D^{20}$ : +1.6 (c 0.66, CH<sub>2</sub>Cl<sub>2</sub>)

**M. p.**: 79-80 °C (CH<sub>2</sub>Cl<sub>2</sub>)

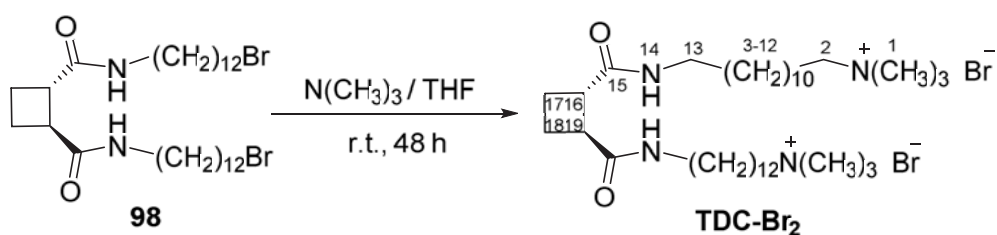
**IR** (ATR):  $\nu$  3286, 2917, 2849, 1626, 1541, 1468, 1346, 1251, 1229, 1188, 994 cm<sup>-1</sup>

**<sup>1</sup>H NMR** (360 MHz, CDCl<sub>3</sub>):  $\delta$  1.26 (broad s., 17H), 1.37-1.44 (c.a., 4H), 1.84-1.94 (c.a., 2H), 2.06-2.14 (c.a., 2H), 3.07-3.15 (c.a., 1H), 3.27-3.40 (c.a., 2H), 6.44 (broad s., 1H).

**<sup>13</sup>C NMR** (90 MHz, CDCl<sub>3</sub>):  $\delta$  20.5, 26.9, 28.2, 28.8, 29.2, 29.5, 29.6, 32.9, 34.1 (C<sub>1</sub>), 39.5 (C<sub>12</sub>), 43.2 (C<sub>15</sub>), 174.0 (CO).

**HRMS**: Calculated for [M + Na]<sup>+</sup>: 659.2583. Found: 659.2598.

#### Bolaamphiphile TDC-Br<sub>2</sub>



Compound (*S,S*)-**98** (100 mg, 0.337 mmol) was dissolved in 2 ml of THF (2 mL) and then DMF (8 mL) was added. The solution was bubbled 10 min with gaseous trimethylamine and left under stirring three days. Afterwards, it was freeze dried to give a solid, which was crystallised from MeOH/Et<sub>2</sub>O affording bolaamphiphile **TDC-Br<sub>2</sub>** (82 mg, 83 % yield).

**Spectroscopic data and physical constants for compound TDC-Br<sub>2</sub>:**

$[\alpha]_D^{20}$ : +47.9 (c 0.93, MeOH)

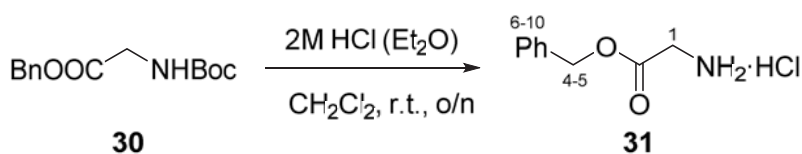
**M. p.:** 84-85 °C (MeOH)

**IR** (ATR):  $\nu$  3290, 2919, 2850, 1632, 1545, 1466, 1349, 1253, 964, 910  $\text{cm}^{-1}$

**<sup>1</sup>H NMR** (360 MHz, MeOD):  $\delta$  1.28 (broad s., 28H), 1.76-1.90 (c.a., 3H), 2.10-2.20 (c.a., 2H), 2.29-2.37 (c.a., 2H), 3.17 (broad s., 18H, H<sub>1</sub>), 3.31-3.42 (a.c., 4H).

**<sup>13</sup>C NMR** (90 MHz, MeOD):  $\delta$  21.8, 23.0, 26.4, 27.1, 29.2, 29.5, 29.5, 29.6, 29.6, 29.7, 39.5, 42.6 (C<sub>13</sub>), 52.6 (C<sub>1</sub>), 66.9 (C<sub>2</sub>), 174.3 (CO).

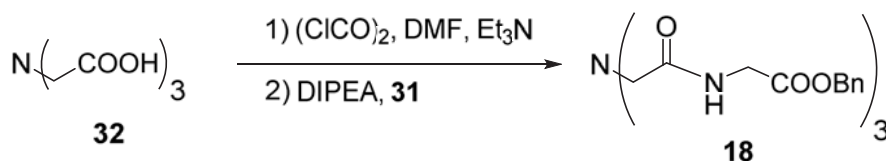
**HRMS** Calculated for [M – Br]<sup>+</sup>: 675.4972. Found: 675.4963.

**HCl·Gly-OBn, 31**

2 M HCl in Et<sub>2</sub>O (30 mL, 60 mmol) was added to a solution of compound **30**<sup>289</sup> (1.23 g, 4.64 mmol) in anhydrous CH<sub>2</sub>Cl<sub>2</sub> (30 mL). The mixture was stirred at room temperature overnight. The solvent was removed under reduced pressure to provide **31** (935 mg, quantitative yield) as an oil.

**Spectroscopic data and physical constants for compound 31:**

**<sup>1</sup>H NMR** (360 MHz, MeOD):  $\delta$  3.89 (s, 2H, H<sub>1</sub>), 5.30 (s, 2H, H<sub>4</sub>), 7.28-7.44 (c.a., 5H, H<sub>6-10</sub>), 7.35 (c.a., 3H, NH<sub>2</sub>·HCl).

**N(CH<sub>2</sub>CO-Gly-OBn)<sub>3</sub>, 18**

2 M solution of oxalyl chloride in CH<sub>2</sub>Cl<sub>2</sub> (2.21 mL) was added to a solution of nitrilotriacetic acid **32** (140 mg, 0.73 mmol) in anhydrous CH<sub>2</sub>Cl<sub>2</sub> (30 mL). Few drops of anhydrous DMF were added and the mixture was stirred under reflux for 2 h. Amino acid **31** (0.84 g, 4.16 mmol) and DIPEA (1.1 mL, 6.5 mmol) were added and the mixture was stirred under reflux for 21 h. The solvent was removed under reduced pressure, EtOAc (50 mL) was added and the solution was washed with saturated aqueous NaHCO<sub>3</sub> solution (2 x 40 mL) and saturated aqueous NaCl solution (1 x 50 mL). The organic layer was dried over anhydrous MgSO<sub>4</sub>, filtered and evaporated in vacuo to provide a dark and gummy oil. The crude was purified by adding EtOAc. Triamide **18** is precipitated as pure white solid (100 mg, 22 %).

**Spectroscopic data and physical constants for compound 18:**

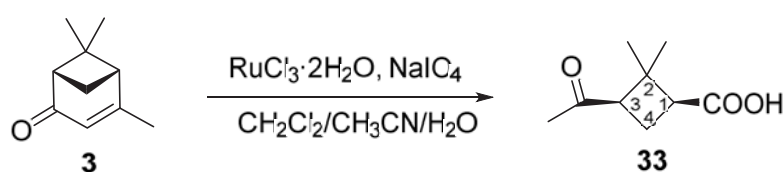
**M. p.:** 104-106 °C (Et<sub>2</sub>O-pentane)

**IR (ATR):**  $\nu$  3290, 3066, 3035, 2919, 2849, 1746, 1662, 1540 cm<sup>-1</sup>

**<sup>1</sup>H NMR** (360 MHz, CDCl<sub>3</sub>):  $\delta$  3.44 (s, 2H, H<sub>1</sub>), 4.07 (d, <sup>3</sup>J<sub>H-H</sub> = 4.3 Hz, 2H, H<sub>4</sub>), 5.13 (s, 2H, H<sub>7</sub>), 7.33 (s, 5H, H<sub>9-13</sub>), 7.73 (broad s, 1H, N-H<sub>3</sub>).

**<sup>13</sup>C NMR** (90 MHz, CDCl<sub>3</sub>):  $\delta$  41.2 (C<sub>4</sub>), 58.7 (C<sub>1</sub>), 67.5 (C<sub>7</sub>), 128.5, 128.7, 128.8 (C<sub>9-13</sub>), 135.2 (C<sub>8</sub>), 170.8 (C<sub>2</sub>, C<sub>5</sub>).

**HRMS:** Calculated [M + Na]<sup>+</sup>: 655.2374. Found: 655.2365.

**(1S,3R)-3-Acetyl-2,2-dimethylcyclobutanecarboxylic acid, 33**

## 10. Experimental Details

To a stirred solution of (–)-verbenone **3** (4.5 mL, 29.3 mmol) in 2:2:3 dichloromethane-acetonitrile-water (240 mL) were added catalytic RuCl<sub>3</sub> hydrate (0.12 g, 0.02 eq) and NaIO<sub>4</sub> (26.3 g, 123.0 mmol, 4.2 eq). The mixture was stirred at room temperature for 18 h. The crude obtained was filtered through Celite® and the organic layer was extracted with dichloromethane (3 x 40 mL). Then, the combined organic extracts were dried over MgSO<sub>4</sub> and concentrated under vacuum to afford the (–)-*cis*-pinonic acid **33** (4.74 g, 95 % yield), which is used without further purification.

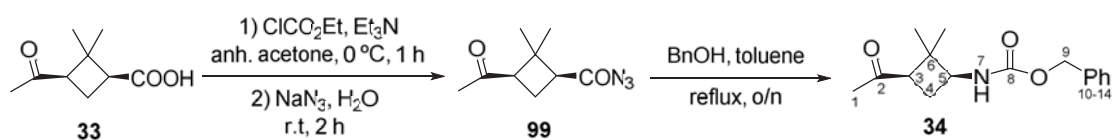
### Spectroscopic data for compound **33**:

<sup>1</sup>H NMR (250 MHz, CDCl<sub>3</sub>): δ 0.97 (s, 3H, *trans*-CH<sub>3</sub>), 1.45 (s, 3H, *cis*-CH<sub>3</sub>), 1.91 (m, 1H, H<sub>4a</sub>), 2.07 (s, 3H, COCH<sub>3</sub>), 2.62 (m, 1H, H<sub>4b</sub>), 2.86 (c.a., 2H, H<sub>1</sub>, H<sub>3</sub>).

Spectroscopic data are consistent with those reported in reference:

Burgess, K.; Li, S.; Rebenspies, J. *Tetrahedron Lett.* **1997**, *38*, 1681-1684.

### (1*R*,3*S*)-3-Azidocarbonyl-2,2-dimethylcyclobutyl methyl ketone, **34**



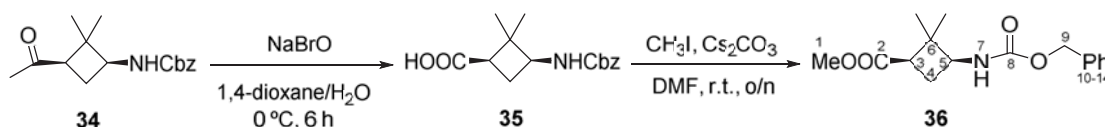
To an ice-cooled solution of **33** (300 mg, 1.7 mmol) in dry acetone, triethylamine (0.29 mL, 2.0 mmol) and ethyl chloroformate (0.2 mL, 2.0 mmol) were subsequently added and the mixture was stirred at 0 °C for 3 h. Then sodium azide (145 mg, 2.2 mmol) in 5 mL of water was added and the resultant solution was stirred at room temperature for 1.5 h. The reaction mixture was extracted with dichloromethane (4 x 15 mL), and the organic extracts were dried over magnesium sulfate. Solvents were removed at reduced pressure to give acyl azide **99** as an oil. A solution of **99** (310 mg, 1.6 mmol) and benzyl alcohol (0.4 mL, 3.3 mmol) in toluene (9 mL) was heated to reflux for 3.5 h. Toluene was removed at a reduced pressure and then excess benzyl alcohol was eliminated by liophilization. The residue was chromatographed on silica gel (1:1 to 2:1 ethyl acetate–hexane) to afford carbamate **34** (402 mg, 92 % yield).

**Spectroscopic data and physical constants for compound 34:**

$^1\text{H NMR}$  (360 MHz,  $\text{CDCl}_3$ ):  $\delta$  0.84 (s, 3H, *trans*- $\text{CH}_3$ ), 1.41 (s, 3H, *cis*- $\text{CH}_3$ ), 2.08 (s, 3H,  $\text{H}_1$ ), 2.1 (m, 2H,  $\text{H}_4$ ), 2.75 (dd,  $J = 4.25$  Hz,  $J = 6.5$  Hz, 1H,  $\text{H}_3$ ), 3.93 (m, 1H,  $\text{H}_5$ ), 4.82 (c. a., 1H, NH), 5.1 (dd,  $J = 6.5$  Hz,  $J_0 = 11$  Hz, 2H,  $\text{H}_9$ ), 7.38 (c. a., 5H,  $\text{H}_{10-14}$ ).

Spectroscopic data are consistent with those reported in reference:

Aguilera, J.; Moglioni, A. G.; Moltrasio, G. Y.; Ortuño, R. M. *Tetrahedron: Asymmetry* **2008**, *19*, 302-308

**Benzyl (1S,3R)-3-methoxycarbonyl-2,2-dimethylcyclobutyl-1-carbamate, 36**

An ice-cooled solution of sodium hypobromite [prepared from bromine (2 mL, 6.3 mmol) and sodium hydroxide (5.5 g, 137 mmol)] in 75 mL of water was added to a solution of ketone **34** (1.2 g, 4.4 mmol) in 3:1 dioxane–water, previously cooled at 5 C. The mixture was diluted with further dioxane (12 mL) and stirred at 5 C for 5 h. Then, the reaction mixture was washed with dichloromethane (2 x 50 mL), treated with sodium sulfite and, finally, 5 % HCl was added to reach pH 2–3. The acid solution was extracted with ethyl acetate (4 x 50 mL) and the organic extracts were dried over magnesium sulfate. The solvent was removed to afford acid **35** (970 mg, 80 % yield), which was used in the next steps without further purification.

**Spectroscopic data and physical constants for compound 35:**

$^1\text{H NMR}$  (360 MHz,  $\text{CDCl}_3$ ):  $\delta$  0.99 (s, 3H, *trans*- $\text{CH}_3$ ), 1.35 (s, 3H, *cis*- $\text{CH}_3$ ), 2.06 (m, 1H), 2.33 (m, 1H), 2.58 (m, 1H), 3.94 (m, 1H), 5.11 (c. a., 3H), 7.37 (c. a., 5H), 10.15 (br s, 1H).

Spectroscopic data are consistent with those reported in reference:

Aguilera, J.; Moglioni, A. G.; Moltrasio, G. Y.; Ortuño, R. M. *Tetrahedron: Asymmetry* **2008**, *19*, 302-308

## 10. Experimental Details

MeI (0.45 mL, 7.2 mmol) and Cs<sub>2</sub>CO<sub>3</sub> (2.4 g, 7.4 mmol) were added to a solution of acid **35** (1.34 g, 4.60 mmol) in DMF (20 mL). The mixture was stirred at room temperature overnight. CH<sub>3</sub>I excess was removed *in vacuo* and EtOAc (30 mL) was added. The solution was washed with saturated aqueous NaHCO<sub>3</sub> solution (3 x 30 mL), saturated aqueous NaCl solution (1 x 30 mL) and with H<sub>2</sub>O (1 x 30 mL). The resulting organic layer was then dried over anhydrous MgSO<sub>4</sub>, filtered and solvents removed under reduced pressure. The solid was purified by silica gel chromatography using EtOAc/hexane (1:3) to afford **36** (1.01 g, 84 %).

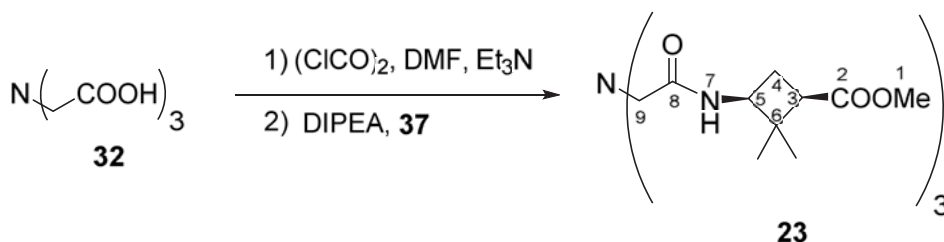
### Spectroscopic data and physical constants for compound **36**:

<sup>1</sup>H NMR (360 MHz, CDCl<sub>3</sub>): δ 0.90 (s, 3H, *trans*-CH<sub>3</sub>), 1.29 (s, 3H, *cis*-CH<sub>3</sub>), 2.05 (m, 1H), 2.36 (m, 1H), 2.57 (dd, *J* = 8 Hz, *J* = 9.75 Hz, 1H), 3.67 (s, 3H), 3.92 (dd, *J* = 8 Hz, *J* = 17.25 Hz, 1H), 4.91 (d, *J* = 11.75 Hz, 1H), 5.05 (d, *J* = 19 Hz, 1H), 5.12 (d, *J* = 20.25 Hz, 1H), 7.36 (complex absorption, 5H).

Spectroscopic data are consistent with those reported in reference:

Aguilera, J.; Moglioni, A. G.; Moltrasio, G. Y.; Ortuño, R. M. *Tetrahedron: Asymmetry* **2008**, *19*, 302-308

### N(CH<sub>2</sub>CO-γCbu-OMe)<sub>3</sub>, **23**



2 M solution of oxalyl chloride in CH<sub>2</sub>Cl<sub>2</sub> (2.40 mL, 4.7 mmol) was added to a solution of nitrilotriacetic acid **32** (270 mg, 1.41 mmol) in anhydrous CH<sub>2</sub>Cl<sub>2</sub> (60 mL). Few drops of anhydrous DMF were added and the mixture was stirred under reflux for 2 h. Amino acid **37**<sup>290</sup> (1.08 g, 6.9 mmol) and DIPEA (2.2 mL, 13 mmol) were added and the mixture was stirred under reflux for 21 h. The solvent was removed under reduced pressure, EtOAc (50 mL) was added and the solution was washed with saturated NaHCO<sub>3</sub> solution (2 x 40 mL)

and saturated NaCl solution (1 x 50 mL). The organic layer was dried over anhydrous MgSO<sub>4</sub>, filtered and evaporated to provide 770 mg of dark brown solid. The crude was first purified by silica gel chromatography using EtOAc and CH<sub>2</sub>Cl<sub>2</sub>/MeOH (20:1) as eluents and later by precipitation using ether and pentane to afford triamide **23** (300 mg, 35 %) as pale yellow solid.

**Spectroscopic data and physical constants for compound 23:**

$[\alpha]_D^{20}$ : -44.3 (c 0.41, CHCl<sub>3</sub>)

**M. p.:** 87-90 °C (Et<sub>2</sub>O/pentane)

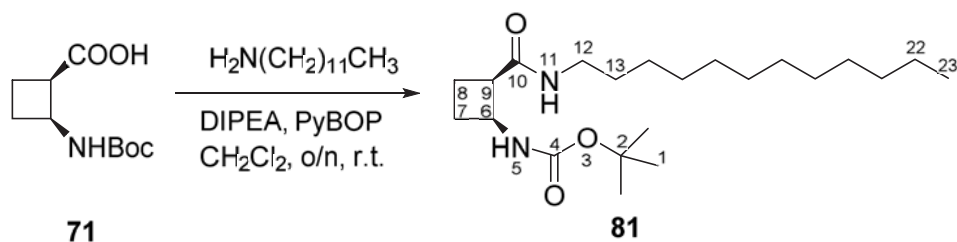
**IR** (ATR):  $\nu$  3271, 2956, 1732, 1653, 1547 cm<sup>-1</sup>

**<sup>1</sup>H NMR** (360 MHz, CDCl<sub>3</sub>):  $\delta$  0.80 (s, 3H, *trans*-CH<sub>3</sub>), 1.22 (s, 3H, *cis*-CH<sub>3</sub>), 2.02-2.34 (c.a., 2H, H<sub>4</sub>), 2.55 (m, 1H, H<sub>3</sub>), 3.07-3.46 (c.a., 2H, H<sub>9</sub>), 3.60 (s, 3H, H<sub>1</sub>), 4.03 (m, 1H, H<sub>5</sub>), 7.26 (broad s, 1H, NH).

**<sup>13</sup>C NMR** (90 MHz, CDCl<sub>3</sub>):  $\delta$  17.5 (CH<sub>3</sub>), 25.7 (C<sub>4</sub>), 29.1 (CH<sub>3</sub>), 43.3 (C<sub>3</sub>), 46.3 (C<sub>6</sub>), 50.2 (C<sub>5</sub>), 51.7 (C<sub>1</sub>), 60.2 (C<sub>9</sub>), 170.6 (C<sub>8</sub>), 173.2 (C<sub>2</sub>).

**HRMS** Calculated for [M + Na]<sup>+</sup>: 631.3314. Found: 631.3322.



***tert*-Butyl ((6*S*,9*R*)-2-(dodecylcarbamoyl)cyclobutyl)carbamate, **81****

To a solution of 154 mg (0.7 mmol) of acid **71** in 10 mL of anhydrous CH<sub>2</sub>Cl<sub>2</sub>, 0.4 mL of DIPEA (2.1 mmol, 3 eq) and 445 mg of PyBOP (0.9 mmol, 1.2 eq) are added. After 10 minutes stirring at room temperature, 145 mg of dodecylamine (0.8 mmol, 1.1 eq) in 5 mL of anhydrous CH<sub>2</sub>Cl<sub>2</sub> are added. The solution is stirred overnight at room temperature. Then, 10 mL of CH<sub>2</sub>Cl<sub>2</sub> are added and the solution is washed with NaHCO<sub>3</sub>. The organic layer is dried with MgSO<sub>4</sub> and the solvent is removed. The crude is purified by column chromatography using 3:1 hexane-EtOAc. 300 mg of compound **81** are obtained as a white solid in a 92 % of yield.

**Spectroscopic data and physical constants for compound **81**:**

$[\alpha]_D^{20}$ : +21.6 (*c* 1.05, CH<sub>2</sub>Cl<sub>2</sub>)

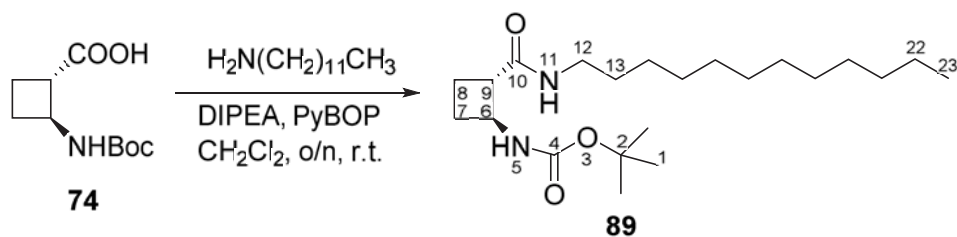
**M. p.**: 106-108 °C (hexane/AcOEt)

**IR** (ATR):  $\nu$  3340, 2918, 1681, 1646, 1516 cm<sup>-1</sup>

**<sup>1</sup>H NMR** (360 MHz, CDCl<sub>3</sub>):  $\delta$  0.80 (t, 3H, H<sub>23</sub>), 1.17 (s, 18H, H<sub>14-22</sub>), 1.33 (s, 9H, H<sub>1</sub>), 1.40 (m, 2H, H<sub>13</sub>), 1.80-2.21 (c.a., 4H, H<sub>7-8</sub>), 3.12 (m, 3H, H<sub>9</sub>, H<sub>12</sub>), 4.30 (q, 1H, H<sub>6</sub>), 5.42 (s, 1H, H<sub>5</sub>), 5.94 (s, 1H, H<sub>11</sub>).

**<sup>13</sup>C NMR** (90 MHz, CDCl<sub>3</sub>):  $\delta$  14.0 (C<sub>23</sub>), 18.2 (C<sub>6</sub>), 22.6 (C<sub>22</sub>), 26.9 (C<sub>7</sub>), 28.3 (C<sub>1</sub>), 29.3 (C<sub>15-20</sub>), 29.5 (C<sub>14</sub>), 29.7 (C<sub>13</sub>), 31.8 (C<sub>21</sub>), 39.5 (C<sub>12</sub>), 46.1 (C<sub>6</sub>), 46.4 (C<sub>9</sub>), 79.1 (C<sub>2</sub>), 155.2 (C<sub>10</sub>), 172.8 (C<sub>4</sub>).

**HRMS** Calculated for [M + Na]<sup>+</sup>: 405.3088. Found: 405.3081.

***tert*-Butyl ((6*S*,9*S*)-2-(dodecylcarbamoyl)cyclobutyl)carbamate, **89****

To a solution of 154 mg (0.7 mmol) of acid **74** in 10 mL of anhydrous  $\text{CH}_2\text{Cl}_2$ , 0.4 mL of DIPEA (2.1 mmol, 3 eq) and 445 mg of PyBOP (0.9 mmol, 1.2 eq) are added. After 10 minutes stirring at room temperature, 145 mg of dodecylamine (0.8 mmol, 1.1 eq) in 5 mL of anhydrous  $\text{CH}_2\text{Cl}_2$  are added. The solution is stirred overnight at room temperature. Then, 10 mL of  $\text{CH}_2\text{Cl}_2$  are added and the solution is washed with  $\text{NaHCO}_3$ . The organic layer is dried with  $\text{MgSO}_4$  and the solvent is removed. The crude is purified by column chromatography using 1:1 hexane-EtOAc. 200 mg of compound **89** are obtained as a white solid in a 82 % of yield.

**Spectroscopic data and physical constants for compound **89**:**

$[\alpha]_D^{20}$ : +18.1 (c 1.1,  $\text{CH}_2\text{Cl}_2$ )

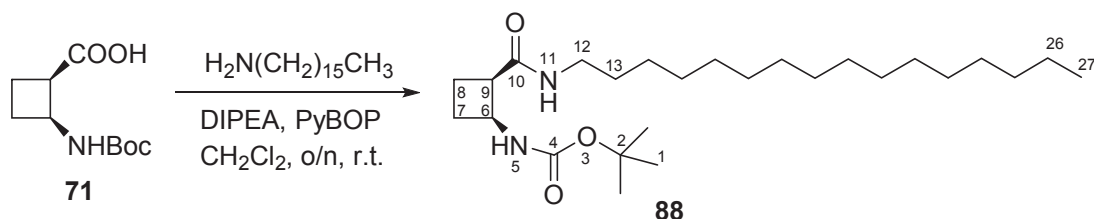
**M. p.**: 166 °C (hexane/AcOEt)

**IR** (ATR):  $\nu$  3318, 2919, 1685, 1638, 1537  $\text{cm}^{-1}$

**$^1\text{H NMR}$**  (360 MHz,  $\text{CDCl}_3$ ):  $\delta$  0.85 (t, 3H,  $\text{H}_{23}$ ), 1.22 (s, 18H,  $\text{H}_{14-22}$ ), 1.42 (s, 9H,  $\text{H}_1$ ), 1.48 (m, 2H,  $\text{H}_{13}$ ), 1.83-2.12 (c.a., 4H,  $\text{H}_{7-8}$ ), 2.88 (m, 1H,  $\text{H}_9$ ), 3.21 (m, 2H,  $\text{H}_{12}$ ), 4.08 (q, 1H,  $\text{H}_6$ ), 5.14 (s, 1H,  $\text{H}_5$ ), 7.92 (s, 1H,  $\text{H}_{11}$ ).

**$^{13}\text{C NMR}$**  (90 MHz,  $\text{CDCl}_3$ ):  $\delta$  14.2 ( $\text{C}_{23}$ ), 18.8 ( $\text{C}_6$ ), 22.8 ( $\text{C}_{22}$ ), 24.8 ( $\text{C}_7$ ), 27.1 ( $\text{C}_1$ ), 28.4 ( $\text{C}_{15-20}$ ), 29.5 ( $\text{C}_{14}$ ), 29.7 ( $\text{C}_{13}$ ), 33.0 ( $\text{C}_{21}$ ), 39.5 ( $\text{C}_{12}$ ), 46.8 ( $\text{C}_6$ ), 50.2 ( $\text{C}_9$ ), 80.3 ( $\text{C}_2$ ), 156.4 ( $\text{C}_{10}$ ), 172.1 ( $\text{C}_4$ ).

**HRMS** Calculated for  $[\text{M} + \text{Na}]^+$ : 405.3088. Found: 405.3091.

***tert*-Butyl ((6*S*,9*R*)-2-(hexadecylcarbamoyl)cyclobutyl)carbamate, **88****

To a solution of 200 mg (0.93 mmol) of acid **71** in 20 mL of anhydrous CH<sub>2</sub>Cl<sub>2</sub>, 0.5 mL of DIPEA (2.79 mmol, 3 eq) and 560 mg of PyBOP (1.11 mmol, 1.2 eq) are added. After 10 minutes stirring at room temperature, 240 mg of hexadecylamine (1.02 mmol, 1.1 eq) in 5 mL of anhydrous CH<sub>2</sub>Cl<sub>2</sub> are added. The solution is stirred overnight at room temperature. Then, 10 mL of CH<sub>2</sub>Cl<sub>2</sub> are added and the solution is washed with NaHCO<sub>3</sub>. The organic layer is dried with MgSO<sub>4</sub> and the solvent is removed. The crude is purified by column chromatography using 3:1 hexane-EtOAc. 320 mg of compound **88** are obtained as a white solid in a 79 % of yield.

**Spectroscopic data and physical constants for compound **88**:**

$[\alpha]_D^{20}$ : -101.4 (c 0.64, CH<sub>2</sub>Cl<sub>2</sub>)

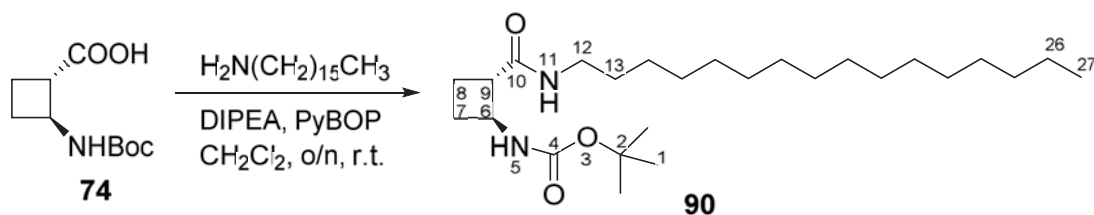
**M. p.:** 108 °C (CH<sub>2</sub>Cl<sub>2</sub>)

**IR** (ATR):  $\nu$  3336, 2916, 1679, 1644, 1514 cm<sup>-1</sup>

**<sup>1</sup>H NMR** (360 MHz, CDCl<sub>3</sub>):  $\delta$  0.90 (t,  $J$  = 6.1 Hz, 3H, H<sub>27</sub>), 1.27 (s, 26H, H<sub>14-26</sub>), 1.43 (s, 9H, H<sub>1</sub>), 1.49 (s, 2H, H<sub>13</sub>), 1.91 (q,  $J$  = 9.4 Hz, 1H, H<sub>8</sub>), 2.09 (t,  $J$  = 10.5 Hz, 1H, H<sub>7</sub>), 2.17 – 2.42 (m, 2H, H<sub>7-8</sub>), 3.23 (m, 3H, H<sub>9</sub>, H<sub>12</sub>), 4.28 – 4.52 (m, 1H, H<sub>6</sub>), 5.38 (d,  $J$  = 7.2 Hz, 1H, H<sub>5</sub>), 5.54 (s, 1H, H<sub>11</sub>).

**<sup>13</sup>C NMR** (90 MHz, CDCl<sub>3</sub>):  $\delta$  14.0 (C<sub>27</sub>), 18.2 (C<sub>6</sub>), 22.6 (C<sub>26</sub>), 26.9 (C<sub>7</sub>), 28.3 (C<sub>1</sub>), 29.2, 29.3, 29.5, 29.5, 29.6, 29.6, 29.6, 29.7 (C<sub>13</sub>), 31.9 (C<sub>21</sub>), 39.5 (C<sub>12</sub>), 46.1 (C<sub>6</sub>), 46.5 (C<sub>9</sub>), 79.2 (C<sub>2</sub>), 155.2 (C<sub>10</sub>), 172.7 (C<sub>4</sub>).

**HRMS** Calculated for [M + Na]<sup>+</sup>: 461.3714. Found: 461.3714.

***tert*-Butyl ((6*S*,9*S*)-2-(hexadecylcarbamoyl)cyclobutyl)carbamate, **90****

To a solution of 140 mg (0.7 mmol) of acid **74** in 15 mL of anhydrous CH<sub>2</sub>Cl<sub>2</sub>, 0.4 mL of DIPEA (2.1 mmol, 3 eq) and 390 mg of PyBOP (0.78 mmol, 1.2 eq) are added. After 10 minutes stirring at room temperature, 174 mg of hexadecylamine (0.72 mmol, 1.1 eq) in 5 mL of anhydrous CH<sub>2</sub>Cl<sub>2</sub> are added. The solution is stirred overnight at room temperature. Then, 10 mL of CH<sub>2</sub>Cl<sub>2</sub> are added and the solution is washed with NaHCO<sub>3</sub>. The organic layer is dried with MgSO<sub>4</sub> and the solvent is removed. The crude is purified by column chromatography using 1:1 hexane-EtOAc. 180 mg of compound **90** are obtained as a white solid in a 78 % of yield.

**Spectroscopic data and physical constants for compound **90**:**

$[\alpha]_D^{20}$ : -4.8 (*c* 0.89, CH<sub>2</sub>Cl<sub>2</sub>)

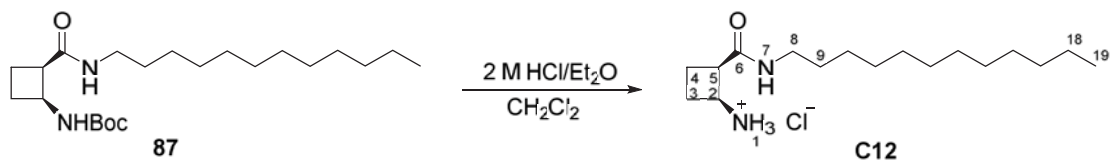
**M. p.:** 104-106 °C (CH<sub>2</sub>Cl<sub>2</sub>)

**IR (ATR):**  $\nu$  3346, 2917, 1684, 1637, 1535 cm<sup>-1</sup>

**<sup>1</sup>H NMR** (360 MHz, CDCl<sub>3</sub>):  $\delta$  0.90 (t, 3H, H<sub>27</sub>), 1.27 (s, 18H, H<sub>14-26</sub>), 1.47 (s, 9H, H<sub>1</sub>), 1.53 (m, 2H, H<sub>13</sub>), 1.74-1.92 (c.a., 2H, H<sub>7-8</sub>), 2.17 (m, 2H, H<sub>7-8</sub>), 2.90 (q, *J* = 9.0 Hz, 1H, H<sub>9</sub>), 3.19 (m, 2H, H<sub>12</sub>), 4.13 (p, *J* = 8.1 Hz, 1H, H<sub>6</sub>), 4.94 (s, 1H, H<sub>5</sub>), 7.92 (s, 1H, H<sub>11</sub>).

**<sup>13</sup>C NMR** (90 MHz, CDCl<sub>3</sub>):  $\delta$  14.1 (C<sub>27</sub>), 18.6 (C<sub>6</sub>), 22.6 (C<sub>26</sub>), 26.9 (C<sub>7</sub>), 28.2 (C<sub>1</sub>), 29.2, 29.3, 29.3, 29.5, 29.6, 29.6, 29.6 (C<sub>13</sub>), 31.9 (C<sub>21</sub>), 39.3 (C<sub>12</sub>), 48.6 (C<sub>6</sub>), 50.2 (C<sub>9</sub>), 79.2 (C<sub>2</sub>), 156.1 (C<sub>10</sub>), 172.8 (C<sub>4</sub>).

**HRMS** Calculated for [M + Na]<sup>+</sup>: 461.3714. Found: 461.3709.

**(2*S*,5*R*)-2-(Dodecylcarbamoyl)cyclobutan-1-ammonium chloride, C12**

To a solution of 144 mg of **87** (0.4 mmol) in 10 mL of anhydrous  $\text{CH}_2\text{Cl}_2$ , 10 mL of 2 M HCl in  $\text{Et}_2\text{O}$  are added. The solution is stirred overnight at room temperature. The solvent is removed under vacuum. The product is purified by precipitation in acetone obtaining 127 mg of surfactant **C12** in a quantitative yield.

**Spectroscopic data and physical constants for compound C12:**

$[\alpha]_D^{20}$ :  $-29.9$  ( $c$  0.53, MeOH)

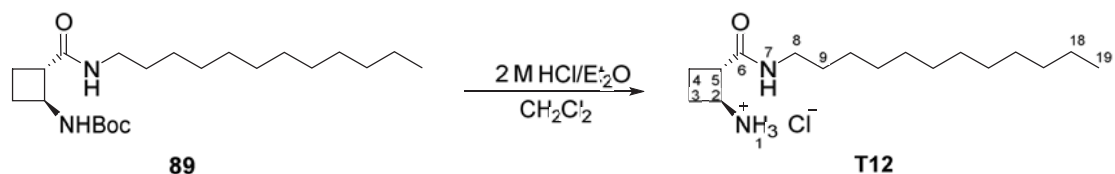
**M. p.:** 120-123 °C (Acetone)

**IR** (ATR):  $\nu$  3328, 2922, 2850, 1638, 1576, 1466  $\text{cm}^{-1}$

**$^1\text{H NMR}$**  (360 MHz,  $\text{MeOD-}d_4$ ):  $\delta$  0.94 (t,  $J$  = 6.8 Hz, 3H,  $\text{H}_{19}$ ), 1.33 (s, 18H,  $\text{H}_{10-18}$ ), 1.55 (m, 2H,  $\text{H}_9$ ), 2.17 – 2.40 (m, 4H,  $\text{H}_{3-4}$ ), 3.22 (m, 3H,  $\text{H}_5, \text{H}_8$ ), 3.99 (m, 1H,  $\text{H}_2$ ).

**$^{13}\text{C NMR}$**  (90 MHz,  $\text{MeOD-}d_4$ ):  $\delta$  14.1, 20.5, 23.4, 24.3, 27.7, 30.1, 30.4, 32.2, 40.3, 45.3, 47.0, 172.9.

**HRMS** Calculated for  $[\text{M} - \text{Cl}]^+$ : 283.2744. Found: 283.2744.

**(2S,5S)-2-(Dodecylcarbamoyl)cyclobutan-1-ammonium chloride, T12**

To a solution of 140 mg of **89** (0.34 mmol) in 10 mL of anhydrous  $\text{CH}_2\text{Cl}_2$ , 10 mL of 2 M HCl in  $\text{Et}_2\text{O}$  are added. The solution is stirred overnight at room temperature. The solvent is removed under vacuum. The product is purified by precipitation in acetone obtaining 104 mg of surfactant **T12** in a quantitative yield.

**Spectroscopic data and physical constants for compound T12:**

$[\alpha]_D^{20}$ : +47.4 (c 0.54, MeOH)

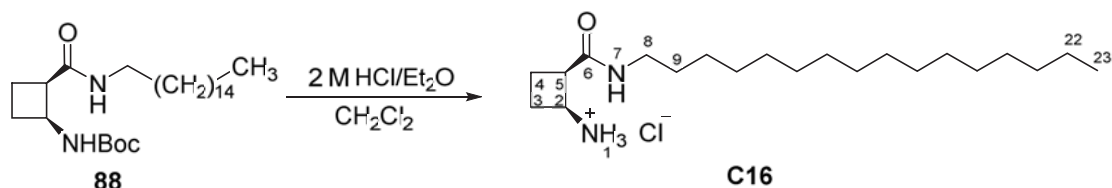
**M. p.:** 66 °C ( $\text{CH}_2\text{Cl}_2$ /pentane)

**IR** (ATR):  $\nu$  3307, 2919, 2850, 1644, 1558, 1460  $\text{cm}^{-1}$

**$^1\text{H NMR}$**  (360 MHz,  $\text{MeOD-}d_4$ ):  $\delta$  0.90 (t, 3H,  $\text{H}_{19}$ ), 1.29 (s, 18H,  $\text{H}_{10-18}$ ), 1.51 (m, 2H,  $\text{H}_9$ ), 1.88-2.24 (c.a., 4H,  $\text{H}_{3-4}$ ), 3.16 (m, 3H,  $\text{H}_5, \text{H}_8$ ), 3.95 (q, 1H,  $\text{H}_2$ ).

**$^{13}\text{C NMR}$**  (90 MHz,  $\text{MeOD-}d_4$ ):  $\delta$  14.5, 20.8, 23.7, 24.5, 28.0, 30.4, 30.7, 33.0, 40.6, 45.6, 47.4, 173.2.

**HRMS** Calculated for  $[\text{M} - \text{Cl}]^+$ : 283.2744. Found: 283.2742.

**(2*S*,5*R*)-2-(Hexadecylcarbamoyl)cyclobutan-1-ammonium chloride, C16**

To a solution of 160 mg of **88** (0.4 mmol) in 10 mL of anhydrous  $\text{CH}_2\text{Cl}_2$ , 10 mL of 2 M HCl in  $\text{Et}_2\text{O}$  are added. The solution is stirred overnight at room temperature. The solvent is removed under vacuum. The product is purified by precipitation in acetone obtaining 140 mg of surfactant **C16** in a quantitative yield.

**Spectroscopic data and physical constants for compound C16:**

$[\alpha]_D^{20}$ :  $-18.8$  ( $c$  0.5, MeOH)

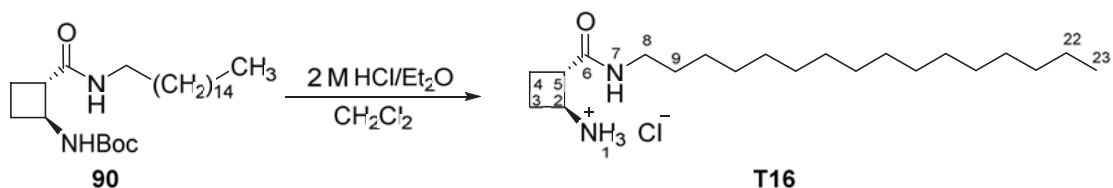
**M. p.:** 107-108 °C (Acetone)

**IR** (ATR):  $\nu$  3287, 2922, 2852, 1641, 1543, 1462  $\text{cm}^{-1}$

**$^1\text{H}$  NMR** (400 MHz,  $\text{MeOD-}d_4$ ):  $\delta$  0.92 (t,  $J$  = 6.8 Hz, 3H,  $\text{H}_{23}$ ), 1.31 (s, 26H,  $\text{H}_{10-22}$ ), 1.44 – 1.63 (m, 2H,  $\text{H}_9$ ), 2.07 – 2.22 (m, 1H,  $\text{H}_3$ ), 2.38 (tdd,  $J$  = 20.6, 11.1, 5.7 Hz, 3H,  $\text{H}_{3-4}$ ), 3.22 (ddt,  $J$  = 26.9, 13.3, 6.8 Hz, 2H,  $\text{H}_8$ ), 3.37 (dd,  $J$  = 9.3, 4.8 Hz, 1H,  $\text{H}_5$ ), 3.99 (q,  $J$  = 7.4 Hz, 1H,  $\text{H}_2$ ).

**$^{13}\text{C}$  NMR** (101 MHz,  $\text{MeOD-}d_4$ ):  $\delta$  13.0, 21.0, 22.3, 25.3, 26.6, 28.9, 29.0, 29.0, 29.2, 29.3, 29.3, 31.6, 38.8, 40.0, 45.8, 173.2.

**HRMS** Calculated for  $[\text{M} - \text{Cl}]^+$ : 339.3370. Found: 339.3380.

**(2S,5S)-2-(Hexadecylcarbamoyl)cyclobutan-1-ammonium chloride, T16**

To a solution of 180 mg of **90** (0.4 mmol) in 10 mL of anhydrous  $\text{CH}_2\text{Cl}_2$ , 10 mL of 2 M HCl in  $\text{Et}_2\text{O}$  are added. The solution is stirred overnight at room temperature. The solvent is removed under vacuum. The product is purified by precipitation in acetone obtaining 151 mg of surfactant **T16** in a quantitative yield.

**Spectroscopic data and physical constants for compound T16:**

$[\alpha]_D^{20}$ : +25.1 (*c* 0.53, MeOH)

**M. p.**: 77-78 °C (Acetone)

**IR** (ATR):  $\nu$  3307, 2917, 2849, 1644, 1559  $\text{cm}^{-1}$

**$^1\text{H NMR}$**  (360 MHz,  $\text{CDCl}_3$ ):  $\delta$  0.92 (t, *J* = 6.7 Hz, 3H,  $\text{H}_{23}$ ), 1.31 (s, 26H,  $\text{H}_{10-22}$ ), 1.45 – 1.60 (m, 2H,  $\text{H}_9$ ), 1.95 m, 1H,  $\text{H}_3$ ), 2.12 (m, 1H,  $\text{H}_4$ ), 2.26 (m, 2H,  $\text{H}_{3-4}$ ), 3.07 – 3.30 (m, 3H,  $\text{H}_5$ ,  $\text{H}_8$ ), 3.98 (q, *J* = 8.2 Hz, 1H,  $\text{H}_2$ ).

**$^{13}\text{C NMR}$**  (101 MHz,  $\text{MeOD-}d_4$ ):  $\delta$  13.0, 19.3, 22.3, 23.1, 26.6, 28.9, 29.0, 29.0, 29.2, 29.3, 29.3, 39.1, 45.9, 46.9, 47.1, 47.3, 47.5, 47.8, 48.0, 48.2, 171.7.

**HRMS** Calculated for  $[\text{M} - \text{Cl}]^+$ : 339.3370. Found: 339.3369.



**Sequence of the DNA: 5' → 3'**

(5')GCTGGCCGATAAGCTCTAAGAAACCATTATTATCATGACATTAACCTATAAAAAT  
 AGGCGTATCACGAGGCCCTTTTCGTCTTCAAGAATTAATCACTGGCCGTCGTTTTAC  
 AACGTCGTGACTGGGAAAACCCTGGCGTTACCCAACCTAATCGCCTTGCAGCACAT  
 CCCCTTTTCGCCAGCAGATCCACATCCTTGAAGGCCGCAGCGACGAGCAGAAGGAA  
 ACCCTCATTCCGGGAAGTCAGCGAGGCCATCTCGCGCTCCCTGGATGCGCCGCTGA  
 CCAGCGTGCAGGTGATTATCACGGAGATGGCCAAGGGCCACTTCGGCATCGGCCG  
 CGAACTGGCCAGCAAGGTGAGACGCTGAAGTGGAGATGCCAAGGGCACTTCGGG  
 TCGAGGAACCCGACCTGCATTGGGACGCGGCCACGGAGAGCGCGGGCAAACGCC  
 GGCATATAGCCAGTGGAGTTTGTAAAACGCTATTTTCAGAGCTTGGAGAGTGTCTAA  
 GAAAGCCGGGCGATGCCAACCAGTCCAGTGATCGAAGTTAGGCTGGTAAGAGCCG  
 CGAGCGATCCTTGAAGCTGTCCCTGATGGTCTGTCATCTACCTGCCTGGACAGCATG  
 GCCTGCAACGCGGGCATCCCGATGCCGCCGAAGCGAGAAGAATCATAATGGGGA  
 AGGCCATCCAGCCTCGCGTCGCGAACGCCAGCAAGACGTAGCCCAGCGCGTTCGGC  
 CGCCATGCCGGCGATAATGGCCTGCTTCTCGCCGAAACGTTTGGTGGCGGGACCA  
 GTGACGAAGGCTTGAGCGAGGGCGTGCAAGATTCCGAATACCGCAAGCGACAGGC  
 CGATCATCGTCGCGCTCCAGCGAAAGCGGTCTCGCCGAAAATGACCCAGAGCGC  
 TGCCGGCACCTGTCCTACGAGTTGCATGATAAAGAAGACAGTCATAAGTGCGGCGA  
 CGATAGTCATGCCCCGCGCCACCGGAAGGAGCTGACTGGGTTGAAGGCTCTCAA  
 GGCATCGGTTCGAGATCCCGGTGCCTAATGAGTGAGCTAACTTACATTAATTGCGTT  
 GCGCTCACTGCCCGCTTTCCAGTCGGGAAACCTGTCGTGCCAGCTGCATTAATGAA  
 TCGGCCAACGCGCGGGGAGAGGCGGTTTTCGTATTGGGCGCCAGGGTGGTTTTTC  
 TTTTACCAGTGAGACGGGCAACAGCTGATTGCCCTTACCAGCCTGGCCCTGAGAG  
 AGTTGCAGCAAGCGGTCCACGCTGGTTTCCCCAGCAGGGCGAAAATCCTGTTTGAT  
 GGTGGTTAACGGCGGGATATAACATGAGCTGTCTTCGGTATCGTCGTATCCCACTAC  
 CGAGATATCCGCACCAACGCGCAGCCCGGACTCGGTAATGGCGCGCATTGCGCCC  
 AGCGCCATCTGATCGTTGGCAACCAGCATCGCAGTGGGAACGATGCCCTCATTGAG  
 CATTGTCATGGTTTGTGAAAACCGGACATGGCACTCCAGTCGCCTTCCCGTTCCGC  
 TATCGGCTGAATTTGATTGCGAGTGAGATATTTATGCCAGCCAGCCAGACGCGAGAC  
 GCGCCGAGACAGAACTTAATGGGCCCGCTAACAGCGCGATTTGCTGGTGACCCAAT  
 GCGACCAGATGCTCCACGCCAGTCGCGTACCGTCTTCATGGGAGAAAATAATACT  
 GTTGATGGGTGTCTGGTCAGAGACATCAAGAAATAACGCCGGAACATTAGTGCAGG  
 CAGCTTCCACAGCAATGGCATCCTGGTCATCCAGCGGATAGTTAATGATCAGCCCA  
 CTGACGCGTTGCGCGAGAAGATTGTGCACCGCCGCTTTACAGGCTTCGACGCCGCT  
 TCGTTCTACCATCGACACCACCAGCTGGCACCCAGTTGATCGGCGCGAGATTTAA  
 TCGCCGCGACAATTTGCGACGGCGCGTGACGGGCCAGACTGGAGGTGGCAACGCC  
 AATCAGCAACGACTGTTTGCCCGCCAGTTGTTGTGCCACGCGGTTGGGAATGTAATT  
 CAGCTCCGCCATCGCCGCTTCCACTTTTTCCCGGTTTTTCGAGAAAACGTGGCTGG  
 CCTGGTTACCACGCGGGAAACGGTCTGATAAGAGACACCGGCATACTCTGCGACA  
 TCGTATAACGTTACTGTTTTACATTCACCACCCTGAATTGACTCTCTTCCGGGCGC  
 TATCATGCCATACCGCGAAAGGTTTTGCGCCATTCGATGGTGTCCGGGATCTCGAC  
 GCTCTCCCTTATGCGACTCCTGCATTAGGAAGCAGCCAGTAGTAGGTTGAGGCCG  
 TTGAGCACCGCCGCGCAAGGAATGGTGCATGCAAGGAGATGGCGCCCAACAGTC  
 CCCCGGCCACGGGGCCTGCCACCATACCCACGCCGAAACAAGCGCTCATGAGCCC  
 GAAGTGGCGAGCCCGATCTTCCCATCGGTGATGTCCGGCGATATAGGCGCCAGCA  
 ACCGCACCTGTGGCGCCGGTGTGCGGCCACGATGCGTCCGGCGTAGAGGATCG  
 AGATCTCGATCCCGCGAAATTAATACGACTCACTATAGGGGAATTGTGAGCGGATAA  
 CAATCCCCTCTAGAAATAATTTTGTTTAACTTTAAGAAGGAGATATCATATGGTACC  
 AAGTAAAGGAGAAGAACTTTTTCACTGGAGTTGTCCAATTCTTGTTGAATTAGATGGT  
 GATGTTAATGGGCACAAATTTTCTGTCACTGGAGAGGGTGAAGGTGATGCAACATAC  
 GGAAAACCTACCCTTAAATTTATTTGCACTACTGGAAAACCTACCTGTTCCATGGCCAA  
 CACTTGTCACTACTTTTCGCGTATGGTCTTCAATGCTTTGCGAGATACCCAGATCACAT  
 GAAGCAGCATGACTTTTTCAAGAGTGCCATGCCCGAAGGTTATGTACAGGAAAGAAC  
 TATATTTTTCAAAGATGACGGGAACTACAAGACACGTGCTGAAGTCAAGTTGAAGG

TGATACCCTTGTTAATAGAATCGAGTTAAAAGGTATTGATTTTAAAGAAGATGGAAAC  
ATTCTTGGACACAAATTGGAATACAACATAACTCACACAATGTATACATCATGGCAG  
ACAAACAAAAGAATGGAATCAAAGTTAACTTCAAATTAGACACAACATTGAAGATGG  
AAGCGTTCAACTAGCAGACCATTATCAACAAAATACTCCAATTGGCGATGGCCCTGT  
CCTTTTACCAGACAACCATTACCTGTCCACACAATCTGCCCTTTCGAAAGATCCCAA  
CGAAAAGAGAGACCACATGGTCCTTCTTGAGTTTGTAAACAGCTGCTGGGATTACACA  
TGGCATGGATGAACTATACAAATAAGGATCCTCTAGCTAGAGTCAGCTTTATGCTTG  
TAAACCGTTTTGTGAAAAAATTTTTAAAATAAAAAAGGGGACCTCTAGGGTCCCAAT  
TAATTAGTAATATAATCTATTAAGGTCATTCAAAGGTCATCCACCGGATCAGCTTA  
GTAAAGCCCTCGCTAGATTTTAATGCGGATGTTGCGATTACTTCGCCAACTATTGCG  
ATAACAAGAAAAAGCCAGCCTTTCATGATATATCTCCAATTTGTGTAGGGCTTATTA  
TGCACGCTTAAAAATAATAAAGCAGACTTGACCTGATAGTTTGGCTGTGAGCAATTA  
TGTGCTTAGTGCATCTAACGCTTGAGTTAAGCCGCGCCGCGAAGCGGCGTCGGCTT  
GAACGAATTGTTAGACATTATTTGCCGACTACCAAGGATCGGGCCTTGATGTTACCC  
GAGAGCTTGGCACCCAGCCTGCGCGAGCAGGGGAATTGATCCGGTGGATGACCTT  
TTGAATGACCTTTAATAGATTATTTACTAATTAATTGGGGACCCTAGAGGTCCCCTT  
TTTTATTTAAAAATTTTTTCAAAAACGGTTTACAAGCATAAAGCTGACCCTCTAGCA  
AGCTTGCGATGCAGGTGGCTGCTGAACCCCCAGCCGGAAGTACCCCAAGGCC  
**CTAGCGTTTGCAATGCACC(3')**

Molecular weight:<sup>‡</sup> 2482498.66 Da

Number of base pairs: 4017

Number of phosphate groups per molecule: 8034

In green: sequence where NruI enzyme cleaves the DNA chain

In yellow: sequence where NdeI enzyme cleaves the DNA chain

---

<sup>‡</sup> Averaged molecular weight obtained from two different sources:

[http://www.bioinformatics.org/sms2/dna\\_mw.html](http://www.bioinformatics.org/sms2/dna_mw.html)

<http://biotools.nubic.northwestern.edu/OligoCalc.html>



## **11. Bibliography**

---



## 11. Bibliography

- (1) *The Encyclopedia of Advanced Materials*, 1st ed.; Mahajan, S., Flemings, M. C., Brook, R. J., Bloor, D., Eds.; Pergamon: Oxford, 1994.
- (2) *Supramolecular Chemistry*, 2nd ed.; Atwood, J. L., Steed, J. W., Eds.; John Wiley & Sons: New York, 2009.
- (3) *Encyclopedia of Supramolecular Chemistry*; Steed, J. W., Atwood, J. L., Eds.; Marcel Dekker: New York, 2004.
- (4) *Core Concepts in Supramolecular Chemistry*; Steed, J. W., Turner, D. R., Wallace, K. J., Eds.; John Wiley & Sons: Chichester, 2007.
- (5) *Comprehensive Supramolecular Chemistry*; Lehn, J.-M., Atwood, J. L., Davies, J. E. D., MacNicol, D. D., Vögtle, F., Eds.; Pergamon: Oxford, 1996.
- (6) *Supramolecular Chemistry of Anions*; Bianchi, E., Bowman, J. K., García-España, E., Eds.; John Wiley & Sons: New York, 1997.
- (7) Ulatowski, F.; Dąbrowa, K.; Bałakier, T.; Jurczak, J. Recognizing the Limited Applicability of Job Plots in Studying Host-Guest Interactions in Supramolecular Chemistry. *J. Org. Chem.* **2016**, *81*, 1746–1756.
- (8) Lehn, J. M. Supramolecular Chemistry - Scope and Perspectives. Molecules - Supermolecules - Molecular Devices. In *Nobel Lectures*; 1987; pp 444–491.
- (9) Fernández, D.; Torres, E.; Avilés, F. X.; Ortuño, R. M.; Vendrell, J. Cyclobutane-Containing Peptides: Evaluation as Novel Metalloprotease Inhibitors and Modelling of Their Mode of Action. *Bioorg. Med. Chem.* **2009**, *17* (11), 3824–3828.
- (10) Torres, E.; Puigmartí-Luis, J.; Pérez del Pino, A.; Ortuño, R. M.; Amabilino, D. B. Use of Unnatural Beta-Peptides as a Self-Assembling Component in Functional Organic Fibres. *Org. Biomol. Chem.* **2010**, *8* (7), 1661–1665.
- (11) Mayans, E.; Gargallo, A.; Álvarez-Larena, Á.; Illa, O.; Ortuño, R. M. Diastereodivergent Synthesis of Chiral Vic -Disubstituted-Cyclobutane Scaffolds: 1,3-Amino Alcohol and 1,3-Diamine Derivatives - Preliminary Use in Organocatalysis. *European J. Org. Chem.* **2013**, *2013* (8), 1425–1433.
- (12) Sans, M.; Illa, O.; Ortuño, R. M. Organobridged Silsesquioxanes Based on Cyclobutane Diamines: Influence of the Stereochemistry on the Morphology of the Materials. *Tetrahedron* **2016**, *72* (22), 2913–2919.
- (13) Torres, E.; Gorrea, E.; Da Silva, E.; Nolis, P.; Branchadell, V.; Ortuño, R. M. Prevalence of Eight-Membered Hydrogen-Bonded Rings in Some Bis(cyclobutane) Beta-Dipeptides Including Residues with Trans Stereochemistry. *Org. Lett.* **2009**, *11* (11), 2301–2304.
- (14) Gorrea, E.; Pohl, G.; Nolis, P.; Celis, S.; Burusco, K. K.; Branchadell, V.; Perczel, A.; Ortuño, R. M. Secondary Structure of Short  $\beta$ -Peptides as the Chiral Expression of Monomeric Building Units: A Rational and Predictive Model. *J. Org. Chem.* **2012**, *77* (21), 9795–9806.
- (15) Aguilera, J.; Favier, I.; Sans, M.; Mor, À.; Álvarez-Larena, Á.; Illa, O.; Gómez, M.; Ortuño, R. M. Synthesis of Chiral Functionalised Cyclobutylpyrrolidines and Cyclobutylamino Alcohols from (-)-(S)-Verbenone - Applications in the Stabilisation of Ruthenium Nanocatalysts. *European J. Org. Chem.* **2015**, *2015* (4), 810–819.
- (16) Gorrea, E.; Carbajo, D.; Gutiérrez-Abad, R.; Illa, O.; Branchadell, V.; Royo, M.; Ortuño, R. M. Searching for New Cell-Penetrating Agents: Hybrid Cyclobutane-proline  $\gamma,\gamma$ -Peptides. *Org. Biomol. Chem.* **2012**, *10* (20), 4050–4057.
- (17) Ospina, J.; Sorrenti, A.; Illa, O.; Pons, R.; Ortuño, R. M. New Chiral Polyfunctional Cyclobutane Derivatives from (-)-Verbenone: Possible Surfactant Behaviour. *Tetrahedron: Asymmetry* **2013**, *24* (12), 713–718.
- (18) Gutiérrez-Abad, R.; Illa, O.; Ortuño, R. M. Synthesis of Chiral Cyclobutane Containing C<sub>3</sub>-Symmetric Peptide Dendrimers. *Org. Lett.* **2010**, *12* (14), 3148–3151.
- (19) Aguilera, J.; Moglioni, A.; Mor, À.; Ospina, J.; Illa, O.; Ortuño, R. M. Divergent Synthetic Routes to Biologically Relevant Types of Compounds: Chiral Polyfunctional  $\gamma$ -Lactams and Amino Acids. *Tetrahedron* **2014**, *70* (37), 6546–6553.
- (20) Ospina, J.; Gutiérrez-Abad, R.; Lope-Piedrafita, S.; Illa, O.; Branchadell, V.; Ortuño, R. M. Stereoselective Synthesis of Highly Branched Chiral Cyclobutane-Cored Triamines and Their Conjugation to Gd-DOTA. *Tetrahedron* **2015**, *71* (42), 8085–8095.
- (21) Weber, E.; Hosel, H. P. A Proposal for Classification and Nomenclature of Host-Guest-Type

## 11. Bibliography

- Compounds. *J. Incl. Phenom.* **1983**, *1*, 79–85.
- (22) Weber, E.; Vögtle, F. Classification and Nomenclature of Coronands, Cryptands, Podands, and of Their Complexes. *Inorganica Chim. Acta* **1980**, *45*, L65–L67.
- (23) Valiyaveettil, S.; Engbersen, J. F. J.; Verboom, W.; Reinhoudt, D. N. Synthesis and Complexation Studies of Neutral Anion Receptors. *Angew. Chemie Int. Ed. English* **1993**, *32* (6), 900–901.
- (24) Dey, S. K.; Das, G. A Selective Fluoride Encapsulated Neutral Tripodal Receptor Capsule: Solvatochromism and Solvatomorphism. *Chem. Commun. (Camb)*. **2011**, *47* (17), 4983–4985.
- (25) Ortuño, J. A.; Expósito, R.; Sánchez-Pedreño, C.; Albero, M. I.; Espinosa, A. A Nitrate-Selective Electrode Based on a tris(2-Aminoethyl)amine Triamide Derivative Receptor. *Anal. Chim. Acta* **2004**, *525* (2), 231–237.
- (26) Beer, P. D.; Chen, Z.; Goulden, A. J.; Graydon, A.; Stokes, S. E.; Wear, T. Selective Electrochemical Recognition of the Dihydrogen Phosphate Anion in the Presence of Hydrogen Sulfate and Chloride Ions by New Neutral Ferrocene Anion Receptors. *J. Chem. Soc. Chem. Commun.* **1993**, No. 24, 1834.
- (27) Öztürk, G.; Çolak, M.; Toğrul, M. Amide-Based Tripodal Receptors for Selective Anion Recognition. *J. Incl. Phenom. Macrocycl. Chem.* **2010**, *68* (1), 49–54.
- (28) Rúa, F.; Boussert, S.; Parella, T.; Díez-Pérez, I.; Branchadell, V.; Giral, E.; Ortuño, R. M. Self-Assembly of a Cyclobutane Beta-Tetrapeptide to Form Nanosized Structures. *Org. Lett.* **2007**, *9* (18), 3643–3645.
- (29) Gorrea, E.; Nolis, P.; Torres, E.; Da Silva, E.; Amabilino, D. B.; Branchadell, V.; Ortuño, R. M. Self-Assembly of Chiral Trans-Cyclobutane-Containing  $\beta$ -Dipeptides into Ordered Aggregates. *Chemistry* **2011**, *17* (16), 4588–4597.
- (30) Celis, S.; Nolis, P.; Illa, O.; Branchadell, V.; Ortuño, R. M. Low-Molecular-Weight Gelators Consisting of Hybrid Cyclobutane-Based Peptides. *Org. Biomol. Chem.* **2013**, *11* (17), 2839–2846.
- (31) Celis, S. The Chiral Cyclobutane Motif in Foldamers, Peptidic Organogelators and Host-Guest Chemistry, Universitat Autònoma de Barcelona, 2013.
- (32) Pi-Boleda, B. Master Thesis, 2013.
- (33) Cox, D. P.; Terpinski, J.; Lawrynowicz, W. “Anhydrous” Tetrabutylammonium Fluoride: A Mild but Highly Efficient Source of Nucleophilic Fluoride Ion. *J. Org. Chem.* **1984**, *49* (17), 3216–3219.
- (34) Hynes, M. J. EQNMR: A Computer Program for the Calculation of Stability Constants from Nuclear Magnetic Resonance Chemical Shift Data. *J. Chem. Soc. Dalton Trans.* **1993**, No. 2, 311.
- (35) Bandyopadhyay, I.; Raghavachari, K.; Flood, A. H. Strong CH...halide Hydrogen Bonds from 1,2,3-Triazoles Quantified Using Pre-Organized and Shape-Persistent Triazolophanes. *ChemPhysChem* **2009**, *10* (14), 2535–2540.
- (36) Schwesinger, R.; Link, R.; Wenzl, P.; Kossek, S. Anhydrous Phosphazanium Fluorides as Sources for Extremely Reactive Fluoride Ions in Solution. *Chemistry* **2005**, *12* (2), 438–445.
- (37) García, F.; Aragón, J.; Viruela, R.; Ortí, E.; Sánchez, L. A Bis(triazole)benzamide Receptor for the Complexation of Halide Anions and Neutral Carboxylic Acid Guests. Guest-Controlled Topicity and Self-Assembly. *Org. Biomol. Chem.* **2013**, *11* (5), 765–772.
- (38) Ota, N.; Stroupe, C.; Ferreira-da-Silva, J. M.; Shah, S. A.; Mares-Guia, M.; Brunger, A. T. Non-Boltzmann Thermodynamic Integration (NBTI) for Macromolecular Systems: Relative Free Energy of Binding of Trypsin to Benzamidine and Benzylamine. *Proteins* **1999**, *37* (4), 641–653.
- (39) Kurinov, I. V.; Harrison, R. W. Prediction of New Serine Proteinase Inhibitors. *Nat. Struct. Biol.* **1994**, *1* (10), 735–743.
- (40) Schwarzl, S. M.; Tschopp, T. B.; Smith, J. C.; Fischer, S. Can the Calculation of Ligand Binding Free Energies Be Improved with Continuum Solvent Electrostatics and an Ideal-Gas Entropy Correction? *J. Comput. Chem.* **2002**, *23* (12), 1143–1149.
- (41) Kang, S. O.; Powell, D.; Day, V. W.; Bowman-James, K. Trapped Bifluoride. *Angew. Chem. Int. Ed. Engl.* **2006**, *45* (12), 1921–1925.
- (42) Kang, S. O.; Day, V. W.; Bowman-James, K. Fluoride: Solution- and Solid-State Structural Binding Probe. *J. Org. Chem.* **2010**, *75* (2), 277–283.
- (43) Perera, S. A.; Bartlett, R. J. NMR Spin–Spin Coupling Constants for Hydrogen Bonds of  $[F(HF)_n]^-$ ,  $n=1-4$ , Clusters. *J. Am. Chem. Soc.* **2000**, *122* (6), 1231–1232.
- (44) Steiner, T. The Hydrogen Bond in the Solid State. *Angew. Chem. Int. Ed. Engl.* **2002**, *41* (1), 49–76.
- (45) Sun, H.; DiMagno, S. G. Anhydrous Tetrabutylammonium Fluoride. *J. Am. Chem. Soc.* **2005**, *127* (7), 2050–2051.
- (46) DiMagno, S. G.; Sun, H. Anhydrous Fluoride Salts and Reagents and Methods for Their Production. *US20060089514* **2006**.

- (47) Goursaud, M.; De Bernardin, P.; Dalla Cort, A.; Bartik, K.; Bruylants, G. Monitoring Fluoride Binding in DMSO: Why Is a Singular Binding Behavior Observed? *Eur. J. Org. Chem.* **2012**, No. 19, 3570–3574.
- (48) Camiolo, S.; Gale, P. A.; Hursthouse, M. B.; Light, M. E. Nitrophenyl Derivatives of Pyrrole 2,5-Diamides: Structural Behaviour, Anion Binding and Colour Change Signalled Deprotonation. *Org. Biomol. Chem.* **2003**, *1* (4), 741–744.
- (49) Graham, T. Liquid Diffusion Applied to Analysis. *Phil. Trans. Roy. Soc.* **1861**, *151*, 183–224.
- (50) Jordan Lloyd, D. *Colloid Chemistry (vol 1)*; Alexander, J., Ed.; The Chemical Catalog Co.: New York, 1926.
- (51) *Thermoreversible Networks (Advances in Polymer Science, Vol 130)*; Nijenhuis, K. te, Ed.; Springer: New York, 1997.
- (52) Li, S.; John, V. T.; Irvin, G. C.; Rachakonda, S. H.; McPherson, G. L.; O'Connor, C. J. Synthesis and Magnetic Properties of a Novel Ferrite Organogel. *J. Appl. Phys.* **1999**, *85* (8), 5965.
- (53) Rodríguez-Llansola, F.; Escuder, B.; Miravet, J. F. Switchable Performance of an L-Proline-Derived Basic Catalyst Controlled by Supramolecular Gelation. *J. Am. Chem. Soc.* **2009**, *131* (32), 11478–11484.
- (54) Díaz-Oltra, S.; Berdugo, C.; Miravet, J. F.; Escuder, B. Study of the Effect of Polymorphism on the Self-Assembly and Catalytic Performance of an L-Proline Based Molecular Hydrogelator. *New J. Chem.* **2015**, *39* (5), 3785–3791.
- (55) Kato, T. Supramolecular Polymers. *Chem. Rev.* **2001**, *101* (12), 4071–4098.
- (56) Puigmartí-Luis, J.; Laukhin, V.; Pérez del Pino, Á.; Vidal-Gancedo, J.; Rovira, C.; Laukhina, E.; Amabilino, D. B. Supramolecular Conducting Nanowires from Organogels. *Angew. Chemie Int. Ed.* **2007**, *46* (1-2), 238–241.
- (57) Mujawar, N. K.; Ghatage, S. L.; Yeligar, V. C. Organogel: Factors and Its Importance. *Int. J. Pharm. Chem. Biol. Sci.* **2014**, *4* (3), 758–773.
- (58) Smith, D. K. Lost in Translation? Chirality Effects in the Self-Assembly of Nanostructured Gel-Phase Materials. *Chem. Soc. Rev.* **2009**, *38* (3), 684–694.
- (59) Duan, P.; Cao, H.; Zhang, L.; Liu, M. Gelation Induced Supramolecular Chirality: Chirality Transfer, Amplification and Application. *Soft Matter* **2014**, *10* (30), 5428–5448.
- (60) Takafuji, M.; Kira, Y.; Tsuji, H.; Sawada, S.; Hachisako, H.; Ihara, H. Optically Active Polymer Film Tuned by a Chirally Self-Assembled Molecular Organogel. *Tetrahedron* **2007**, *63* (31), 7489–7494.
- (61) Anuradha; La, D. D.; Al Kobaisi, M.; Bhosale, S. V. Right Handed Chiral Superstructures from Achiral Molecules: Self-Assembly with a Twist. *Sci. Rep.* **2015**, *5*, 15652.
- (62) Abdallah, D. J.; Weiss, R. G. Organogels and Low Molecular Mass Organic Gelators. *Adv. Mater.* **2000**, *12* (17), 1237–1247.
- (63) *Organic Nanostructures*; Atwood, J. L., Steed, J. W., Eds.; Wiley-VCH: Weinheim, 2008.
- (64) *Functional Molecular Gels*; Escuder, B., Miravet, J. F., Eds.; Royal Society of Chemistry: Cambridge, 2014.
- (65) Lan, Y.; Corradini, M. G.; Weiss, R. G.; Raghavan, S. R.; Rogers, M. A. To Gel or Not to Gel: Correlating Molecular Gelation with Solvent Parameters. *Chem. Soc. Rev.* **2015**, *44* (17), 6035–6058.
- (66) Abdallah, D. J.; Weiss, R. G. N-Alkanes Gel N-Alkanes (and Many Other Organic Liquids). *Langmuir* **2000**, *16* (2), 352–355.
- (67) Abdallah, D. J.; Sirchio, S. A.; Weiss, R. G. Hexatriacontane Organogels. The First Determination of the Conformation and Molecular Packing of a Low-Molecular-Mass Organogelator in Its Gelled State. *Langmuir* **2000**, *16* (20), 7558–7561.
- (68) Terech, P.; Pasquier, D.; Bordas, V.; Rossat, C. Rheological Properties and Structural Correlations in Molecular Organogels. *Langmuir* **2000**, *16* (10), 4485–4494.
- (69) Mieden-Gundert, G.; Klein, L.; Fischer, M.; Vögtle, F.; Heuzé, K.; Pozzo, J.-L.; Vallier, M.; Fages, F. Rational Design of Low Molecular Mass Organogelators: Toward a Library of Functional N-Acyl-1,ω-Amino Acid Derivatives. *Angew. Chemie Int. Ed.* **2001**, *40* (17), 3164–3166.
- (70) Knight, D. W.; Morgan, I. R. A New Organogelator Effective at Both Extremes of Solvent Polarity. *Tetrahedron Lett.* **2009**, *50* (47), 6610–6612.
- (71) John, G.; Jung, J. H.; Masuda, M.; Shimizu, T. Unsaturation Effect on Gelation Behavior of Aryl Glycolipids. *Langmuir* **2004**, *20* (6), 2060–2065.
- (72) Hanabusa, K.; Yamada, M.; Kimura, M.; Shirai, H. Prominent Gelation and Chiral Aggregation of Alkylamides Derived Fromtrans-1,2-Diaminocyclohexane. *Angew. Chemie Int. Ed. English* **1996**, *35* (17), 1949–1951.
- (73) Cao, X.; Zhao, X.; Gao, A.; Xu, R. Organogel Formation Based on Bis-Urea Derivative. *Supramol. Chem.*



## 11. Bibliography

- 2014**, 26 (10-12), 804–808.
- (74) Pal, A.; Ghosh, Y. K.; Bhattacharya, S. Molecular Mechanism of Physical Gelation of Hydrocarbons by Fatty Acid Amides of Natural Amino Acids. *Tetrahedron* **2007**, 63 (31), 7334–7348.
- (75) Willemsen, H. M.; Vermonden, T.; Marcelis, A. T. M.; Sudhölter, E. J. R. Alkyl Derivatives of Cholic Acid as Organogelators: One-Component and Two-Component Gels. *Langmuir* **2002**, 18 (19), 7102–7106.
- (76) Taboada, E.; Feldborg, L. N.; Pérez del Pino, Á.; Roig, A.; Amabilino, D. B.; Puigmartí-Luis, J. Nanocomposites Combining Conducting and Supermagnetic Components Prepared via an Organogel. *Soft Matter* **2011**, 7 (6), 2755–2761.
- (77) Celis, S.; Gorrea, E.; Nolis, P.; Illa, O.; Ortuño, R. M. Designing Hybrid Foldamers: The Effect on the Peptide Conformational Bias of Beta- versus Alfa- and Gamma-Linear Residues in Alternation with (1R,2S)-2-Aminocyclobutane-1-Carboxylic Acid. *Org. Biomol. Chem.* **2012**, 10, 861–868.
- (78) Zweep, N.; Hopkinson, A.; Meetsma, A.; Browne, W. R.; Feringa, B. L.; van Esch, J. H. Balancing Hydrogen Bonding and van Der Waals Interactions in Cyclohexane-Based Bisamide and Bisurea Organogelators. *Langmuir* **2009**, 25 (15), 8802–8809.
- (79) *Rheology: Principles, Measurements and Applications*; Macosko, C. W., Ed.; VCH Publishers: New York, 1994.
- (80) *Molecular Light Scattering and Optical Activity*, 2nd ed.; Barron, L. B., Ed.; Cambridge University Press: New York, 2004.
- (81) Makarević, J.; Jokić, M.; Raza, Z.; Štefanić, Z.; Kojić-Prodić, B.; Žinić, M. Chiral Bis(amino Alcohol)oxalamide Gelators—Gelation Properties and Supramolecular Organization: Racemate versus Pure Enantiomer Gelation. *Chem. - A Eur. J.* **2003**, 9 (22), 5567–5580.
- (82) Hunter, C. A.; Anderson, H. L. What Is Cooperativity? *Angew. Chem. Int. Ed. Engl.* **2009**, 48 (41), 7488–7499.
- (83) Mahadevi, A. S.; Sastry, G. N. Cooperativity in Noncovalent Interactions. *Chem. Rev.* **2016**, 116 (5), 2775–2825.
- (84) de Loos, M.; van Esch, J.; Kellogg, R. M.; Feringa, B. L. Chiral Recognition in Bis-Urea-Based Aggregates and Organogels through Cooperative Interactions. *Angew. Chemie* **2001**, 113 (3), 633–636.
- (85) Hirst, A. R.; Coates, I. A.; Boucheteau, T. R.; Miravet, J. F.; Escuder, B.; Castelletto, V.; Hamley, I. W.; Smith, D. K. Low-Molecular-Weight Gelators: Elucidating the Principles of Gelation Based on Gelator Solubility and a Cooperative Self-Assembly Model. *J. Am. Chem. Soc.* **2008**, 130 (28), 9113–9121.
- (86) Cotton, A. Absorption Inégale Des Rayons Circulaires Droit et Gauche Dans Certain Corps Actifs. *C. R. H. Acad. Sci.* **1895**, 120, 989–991.
- (87) Cotton, A. Dispersion Rotatoire Anomale Des Corps Absorbants. *C. R. H. Acad. Sci.* **1895**, 120, 1044–1046.
- (88) *Circular Dichroism: Principles and Applications*, 2nd ed.; Berova, N., Nakanishi, K., Woody, R. W., Eds.; Wiley-VCH: Weinheim, 1994.
- (89) Yu, G.; Yan, X.; Han, C.; Huang, F. Characterization of Supramolecular Gels. *Chem. Soc. Rev.* **2013**, 42 (16), 6697.
- (90) Rodríguez-Llansola, F.; Miravet, J. F.; Escuder, B. Supramolecular Gel Formation and Self-Correction Induced by Aggregation-Driven Conformational Changes. *Chem. Commun.* **2009**, 46 (2), 209–211.
- (91) *Comprehensive Chiroptical Spectroscopy, Applications in Stereochemical Analysis of Synthetic Compounds, Natural Products and Biomolecules.*; Berova, N., Polavarapu, P. L., Nakanishi, K., Woody, R. W., Eds.; John Wiley & Sons, Inc: New Jersey, 2012.
- (92) Gottarelli, G.; Lena, S.; Masiero, S.; Pieraccini, S.; Spada, G. P. The Use of Circular Dichroism Spectroscopy for Studying the Chiral Molecular Self-Assembly: An Overview. *Chirality* **2008**, 20 (3-4), 471–485.
- (93) Sly, J.; Kasák, P.; Gomar-Nadal, E.; Rovira, C.; Górriz, L.; Thordarson, P.; Amabilino, D. B.; Rowan, A. E.; Nolte, R. J. M.; MacDiarmid, A. G.; et al. Chiral Molecular Tapes from Novel Tetra(thiafulvalene-Crown-Ether)-Substituted Phthalocyanine Building Blocks. *Chem. Commun.* **2005**, 40 (10), 1255–1257.
- (94) Amabilino, D. B. Chapter 3: Chiral Organic Nanomaterials. In *Organic Nanomaterials: synthesis, characterization and device application*; Torres, T., Bottoni, G., Eds.; John Wiley & Sons, Inc: New Jersey, 2013.
- (95) Lascialfari, L.; Pescitelli, G.; Brandi, A.; Mannini, M.; Berti, D.; Cicchi, S. Urea vs. Carbamate Groups: A Comparative Study in a Chiral C2 Symmetric Organogelator. *Soft Matter* **2015**, 11 (42), 8333–8341.
- (96) Maity, S.; Das, P.; Reches, M. Inversion of Supramolecular Chirality by Sonication-Induced Organogelation. *Nat. Publ. Gr.* 1–11.

- (97) Zhou, P.; Zhao, N.; Rele, D. N.; Berova, N.; Nakanishi, K. A Chiroptical/chemical Strategy for Configurational Assignments of Acyclic 1,3-Skipped Polyols: Model 1,2,4,6-Tetrols. *J. Am. Chem. Soc.* **1993**, *115*, 9313–9314.
- (98) Pescitelli, G.; Di Bari, L.; Berova, N. Conformational Aspects in the Studies of Organic Compounds by Electronic Circular Dichroism. *Chem. Soc. Rev.* **2011**, *40* (9), 4603.
- (99) Harada, N.; Saito, A.; Ono, H.; Gawronski, J.; Gawronska, K.; Sugioka, T.; Uda, H.; Kuriki, T. A CD Method for Determination of the Absolute Stereochemistry of Acyclic Glycols. 1. Application of the CD Exciton Chirality Method to Acyclic 1,3-Dibenzoate Systems. *J. Am. Chem. Soc.* **1991**, *113* (10), 3842–2850.
- (100) Edelsztejn, V. C.; Mac Cormack, A. S.; Ciarlantini, M.; Di Chenna, P. H. Self-Assembly of 2,3-Dihydroxycholestane Steroids into Supramolecular Organogels as a Soft Template for the in-Situ Generation of Silicate Nanomaterials. *Beilstein J. Org. Chem.* **2013**, *9*, 1826–1836.
- (101) Lan, Y.; Corradini, M. G.; Liu, X.; May, T. E.; Borondics, F.; Weiss, R. G.; Rogers, M. A. Comparing and Correlating Solubility Parameters Governing the Self-Assembly of Molecular Gels Using 1,3:2,4-Dibenzylidene Sorbitol as the Gelator. *Langmuir* **2014**, *30* (47), 14128–14142.
- (102) Katritzky, A. R.; Fara, D. C.; Yang, H.; Tämm, K.; Tamm, T.; Karelson, M. Quantitative Measures of Solvent Polarity. *Chem. Rev.* **2004**, *104* (1), 175–198.
- (103) Sangster, J. Octanol-Water Partition Coefficients of Simple Organic Compounds. *J. Phys. Chem. Ref. Data* **1989**, *18* (3), 1111–1229.
- (104) Brooker, L. G. S.; Keyes, G. H.; Heseltine, D. W. Color and Constitution. XI. Anhydronium Bases of P-Hydroxystyryl Dyes as Solvent Polarity Indicators. *J. Am. Chem. Soc.* **1951**, *73* (11), 5350–5356.
- (105) Cerón-Carrasco, J. P.; Jacquemin, D.; Laurence, C.; Planchat, A.; Reichardt, C.; Sraïdi, K. Solvent Polarity Scales: Determination of New ET (30) Values for 84 Organic Solvents. *J. Phys. Org. Chem.* **2014**, *27* (6), 512–518.
- (106) Reichardt, C. Polarity of Ionic Liquids Determined Empirically by Means of Solvatochromic Pyridinium N-Phenolate Betaine Dyes. *Green Chem.* **2005**, *7* (5), 339–351.
- (107) Dong, D. C.; Winnik, M. A. The Py Scale of Solvent Polarities. *Can. J. Chem.* **1984**, *62* (11), 2560–2565.
- (108) Hildebrand, J. H.; Scott, R. L. *The Solubility of Nonelectrolytes*, 3rd ed.; Dover Publications: Reinhold, NY, 1959.
- (109) Scatchard, G. Equilibrium in Non-Electrolyte Mixtures. *Chem. Rev.* **1949**, *44* (1), 7–35.
- (110) Lagalante, A. F.; Wood, C.; Clarke, A. M.; Bruno, T. J. Kamlet–Taft Solvatochromic Parameters for 25 Glycol Ether Solvents and Glycol Ether Aqueous Solutions. *J. Solution Chem.* **1998**, *27* (10), 887–900.
- (111) Wyatt, V. T.; Bush, D.; Lu, J.; Hallett, J. P.; Liotta, C. L.; Eckert, C. A. Determination of Solvatochromic Solvent Parameters for the Characterization of Gas-Expanded Liquids. *J. Supercrit. Fluids* **2005**, *36* (1), 16–22.
- (112) Edwards, W.; Lagadec, C. A.; Smith, D. K. Solvent–gelator Interactions—using Empirical Solvent Parameters to Better Understand the Self-Assembly of Gel-Phase Materials. *Soft Matter* **2011**, *7* (1), 110–117.
- (113) Catalán, J.; López, V.; Pérez, P.; Martín-Villamil, R.; Rodríguez, J.-G. Progress towards a Generalized Solvent Polarity Scale: The Solvatochromism of 2-(dimethylamino)-7-Nitrofluorene and Its Homomorph 2-Fluoro-7-Nitrofluorene. *Liebigs Ann.* **1995**, *1995* (2), 241–252.
- (114) Catalán, J.; Díaz, C.; López, V.; Pérez, P.; De Paz, J.-L. G.; Rodríguez, J. G. A Generalized Solvent Basicity Scale: The Solvatochromism of 5-Nitroindoline and Its Homomorph 1-Methyl-5-Nitroindoline. *Liebigs Ann.* **1996**, *1996* (11), 1785–1794.
- (115) Catalán, J.; Díaz, C. A Generalized Solvent Acidity Scale: The Solvatochromism of *tert*-Butylstilbazolium Betaine Dye and Its Homomorpho, *O'*-Di-*tert*-Butylstilbazolium Betaine Dye. *Liebigs Ann.* **1997**, *1997* (9), 1941–1949.
- (116) Hansen, C. M. *Hansen Solubility Parameters*, 2nd ed.; CRC Press: Boca Raton, FL, 2007.
- (117) Raynal, M.; Bouteiller, L. Organogel Formation Rationalized by Hansen Solubility Parameters. *Chem. Commun. (Camb)*. **2011**, *47* (29), 8271–8273.
- (118) Hansen, C. M.; Abbot, S.; Yamamoto, H. HSPiP (Hansen Solubility Parameters in Practice) Software. 2015.
- (119) Gao, J.; Wu, S.; Rogers, M. A. Harnessing Hansen Solubility Parameters to Predict Organogel Formation. *J. Mater. Chem.* **2012**, *22* (25), 12651–12658.
- (120) Aparicio, F.; García, F.; Sánchez, L. Supramolecular Polymerization of C<sub>3</sub>-Symmetric Organogelators: Cooperativity, Solvent, and Gelation Relationship. *Chemistry* **2013**, *19* (9), 3239–3248.
- (121) Xu, H.; Song, J.; Tian, T.; Feng, R. Estimation of Organogel Formation and Influence of Solvent

## 11. Bibliography

- Viscosity and Molecular Size on Gel Properties and Aggregate Structures. *Soft Matter* **2012**, *8* (12), 3478.
- (122) Bonnet, J.; Suissa, G.; Raynal, M.; Bouteiller, L. Organogel Formation Rationalized by Hansen Solubility Parameters: Dos and Don'ts. *Soft Matter* **2014**, *10* (18), 3154–3160.
- (123) Mori, T.; Inoue, Y.; Grimme, S. Time Dependent Density Functional Theory Calculations for Electronic Circular Dichroism Spectra and Optical Rotations of Conformationally Flexible Chiral Donor-Acceptor Dyad. *J. Org. Chem.* **2006**, *71* (26), 9797–9806.
- (124) Pescitelli, G.; Di Bari, L.; Caporusso, A. M.; Salvadori, P. The Prediction of the Circular Dichroism of the Benzene Chromophore: TDDFT Calculations and Sector Rules. *Chirality* **2008**, *20* (3-4), 393–399.
- (125) Pescitelli, G.; Di Bari, L.; Berova, N. Application of Electronic Circular Dichroism in the Study of Supramolecular Systems. *Chem. Soc. Rev.* **2014**, *43* (15), 5211–5233.
- (126) Person, R. V.; Monde, K.; Humpf, H.; Berova, N.; Nakanishi, K. A New Approach in Exciton-Coupled Circular Dichroism (ECCD)-Insertion of an Auxiliary Stereogenic Center. *Chirality* **1995**, *7* (3), 128–135.
- (127) *J-Aggregates (Volume 2)*; Kobayashi, T., Ed.; World Scientific Publishing Co. Pte. Ltd.: Singapore, 1996.
- (128) *Surfactants and Interfacial Phenomena*; Rosen, M. J., Kunjappu, J. T., Eds.; John Wiley & Sons, Inc: Hoboken, New Jersey, 2012.
- (129) *Surfactants and Polymers in Aqueous Solution*, 2nd ed.; Holmberg, K., Jönsson, B., Kronberg, B., Lindman, B., Eds.; John Wiley & Sons, Ltd: Chichester, 2002.
- (130) *Giant Micelles: Properties and Applications*; Zana, R., Kaler, E. W., Eds.; Taylor & Francis Group: Boca Raton, 2007.
- (131) *Industrial Applications of Surfactants*; Karsa, D. R., Ed.; Royal Society of Chemistry: Cambridge, 1999.
- (132) *Encyclopedia of Colloid and Interface Science*; Tadros, T., Ed.; Springer Berlin Heidelberg: Berlin, Heidelberg, 2013.
- (133) *DNA Interaction with Polymers and Surfactants*; Dias, R. S., Lindman, B., Eds.; John Wiley & Sons, Inc: New Jersey, 2008.
- (134) Presto, W. C.; Preston, W. Some Correlating Principles of Detergent Action. *J. Phys. Colloid Chem.* **1948**, *52* (1), 84–97.
- (135) *Handbook of Applied Surface and Colloid Chemistry*; Holmberg, K., Ed.; John Wiley & Sons: New York, 2002.
- (136) Noüy, P. L. An Interfacial Tensiometer for Universal Use. *J. Gen. Physiol.* **1925**, *7*, 625–631.
- (137) *Essentials of Physics*, 6th ed.; Cutnell, J. D., Johnson, K. W., Eds.; John Wiley & Sons: New York, 2006.
- (138) Anastasiadis, S. H.; Chen, J. K.; Koberstein, J. T.; Siegel, A. F.; Sohn, J. E.; Emerson, J. A. The Determination of Interfacial Tension by Video Image Processing of Pendant Fluid Drops. *J. Colloid Interface Sci.* **1987**, *119* (1), 55–66.
- (139) Atae-Allah, C.; Cabrerizo-Vílchez, M.; Gómez-Lopera, J. F.; Holgado-Terriza, J. A.; Román-Roldán, R.; Luque-Escamilla, P. L. Measurement of Surface Tension and Contact Angle Using Entropic Edge. *Meas. Sci. Technol.* **2001**, *12*, 288–298.
- (140) *Surfaces, Interfaces and Colloids — Principles and Applications*, 2nd ed.; Myers, D., Ed.; Wiley-VCH: New York, 1999.
- (141) *Colloidal Foundations of Nanoscience*; Berti, D., Palazzo, G., Eds.; Elsevier: Florence, 2014.
- (142) Bordes, R.; Tropsch, J.; Holmberg, K. Role of an Amide Bond for Self-Assembly of Surfactants. *Langmuir* **2010**, *26* (5), 3077–3083.
- (143) Tanford, C. The Hydrophobic Effect and the Organization of Living Matter. **2009**, *200* (4345), 1012–1018.
- (144) Sorrenti, A.; Illa, O.; Ortuño, R. M. Amphiphiles in Aqueous Solution: Well beyond a Soap Bubble. *Chem. Soc. Rev.* **2013**, *42* (21), 8200–8219.
- (145) Fuhrhop, J.-H.; Wang, T. Bolaamphiphiles. *Chem. Rev.* **2004**, *104* (6), 2901–2937.
- (146) <http://huntsofficefurniturefvq.blogspot.com.es>  
<http://huntsofficefurniturefvq.blogspot.com.es/2012/06/1865-wood-engraving-hunt-ostrich-bola.html>.
- (147) <http://legacyofkain.wikia.com> <http://legacyofkain.wikia.com/wiki/File:Nosgoth-Character-Hunter-Bola-Weapon.jpg>. **2016**.
- (148) Shimizu, T. Bottom-Up Synthesis and Structural Properties of Self-Assembled High-Axial-Ratio Nanostructures. *Macromol. Rapid Commun.* **2002**, *23* (5-6), 311–331.
- (149) Nagarajan, R. Self-Assembly of Bola Amphiphiles. *Chem. Eng. Commun.* **1987**, *55*, 251–273.

- (150) Li, Q.; Mittal, R.; Huang, L.; Travis, B.; Sanders, C. R. Bolaamphiphile-Class Surfactants Can Stabilize and Support the Function of Solubilized Integral Membrane Proteins. *Biochemistry* **2009**, *48* (49), 11606–11608.
- (151) De Rosa, M.; Gambacorta, A. The Lipids of Archaeobacteria. *Prog. Lipid Res.* **1988**, *27* (3), 153–175.
- (152) Petkovich, N. D.; Stein, A. Controlling Macro- and Mesostructures with Hierarchical Porosity through Combined Hard and Soft Templating. *Chem. Soc. Rev.* **2013**, *42* (9), 3721–3739.
- (153) Kobayashi, S.; Hamasaki, N.; Suzuki, M.; Kimura, M.; Shirai, H.; Hanabusa, K. Preparation of Helical Transition-Metal Oxide Tubes Using Organogelators as Structure-Directing Agents. *J. Am. Chem. Soc.* **2002**, *124* (23), 6550–6551.
- (154) Jung, J. H.; Ono, Y.; Hanabusa, K.; Shinkai, S. Creation of Both Right-Handed and Left-Handed Silica Structures by Sol–Gel Transcription of Organogel Fibers Comprised of Chiral Diaminocyclohexane Derivatives. *J. Am. Chem. Soc.* **2000**, *122* (20), 5008–5009.
- (155) Sans, M.; Illa, O.; Ortuño, R. M. Stereoselective Synthesis of All Stereoisomers of Orthogonally Protected Cyclobutane-1,2-Diamine and Some Chemoselective Transformations. *Org. Lett.* **2012**, *14* (10), 2431–2433.
- (156) Sans, M. The Chiral Cyclobutane Motif in Advanced Materials and Catalysis: Organogelators, Surfactants, Hybrid Silicas and Metal Ligands, Universitat Autònoma de Barcelona, 2014.
- (157) House, T. H. E. P.; The, O. F.; Academy, R. Improved Method for Determining the Temperature Dependence of Interfacial Tension at Liquid Crystal-Isotropic Liquid Interface. **2006**, *7* (1), 1–6.
- (158) *Lange's Handbook of Chemistry*, 11th ed.; Dean, J. A., Ed.; McGraw-Hill, Inc., 1967.
- (159) Czajka, A.; Hazell, G.; Eastoe, J. Surfactants at the Design Limit. *Langmuir* **2015**, *31* (30), 8205–8217.
- (160) Meher, J.; Dash, U.; Jena, S.; Misra, P. K. Investigation on Surface Activity and Aggregation Property of Mixed Solution of Cetyl Trimethyl Ammonium Bromide with Novel Gemini Surfactants with Ethoxy Ethyl Spacer. *Int. J. Adv. Chem. Sci. App.* **2013**, *1* (1), 16–20.
- (161) Menger, F. ; Wrenn, S. Interfacial and Micellar Properties of Bolaform Electrolytes &. *J. Phys. Chem.* **1974**, *78* (14), 1387–1390.
- (162) Kunitake, T.; Okahata, Y.; Shimomura, M.; Sho-ichiro, Y.; Takarabe, K. Formation of Stable Bilayer Assemblies. *J. Am. Chem. Soc.* **1981**, *103*, 5401–5413.
- (163) Wagner, J.; Härtl, W.; Hempelmann, R. Characterization of Monodisperse Colloidal Particles: Comparison between SAXS and DLS. *Langmuir* **2000**, *16* (9), 4080–4085.
- (164) Svergun, D. Basics of X-Ray Scattering by Solutions; 2012.
- (165) Anton Paar, G. The SAXS Guide. Anton Paar: Graz, Austria 2013.
- (166) Mezei, A.; Pérez, L.; Pinazo, A.; Comelles, F.; Infante, M. R.; Pons, R. Self Assembly of pH-Sensitive Cationic Lysine Based Surfactants. *Langmuir* **2012**, *28* (49), 16761–16771.
- (167) Ramakanth, I.; Patnaik, A. Novel Two-Component Gels of Cetylpyridinium Chloride and the Bola-Amphiphile 6-Amino Caproic Acid: Phase Evolution and Mechanism of Gel Formation. *J. Phys. Chem. B* **2012**, *116* (9), 2722–2729.
- (168) Pauw, B. R. How to Do a Perfect SAXS Measurement. **2011**.
- (169) Ferrer, S. ALBA Synchrotron Facility. *Synchrotron Radiat. News* **2016**, *29* (2), 23–28.
- (170) *Neutrons, X-Rays and Light Scattering Methods Applied to Soft Condensed Matter*; Lindner, P., Zemb, T., Eds.; Elsevier: Paris, 2002.
- (171) Chen, X.; Wang, J.; Shen, N.; Luo, Y.; Li, L.; Liu, M.; Thomas, R. K. Gemini Surfactant/DNA Complex Monolayers at the Air–Water Interface: Effect of Surfactant Structure on the Assembly, Stability, and Topography of Monolayers. *Langmuir* **2002**, *18* (16), 6222–6228.
- (172) Nagarajan, R. Self Assembly of Bola Amphiphiles. *Chem. Eng. Commun.* **1987**, *55* (1-6), 251–273.
- (173) Nagarajan, R. Amphiphilic Surfactants and Amphiphilic Polymers : Principles of Molecular Assembly. *ACS Symp. Ser.* **2011**, *Chapter 1*, 1–22.
- (174) Gouzy, M.-F.; Guidetti, B.; André-Barres, C.; Rico-Lattes, I.; Lattes, a.; Vidal, C. Aggregation Behavior in Aqueous Solutions of a New Class of Asymmetric Bipolar Amphiphiles Investigated by Surface Tension Measurements. *J. Colloid Interface Sci.* **2001**, *239* (2), 517–521.
- (175) Batsanov, S. Van Der Waals Radii of Elements. *Inorg. Mater.* **2001**, *37* (9), 871–885.
- (176) Nagarajan, R.; Ruckenstein, E. Aggregation of Amphiphiles as Micelles or Vesicles in Aqueous Media. *J. Colloid Interface Sci.* **1979**, *71* (3), 580–604.
- (177) R. Nagarajan. Mixed Surfactant Systems. *ACS Symp. Ser.* **1992**, *501*, 54–95.
- (178) Hartung, J.; Kopf, T.; Svoboda, I.; Fuess, H. Trimethylammonium Bromide at 100 K. *Acta Crystallogr. Sect. E Struct. Reports Online* **2006**, *62* (2), o570–o572.
- (179) Cavazzana-Calvo, M. Gene Therapy of Human Severe Combined Immunodeficiency (SCID)-X1

## 11. Bibliography

- Disease. *Science* (80- ). **2000**, *288* (5466), 669–672.
- (180) Manno, C. S.; Pierce, G. F.; Arruda, V. R.; Glader, B.; Ragni, M.; Rasko, J. J.; Rasko, J.; Ozelo, M. C.; Hoots, K.; Blatt, P.; et al. Successful Transduction of Liver in Hemophilia by AAV-Factor IX and Limitations Imposed by the Host Immune Response. *Nat. Med.* **2006**, *12* (3), 342–347.
- (181) *Gene and Stem Cell Therapy*; Boyd, A. C., Ed.; Karger: Basel: New York, 2006.
- (182) Maguire, A. M.; Simonelli, F.; Pierce, E. A.; Pugh, E. N.; Mingozzi, F.; Bencicelli, J.; Banfi, S.; Marshall, K. A.; Testa, F.; Surace, E. M.; et al. Safety and Efficacy of Gene Transfer for Leber’s Congenital Amaurosis. *N. Engl. J. Med.* **2008**, *358* (21), 2240–2248.
- (183) Kaplitt, M. G.; Feigin, A.; Tang, C.; Fitzsimons, H. L.; Mattis, P.; Lawlor, P. A.; Bland, R. J.; Young, D.; Strybing, K.; Eidelberg, D.; et al. Safety and Tolerability of Gene Therapy with an Adeno-Associated Virus (AAV) Borne GAD Gene for Parkinson’s Disease: An Open Label, Phase I Trial. *Lancet* **2007**, *369* (9579), 2097–2105.
- (184) Yang, Z. R.; Wang, H. F.; Zhao, J.; Peng, Y. Y.; Wang, J.; Guinn, B.-A.; Huang, L. Q. Recent Developments in the Use of Adenoviruses and Immunotoxins in Cancer Gene Therapy. *Cancer Gene Ther.* **2007**, *14* (7), 599–615.
- (185) *Advances in Genetics, Volume 89*; Friedmann, T., Dunlap, J. C., Goodwin, S. F., Eds.; Elsevier Inc.: Oxford, 2015.
- (186) Mintzer, M. A.; Simanek, E. E. Nonviral Vectors for Gene Delivery. *Chem. Rev.* **2009**, *109* (2), 259–302.
- (187) Niven, R.; Pearlman, R.; Wedeking, T.; Mackeigan, J.; Noker, P.; Simpson-Herren, L.; Smith, J. G. Biodistribution of Radiolabeled Lipid-DNA Complexes and DNA in Mice. *J. Pharm. Sci.* **1998**, *87* (11), 1292–1299.
- (188) Stekar, J.; Nössner, G.; Kutscher, B.; Engel, J.; Hilgard, P. Synthesis, Antitumor Activity, and Tolerability of Phospholipids Containing Nitrogen Homologues. *Angew. Chemie Int. Ed. Engl.* **1995**, *34* (2), 238–240.
- (189) Wettig, S. D.; Verrall, R. E.; Foldvari, M. Gemini Surfactants : A New Family of Building Blocks for Non-Viral Gene Delivery Systems. *Curr. Gene Ther.* **2008**, *8*, 9–23.
- (190) Boussif, O.; Lezoualc’h, F.; Zanta, M. A.; Mergny, M. D.; Scherman, D.; Demeneix, B.; Behr, J. P. A Versatile Vector for Gene and Oligonucleotide Transfer into Cells in Culture and in Vivo: Polyethylenimine. *Proc. Natl. Acad. Sci.* **1995**, *92* (16), 7297–7301.
- (191) Veeralakshmi, S.; Nehru, S.; Sabapathi, G.; Arunachalam, S.; Venuvanalingam, P.; Kumar, P.; Anusha, C.; Ravikumar, V. Single and Double Chain surfactant–cobalt(III) Complexes: The Impact of Hydrophobicity on the Interaction with Calf Thymus DNA, and Their Biological Activities. *RSC Adv.* **2015**, *5* (40), 31746–31758.
- (192) Buhleier, E.; Wehner, W.; Vögtle, F. “Cascade”- and “Nonskid-Chain-like” Syntheses of Molecular Cavity Topologies. *Synthesis (Stuttg.)*. **1978**, *1978* (02), 155–158.
- (193) Ahmed, T.; Kamel, A. O.; Wettig, S. D. Interactions between DNA and Gemini Surfactant: Impact on Gene Therapy: Part I. *Nanomedicine* **2016**, *10*.2217/nnm.15.203.
- (194) Ahmed, T.; Kamel, A. O.; Wettig, S. D. Interactions between DNA and Gemini Surfactant: Impact on Gene Therapy: Part II. *Nanomedicine* **2016**, *10*.2217/nnm.15.204.
- (195) Zhu, D.-M.; Evans, R. K. Molecular Mechanism and Thermodynamics Study of Plasmid DNA and Cationic Surfactants Interactions. *Langmuir* **2006**, *22* (8), 3735–3743.
- (196) Shirahama, K.; Takashima, K.; Takisawa, N. Interaction between Dodecyltrimethylammonium Chloride and DNA. *Bull. Chem. Soc. Jpn.* **1987**, *60* (1), 43–47.
- (197) Guo, X.; Huang, L. Recent Advances in Nonviral Vectors for Gene Delivery. *Acc. Chem. Res.* **2012**, *45* (7), 971–979.
- (198) Wang, W.; Li, W.; Ma, N.; Steinhoff, G. Non-Viral Gene Delivery Methods. *Curr. Pharm. Biotechnol.* **2013**, *14* (1), 46–60.
- (199) Matulis, D.; Rouzina, I.; Bloomfield, V. A. Thermodynamics of Cationic Lipid Binding to DNA and DNA Condensation: Roles of Electrostatics and Hydrophobicity. *J. Am. Chem. Soc.* **2002**, *124* (25), 7331–7342.
- (200) Husale, S.; Grange, W.; Karle, M.; Bürgi, S.; Hegner, M. Interaction of Cationic Surfactants with DNA: A Single-Molecule Study. *Nucleic Acids Res.* **2008**, *36* (5), 1443–1449.
- (201) Bathaie, S. Z.; Moosavi-Movahedi, A. A.; Saboury, A. A. Energetic and Binding Properties of DNA upon Interaction with Dodecyl Trimethylammonium Bromide. *Nucleic Acids Res.* **1999**, *27* (4), 1001–1005.
- (202) Carlstedt, J.; Lundberg, D.; Dias, R. S.; Lindman, B. Condensation and Decondensation of DNA by Cationic Surfactant, Spermine, or Cationic Surfactant-Cyclodextrin Mixtures: Macroscopic Phase

- Behavior, Aggregate Properties, and Dissolution Mechanisms. *Langmuir* **2012**, *28* (21), 7976–7989.
- (203) Dias, R. S.; Magno, L. M.; Valente, A. J. M.; Das, D.; Das, P. K.; Maiti, S.; Miguel, M. G.; Lindman, B. Interaction between DNA and Cationic Surfactants: Effect of DNA Conformation and Surfactant Headgroup. *J. Phys. Chem. B* **2008**, *112* (46), 14446–14452.
- (204) Cheng, C.; Ran, S.-Y. Interaction between DNA and Trimethyl-Ammonium Bromides with Different Alkyl Chain Lengths. *Sci. World J.* **2014**, *2014* (863049), 1–9.
- (205) Dias, R.; Rosa, M.; Canelas Pais, A.; Miguel, M.; Lindman, B. DNA-Surfactant Interactions. Compaction, Condensation, Decompaction and Phase Separation. *J. Chinese Chem. Soc.* **2004**, *51*, 447–469.
- (206) Grueso, E.; Cerrillos, C.; Hidalgo, J.; Lopez-Cornejo, P. Compaction and Decompaction of DNA Induced by the Cationic Surfactant CTAB. *Langmuir* **2012**, *28* (30), 10968–10979.
- (207) Pinnaduwaage, P.; Schmitt, L.; Huang, L. Use of a Quaternary Ammonium Detergent in Liposome Mediated DNA Transfection of Mouse L-Cells. *Biochim. Biophys. Acta* **1989**, *985* (1), 33–37.
- (208) Ainalem, M.-L.; Bartles, A.; Muck, J.; Dias, R. S.; Carnerup, A. M.; Zink, D.; Nylander, T. DNA Compaction Induced by a Cationic Polymer or Surfactant Impact Gene Expression and DNA Degradation. *PLoS One* **2014**, *9* (3), e92692 (1–12).
- (209) Pérez, N.; Pérez, L.; Infante, M. R.; García, M. T. Biological Properties of Arginine-Based Glycerolipidic Cationic Surfactants. *Green Chem.* **2005**, *7*, 540–546.
- (210) Infante, M. R.; Pérez, L.; Morán, M. C.; Pons, R.; Mitjans, M.; Vinardell, M. P.; Garcia, M. T.; Pinazo, A. Biocompatible Surfactants from Renewable Hydrophiles. *Eur. J. Lipid Sci. Technol.* **2010**, *112* (1), 110–121.
- (211) Pinazo, A.; Pons, R.; Pérez, L.; Infante, M. R. Amino Acids as Raw Material for Biocompatible Surfactants. *Ind. Eng. Chem. Res.* **2011**, *50* (9), 4805–4817.
- (212) Chandra, N.; Tyagi, V. K. Synthesis, Properties, and Applications of Amino Acids Based Surfactants: A Review. *J. Dispers. Sci. Technol.* **2013**, *34* (6), 800–808.
- (213) Foley, P.; Kermanshahi pour, A.; Beach, E. S.; Zimmerman, J. B. Derivation and Synthesis of Renewable Surfactants. *Chem. Soc. Rev.* **2012**, *41* (4), 1499–1518.
- (214) Fielden, M. L.; Perrin, C.; Kremer, A.; Bergsma, M.; Stuart, M. C.; Camilleri, P.; Engberts, J. B. F. N. Sugar-Based Tertiary Amino Gemini Surfactants with a Vesicle-to-Micelle Transition in the Endosomal pH Range Mediate Efficient Transfection in Vitro. *Eur. J. Biochem.* **2001**, *268* (5), 1269–1279.
- (215) Al-Dosari, M. S.; Gao, X. Nonviral Gene Delivery: Principle, Limitations, and Recent Progress. *AAPS J.* **2009**, *11* (4), 671–681.
- (216) Sorrenti, A.; Illa, O.; Pons, R.; Ortuño, R. M. Chiral Cyclobutane  $\beta$ -Amino Acid-Based Amphiphiles: Influence of *Cis* / *Trans* Stereochemistry on Solution Self-Aggregation and Recognition. *Langmuir* **2015**, *31* (35), 9608–9618.
- (217) Sorrenti, A.; Illa, O.; Ortuño, R. M.; Pons, R. Chiral Cyclobutane  $\beta$ -Amino Acid-Based Amphiphiles: Influence of *Cis*/*Trans* Stereochemistry on Condensed Phase and Monolayer Structure. *Langmuir* **2016**, *32*, 6977–6984.
- (218) Bouzas, M. Master Thesis, 2012.
- (219) *Química Analítica Cualitativa*, 18th ed.; Burriel Martí, F., Lucena Conde, F., Arribas Jimeno, S., Hernández Méndez, J., Eds.; Internation Thomson Editores: Madrid, 2008.
- (220) Goldsipe, A.; Blankschtein, D. Molecular-Thermodynamic Theory of Micellization of pH-Sensitive Surfactants. *Langmuir* **2006**, *22* (8), 3547–3559.
- (221) Goldsipe, A.; Blankschtein, D. Titration of Mixed Micelles Containing a pH-Sensitive Surfactant and Conventional (pH-Insensitive) Surfactants: A Regular Solution Theory Modeling Approach. *Langmuir* **2006**, *22* (24), 9894–9904.
- (222) Söderman, O.; Jönsson, B.; Olofsson, G. Titration of Fatty Acids Solubilized in Cationic and Anionic Micelles. Calorimetry and Thermodynamic Modeling. *J. Phys. Chem. B* **2006**, *110* (7), 3288–3293.
- (223) Kleven, H. B. Critical Micelle Concentrations as Determined by Refraction. *J. Phys. Colloid Chem.* **1948**, *52* (1), 130–148.
- (224) Okuda, H.; Imae, T.; Ikeda, S. The Adsorption of Cetyltrimethylammonium Bromide on Aqueous Surfaces of Sodium Bromide Solutions. *Colloids and Surfaces* **1987**, *27* (4), 187–200.
- (225) Chiappisi, L.; Yalcinkaya, H.; Gopalakrishnan, V. K.; Gradzielski, M.; Zemb, T. Catanionic Surfactant Systems—thermodynamic and Structural Conditions Revisited. *Colloid Polym. Sci.* **2015**, *293* (11), 3131–3143.
- (226) Nobbmann, U. Polydispersity – what does it mean for DLS and chromatography?

## 11. Bibliography

- <http://www.materials-talks.com/blog/2014/10/23/polydispersity-what-does-it-mean-for-dls-and-chromatography/>.
- (227) Koppel, D. E. Analysis of Macromolecular Polydispersity in Intensity Correlation Spectroscopy: The Method of Cumulants. *J. Chem. Phys.* **1972**, *57* (11), 4814–4820.
- (228) Mohanty, A.; Dey, J. Effect of the Headgroup Structure on the Aggregation Behavior and Stability of Self-Assemblies of Sodium N-[4-(n-Dodecyloxy)benzoyl]-L-Aminoacidates in Water. *Langmuir* **2007**, *23* (3), 1033–1040.
- (229) El-Hachemi, Z.; Mancini, G.; Ribó, J. M.; Sorrenti, A. Role of the Hydrophobic Effect in the Transfer of Chirality from Molecules to Complex Systems: From Chiral Surfactants to Porphyrin/surfactant Aggregates. *J. Am. Chem. Soc.* **2008**, *130* (45), 15176–15184.
- (230) Shinitzky, M.; Haimovitz, R. Chiral Surfaces in Micelles of Enantiomeric N-Palmitoyl-and N-Stearoylserine. *J. Am. Chem. Soc.* **1993**, *115* (9), 12545–12549.
- (231) Domínguez, A.; Fernández, A.; González, N.; Iglesias, E.; Montenegro, L. Determination of Critical Micelle Concentration of Some Surfactants by Three Techniques. *J. Chem. Educ.* **1997**, *74* (10), 1227–1231.
- (232) Tahirat, N.; Luis, A.; Mindy, L. Determination of Critical Micelle Concentrations Using UV-Visible Spectroscopy. *J. High Sch. Res.* **2011**, *2* (1), 1–6.
- (233) Yu, D.; Huang, F.; Xu, H. Determination of Critical Concentrations by Synchronous Fluorescence Spectrometry. *Anal. Methods* **2012**, *4* (1), 47–49.
- (234) Tanhaei, B.; Saghatoleslami, N.; Chenar, M. P.; Ayati, A.; Hesampour, M.; Mänttari, M. Experimental Study of CMC Evaluation in Single and Mixed Surfactant Systems, Using the UV-Vis Spectroscopic Method. *J. Surfactants Deterg.* **2012**, *16* (3), 357–362.
- (235) Polavarapu, P. L.; Vijay, R. Chiroptical Spectroscopy of Surfactants. *J. Phys. Chem. A* **2012**, *116* (21), 5112–5118.
- (236) Boleda, M. D.; Briones, P.; Farrés, J.; Tyfield, L.; Pi, R. Experimental Design: A Useful Tool for PCR Optimization. *Biotechniques* **1996**, *21* (1), 134–140.
- (237) Chien, A.; Edgar, D. B.; Trela, J. M. Deoxyribonucleic Acid Polymerase from the Extreme Thermophile *Thermus Aquaticus*. *J. Bacteriol.* **1976**, *127* (3), 1550–1557.
- (238) Haugand, R. P.; Yue, S. T.; Millard, P. J.; Roth, B. L. Cyclic-Substituted Unsymmetrical Cyanine Dyes. US5436134, 1995.
- (239) Jadhav, V. M.; Valaske, R.; Maiti, S. Interaction between 14mer DNA Oligonucleotide and Cationic Surfactants of Various Chain Lengths. *J. Phys. Chem. B* **2008**, *112* (29), 8824–8831.
- (240) *The Colloidal Domain: Where Physics, Chemistry, Technology and Biology Meet*; Evans, D. F., Wennerström, H., Eds.; VCH: New York, 1994.
- (241) Zhu, D.-M.; Evans, R. K. Molecular Mechanism and Thermodynamics Study of Plasmid DNA and Cationic Surfactants Interactions. *Langmuir* **2006**, *22* (8), 3735–3743.
- (242) Diamant, H.; Andelman, D. Self-Assembly in Mixtures of Polymers and Small Associating Molecules. *Macromolecules* **2000**, *33* (21), 8050–8061.
- (243) Kypr, J.; Kejnovská, I.; Renčuk, D.; Vorlíčková, M. Circular Dichroism and Conformational Polymorphism of DNA. *Nucleic Acids Res.* **2009**, *37* (6), 1713–1725.
- (244) Grueso, E.; Kuliszewska, E.; Roldan, E.; Perez-Tejeda, P.; Prado-Gotor, R.; Brecker, L. DNA Conformational Changes Induced by Cationic Gemini Surfactants: The Key to Switching DNA Compact Structures into Elongated Forms. *RSC Adv.* **2015**, *5* (37), 29433–29446.
- (245) Hourii, S. J.; Buss, V. Circular Dichroism and Derivative Spectra Study of the Excitonic Aggregation of Pinacyanol by Aerosol-OT. *Open J. Phys. Chem.* **2012**, *2*, 34–40.
- (246) Chang, Y.-M.; Chen, C. K.-M.; Hou, M.-H. Conformational Changes in DNA upon Ligand Binding Monitored by Circular Dichroism. *Int. J. Mol. Sci.* **2012**, *13* (3), 3394–3413.
- (247) *Chapter 9 - Quantitative DNase Footprint Titration: A Method for Studying Protein-DNA Interactions*; Brenowitz, M., Seneor, D. F., Shea, M. A., Ackers, G. K., Eds.; Methods in Enzymology; Elsevier, 1986; Vol. 130.
- (248) Watson, R. J.; Schildkraut, I.; Qiang, B.-Q.; Martin, S. M.; Visentin, L. P. NdeI: A Restriction Endonuclease from *Neisseria Denitrificans* Which Cleaves DNA at 5'-CATATG-3' Sequences. *FEBS Lett.* **1982**, *150* (1), 114–116.
- (249) Motais, R.; Guizouarn, H.; Garcia-Romeu, F. Red Cell Volume Regulation: The Pivotal Role of Ionic Strength in Controlling Swelling-Dependent Transport Systems. *Biochim. Biophys. Acta* **1991**, *1075*, 169–180.
- (250) Mouat, M. F.; Manchester, K. L. The Intracellular Ionic Strength of Red Cells and the Influence of

- Complex Formation. *Comp. Haematol. Int.* **1998**, *8*, 58–60.
- (251) Lindman, B.; Antunes, F.; Aidarova, S.; Miguel, M.; Nylander, T. Polyelectrolyte-Surfactant Association—from Fundamentals to Applications. *Colloid J.* **2014**, *76* (5), 585–594.
- (252) Thalberg, K.; Lindman, B.; Karlström, G. Phase Behavior of a System of Cationic Surfactant and Anionic Polyelectrolyte: The Effect of Salt. *J. Phys. Chem.* **1991**, *95*, 6004–6011.
- (253) Engel, R. H.; Riggitt, S. J. Intestinal Absorption of Heparin Facilitated by Sulfated or Sulfonated Surfactants. *J. Pharm. Sci.* **1969**, *58* (6), 706–710.
- (254) Song, W. W.; Li, N. B.; Luo, H. Q. Gemini Surfactant Applied to the Heparin Assay at the Nanogram Level by Resonance Rayleigh Scattering Method. *Anal. Biochem.* **2012**, *422* (1), 1–6.
- (255) Sun, W.; Han, J.; Li, Q.; Jiao, K. Spectrophotometric and Voltammetric Studies on the Interaction of Heparin with Crystal Violet and Its Analytical Application. *South African J. Chem.* **2015**, *60*, 42–46.
- (256) Yongliang, C.; Malek, M.; Gulilat, G. Transfection Reagents. US8785200(B2), 2012.
- (257) Zhou, T.; Llizo, A.; Li, P.; Wang, C.; Guo, Y.; Ao, M.; Bai, L. High Transfection Efficiency of Homogeneous DNA Nanoparticles Induced by Imidazolium Gemini Surfactant as Nonviral Vector. *J. Phys. Chem. C* **2013**, *117*, 26573–26581.
- (258) Perrone, S.; Usai, M.; Lazzari, P.; Tucker, S. J.; Wallace, H. M.; Zanda, M. Efficient Cell Transfection with Melamine-Based Gemini Surfactants. **2013**.
- (259) Guo, X.; Yu, F.; Ran, X.; Song, X.; Ding, J.; Wang, Y. Vesicle Formation between Single-Chained Cationic Surfactant and Plasmid DNA and Its Application in Cell Transfection. *Colloid Polym. Sci.* **2014**, *292* (12), 3103–3111.
- (260) Cardoso, A. M.; Morais, C. M.; Cruz, A. R.; Silva, S. G.; Luísa, M.; Marques, E. F.; Pedroso, M. C.; Lima, D.; Jurado, A. S. New Serine-Derived Gemini Surfactants as Gene Delivery Systems. *Eur. J. Pharm. Biopharm.* **2015**, *89*, 347–356.
- (261) Kolossváry, I.; Guida, W. C. Low Mode Search. An Efficient, Automated Computational Method for Conformational Analysis: Application to Cyclic and Acyclic Alkanes and Cyclic Peptides. *J. Am. Chem. Soc.* **1996**, *118* (21), 5011–5019.
- (262) Kaminski, G. A.; Friesner, R. A.; Tirado-Rives, J.; Jorgensen, W. L. Evaluation and Reparametrization of the OPLS-AA Force Field for Proteins via Comparison with Accurate Quantum Chemical Calculations on Peptides. *J. Phys. Chem. B* **2001**, *105* (28), 6474–6487.
- (263) Mohamadi, F.; Richards, N. G. J.; Guida, W. C.; Liskamp, R.; Lipton, M.; Caufield, C.; Chang, G.; Hendrickson, T.; Still, W. C. MacroModel: An Integrated Software System for Modeling Organic and Bioorganic Molecules Using Molecular Mechanics. *J. Comput. Chem.* **1990**, *11* (4), 440–467.
- (264) Zhao, Y.; Truhlar, D. G. Density Functional for Spectroscopy: No Long-Range Self-Interaction Error, Good Performance for Rydberg and Charge-Transfer States, and Better Performance on Average than B3LYP for Ground States. *J. Phys. Chem. A* **2006**, *110* (49), 13126–13130.
- (265) Frisch, M. J.; Trucks, G. W.; Schlegel, H. B.; Scuseria, G. E.; Robb, M. A.; Cheeseman, J. R.; Scalmani, G.; Barone, V.; Mennucci, B.; Petersson, G. A.; et al. Gaussian 09. Wallingford CT 2009.
- (266) Zhao, Y.; Truhlar, D. G. The M06 Suite of Density Functionals for Main Group Thermochemistry, Thermochemical Kinetics, Noncovalent Interactions, Excited States, and Transition Elements: Two New Functionals and Systematic Testing of Four M06-Class Functionals and 12 Other Function. *Theor. Chem. Acc.* **2007**, *120*, 215–241.
- (267) Zhao, Y.; Truhlar, D. G. A New Local Density Functional for Main-Group Thermochemistry, Transition Metal Bonding, Thermochemical Kinetics, and Noncovalent Interactions. *J. Chem. Phys.* **2006**, *125* (19), 194101.
- (268) Boys, S. F.; Bernardi, F. The Calculation of Small Molecular Interactions by the Differences of Separate Total Energies. Some Procedures with Reduced Errors. *Mol. Phys.* **1970**, *19* (4), 553–566.
- (269) Davidson, E. R.; Feller, D. Basis Set Selection for Molecular Calculations. *Chem. Rev.* **1986**, *86* (4), 681–696.
- (270) Muddana, H. S.; Gilson, M. K. Calculation of Host-Guest Binding Affinities Using a Quantum-Mechanical Energy Model. *J. Chem. Theory Comput.* **2012**, *8* (6), 2023–2033.
- (271) Marenich, A. V.; Cramer, C. J.; Truhlar, D. G. Universal Solvation Model Based on Solute Electron Density and on a Continuum Model of the Solvent Defined by the Bulk Dielectric Constant and Atomic Surface Tensions. *J. Phys. Chem. B* **2009**, *113* (18), 6378–6396.
- (272) Tomasi, J.; Mennucci, B.; Cammi, R. Quantum Mechanical Continuum Solvation Models. *Chem. Rev.* **2005**, *105* (8), 2999–3093.
- (273) *Quantum Chemistry*; Levine, I. N., Ed.; Prentice Hall: New Jersey, 2001.
- (274) Foster, J. P.; Weinhold, F. Natural Hybrid Orbitals. *J. Am. Chem. Soc.* **1980**, *102* (24), 7211–7218.



## 11. Bibliography

- (275) Bryantsev, V. S.; Diallo, M. S.; Goddard, W. A. Calculation of Solvation Free Energies of Charged Solutes Using Mixed Cluster/continuum Models. *J. Phys. Chem. B* **2008**, *112* (32), 9709–9719.
- (276) Kelly, C. P.; Cramer, C. J.; Truhlar, D. G. SM6: A Density Functional Theory Continuum Solvation Model for Calculating Aqueous Solvation Free Energies of Neutrals, Ions, and Solute–Water Clusters. *J. Chem. Theory Comput.* **2005**, *1* (6), 1133–1152.
- (277) Cramer, C. J. *Essentials of Computational Chemistry*, 2nd editio.; John Wiley & Sons, 2004.
- (278) Kobko, N.; Paraskevas, L.; del Rio, E.; Dannenberg, J. J. Cooperativity in Amide Hydrogen Bonding Chains: Implications for Protein-Folding Models. *J. Am. Chem. Soc.* **2001**, *123* (18), 4348–4349.
- (279) Bauernshmitt, R.; Ahlrichs, R. Treatment of Electronic Excitations within the Adiabatic Approximation of Time Dependent Density Functional Theory. *Chem. Phys. Lett.* **1996**, *256*, 454–464.
- (280) Autschbach, J.; Ziegler, T.; van Gisbergen, S. J. A.; Baerends, E. J. Chiroptical Properties from Time-Dependent Density Functional Theory. I. Circular Dichroism Spectra of Organic Molecules. *J. Chem. Phys.* **2002**, *116* (16), 6930.
- (281) Stratmann, R. E.; Scuseria, G. E.; Frisch, M. J. An Efficient Implementation of Time-Dependent Density-Functional Theory for the Calculation of Excitation Energies of Large Molecules. *J. Chem. Phys.* **1998**, *109* (19), 8218.
- (282) Yanai, T.; Tew, D. P.; Handy, N. C. A New Hybrid Exchange–correlation Functional Using the Coulomb-Attenuating Method (CAM-B3LYP). *Chem. Phys. Lett.* **2004**, *393* (1-3), 51–57.
- (283) O’Boyle, N. M.; Tenderholt, A. L.; Langner, K. M. Cclib: A Library for Package-Independent Computational Chemistry Algorithms. *J. Comput. Chem.* **2008**, *29* (5), 839–845.
- (284) Pinazo, A.; Angelet, M.; Pons, R.; Lozano, M.; Infante, M. R.; Pérez, L. Lysine-Bisglycidol Conjugates as Novel Lysine Cationic Surfactants. *Langmuir* **2009**, *25* (14), 7803–7814.
- (285) Maurstad, G.; Danielsen, S.; Stokke, B. T. Analysis of Compacted Semiflexible Polyanions Visualized by Atomic Force Microscopy: Influence of Chain Stiffness on the Morphologies of Polyelectrolyte Complexes †. *J. Phys. Chem. B* **2003**, *107* (32), 8172–8180.
- (286) Castiglioni, E.; Biscarini, P.; Abbate, S. Experimental Aspects of Solid State Circular Dichroism. *Chirality* **2009**, *21*, 28–36.
- (287) Kekicheff, P.; Spalla, O. Refractive Index of Thin Aqueous Films Confined between Two Hydrophobic Surfaces. *Langmuir* **1994**, *10* (5), 1584–1591.
- (288) Yu, C.; Irudayaraj, J. Quantitative Evaluation of Sensitivity and Selectivity of Multiplex nanoSPR Biosensor Assays. *Biophys. J.* **2007**, *93* (10), 3684–3692.
- (289) Matsoukas, J.; Moharir, Y. E.; Findlay, J. A. A Convenient Method for the Isolation of Free Amino Acids from Marine Invertebrates. *J. Nat. Prod.* **1983**, *46* (4), 582–585.
- (290) Aguilera, J.; Moglioni, A. G.; Moltrasio, G. Y.; Ortuño, R. M. Stereodivergent Synthesis of the First Bis(cyclobutane)  $\beta$ -Dipeptides and Mixed  $\beta$ -Oligomers. *Tetrahedron: Asymmetry* **2008**, *19* (3), 302–308.
- (291) Mintzer, M. A.; Simanek, E. E. Nonviral Vectors for Gene Delivery. **2009**, No. 979, 259–302.

## **12. Annex**

---



## 12. Annex

### 12.1 CryoTEM images of pH-dependent surfactants

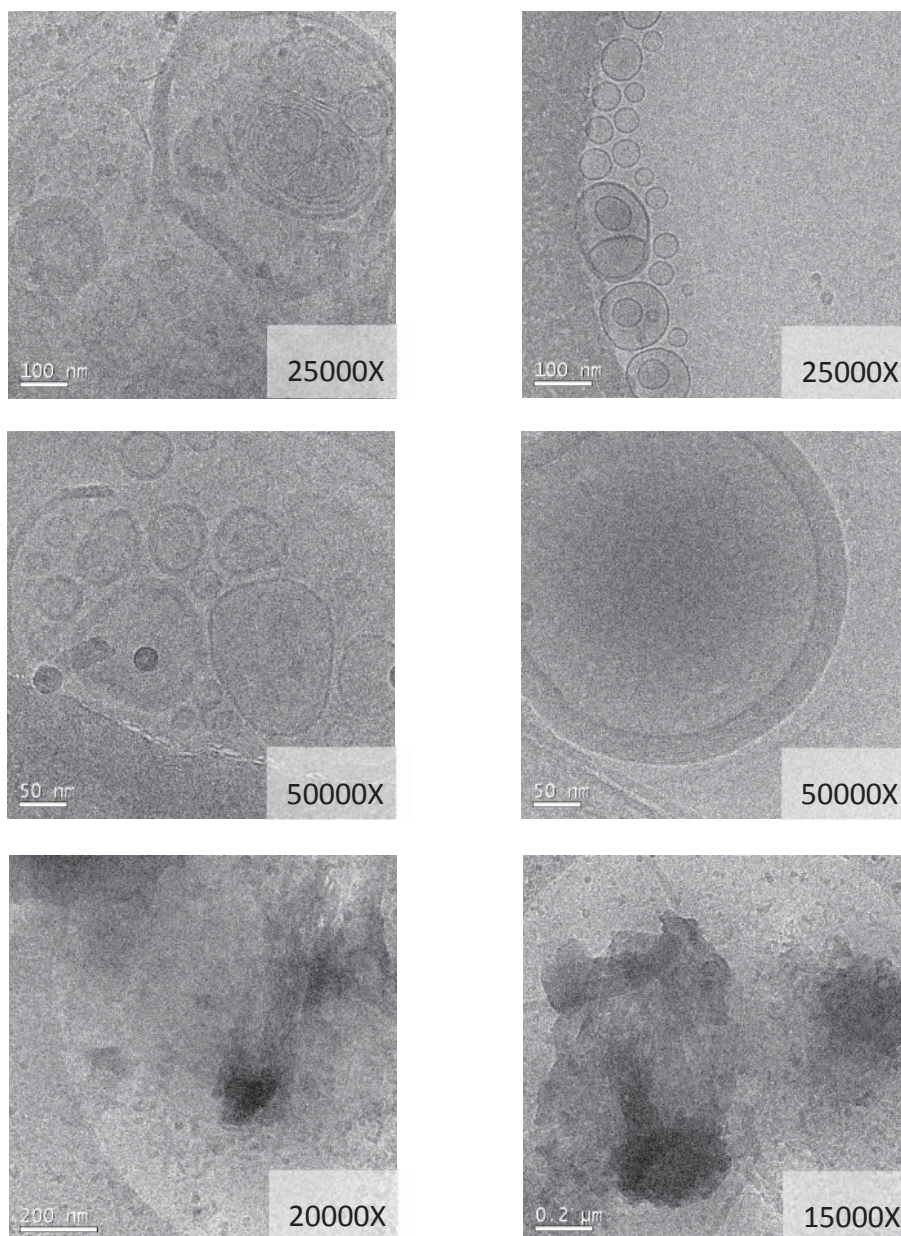


**Figure 142.** CryoTEM images of **C12** at three different pH's: 2 (top), natural (middle) and 12 (bottom).

12. Annex

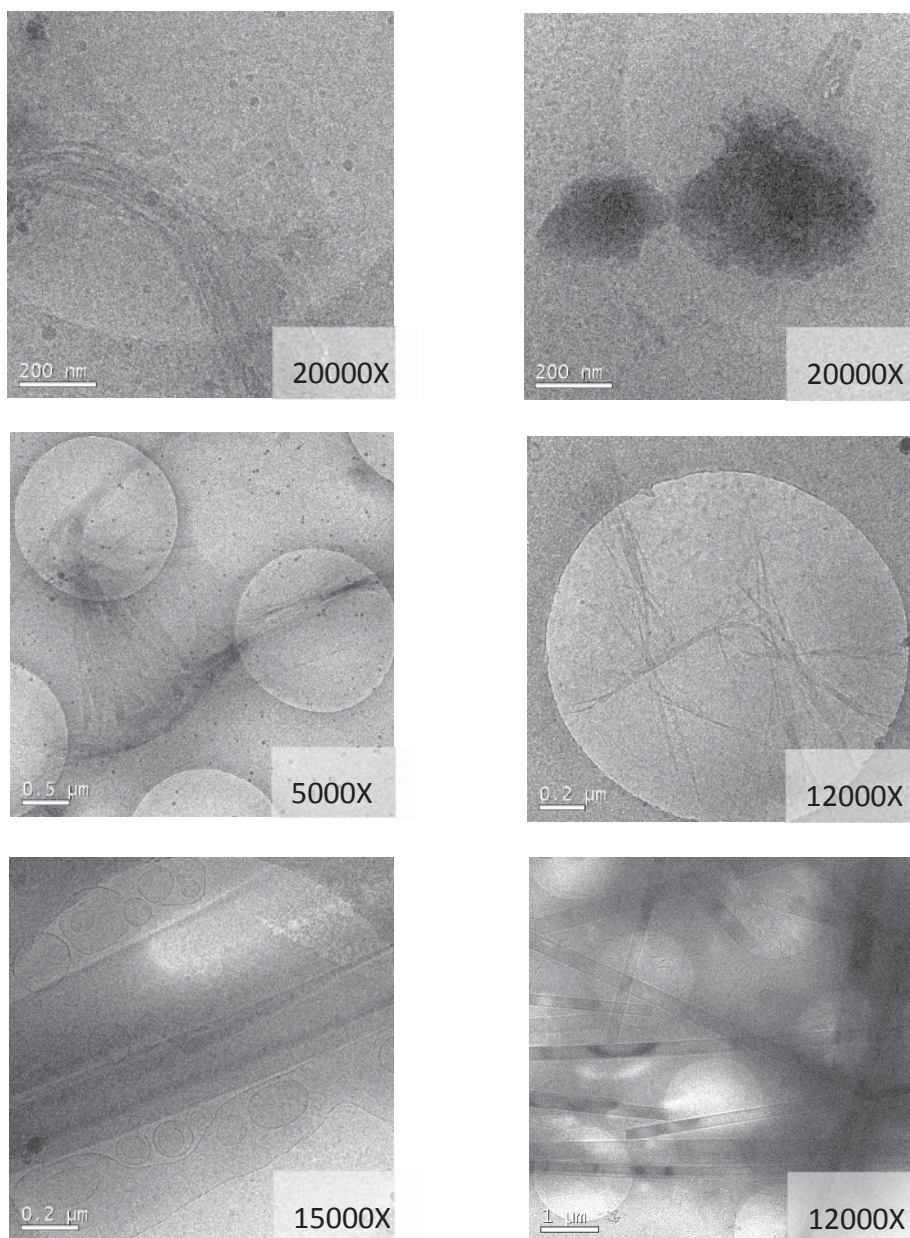


**Figure 143.** CryoTEM images of **T12** at three different pH's: 2 (top), natural (middle) and 12 (bottom).

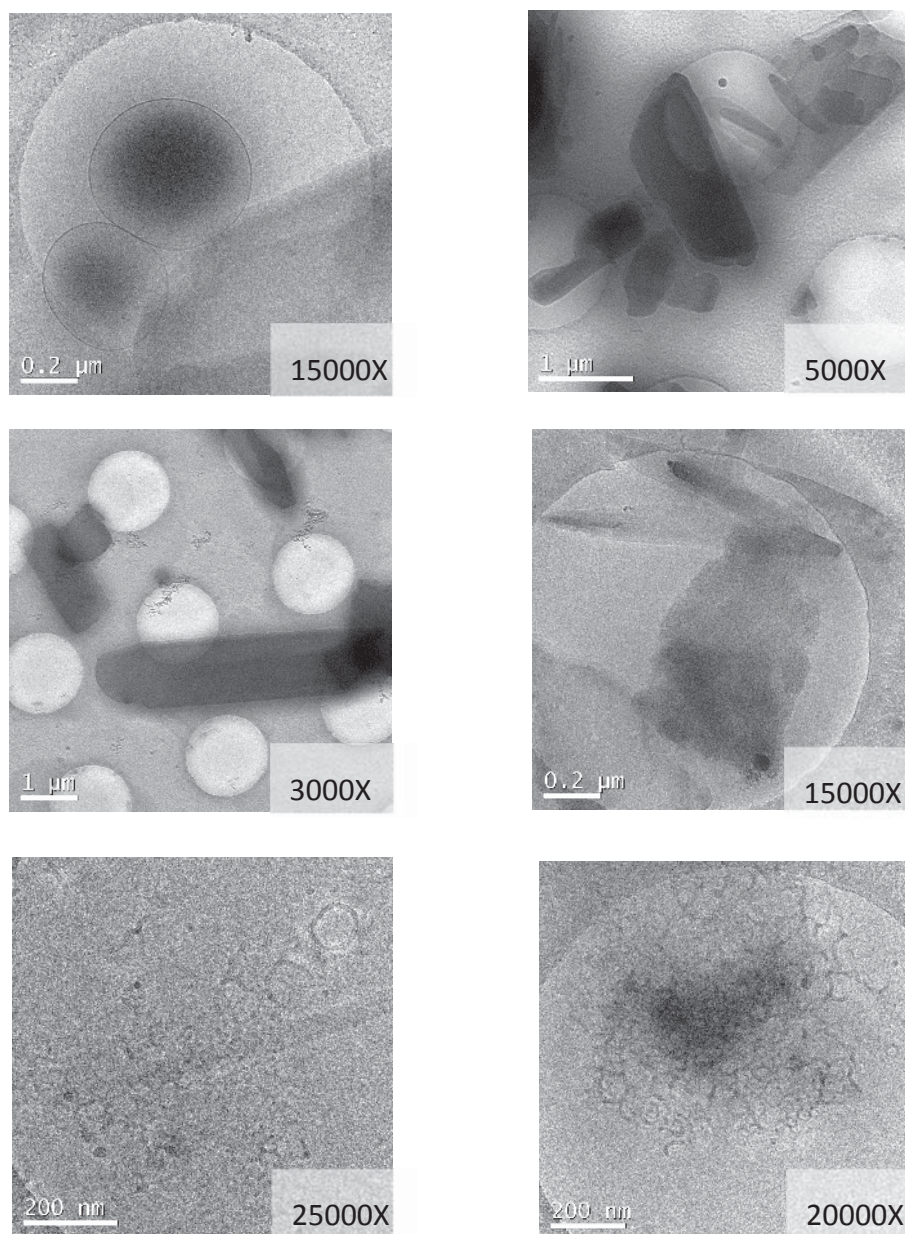


**Figure 144.** CryoTEM images of **C16** at three different pH's: 2 (top), natural (middle) and 12 (bottom).

12. Annex

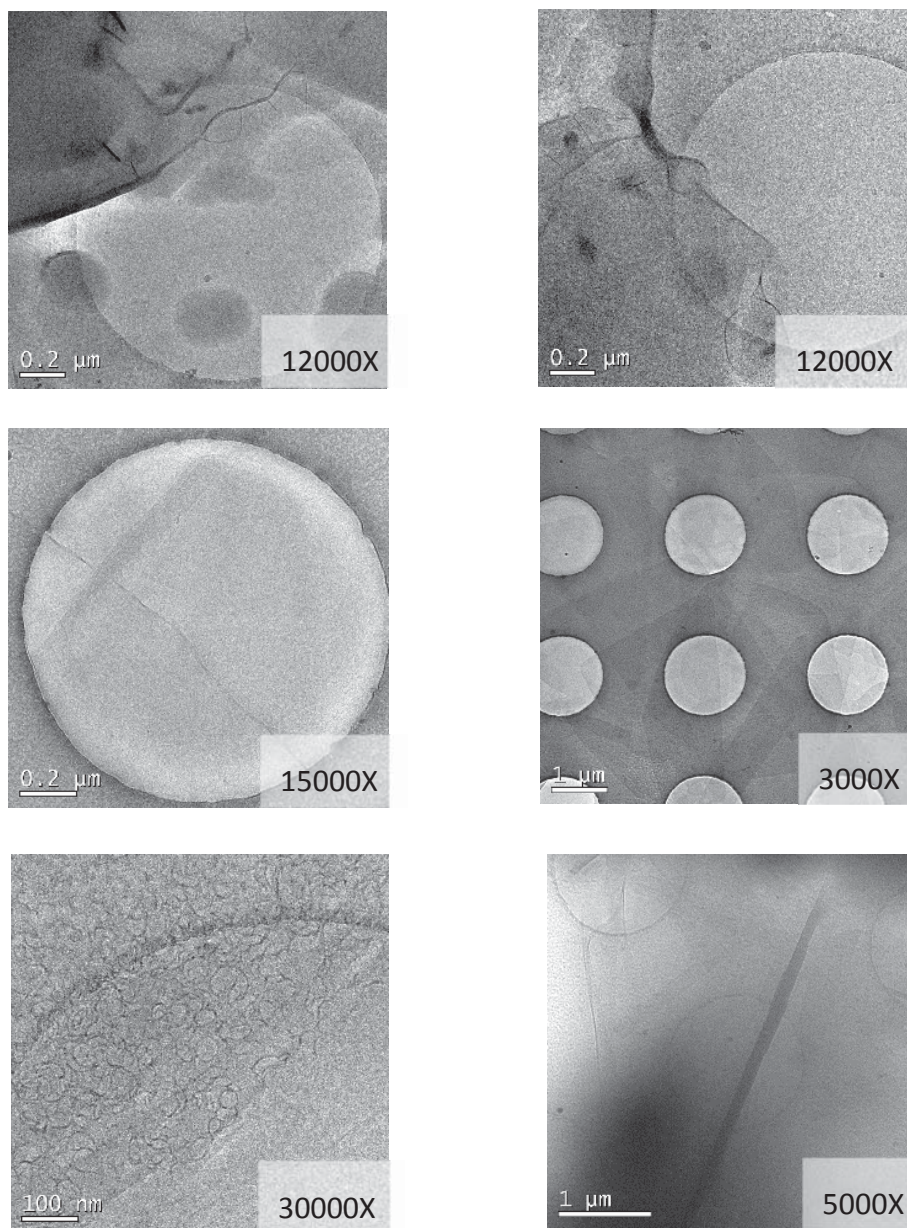


**Figure 145.** CryoTEM images of **T16** at three different pH's: 2 (top), natural (middle) and 12 (bottom).

## 12.2 Correlation curves of DLS

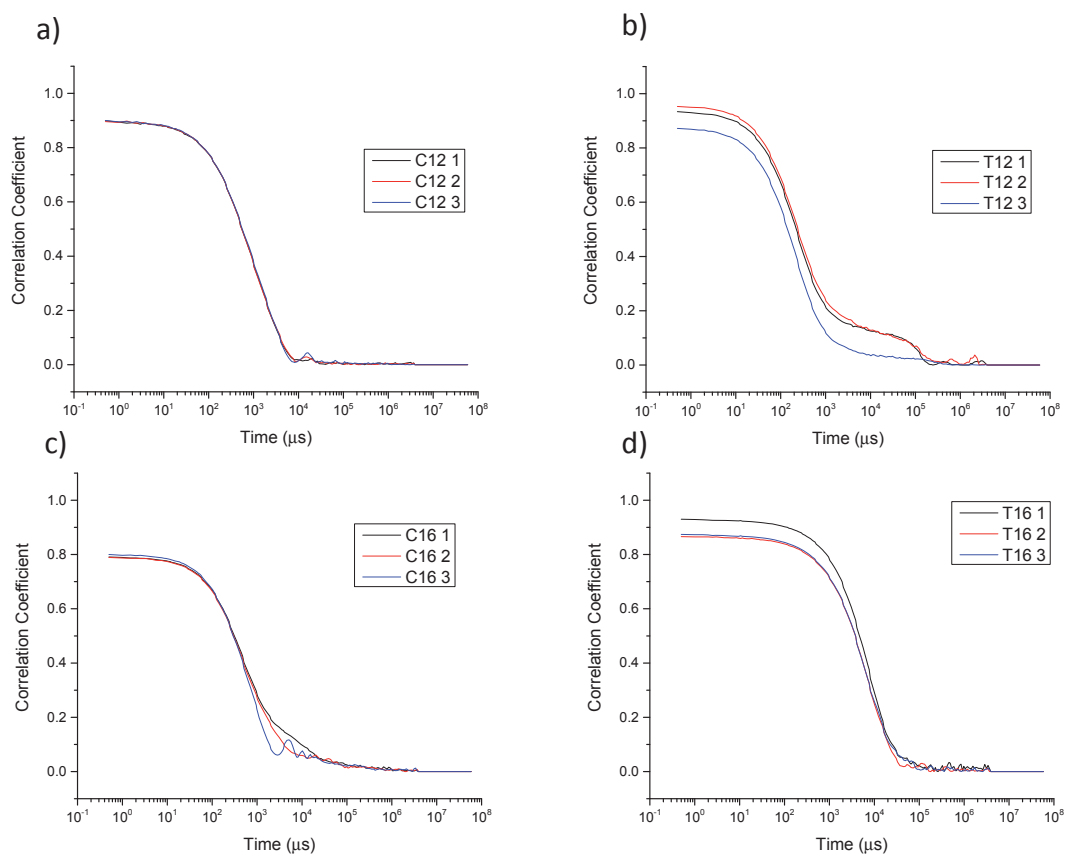


**Figure 146.** Correlation function of the DLS measurements of surfactant a) **C12**, b) **T12**, c) **C16** and d) **T16**.



### 12.3 Emission Spectra of DNA-GelStar® complexes at different surfactant concentrations

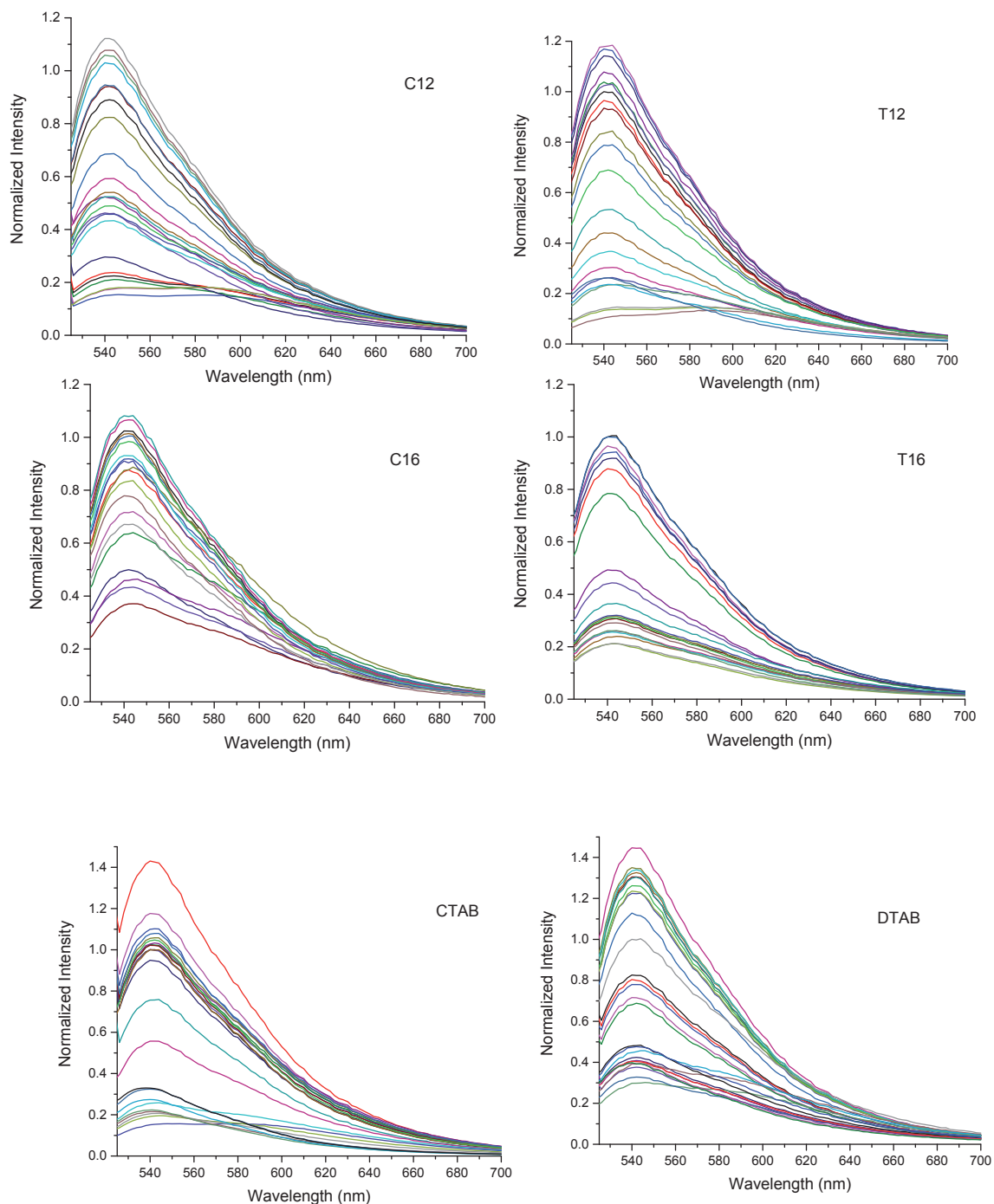


**Figure 147.** Emission Spectra of DNA-GelStar complexes at different surfactant concentrations.

## 12.4 Comparison between the results obtained from DEA and EMSA

To compare the obtained results, the superposition of the DEA and the EMSA results were represented. These two techniques give us different information about the formed complexes, but the behaviour of these surfactants with DNA can be compared. Superposed graphics are shown in Figure 148. Blue line represents the  $Z_{hp-3}$  and purple line show the CMC of the surfactant.

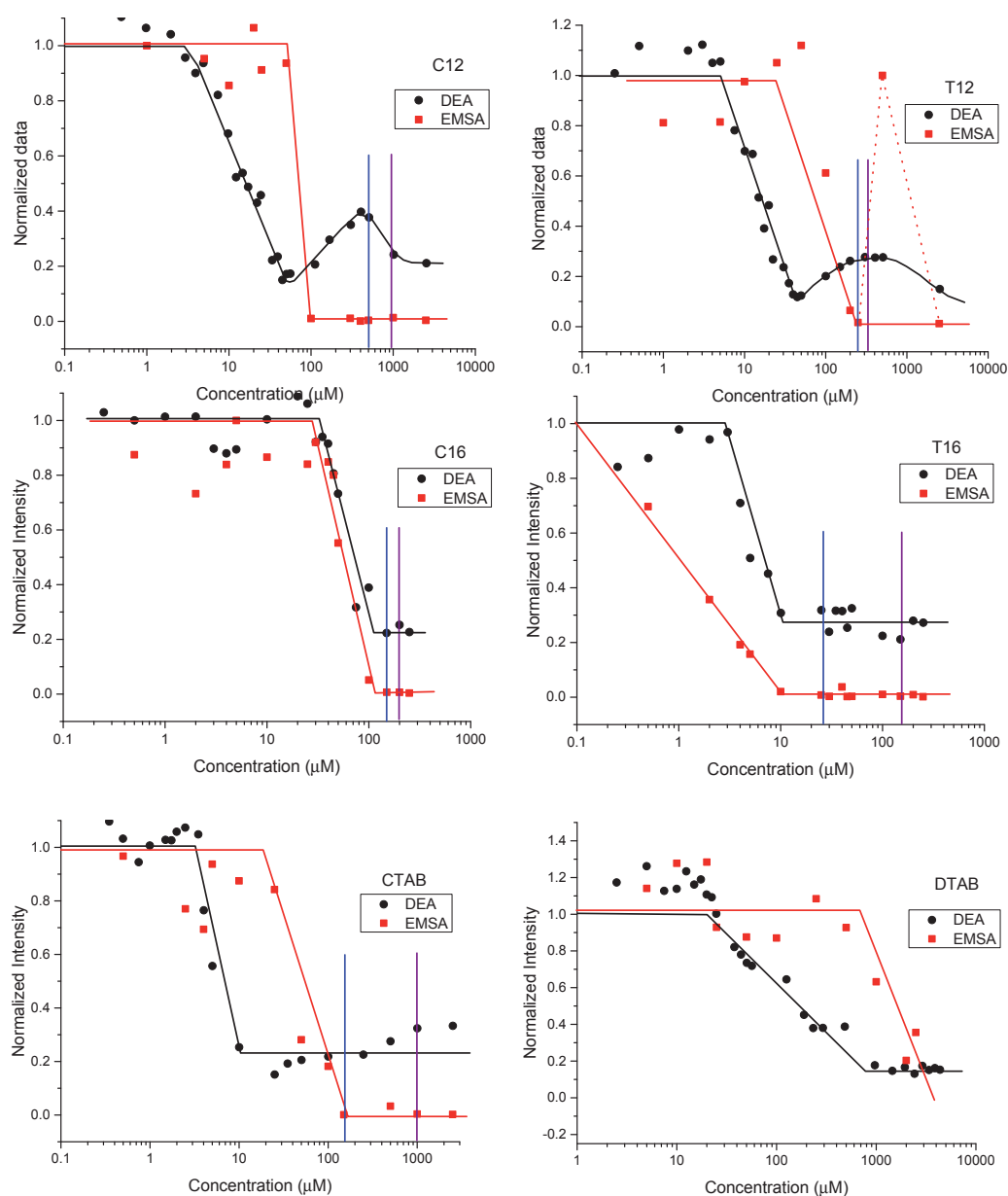


**Figure 148.** Superposed results of DEA and EMSA experiments. Blue line represents the  $Z_{hp-3}$  and purple line show the CMC of the surfactant.

## 12. Annex

Results of both techniques are in very good agreement with each other and they verify that all the obtained results are reproducible and correct.

As it is shown, some information about the mechanism of the formation of the complexes can be found out. Difference between the 12-carbon and 16-carbon chain length can be observed. On the one hand, in both **C12** and **T12**, the concentration of the critical intensity (from DEA) corresponds to the starting point of the decrease of the free DNA concentration (from EMSA), while in **C16** and **T16**, the concentration of the critical intensity (from DEA) corresponds to the final point of the decrease of the free DNA concentration (from EMSA). It clearly means that the mechanism of the complex formation is different depending on the chain length and it seems to be independent on the stereochemistry.

Once the concentration of surfactant is above the CAC, surfactant aggregates start to form a complex with free DNA. In the case of **C12** and **T12**, the binding avoids GelStar® to bind DNA, reducing the intensity in DEA but they do not decrease the negative charges of the DNA. Once the  $C_{Cl}$  is reached, concentration of free DNA starts to decrease. After the  $Z_{hp-2}$  (in DEA), they show a broad peak where the intensity is increased and then it is decreased again. Comparing the results of DEA and EMSA, it is observed that the maximum of this broad peak corresponds to the  $Z_{hp-3}$  (blue line). After this point, the formation of the positively charged complex or the precipitation starts.

On the other hand, **C16** and **T16** not only avoid GelStar® to bind DNA but also reduce the negative charges of the DNA until the  $Z_{hp-2}$  is reached. Then, the non-charged complex is obtained ( $Z_{hp-3}$ , blue line) and the formation of the positively charged complex or the precipitation starts.

In all cases, CMC is above the concentration at which the positively charged complex starts to be formed. The formation of micelles (or other surfactant aggregates) in solution favours that these new aggregates bind DNA forming the cationic complex.

## 12.5 DNase Foot Printing Assay

Nrul:

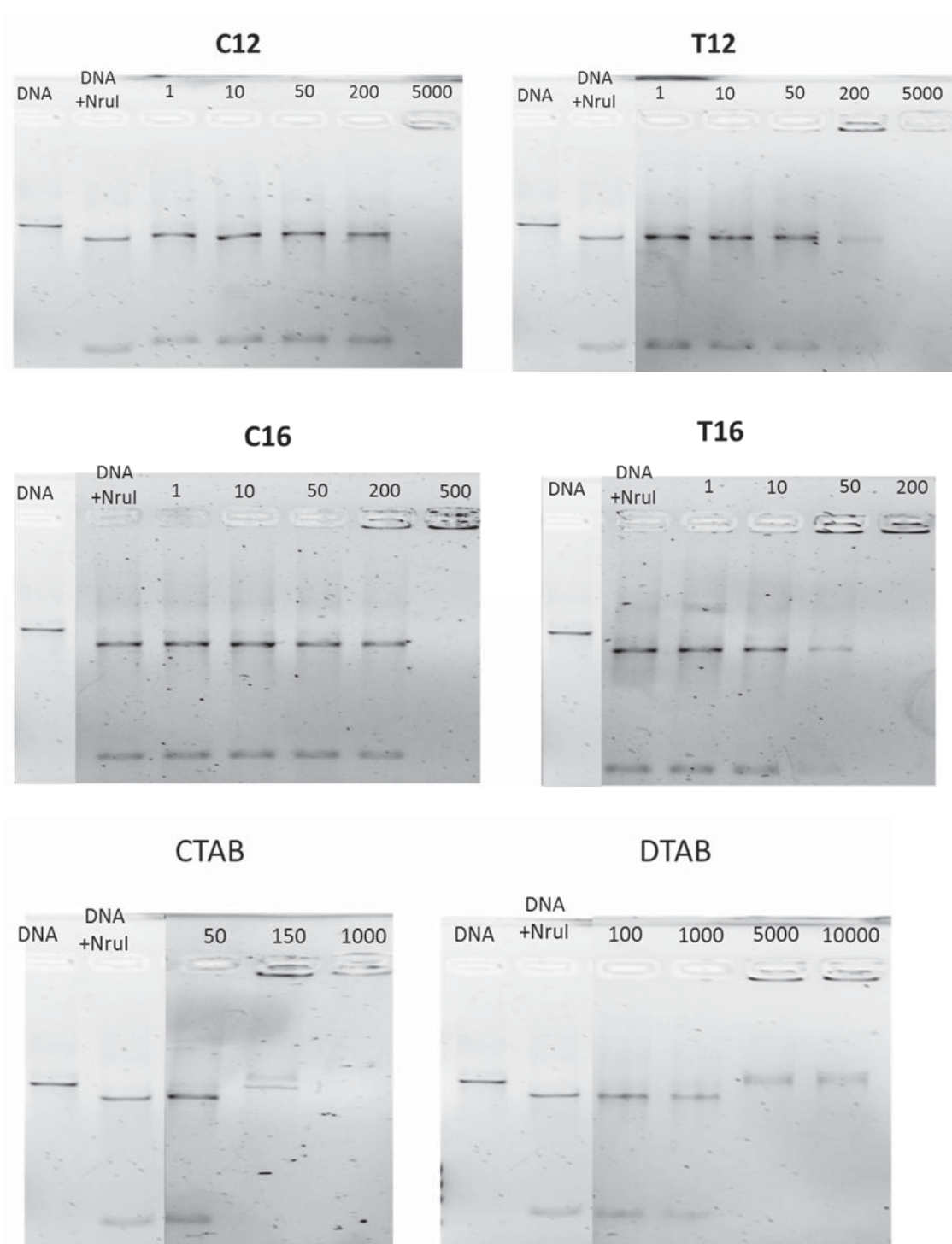


**Figure 149.** Resulting images from the electrophoresis of the NruI DNase Foot Printing Assays. Concentrations are shown in  $\mu\text{M}$  of surfactant/ppm of DNA.

Standard DNase:

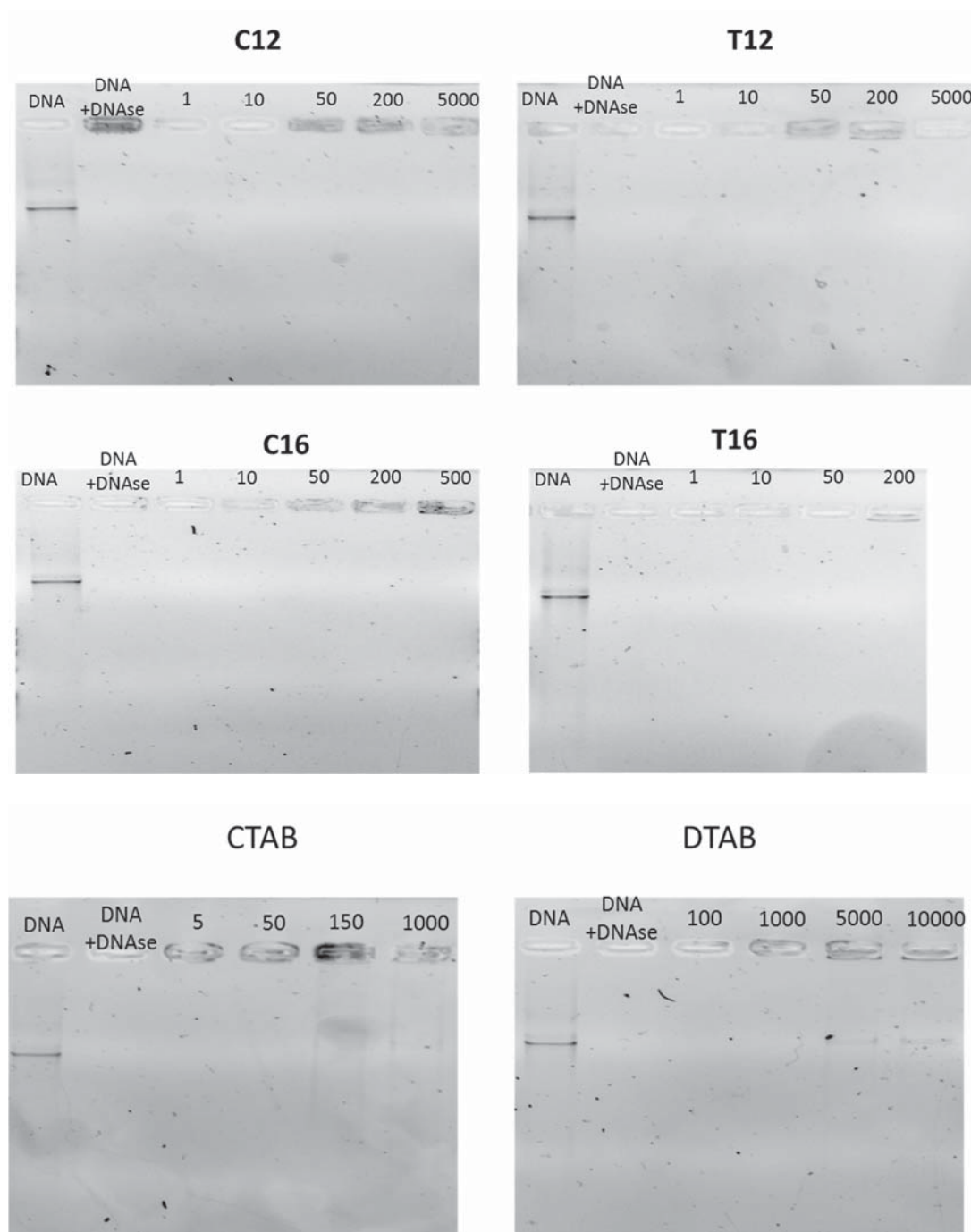


**Figure 150.** Resulting images from the electrophoresis of the DNase Foot Printing Assays. Concentrations are shown in  $\mu\text{M}$  of surfactant/ppm of DNA.

## 12.6 Transfection studies

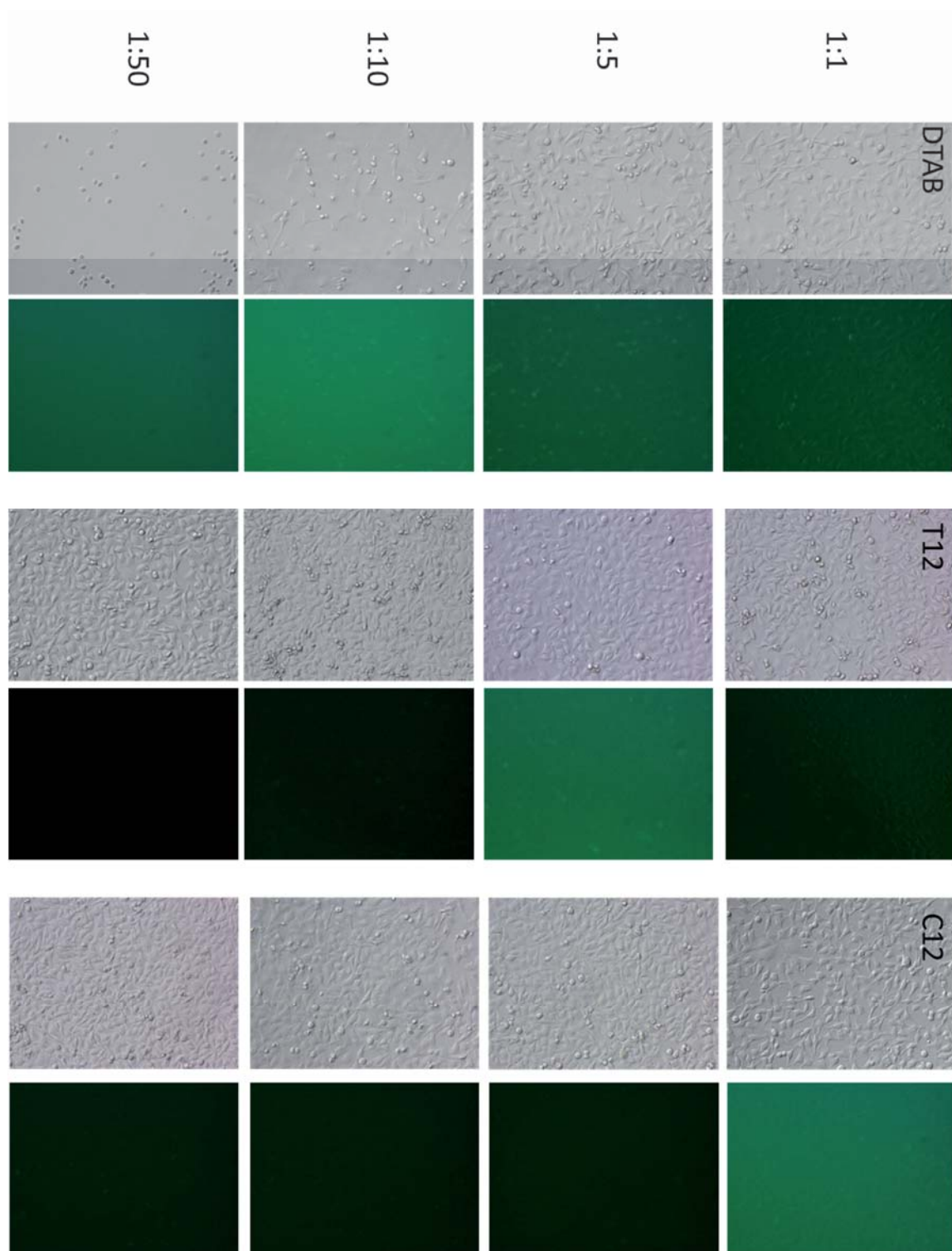


**Figure 151.** Images of the cells and images of the fluorescence microscope of the transfection studies of compounds DTAB, T12 and C12.



**Figure 152.** Images of the cells and mages of the fluorescence microscope of the transfection studies of compounds CTAB, T16 and C16.





## 12. Annex

```
echo ""
echo -e "\e[0;31m ***** \e[0m"
echo ""
exit
fi

touch /users/bernat/bin/estatcalculs/noms_antic1
touch /users/bernat/bin/estatcalculs/noms_antic2
touch /users/bernat/bin/estatcalculs/noms_antic3
touch /users/bernat/bin/estatcalculs/date_antic
touch /users/bernat/bin/estatcalculs/num_antic

username=$(whoami)
hora=$(date | awk '{print $4}')
dia=$(date +%d/%m/%y")
echo ""
echo -e "\e[0;31m ***** \e[0m"
echo ""
echo -e "\e[0;36m Hola ${username}! Avui es dia $dia, son les $hora i aquests son els teus calculs: \e[0m"
echo ""

gruppropi=$(id -gn)
grup=$(infocues $gruppropi | grep "Estat" | awk '{print $6}')

for i in $grup;do
  cua=$(qstat -u $username $i)
  if test -n "$cua";then
    total=$(qstat -u ${username} $i | grep $username -c)
    #a = Job Id, Username and Queue
    a=$(qstat -i -u ${username} | awk 'NR>5 {print " "$1"s" " "$2" " "$3 " "}')
    #b = Jobname
    b=$(qstat -f $(qstat -u ${username} $i | awk 'NR>5 {print $1"es"}') | grep -e "Job_Name" | awk '{print $3}')
    #c = NDS and Nodes
    c=$(qstat -i -n1u ${username} | awk 'NR>5 {print " "$6 " " "$7}')
    #d = Status and Time
    d=$(qstat -i -n1u ${username} | awk 'NR>5 {print $10 " " "$11}')
    #e = starting date
    e=$(qstat -f $(qstat -u ${username} $i | awk 'NR>5 {print $1"es"}') | grep -e "start_time" | awk '{print $4 " " "$5 " " "$6}')

    #nombre de calculs
    run_borg=$(qstat -u $username $i |grep " R " -c)
    queue_borg=$(qstat -u $username $i |grep " Q " -c)
    maxprocs=$(infocues $i | awk 'NR>9 && NR<11 {print $3}')

    # comença el programa!
    echo " Job ID      Username Queue" >> output
    echo " -----" >> output
    if test -n "${total}";then
      echo "${a}" >> output
      echo "Jobname" >> output
      echo "-----" >> output
      echo "${b}" >> output
      echo "NDS Nodes" >> output
      echo "-----" >> output
      echo "${c}" >> output
      echo "S Time" >> output
      echo "- ----" >> output
      echo "${d}" >> output
      echo "Main Borg" >> output
      echo "-----" >> output
      long=$(qstat -i -n1u ${username} | awk 'NR>5 {print $12 }')
      for j in ${long};do
        short=${j:0:8}
        echo $short >> output
      done
      echo "Starting time" >> output
      echo "-----" >> output
      echo "${e}" >> output
    fi

    #fila on comença cada bloc
    inb1=$((0 + 1))
    inb2=$((0 + $total + 3))
    inb3=$((0 + 2 * $total + 5))
    inb3b=$((0 + 3 * $total + 7))
    inb4=$((0 + 4 * $total + 9))
    inb5=$((0 + 5 * $total + 11))

    #fila on acaba cada bloc
    fib1=$((0 + $total + 2 ))
    fib2=$((0 + 2 * $total + 4))
    fib3=$((0 + 3 * $total + 6))
    fib3b=$((0 + 4 * $total + 8))
    fib4=$((0 + 5 * $total + 10))
    fib5=$((0 + 5 * $total + $run_borg + 12))

    #el que conte cada bloc
```

```

(sed -n ${inb1},${fib1}p output) > file1
(sed -n ${inb2},${fib2}p output) > file2
(sed -n ${inb3},${fib3}p output) > file3
(sed -n ${inb3b},${fib3b}p output) > file4
(sed -n ${inb4},${fib4}p output) > file5
(sed -n ${inb5},${fib5}p output) > file6
echo -e "\e[0;31m ***** \e[0m"
echo ""
if [ "$i" == "borg1" ];then
    echo -e "\e[0;32m BORG1\e[0m: max 10 jobs, 32 procs"
    else if [ "$i" == "borg2" ];then
        echo -e "\e[0;32m BORG2\e[0m: max 12 jobs, 96 procs"
        else if [ "$i" == "borg3" ];then
            echo -e "\e[0;32m BORG3\e[0m: "
        fi
    fi
fi

echo ""
paste file1 file2 file3 file4 file5 file6 | column -s $'\t' -t
echo ""
echo " # Total $i: $total ($run_borg + $queue_borg)"
suma=$(qstat -u $username $i | grep 'R ' | awk '{print $7}')
n=0
for k in $suma;do
    n=$((k + $n))
done
echo " # Estas fent servir $n procs"
echo ""
#elimina els fitxers temporals creats
rm file{1..6}
rm output
fi
done

echo -e "\e[0;31m ***** \e[0m"

totalborg1=$(qstat -u bernat borg1)
totalborg2=$(qstat -u bernat borg2)
totalborg3=$(qstat -u bernat borg3)
total=$(qstat -u bernat | grep bernat -c)

antic1=$(cat /users/bernat/bin/estatcalculs/noms_antic1)
antic2=$(cat /users/bernat/bin/estatcalculs/noms_antic2)
antic3=$(cat /users/bernat/bin/estatcalculs/noms_antic3)
dateantic=$(cat /users/bernat/bin/estatcalculs/date_antic | awk '{print $2 " " $3 " " $4}')

if test -n "$totalborg1";then
    noms1=$(qstat -f $(qstat -u ${username} borg1 | awk 'NR>5 {print $1"es"}') | grep -e "Job_Name" | awk '{print $3}')
    echo "noms1" >> actual1
    for i in $antic1;do
        comproba1=$(grep "$i" actual1 | grep "$i" -c)
        if [ "$comproba1" == 0 ];then
            echo $i >> /users/bernat/bin/estatcalculs/acabats_borg1
        fi
    done
    rm actual1
    else
    for i in $antic1;do
        echo $i >> /users/bernat/bin/estatcalculs/acabats_borg1
    done
fi

if test -n "$totalborg2";then
    noms2=$(qstat -f $(qstat -u ${username} borg2 | awk 'NR>5 {print $1"es"}') | grep -e "Job_Name" | awk '{print $3}')
    echo "noms2" >> kk2
    for i in $antic2;do
        comproba=$(grep "$i" kk2 | grep "$i" -c)
        if [ "$comproba" == 0 ];then
            echo $i >> /users/bernat/bin/estatcalculs/acabats_borg2
        fi
    done
    rm kk2
    else
    for i in $antic2;do
        comproba2=$(grep "$i" /users/bernat/bin/estatcalculs/acabats_borg2 | grep "$i" -c)
        if [ "$comproba2" == 0 ];then
            echo $i >> /users/bernat/bin/estatcalculs/acabats_borg2
        fi
    done
fi

if test -n "$totalborg3";then
    noms3=$(qstat -f $(qstat -u ${username} borg3 | awk 'NR>5 {print $1"es"}') | grep -e "Job_Name" | awk '{print $3}')
    echo "noms3" >> kk3
    for i in $antic3;do
        comproba=$(grep "$i" kk3 | grep "$i" -c)

```



## 12.8 Posters

## 16th Tetrahedron Symposium

Berlin, June 2015

**Carbocyclic diamide-based LMWOGs: influence of ring size, substitution and stereochemistry**

Bernat Pi-Boleda,<sup>a</sup> Marta Sans,<sup>a</sup> María Campos,<sup>b</sup> Ona Illa,<sup>a</sup> Ramón Estévez,<sup>b</sup> Vicenç Branchadell,<sup>a</sup> Juan Carlos Estévez,<sup>b</sup> Rosa M. Ortuño<sup>a</sup>

<sup>a</sup> Departament de Química, Universitat Autònoma de Barcelona (UAB), Spain  
<sup>b</sup> Centro Singular de Investigación en Química Biológica y Materiales Moleculares (CIQUUS), Spain  
[bernat.pi@uab.cat](mailto:bernat.pi@uab.cat)

Berlin, June 2015

---

### Introduction

Low molecular weight organogelators (LMWOGs) are molecules consisting of organic compounds with a molecular weight of less than 2000 Da which show gelation behaviour in organic solvents.<sup>1</sup> According to one of our research programs,<sup>2</sup> the aim of the study is to find out the influence of the ring size, different substitution and relative stereochemistry of some carbocyclic diamides on their gelation abilities.

### Studied diamide-based LMWOGs

---

### Results: gelation study

	THF	EtOH	MeOH	CH <sub>2</sub> Cl <sub>2</sub>	CH <sub>3</sub> OH	CH <sub>3</sub> CO <sub>2</sub> Me	CH <sub>2</sub> Cl <sub>2</sub>	EtOH	MeOH	CH <sub>2</sub> Cl <sub>2</sub>	EtOH	MeOH
A	1	1	1	1	1	1	1	1	1	1	1	1
B	1	1	1	1	1	1	1	1	1	1	1	1
C	1	1	1	1	1	1	1	1	1	1	1	1
D	1	1	1	1	1	1	1	1	1	1	1	1
E	1	1	1	1	1	1	1	1	1	1	1	1
F	1	1	1	1	1	1	1	1	1	1	1	1
G	1	1	1	1	1	1	1	1	1	1	1	1
H	1	1	1	1	1	1	1	1	1	1	1	1
I	1	1	1	1	1	1	1	1	1	1	1	1

1: Soluble; 0: Insoluble; minimum gelation concentration (mg/L) in mg/mL.

**Aggregation Energies**

**Gelation Temperatures**

**SEM**

**Conclusions**

- Stereochemistry has an effect only on the non-substituted cyclohexane-based LMWOGs.
- Cyclobutane-based compounds A and B are toluene-selective organogelators.
- TBDMS protection favors gelation of alcohols, while free OH groups favors gelation of apolar solvents.
- Two or more free OH groups promote two different aggregation patterns.
- Theoretical calculations help us to understand the gelation abilities.

**2<sup>nd</sup> experimental design nrgc in toluene**

**Unexpected behavior can be explained with theoretical calculations**

**Theoretical calculations are in agreement with HSP**

**Aggregation Energies**

**SEM**

**References**

- (a) Abdallah, D. J.; Weiss, R. G. *Adv. Mater.* **2000**, *12*, 17, 1237.
- (a) Celis, S.; Nolis, P.; Illa, O.; Branchadell, V.; Ortuño, R. M. *Org. Biomol. Chem.* **2013**, *11*, 1839. (b) Gorrea, E.; Nolis, P.; Torres, E.; Da Silva, E.; Amabilino, D. B.; Branchadell, V.; Ortuño, R. M. *Chem. Eur. J.* **2011**, *17*, 4588.
- (a) Raynal, M.; Boutellier, L. *Chem. Commun.* **2011**, 47, 8271. (b) Edelshtein, V. C.; Mac Cormack, A. S.; Ciarlantini, M.; Di Chenna, P. H. *Beilstein J. Org. Chem.* **2013**, *9*, 1826.

---

### Computational details

**Monomer to Tetramer:**

- Conformational Search: OPLS-2005, Mixed low mode/torsional sampling, gas phase, *MacroModel*
- DFT Optimization: M06-2X, 6-31G(d), gas phase, *Gaussian09*
- Minimization: OPLS-2005, in toluene, *MacroModel*

**Hexamer to Octamer:**

- Minimization: OPLS-2005, in toluene, *MacroModel*
- DFT Energy calculation: M06-2X, 6-31G(d), gas phase, *Gaussian09*

### Download this poster:

## 16th Tetrahedron Symposium

Berlin, June 2015

## Cationic bolaamphiphiles with a cyclobutane scaffold: behavior as surfactants

Bernat Pi-Boleda,<sup>a</sup> Marta Sans,<sup>a</sup> Alessandro Sorrenti,<sup>a</sup> Ona Illa,<sup>a</sup> Vicenç Branchadell,<sup>a</sup> Ramon Pons,<sup>b</sup> Rosa M. Ortuño<sup>a</sup>

<sup>a</sup> Departament de Química, Universitat Autònoma de Barcelona (UAB), Spain  
<sup>b</sup> Departament de Tecnologia Química i de Tensioactius, Institut de Química Avançada de Catalunya (IQAC-CSIC), Spain

bernat.pi@uab.cat

Berlin, June 2015

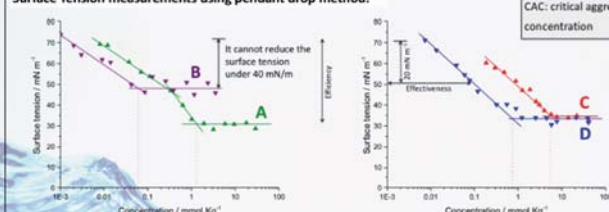
## Introduction:

There is a family of amphiphiles called bola which have two polar head groups attached at the ends of a hydrophobic chain.<sup>1</sup> In this work, four cyclobutane-containing bolaamphiphiles have been synthesized and their ability to act as surfactants has been studied. The cyclobutane unit could introduce some rigidity to the amphiphile favouring a "wicket" configuration. The influence of the regio- and stereochemistry on their behavior has been analyzed.

## Studied molecules:



## Results:

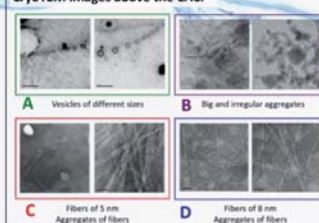
Surface Tension measurements using pendant drop method:<sup>2</sup>

CAC: critical aggregation concentration

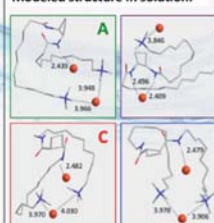
	Area $A_{CAC}$ ( $\text{\AA}^2$ )	Efficiency $\Pi_{CAC}$ (mN/m)	Effectiveness $PC_{20}$ (mM)	CAC (mM)	$\Delta G_{mix}^{\ddagger}$ (kcal/mol)
A	100.2 ± 5.3	41.5	0.853	1.30	-4.25
B	223.5 ± 21.8	22.9	1.509	0.06	-2.44
C	141.0 ± 4.0	36.2	0.168	5.41	-5.10
D	147.6 ± 3.8	38.9	1.108	0.72	-3.90

B cannot be considered as a surfactant whereas the others can ( $\Pi_{CAC} > 30$  mN/m).

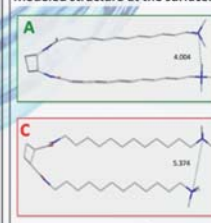
## CryoTEM images above the CAC:



## Modeled structure in solution:

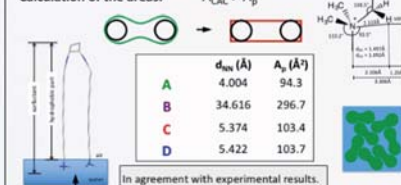


## Modeled structure at the surface:



All of them have a "wicket" configuration except B, which has an opened configuration.

## Calculation of the areas:



## Conclusions:

- The cyclobutane moiety favours a "wicket" configuration. However, other factors such as stereochemistry play an important role.
- Stereochemistry has an effect on the solubility and thus, on the CAC and on the efficiency.
- The structure of the aggregates depends on the regiochemistry.
- A theoretical approach can be used to calculate the aggregation on the surface and to predict their behavior.

## References:

- <sup>1</sup> (a) Fuhrhop, J.; Wang, T. *Chem. Rev.* **2004**, *104*, 2901; (b) Sorrenti, A.; Illa, O.; Ortuño, R. M. *Chem. Soc. Rev.* **2013**, *42*, 21, 8200.  
<sup>2</sup> Anastasiadis S. H.; Chen, J. -K.; Koberstein, J. T.; Siegel, A. F.; Sohn, J. E.; Emerson, J. A. *J. Colloid Interface Sci.*, **1987**, *119*, 1, 55.

Download this poster:



View this poster with the Poster-It app  
[www.poster-it.com](http://www.poster-it.com)

C. Search: OPLS-2005, Mixed Low Mode/Torsional Sampling, Macromodel DFT Optimization: M06-2X/6-31G(d), Gaussian09

## Jornades Doctorals

Bellaterra, June 2016

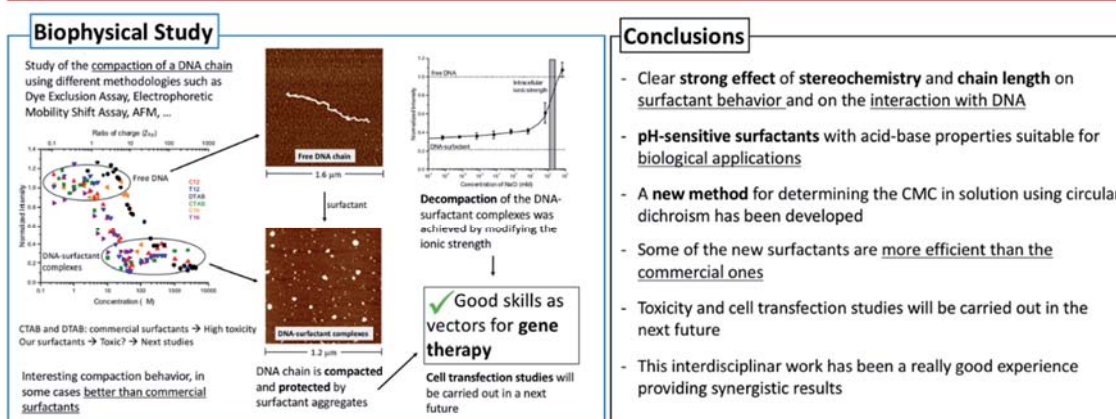
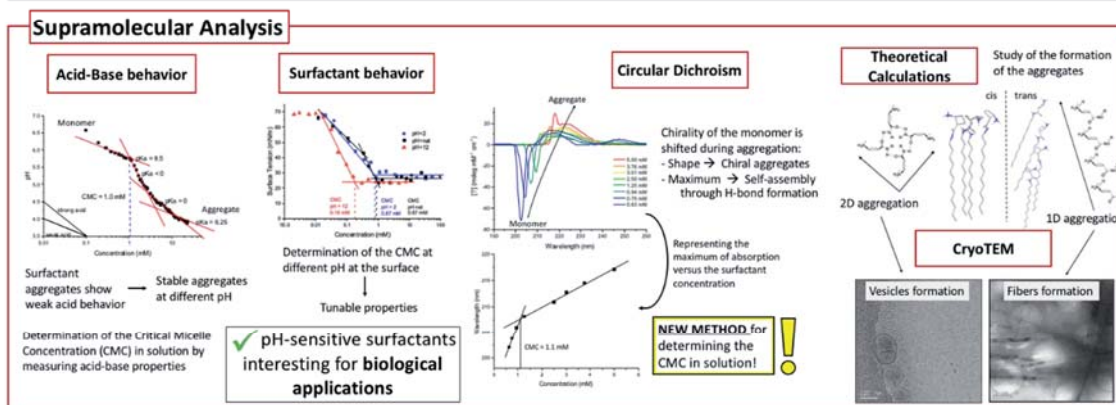
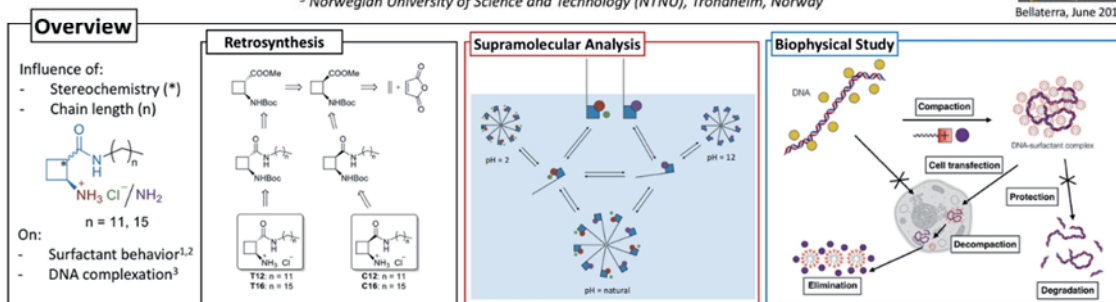
## Chiral pH-dependent $\beta$ -amino acid-based surfactants: synthesis, supramolecular analysis and study as potential new vectors for gene therapy

Bernat Pi-Boleda,<sup>1</sup> Ramon Pons,<sup>2</sup> Rita S. Dias,<sup>3</sup> Vicenç Branchadell,<sup>1</sup> and Rosa M. Ortuño<sup>1</sup>

bernat.pi@uab.cat

<sup>1</sup>Universitat Autònoma de Barcelona (UAB), Bellaterra, Spain<sup>2</sup>Institut de Química Avançada de Catalunya (IQAC-CSIC), Barcelona, Spain<sup>3</sup>Norwegian University of Science and Technology (NTNU), Trondheim, Norway

Bellaterra, June 2016



## References

- (1) Sorrenti, A.; Illa, O.; Pons, R.; Ortuño, R. M. *Langmuir* **2015**, *31*, 9608–9618.
- (2) Pinazo, A.; Angelet, M.; Pons, R.; Lozano, M.; Infante, M. R.; Pérez, L. *Langmuir* **2009**, *25*, 7803–7814.
- (3) Dias, R. S.; Lindman, B. *DNA Interaction with Polymers and Surfactants*; John Wiley & Sons, Inc., New Jersey, **2008**.

Download this poster:



It was awarded with the First Price.